DIPARTIMENTO DI INGEGNERIA PER L'AMBIENTE E IL TERRITORIO E INGEGNERIA CHIMICA
UNIVERSITA' DELLA CALABRIA

Dottorato di Ricerca in Ingegneria Chimica e dei Materiali

CICLO XXVII

Erasmus Mundus Doctorate in Membrane Engineering – EUDIME

---

in co-supervisione con:

Université Toulouse 3 Paul Sabatier (FRANCE)

Institute of Chemical Technology Prague (CZECH REPUBLIC)

TESI

Evaluation of thermal polarization and membrane characteristics for membrane distillation

Settore Scientifico Disciplinare: CHIM/07- Fondamenti Chimici delle Tecnologie

I supervisori

Dr. Pierre Aimar

Prof. Enrico Drioli

Prof. Karel Bouzek

Dr. Vlastimil Fila

Il Dottorando

Aamer Ali

Il Coordinatore del Dottorato di Ricerca
in Ingegneria Chimica e dei Materiali
Ch.mo Prof. Raffaele MOLINARI

ANNO ACCADEMICO 2013-2014

ACKNOWLEDGEMENT

At first place, I am thankful to almighty Allah who bestowed me with health, courage and strength to pursue this research, along with countless other blessings.

I greatly acknowledge the generous financial support from The Education, Audiovisual and Culture Executive Agency – EACEA/European Commission within the "Erasmus Mundus Doctorate in Membrane Engineering – EUDIME" (ERASMUS MUNDUS Program 2009-2013, FPA n. 2011-0014, SGA n. 2011-1599) for pursuing the current study.

I would like to express my deepest gratitude to Prof. Enrico Dioli, Dr. Pierre Aimar and Dr. Vlastimil Fila not only for supervising my research but also for making the practical arrangements to host my visits to their laboratories. I am also thankful to Dr. Francesca Macedonio for her technical support and valuable advice during my research.

I would like to extend my gratitude to current director of ITM-CNR Dr. Ledietta Giorno for providing me an excellent research environment during my stay at University of Calabria. I would also like to acknowledge the valuable cooperation from Prof. Molinari, Dr. Efrem and the other technical and administrative staff throughout my PhD.

I am also thankful to all my friends and colleagues from University of Calabria, University of Paul Sabatier Toulouse and Institute of Chemical Technology Prague for their multi-aspect provision. All the good moments that we spent together will always occupy a fraction of my mind in the form of golden memories. It is hard to move ahead without mentioning the support from Cejna, Fitim, Alessio Fuoco and Han Lee. The last three are specially acknowledged for their useless efforts to improve my football and basketball skills.

Last but not the least, I would like to express my sincere gratitude to all my family members for their encouragement, support and prayers that have been with me throughout my life.

Aamer Ali

Abstract

The current PhD work emphasizes on various aspects of membrane distillation for approaching zero liquid discharge in seawater desalination. In broader sense, two themes have been discussed in detail: (i) correlation between membrane features and their performance in MD (ii) understanding and control of thermal polarization in MD. Introduction and state-of-the-art studies of MD including progress in membrane development, understanding the transport phenomenon, recent developments in module fabrication, fouling and related phenomenon and innovative applications have been discussed in introductory part of the thesis. The effect of operating conditions and dope compositions on membrane characteristics and correlation between membrane features and their performance has been discussed in subsequent section. It has been established that membrane morphology plays a crucial role in performance of the membrane for real applications. Furthermore, it has been demonstrated that the effect of membrane morphology is different for direct contact and vacuum configurations.

Theoretical and experimental aspects of thermal polarization in direct contact membrane distillation have also been investigated. Thermal polarization phenomenon in a flat sheet membrane has been studied by using a specifically designed cell. The effect of operating conditions and solution concentration on thermal polarization has been explored experimentally. It has been observed that increased solution concentration favors the thermal polarization due to resulting poor hydrodynamic at the membrane surface and increase in diffusion resistance to the water vapors migrating from bulk feed phase to the membrane surface. Some active and passive techniques to decrease thermal polarization and possible fouling in membrane distillation have also been discussed in the current study. Thermal polarization can be greatly reduced by inducing secondary flows in the fluid flowing inside the fiber. The induction of secondary flows in the current study has been realized by using the fibers twisted in helical and wavy configurations. Due to improvement of thermal polarization coefficient on up and downstream, the undulating fiber geometries provide high flux and superior performance ratio. Application of intermittent and pulsatile flow to control thermal polarization in MD has also been discussed. It has been inferred that these flows have positive impact on performance ratio and volume based enhancement factors without compromising on packing density of the system.

The application of MD for treatment of produced water has also been studied. The effect of membrane features on their performance for the treatment of this complex solution has been discussed. The desirable membrane features for successful application of MD for such treatment have been distinguished. It has been inferred that MD possesses the capability to produce a distillate of excellent quality and is an interesting candidate to recover the minerals present in the produced water. The fouling tendency of the membranes with different characteristics towards different types of feed solutions has also been discussed in this study. It has been shown that the porosity enhanced through the introduction of macrovoids in non-solvent induced phase separation technique creates problems

related with wetting and pore scaling during practical application of such membranes. The fouling related issues are less severe in the membranes with sponge like microstructure but the overall porosity of such membranes is relatively less. Thus it has been concluded that there should be an optimum between the high throughput and stable performance of the membranes synthesized through phase inversion techniques. Conclusions of the study and future perspectives have been discussed in the last section of the study.

Table of Contents

List of figures

List of tables

CHAPTER 1

Introduction

1. Membrane operations and modern process industry

Separation, concentration and purification of molecular mixtures are the key requirements in process industry, underlying the importance of efficient separation in this sector. The state-of-the-art norms to achieve these objectives include distillation, extraction, crystallization, adsorption and ion exchange technology. These technologies are energy intensive in nature and generally mark a large footprint. For instance, it has been estimated that 60-70% of the energy requirement in petrochemical industry is anticipated in particular field of separation and purification. Thus the basic characteristics features of the conventional separation processes are contradictory to the basis of process intensification strategy [1]. Consequently, improvement or replacement of traditional separation techniques can offer a substantial impact on the process feasibility.

Contrary to the practice of the conventional process industry, depleting resources of energy and raw materials combined with environmental issues emphasize on sustainable industrial growth across the globe. The sustainable growth can be realized by using the material and energy resources more efficiently and rationally while at the same time, eliminating or minimizing the hazards associated with processes. Modern membrane engineering represents one of the possible and the most interesting way for developing processes in accordance with the guidelines provided by process intensification strategy to meet the challenges of the modern world [2]. Membrane engineering appears as a powerful discipline with characteristic features of efficient molecular separation, compatibility between different membrane operations in integrated systems to achieve the specific separation requirements, easy control and scale-up, chemical transformation and mass and energy transfer between different phases to realize the objectives of process intensification strategy.

Membrane engineering, at present, is providing interesting solutions to some of the major problems of our modern industrialized society for decreasing energy consumption, resolving environmental concerns and exploring the potential of many processes in a better and improved way. For instance, in many regions in the world conventional thermal desalination plants have been replaced with membrane process due to their 10-fold more energy efficient nature than thermal options; conventional activated sludge plants have been turned into membrane bioreactors due to their compactness (up to 5 times more compact than conventional plants), reduced sludge production and considerable level of physical disinfection [3]. In food industry, the membrane operations are availing interesting opportunities of concentrating the products and treating the wastewater streams. The use of membrane technology in energy production sector has opened the innovative gateways to produce electricity by using the concept of blue energy and fuel cells.

In addition to the conventional traditional pressure driven membrane processes, numerous new membrane operations have emerged recently with significant potential in various area. The new operations differ from the conventional ones mainly in terms of driving force and/or separation mechanism. The driving force for majority of the conventional membrane operations including microfiltration (MF), ultrafiltration (UF), nanofiltration (NF) and reverse osmosis (RO) is the pressure gradient. The processes such as electrodilaysis (ED), electrodilaysis reversal (EDR) and electrodeionization are driven by the electrochemical potential whereas temperature gradient is the

driving force for the membrane distillation (MD) and membrane dryers. The separation ranges for the conventional pressure driven processes have been provided in Figure 1.1 while a summary of the driving forces, mode of separation and permeating and retaining species for conventional and some new processes has been provided in Table 1.1. Size exclusion is the main governing separation mechanism for conventional pressure driven processes, however, chemical nature of the species also plays an important role in NF and RO.

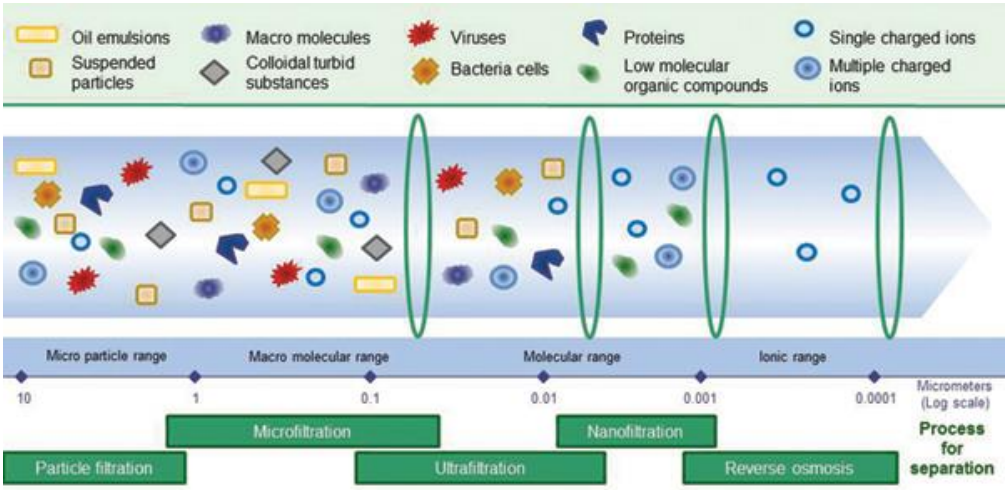

Figure 1.1: Separation ranges for various membrane processes

Table 1.1: An overview of various membrane operations

Process	*Driving Force*	*Mode of transport*	*Species Passed*	*Species Retained*
Microfiltration (MF)	Pressure difference 100 - 500 kpa	Size exclusion convection	Solvent (water) and dissolved solutes	Suspended solids, fine particulates, some colloids
Ultrafiltration (UF)	Pressure difference 100 - 800 kpa	Size exclusion convection	Solvent (water) and low molecular weight solutes (<1000 da)	Macrosolutes and colloids
Nanofiltration (NF)	Pressure difference 0.3 - 3 mpa	Size exclusion solution diffusion Donnan exclusion	Solvent (water), low molecular, weight solutes, monovalent ions	Molecular weight compounds > 200 da multivalent ions
Reverse osmosis (RO)	Pressure difference 1 - 10 mpa	Solution diffution mechanism	Solvent (water)	Dissolved and suspended solids

Gas Separation (GS)	Pressure difference 0.1 – 10 mpa	Solution diffusion mechanism	Gas molecules having low molecular weight or high solubility-diffusivity	Gas molecules having high molecular weight or low solubility-diffusivity
Pervaporation (PV)	Chemical potential or concentration difference	Solution diffusion mechanism	High permeable solute or solvents	Less permeable solute or solvents
Electrodialysis (ED)	Electrical potential difference,1 – 2 v / cell pair	Donnan exclusion	Solutes (ions) small quantity of solvent	Non-ionic and macromolecular species
Dialysis (D)	Concentration difference	Diffusion	Solute (ions and low mw organics) small solvent quantity	Dissolved and suspended solids with mw > 1000 da
Membrane contactors (MC)	Chemical potential, concentration difference; temperature difference	Diffusion	Compounds soluble in the extraction solvent; volatiles	Compounds non soluble in the extraction solvent; non volatiles
Membrane based solvent extraction (MBSX)	Chemical potential or concentration difference	Diffusion partition	Compounds soluble in the extraction solvent	Compounds non soluble in the extraction solvent
Membrane distillation (MD)	Temperature difference	Diffusion	Volatiles	Non volatiles
Supported liquid membranes (SLM)	Concentration difference	Diffusion	Ions, low MW organics	Ions, less permeable organics
Membrane reactors (MR)	Various	Various	Permeable product	Non permeable reagents
Membrane crystallization	Temperature difference	Diffusion	Volatiles	Non volatiles
Forward osmosis	Osmotic gradient	Solution diffusion	Solvent	Dissolved and suspended solids
Membrane emulsification	Pressure gradient	Convection	Dispersed phase	
Membrane dryers	Vapor pressure gradient	Diffusion	Volatile	Non volatiles

In many parts of the world, the dependence on seawater for industrial, drinking and household purposes has greatly increased. Conventionally, seawater desalination is carried out through state-of-the-art pressure driven membrane based processes due to their significant advantages compared to thermal processes. However, the pressure driven processes face some challenges that need to be

addressed, operation at high pressure and disposal of brine being the most significant obstacles that negatively affect the process economy and cause environmental problems. New membrane based operations offer promising solutions to desalination problems. The use of new processes in integration with the traditional ones can not only resolve the problem of waste handling but also provides the opportunity to boost the overall recovery factor and economy of the process. Integrated approach takes into account energy saving, water rationalization, minimization of resource utilization and waste production [4]. Therefore, integrated systems can contribute significantly to the solution of strategic aspects of industrial productions. Different membrane operations can be coupled in integrated systems for approaching the ambitious objective of "zero liquid discharge". For instance, in seawater desalination conventional pressure driven membrane operations can be combined with other innovative membrane processes such as membrane distillation (MD) or membrane crystallization (MCr) for achieving the aspiring objective of reaching very high recovery factor (around 85-90%) [5] (Figure 1.2).

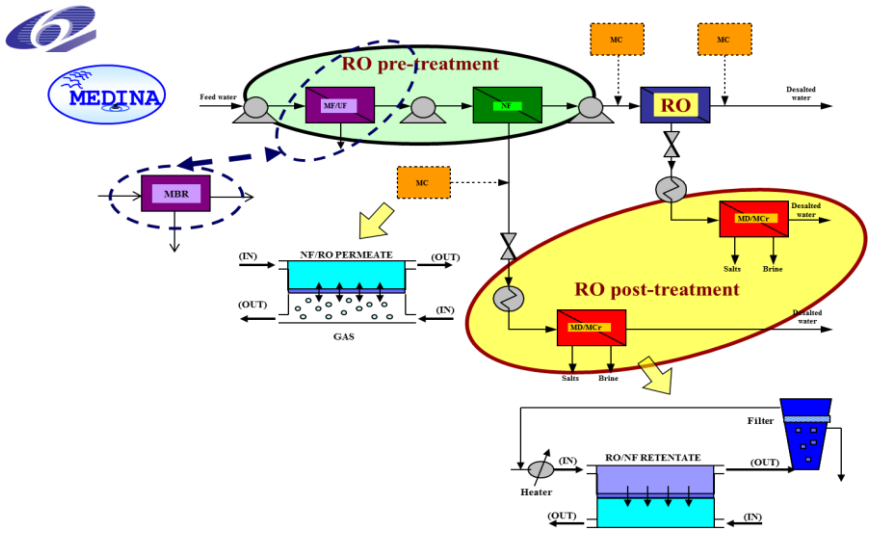

Figure 1.2: Integrated membrane systems for desalination proposed in MEDINA project [5]

2. Membrane Distillation

Membrane distillation (MD) is one of the innovative membrane based processes that was documented for the first time in 1963 [6]. However, only recently, it gained significant popularity among the scientific and engineering community. Different terminologies have been used for the process till the ''Workshop on Membrane Distillation'' held in Rom during May, 1986. The definition of MD was confined in the workshop to the process utilizing the hydrophobic, porous membrane with the pores allowing the transport of vapors without capillary condensation. It was also acclimatized that membranes must not alter the vapor liquid equilibrium, at least one side of the membrane must be in contact with liquid feed and the necessary driving force is provided by vapor pressure gradient across the membrane. The process finds promising applications in various areas of membrane engineering including water desalination, treatment of industrial effluent, pharmaceutical industry, food industry, removal of organic compounds from aqueous streams and in a number of other applications. The process is based on temperature gradient created across a microporous membrane that separates vapor-liquid phases in equilibrium as illustrated in Figure 1.3 and therefore the process performance is relatively insensitive to the feed concentration. The hydrophobic nature of the membranes ensures the passage of only vapor phase through the membrane. The process possesses some unique advantages in comparison to conventional distillation or pressure driven membrane based processes: theoretically complete rejection of all non-volatile components, lower operating temperatures and pressures,

possibility to use waste grade heat or energy, less stringent requirements in terms of mechanical strength of membranes and possibility to concentrate the solutions to their saturation level [7].

MD has the capability to replace reverse osmosis process if cheap or low grade waste energy is available [8]. Substantial potential of practical application of MD in processes such as water desalination exists in the areas with relatively hot climate. In Middle East, half of the domestic oil consumption is associated with water purification every year. MD can play a crucial role in decreasing this proportion significantly due to the abundant solar energy available in Middle East. However, it is worthy to note that in most of the cases, MD should be considered as an optimum compromise between its energy intensive nature and healthy impact on environment.

MD can be easily adapted to other systems. It can be coupled with the solar energy systems to utilize the low grade energy; it can be used separately or in integration with other processes such as membrane bioreactors (MBRs), forward osmosis (FO), microfiltration (MF), ultrafiltration (UF), nanofiltration (NF) and RO to improve the efficiency of the process in terms of purity and recovery factor. In case of seawater desalination, MBR and UF/MF can improve the pre-treatment whereas MD can be used to recover the water from the residual brine. Moreover, the use of MD as membrane crystallization unit allows to extract not only further water but also the minerals contained in the brine streams (e.g., sodium, chlorine, magnesium, sulphate, calcium, potassium, bicarbonate, and eventually also lithium, bromine, and many more) [9][10]. MD based processes, such as membrane crystallization and osmotic membrane distillation, have opened innovative gateway to obtain the crystals from salt solutions and to concentrate various solutions to the limits which are not achievable through conventional pressure driven processes. Another interesting application of MD is its potential to recover toxic or/and useful compounds and heavy metals from various sorts of industrial effluents which can be reused in the process or can be separated from the effluent to avoid their adverse environmental impact [11][12]. Hence, MD can provide an innovative, cost effective and easy-to-adopt pathway with significant impact in terms of benefits obtained to achieve the goals of green chemistry.

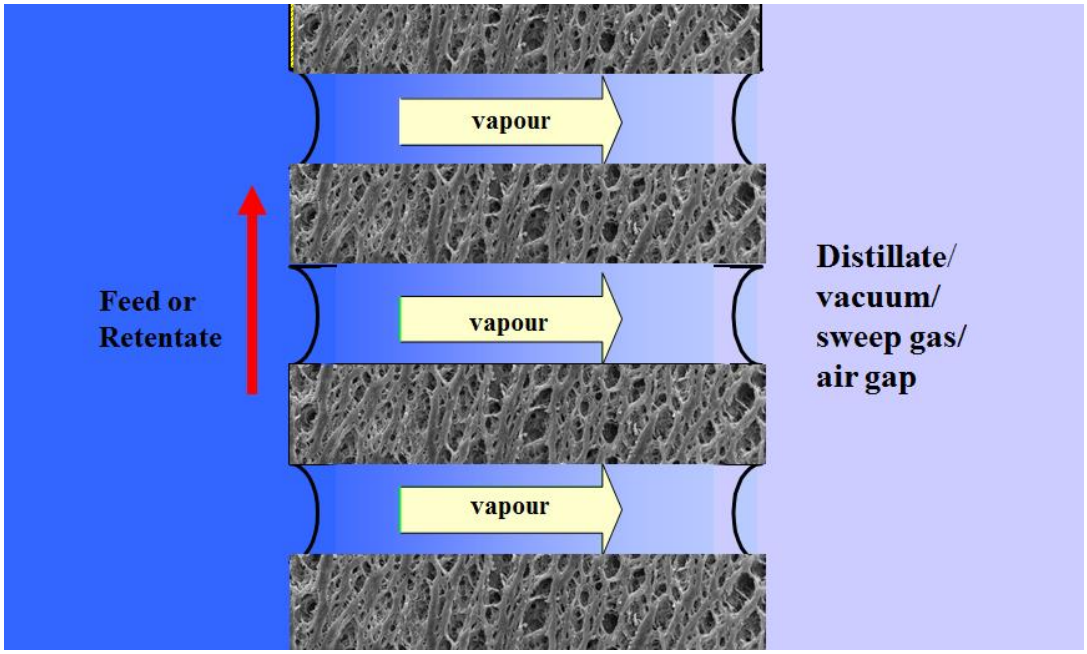

Figure 1.3: Schematic of basic MD process

2.1 Main challenges for MD

2.1.1 Inappropriate membranes

The unavailability of the membranes specifically designed for MD is the biggest obstacle for widespread applications of MD. Traditionally, the membranes prepared for ultrafiltration and microfiltration through phase inversion processes have been utilized for MD applications. These membranes generally have low porosity, limited hydrophobicity, broader pore size distribution and pore size not engineered for MD requirements. The thickness of these membranes has been design to withstand relatively high pressure of UF and MF which is not encountered in MD. Accordingly, MD flux for such membranes is low and at the same time conductive losses are high.

2.1.2. Thermal polarization

Thermal losses associated with the thermal polarization (also referred as temperature polarization) is another issue that suppresses the process performance. In direct contact membrane distillation (DCMD), a hot feed and a cold permeate are in direct contact with the opposite sides of the membrane. The transport of heat across the membrane takes place through conduction and transport of the hot vapors through the membrane (Figure 1.4). Consequently, the temperatures at the membrane surfaces are different from their values in the bulk. Temperature or thermal polarization coefficient is used to describe the thermal efficiency of the process. It is defined as the ratio of the difference of feed and distillate temperatures at membrane surfaces to the corresponding difference in the bulk.

$$TPC = \frac{T_{fm} - T_{pm}}{T_f - T_p}$$

The value of temperature polarization coefficient approaching to unity describes a thermally efficient process. In poorly designed system, significant heat is lost due to thermal polarization.

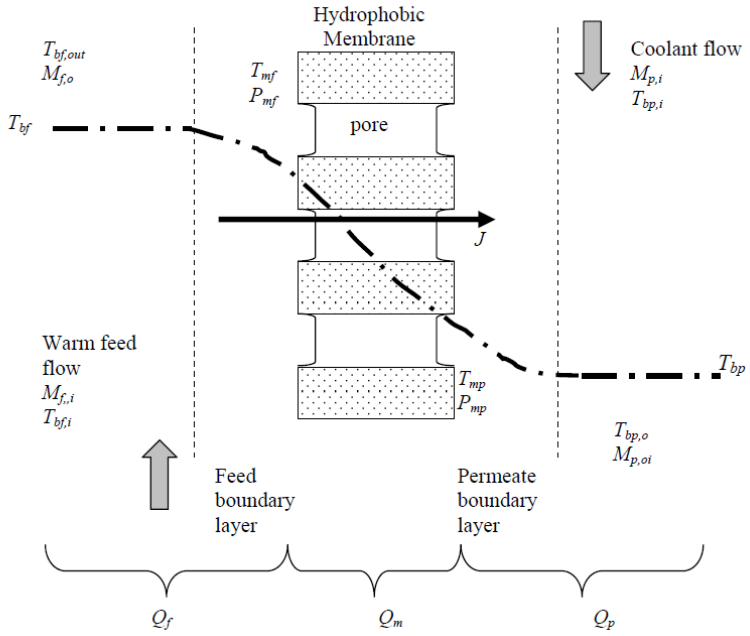

Figure 1.4: Illustration of heat transfer and thermal polarization in MD process

2.1.3 Nontraditional fouling

Due to different transport phenomenon and operating mechanism, generally rigorous feed characteristics and use of hydrophobic membranes, the nature of fouling in MD is different from other low pressure membrane processes. Scale formation at membrane surface is the most common form of fouling observed in MD process when applied to concentrated salt solutions. Wetting of pores has the similar effect as that of the fouling in conventional pressure driven membrane operations. With the advent of novel applications of MD, other types of fouling can also be seen in various studies. For example, the fouling phenomenon becomes more significant and sever while treating the solutions rich in organic contents [13] [14]. The thickness of the fouling layer can play a decisive role in controlling the heat and mass transfer across the membrane [15].

2.1.4 Loss of membrane hydrophobicity

MD process essentially relies on the hydrophobic nature of the membranes to retain the liquid on one side of the membrane while allowing the passage of only vapors. The intrusion of liquid inside the membrane pores is referred to as pore wetting. The successful application of the membrane distillation has been associated with the fulfilment of non-wettability criteria of membrane pores. When the hydraulic pressure exceeds the liquid entry pressure, the membranes are prone to wetting. The effect of wetting is not only possible reduction in flux and degradation of permeate quality but also a severe fouling inside the pores caused by the precipitated/adsorbed materials. Certain components from aggressive feed solutions can interact with the membrane material to alter its hydrophobic nature. Similarly, low surface additives present in the feed can penetrate through the pores and can damage the hydrophobic character of the pores. Biofouling can also play a role in decreasing the hydrophobicity of the membranes.

2.1.5 Large scale applications

Traditionally, MD has been utilized for desalination purposes as an alternative to RO or to overcome limited recovery of RO and other thermal desalination techniques [16]. Moreover, MD has been considered as a viable candidate in arid areas which lie in the region with abundant solar energy available, thus further confining its application mostly for desalination [17]. However, a lot of other interesting applications of MD have been explored due to less fouling tendency of the process, the potential to treat the complex feed solutions and due to the fact that the separation is driven by the temperature induced phase equilibrium establish at a particular temperature. The temperature gradient base nature of the process also opens new novel opportunities to use it for vapor/gas separation applications where the equilibrium composition at any temperature is enriched with the more volatile component. Consequently, the sphere of applications of the process has extended beyond the traditional use of desalination. However, most of these studies have been carried out at lab scale and require more pilot scale studies to bridge the gap between lab scale testing and commercial scale application.

3. Thesis statement

The aim of this thesis is to further enhance the understanding of fundamental identified constraints of MD, specifically thermal polarization and membrane characteristics required for MD. The qualitative application of the conclusions drawn is believed to be applicable for practical applications of MD, though the carried out research and mentioned results are based on laboratory work. A brief overview of each chapter included into the thesis has been described below.

A general overview of state-of-the-art of MD has been provided in **chapter 2**. The chapter elaborates different conventional and emerging configurations of MD, recent trends in membrane synthesis and module fabrication, new attempts to elaborate heat and mass transport mechanism in MD, fouling in MD and novel applications of the process.

There is a strong need to understand the correlation between membrane features including morphology, porosity, mean pore size, pore size distribution and their performance in MD. On one hand, it is well established that the membranes with high overall porosity and large pore size favor the mass transport of vapors from feed to the permeate side while on the other hand, the presence of large pores in the membrane can make the membranes more prone to wetting. Furthermore, it is not only the overall porosity that favors the high flux but the microstructure of the membrane also plays a key role in dictating the membrane performance. **Chapter 3** describes the relationship between the membrane properties and their performance against different solutions. The lab made membranes have been tested in vacuum and direct contact configurations for different feed solutions and the relationships between the membrane characteristics and performance has been explored.

As stated previously, thermal polarization severely affect MD process in an environment characterized by poor hydrodynamic and high feed temperature. There are several correlations in the literature relating the hydrodynamic of the system with thermal polarization, yet still literature suffers from the lack of direct experimental realization of temperature polarization based on the experimentally measured temperatures at membrane surface. The experimental study of temperature polarization carried out by using a cell specifically designed for this purpose has been described in **chapter 4**.

Various approaches have been used in the literature to minimize the temperature polarization in MD. Module designing and flow patterns can play a significant role in decreasing the thermal polarization in MD. **Chapter 5** describes the effect of wavy and helical shaped fibers on temperature polarization on MD process. The effect of pulsatile and intermittent flow patterns has also been described in this chapter.

The sphere of potential applications of MD is growing rapidly. The process has been tested for the applications ranging from the separation of volatile aroma components to the recovery of organic and inorganic crystals from various solutions. One growing field of potential interest is the oil and gas industry. With exhausting oil reserves and discovery of the non-conventional reservoirs of natural gas, the handling and treatment of produced water is becoming increasingly important. Produced water is characterized with the presence of very high salt content and small fractions of oil and greases. The treatment of such complex water is challenging for the conventional membranes based processes. MD is considered as an appropriate candidate for the treatment of this complex solution. **Chapter 6** discusses the feasibility of MD process for the treatment of gas field produced water by using membranes with different characteristics. Initial studies to recover crystals from produced water have also been discussed in this chapter.

Fouling is a major operational problem in all pressure driven membrane processes. The nature of fouling in MD is different from traditional pressure driven processes. Nontraditional fouling in MD has been discussed in **chapter 7**. MD has been operated on various feed solutions including whey solution, MBR effluent from a hospital industry, RO brine and produced water to study the fouling tendency of various membranes. The possible concept of critical flux in MD has also been described in this chapter.

The main conclusions of the work and future directions have been highlighted in **chapter 8**. The potential directions for the membrane preparation, fouling and temperature polarization control have been discussed in this chapter.

References

[1] A. I. Stankiewicz and J. A. Moulijn, "Process Intensification: Transforming Chemical Engineering," *Chem. Eng. Prog.*, no. January, pp. 22–34, 2000.

[2] E. Drioli, A. Brunetti, D. Pro, and G. Barbieri, "Process intensi fi cation strategies and membrane engineering," *Green Chem.*, vol. 14, pp. 1561–1572, 2012.

[3] E. Drioli, A. I. Stankiewicz, and F. Macedonio, "Membrane engineering in process intensification — An overview," *J. Memb. Sci.*, vol. 380, pp. 1–8, 2011.

[4] E. Drioli, E. Curcio, G. Di Profio, F. Macedonio, and a. Criscuoli, "Integrating Membrane Contactors Technology and Pressure-Driven Membrane Operations for Seawater Desalination," *Chem. Eng. Res. Des.*, vol. 84, no. 3, pp. 209–220, Mar. 2006.

[5] E. Drioli, A. Criscuoli, and F. Macedonio, *Membrane Based Desalination: An Integrated Approach (MEDINA)*. IWA Publishing, 2010.

[6] B. R. Budel, "Silicone Rubber Vapor Diffusionin Saline Water Distillation," US Patent 285,032,1963.

[7] M. Khayet, "Membranes and theoretical modeling of membrane distillation : A review," *Adv. Colloid Interface Sci.*, vol. 164, no. 1–2, pp. 56–88, 2011.

[8] S. Alobaidani, E. Curcio, F. Macedonio, G. Diprofio, H. Alhinai, and E. Drioli, "Potential of membrane distillation in seawater desalination: Thermal efficiency, sensitivity study and cost estimation," *J. Memb. Sci.*, vol. 323, no. 1, pp. 85–98, Oct. 2008.

[9] F. Macedonio, C. A. Quist-jensen, O. Al-harbi, H. Alromaih, S. A. Al-jlil, F. Al Shabouna, and E. Drioli, "Thermodynamic modeling of brine and its use in membrane crystallizer," *Desalination*, vol. 323, pp. 83–92, 2013.

[10] C. M. Tun and A. M. Groth, "Sustainable integrated membrane contactor process for water reclamation , sodium sulfate salt and energy recovery from industrial ef fl uent," *Dsalination*, vol. 283, pp. 187–192, 2011.

[11] A. El-abbassi, A. Ha, M. Khayet, and M. C. García-payo, "Integrated direct contact membrane distillation for olive mill wastewater treatment," *Desalination*, vol. 323, pp. 31–38, 2013.

[12] E. Drioli, E. Curcio, A. Criscuoli, and G. Di, "Integrated system for recovery of CaCO 3 , NaCl and MgSO 4 · 7H 2 O from nanofiltration retentate," *J. Memb. Sci.*, vol. 239, pp. 27–38, 2004.

[13] S. Goh, J. Zhang, Y. Liu, and A. G. Fane, "Fouling and wetting in membrane distillation (MD) and MD-bioreactor (MDBR) for wastewater reclamation," *DES*, vol. 323, pp. 39–47, 2013.

[14] A. Hausmann, P. Sanciolo, T. Vasiljevic, M. Weeks, K. Schroën, S. Gray, and M. Duke, "Fouling mechanisms of dairy streams during membrane distillation," *J. Memb. Sci.*, vol. 441, pp. 102–111, 2013.

[15] Z. Ding, L. Liu, J. Yu, R. Ma, and Z. Yang, “Concentrating the extract of traditional Chinese medicine by direct contact membrane distillation,” *J. Memb. Sci.*, vol. 310, no. 1–2, pp. 539–549, Mar. 2008.

[16] S. Adham, A. Hussain, J. M. Matar, R. Dores, and A. Janson, “Application of Membrane Distillation for desalting brines from thermal desalination plants,” *Desalination*, vol. 314, pp. 101–108, 2013.

[17] M. Rasool and F. Banat, “Desalination by solar powered membrane distillation systems,” *Desalination*, vol. 308, pp. 186–197, 2013.

CHAPTER 2

Membrane Distillation-an overview

Recently, numerous studies have been carries out with the aim to develop the appropriate membranes for MD, to improve the process understanding, appropriate module fabrication and to confirm the feasibility of the process for several applications. In order to improve the process efficiency, some new configurations have also been investigated. An overview of recent state-of-the-art developments in various aspects of MD has been provided in current chapter.

1. MD configurations

Depending on the methods to induce vapor pressure gradient across the membrane and to collect the transported vapors from the permeate side, MD processes can be classified into four basic configurations (Figure 2.1a). A common feature of all the configurations is the direct exposure of one side of the membrane to the feed solution used. DCMD has been the most studied mode due to its inherent simplicity [1]. On the other hand, vacuum membrane distillation (VMD) can be used for high output while air gap membrane distillation (AGMD) and sweep gas membrane distillation (SGMD) enjoy the benefit of low energy losses and high performance ratio [2][3][4]. Some new configurations with improved energy efficiency, better permeation flux or smaller foot print have been proposed such as material gap membrane distillation (MGMD) [5], multi effect membrane distillation (MEMD) [6], vacuum-multi effect membrane distillation (V-MEMD) [7] and permeate gap membrane distillation (PGMD) shown in Figure 2.1b [8]. A pros and cons analysis of conventional configurations has been provided in Table 2.1.

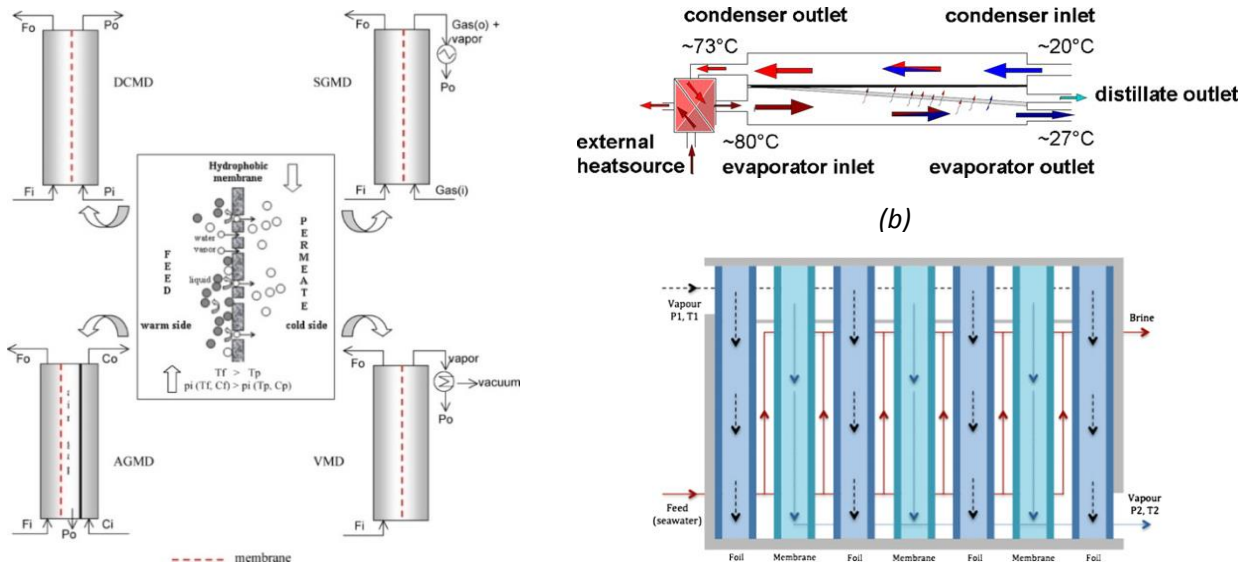

(a) *(b)* *(c)*

Figure 2.1: (a) Conventional MD configurations (b) Module arrangement for PGMD [9] (c) Schematic illustration of streams in V-MEMD module [7].

Table 2.1: Advantages and disadvantages of the four main MD configurations.

Configuration	*Pros*	*Cons*
DCMD	The easiest and simplest configuration to realize practically, flux is more stable than VMD for the feeds with fouling tendency, high gained output ratio [2], it might be the most appropriate configuration for removal of volatile components [4].	Flux obtained is relatively lower than vacuum configurations under the identical thermal conditions, thermal polarization is highest among all the configurations, flux is relatively more sensitive to feed concentration, the permeate quality is sensitive to membrane wetting, suitable mainly for aqueous solutions.
VMD	High flux, can be used for recovery of aroma compounds and related substances, the permeate quality is stable despite of some wetting; no possibility of wetting from distillate side, thermal polarization is very low.	Higher probability of pore wetting, higher fouling, minimum selectivity of volatile components [4], require vacuum pump and external condenser.
AGMD	Relatively high flux than SGMD, low thermal losses, no wetting on permeate side, less fouling tendency.	Air gap provides an additional resistance to vapors, difficult module designing, difficult to model due to the involvement of too many variables, lowest gained output ratio[2].
SGMD	Thermal polarization is lower, no wetting from permeate side, permeate quality independent of membrane wetting.	Additional complexity due to the extra equipment involved, heat recovery is difficult, low flux, pretreatment of sweep gas might be needed.

Recently, Memsys have applied a patented concept of integrating vacuum with multi effects in their module designing for MD. V-MEMD is a modified form of VMD that integrates the concept of state-of-the-art multi effect distillation into the VMD. As a general principle of the process, the vapors produced in each stage are condensed during the subsequent stage. Vapors are generated in steam raiser working under vacuum by exchanging the heat provided by external source. The vapors are condensed by exchanging the heat with feed separated with a foil. The vapors generated in 1st stage are transported through the membrane and collected on the foil in the 2nd stage. The flow of different streams in a single stage has been illustrated in Figure 2.1c. It has been claimed that these modules has excellent gained to output ratio which is crucial parameter for industrial applications [7]. A condenser is used to condense the vapors generated in final stage. The vapor pressure in each stage is less than its preceding stage.

2. Membranes for MD

As briefly discussed in Chapter 1, traditionally the membranes prepared for low pressure membranes processes have been utilized for MD applications. There are several aspects of these membranes that need further improvement for successful application in MD. For example, the thickness of the conventional membranes for MD has been designed for MF/UF requirements. While considering such membranes for MD, on one side, low thickness offers less resistance to the mass transfer, while on the other hand,

membranes with low thickness suffer from more energy losses due to heat flux flowing through conduction across the membranes [10]. In order to address the thickness issue, dual and even triple layer membranes have been introduced [11]. These membranes contain a hydrophobic active layer and a hydrophilic support layer. The support layer provides thermal insulation and ensures the required mechanical robustness of the membrane while the active layer retains the liquid. Care must be taken in selection of thickness of the active layer as too less thickness can allow the passage of the liquid through the pores and may not be sufficient to resist the chemical attack from the feed side during long term operations. According to Laganà et al [12] optimum thickness of active layer is 30-60 um. However, a broad look at thickness effect on MD performance reveals that the literature lacks of clear and conclusive statements. For example, for concentrated salt solutions, Gosteli et al [13] have observed that the performance of thin membrane is more sensitivity towards concentration, however, no further investigations have addressed this issue. Wu et al [14] have demonstrated that the optimal thickness for electro spun PVDF based membrane increases with reduced heat transfer coefficient, decreased feed inlet temperature and increased permeability and salinity level. Contrary to this, Jansen et al [15] have found that conduction losses are directly related with the temperature gradient at the membranes surfaces and inversely related with the membranes thickness.

For what concerns pore size, the utilized porous membranes don't show a single pore size; rather they exhibit a range of pore size distribution (PSD). A membrane with good PSD shows a Guassian distribution curve with a sharp peak and very narrow width. As evident from Table 2.2, the membranes used for UF show quite a broad range of minimum and maximum pore sizes which is somehow acceptable for UF applications. On the other hand, both mean pore size and pore size distributions are crucial for MD process. Although higher flux has been reported for the membranes with bigger pores, yet the large pore dimensions make the membrane vulnerable to wetting. The presence of even a few oversized pores can kill the efficiency of the entire process by allowing the passage of liquid through the pores. Therefore, for pore size, an optimization is required between the stable performance and high flux [16]. The commonly used pore size for MD is in the range of 100 nm to 1um [17]. The sensitivity of process performance towards pore size is different for different configurations of MD. The hydrophobicity of the membrane material and surface tension of the feed solution used will play a decisive role in deciding the pore size. The presence of pores with different dimensions gives rise to the involvement of different mass transport mechanisms in a single membrane [18].

Regarding the membrane material, it has to be hydrophobic to ensure the retention of liquid and the passage of only vapor phase through the membrane pores. PVDF, PP and PTFE are the most commonly used polymeric materials used for membrane preparation for MD applications. Among these, PTFE exhibits the best hydrophobic characteristics, yet the most research on membrane preparation has been carried out by using PVDF membranes due to its easy processability. PTFE is not soluble in any solvents and therefore, poses serious issues with processing. In order to render/improve the hydrophobic character, various techniques have been applied including the coating of different low energy flouro polymers at the membrane surface [19], plasma modification [20], formation of various hierarchical structures [21], incorporation of nano particles into the dope solution during membrane synthesis [22], making the surface rough [23] etc. Surface roughness is an interesting technique to render the super hydrophobicity to the membrane surface; however, its further effects on surface scaling/fouling and thermal polarization still need to be addressed.

Table 2.2: Characteristic features of some state-of-the-art UF membranes mentioned in literature (For details of abbreviation used to describe the membranes, please consult the corresponding reference)

Membrane type	r_{min}*(nm)*	r_{min}*(nm)*	r_{av}*(nm)*	ε*(%)*	*Ref.*
XM 100A	5	12	9	0.75	[24]
XM 300	6	19	12.5	0.3	[24]
Milipre PTSG	1	15	3	7-12	[25]
PVDF	3	4	-	10	[26]
Polyimide UF	1.5	6	-	0.7-0.9	[27]
PCTE 10	134	258	181	6	[28]
PCTE 50	553	821	657	14	[28]
PCTE 100	98 5	1233	113 3	45	[28]
PTHK	16 8	33 6	22 1	34	[28]
YM	6.3	18	11.3	-	[29]
PM30	16.7	62.7	30.6	-	[29]
GVHP	-	-	283.2	70.1	[16]
PVHP	-	-	463.9	71.3	[16]

In addition to the above all parameters, membrane porosity plays a crucial role in dictating the flux. More porous membranes offer more diffusion surface for the vapors and at the same time decrease the thermal conductivity of the membrane as the air trapped inside the pores has conductivity 10 times less than typical polymeric materials used. Overall porosity also dictates the mechanical stability of the membrane. However, it must be highlighted that it is not only the overall porosity that is important for the successful application but also the mechanism of achieving the porosity. The membranes having macro voids usually show very good porosity or void fraction but on the other hand are more prone to the wetting [30]. Related to the porosity is the tortuosity of the pores which indicates the effective length that vapors have to travel to move from feed side to the permeate side. The commonly used value for tortuosity factor is close to 2, though some studies have taken the tortuosity factor as the inverse of porosity [16].

Properties of some commercial membranes used for MD applications have been provided in Table 2.3. Comparison of Table 2.2 and Table 2.3 indicates that the membranes properties required for two applications are very different. The second significant conclusion is that the required MD membrane properties have been incorporates to some extent in some commercial membranes (for example see the r_{av}, r_{min}, r_{max}, and porosity for TF1000, TF450 ,TF200, GVHP), however, the optimization of these features, further ‘’engineering’’ of the membranes and additional improvement in module design can make them further attractive.

Table 2.3: Some features of the commercial membranes used for MD

Membrane type	*Manufacturer*	*Material*	r_{min} *(nm)*	r_{max} *(nm)*	r_{av} *(nm)*	δ *(μm)*	*LEP (bar)*	ε *(%)*	*Ref.*
TF1000	Gelman	PTFE/PP	280	420	325	178	282	80	[18], [127]
TF450	Gelman	PTFE/PP	180	300	235	178	138	80	
TF200	Gelman	PTFE/PP	120	210	155	178	48	80	
PV22	Millipore	PVDF	-	-	220	126	2.29	62	[128]
PTS20	Gore	PTFE/PP	-	-	200	184	4.63	44	
PT45	Gore	PTFE/PP	-	-	450	77	2.88	89	
Accurel® S6/2	AkzoNobel	PP	-	600	200	450	1.4	70	[129]
HVHP	Millipore	PVDF	280	680	451.23		105	33.64	[129]
GVHP	Millipore	PVDF	200	350	265.53		204	32.74	
MD080CO2N	Enka Microdyn	PP	-	-	200	650		70	[18]
Accurel®	Enka A.G	PP		600		400		74	
Celgard X-20	Hoechst Celanese Co	PP	-	70	50	25		35	
EHF270FA-16	Mitsubishi	PE	-	-	100	55		70	

Besides optimizing the features (pore size, pore size distribution, overall porosity etc.), some efforts have also been devoted to engineer the structure of membrane. Wang and Chang [31] have fabricated multi bore PVDF hollow fiber membranes by using especially designed spinneret. The membranes are claimed to have better mechanical strength and provide easy module fabrication. Edwie and Chung [32] have investigated the ‘‘layer effects’’ on performance of MD process. The authors have prepared and compared the performance of single layer PVDF membrane, dual layer hydrophilic/hydrophobic PVDF membrane and dual layer hydrophobic/hydrophilic PVDF/PAN membrane. The most stable performance was achieved by using the single layer membrane with small pore size having cellular morphology.

Thermal induced phase separation (TIPS) is another interesting technique to synthesize the membranes with narrow and controlled pore size distribution. Recently, some investigations have been performed to fabricate and analyze the performance of PP membranes prepared through TIPS. Tang et al [33] have prepared isotactic polypropylene based membranes with narrow pore size distribution by using TIPS. The factors affecting the structure and performance of these membranes were studied. The method seems to be very promising to fabricate the membranes with specific features for MD applications.

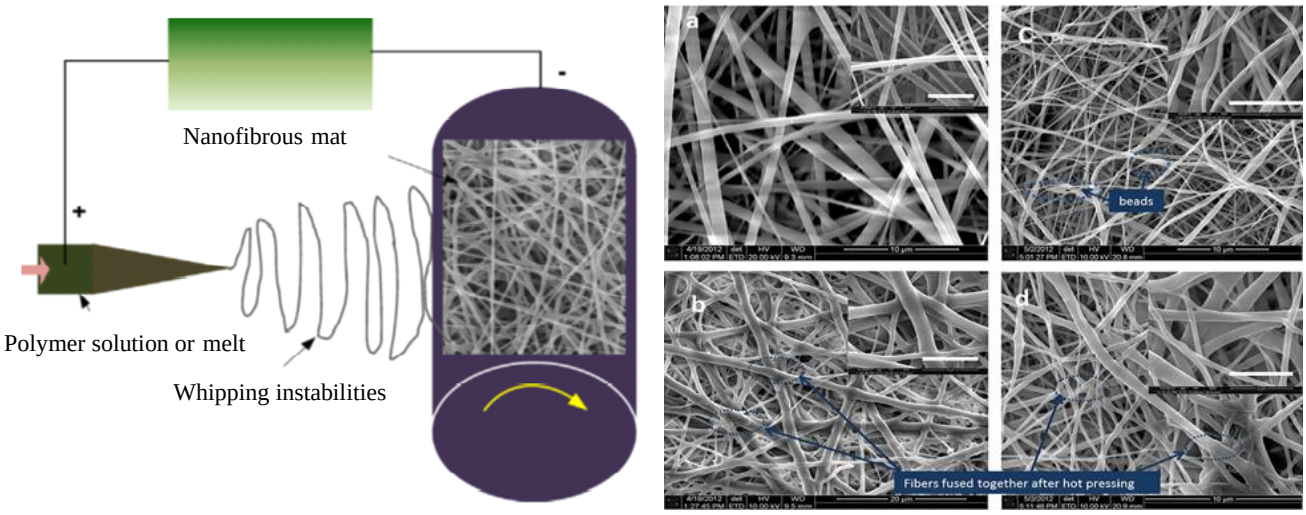

(a) (b)

Figure 2.2: (a) A schematic diagram of the electrospinning process [34] (b) SEM image of electrospun membranes [30]

Recent trends in membrane synthesis process for MD incorporate the use of innovative technologies such as nanotechnology having a significantly potential role in membrane based desalination techniques including MD. For instance, electrospun nano fiber membranes have been reported in many studies recently and have shown very interesting results. In electrospinning process, the fibers are spun under the pressure and electric field applied and form non-woven mat at the grounded rotating collectors (Figure 2.2). The mat formed shows very high porosity, excellent hydrophobicity, very good interconnectivity and very high surface to volume ratio making them interesting candidates for desalination applications. Eletrospinning can be performed with polymer solution or melt and the properties of the mat can be tuned by changing the process parameters, material used and the post treatment step applied [34][35][36]. Due to the possibility to use polymer melt, instead of solution, electrospinning provides opportunities to make the membranes with vast variety of polymers. Different functional materials can be incorporated into the nano fibers during or after their spinning thus incorporating multi functionality into the fibers. Some lab scale applications of electrospun nano fiber membranes have also been reported in recent literature [35][36] [37].

Graphene is an interesting material with several applications due to its very high strength to weight ratio. In addition to its use in various fields (foldable electronics, biological engineering, composite materials, energy storage), the new research has shown that it exhibits amazing selective permeability towards various components. For example, a sub-micron thin graphene oxide membrane can retain all gases and liquids except water molecules [38]. The separation of water from organic mixtures has been demonstrated excellently by these membranes [39]. Similarly, graphene membranes can selectively permeate some metals ions present into a solution containing different types of ions [40]. Graphene membrane with thickness about 1 nm has shown excellent selectivity towards various gases [41]. Due to these facts combined with their high strength, it is possible to tremendously reduce the thickness of the graphene based membranes that can open broad opportunities for these membranes in desalination applications including MD. The applications of graphene membranes in water treatment sections are being tested by different researchers [42], [43], [44].

Biomimic membranes like aquaporin have shown a great potential for desalination applications due to their high permeability and selectivity towards water molecules. Under the right conditions, aquaporin membranes form the water channels allowing the passage of only water molecules and exclusion of all ions. It has been postulated that aquaporin based membranes can achieve a water flux as high as 601 $Lm^{-2}h^{-1}bar^{-1}$ which is an order of magnitude higher than conventional RO process [45]. The commercial application of such membranes for water desalination is however still far away due to insufficient stability of the membranes, difficulties associated with commercial scale production and limited rejection of salts exhibited by the existing membranes [46].

The use of carbon nanotubes (CNTs) in water desalination is also emerging in lab scale investigations. CNTs comprise of rolled up cylinder of graphene with nano scale dimensions. Their exceptional mechanical strength, chemical resistance and thermal properties are well known. As illustrated in Figure 2.3, very high transport of water molecules inside the CNTs and their potential to change the water-membrane interaction to stop the permeation of liquid water molecules while favoring the preferential transport of vapors through the pores have encouraged their incorporation into the membrane matrix [47] [48]. On the other hand, for desalination through MD, CNTs based membranes provide excellent porosity and hydrophobicity. The initial studies to demonstrate the potential of CNTs membranes for desalination through MD have been provided in references [49] and [50]. The application of CNT based membranes in MD has caused considerable increase in flux enhancement for salt solution [48].

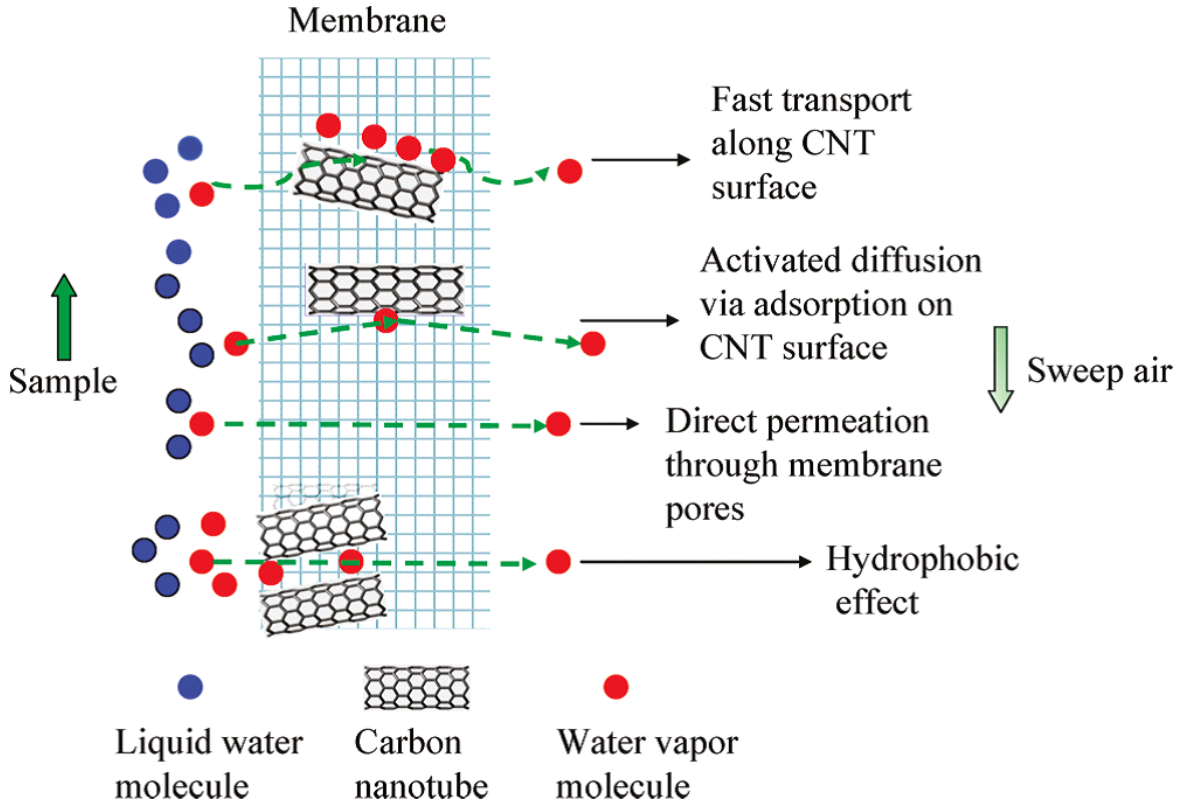

Figure 2.3: MD mechanism for the membranes containing CNTs in their matrix [47]

3. Process understanding and modeling

Numerous recent publications aim to address the understanding of heat and mass transport phenomenon in MD from different perspectives. Like past, the most of the studies are based on theoretical approaches. New

modeling tools and computational software such as CFD, ASPEN, MATLAB etc. have also been introduced to better elucidate the phenomenon. The most published literature discusses the heat and mass transfer in DCMD and VMD with some evolving significance devoted to AGMD. The main challenge is to incorporate quantitatively thermal polarization and concentration affect in heat and mass transport analysis.

In order to overcome the problems associated with the determination of heat transfer coefficients by the conventional approaches, the use of different numerical approaches have been introduced. By applying the heat, mass and momentum balance under the given boundary conditions, the temperature at the membrane surfaces can be predicted. Al-Sharif et al [51] have modeled the effect of three different spacers types on heat and mass transport in DCMD by using open source computational fluid dynamic (CFD) code. Yu et al [52] have investigated local heat flux, membrane surface temperature, thermal polarization and thermal efficiency of DCMD system in counter current configuration. The effect of hollow fiber microstructures on hydrodynamic, thermal polarization and flux for wavy and geared shaped geometries by using CFD analysis has been provided by Yang et al [53]. Manawi et al have developed a predictive model for MD incorporating the effect of various operating parameters including feed and permeate temperatures and flow rates, flow configurations and flow regimes [54]. The membrane has been divided into n control volumes on each hot and cold side, exchanging heat and mass transfer with each other. The experimental results have been claimed in good agreement with the models predictions. Kurdian et al [55] have used mass and energy balance to model the flux behavior of GVHP hydrophobic membranes operating on aqueous solution of sodium chloride and sodium sulphate.

Recently some ambitious attempts have been observed in measuring the membrane surface temperature directly by using different techniques. Tamburini et al [56] have used a technique based on thermochromic liquid crystals and digital image analysis tool to investigate the thermal polarization in spaced filled channels used in MD studies. The hot and cold channels were fabricated between plexi glass chambers and a polycarbonate thin sheet that mimics the membrane. Thermochromic Liquid Crystals was incorporated at the hot feed side adhering with the polycarbonate sheet by using silicon grease. The surface of TLC was illuminated and images were recorded at various experimental conditions for further analysis of temperature distribution along and across the channels by using Matlab image processing toolbox. On the basis of experimental results obtained, a correlation between Nusselt number and *Re* and *Pr* was proposed for the system. Ali et al [57]have used a cell equipped with 16 temperature sensors to measure the temperature profiles on feed and permeate side in DCMD. The effect of different parameters on thermal polarization has been investigated by directly monitoring the bulk and interfacial temperatures. The authors have concluded that heat transfer coefficient can be predicted under certain assumptions by using the relationship predicted by Gryta el al. [58] under certain assumptions.

Various activities can be seen in recent literature to optimize and understand the AGMD process. The effect of removal of air from the membrane pores and feed water deaeration has been discussed by Winter et al. [9]. The air entrapped in the pore and air gap can significantly reduce the mass transfer in AGMD. The use of deaerated water has been claimed to increase the flux and reduce the thermal energy demand. It was further claimed that the additional energy consumed in deaeration can be compensated by the additional product obtained. The concept of directly heating the composite membrane for desalination purposes through AGMD has been introduced in reference [59]. The top surface of the composite membrane can absorb the solar energy while the underneath hydrophobic surface ensures the required non wettability. The important of reducing the pressure in air gap has also been highlighted in the same study. Geng et al [60] have used the energy recovery hollow fiber to directly heat the feed by using the latent heat of vapors condensed at the surface of heat exchanger hollow fiber. Alsaadi et al [61] have used the mathematical equations applied to

explain heat and mas transfer phenomenon in single stage AGMD to develop a one dimensional AGMD model. The model was validated for various operating conditions, process parameters and membrane features. It was also claimed that the model can predict the upscale AGMD installation.

Zhang et al [62] have proposed a new method based on gas permeability data to measure the properties of hollow fiber membranes to be used in modeling of VMD. The modeling predictions agree well with the experimental flux, although the difference diverged at high temperatures. Zuo et al [63] have built and solved a two dimensional model with finite element method for VMD by using hollow fibers. The model incorporates the effect of feed inlet temperature, feed flow rate, fiber length and degree of vacuum applied on temperature, velocity and pressure distribution along and across the fiber. It has been predicted that water production cost through VMD can be reduced to ~38% by using the optimized design and conditions. Similarly, Lee and Kim [64] have proposed a one dimensional model to predict the performance of hollow fibers in VMD by simultaneously solving the energy, mass and momentum conservation equations. Kim [65] has modeled temperature distribution across the feed and permeate channels by using perturbation theory and method of separation of variables.

Lovineh et al [66] have developed a simultaneous heat and mass transport model to predict the effect of operating conditions and membrane characteristics on the performance of VMD process. The authors have concluded the insensitiveness of the process performance towards membrane materials when the pore size is tiny. Shim et al [108] have proposed a one-dimensional model to predict the performance of multi vacuum membrane distillation modules connected with each other's. The optimum number of modules connected in series was calculated on the basis of variation in hydraulic pressure and feed temperature.

4. Module designing for MD

After the availability of appropriate membranes for any application, the next most important step is to assemble these membranes in a particular configuration to ensure the required membrane area enclosed in a particular module volume. In addition to provide compactness, an appropriate module design can reduce the thermal/concentration polarization, fouling and energy consumption of the process. These advantages can be realized by disturbing the normal flow pattern that develops along the fiber. Adequate module design can improve the hydrodynamic on shell and lumen side, thus imparting a positive impact on the process. In this context, the module designing provides an economical alternative of the active techniques to change the hydrodynamic conditions in the membrane. Despite of these benefits, the investigations on module design are limited in number generally for membrane operations and particularly for MD.

Similar to the other membrane based processes, module design for MD is crucial to use the process more rationally. An appropriate module design for MD applications should take into consideration the minimization of thermal polarization on up and down stream, appropriate packing density to ensure the module compactness, robustness, achievement of high energy efficiency, suitable length, high volume based enhancement factor and relatively easy fabrication with the flexibility to apply for the maximum configurations. In addition, the material implied for module fabrication must ensure the minimum thermal losses and must be heat resistance. There are several different industrial sectors looking at MD with different demands that further underline the importance of flexibility in module design. In MD, several possibilities have been considered to design an appropriate module:

- Use of appropriate flow scheme to maximize the temperature gradient along the membrane (counter flow, cross flow, concurrent)

- Use of baffles and spacers (Figure 2.4) to homogenize the temperature distribution within a stream
- Use of different fiber geometries to ensure the uniform heat distribution within the module
- Use of heat recovery devices

He et al [67] have provided the concept of heat recovery by interstate heating of the cold feed by using the permeate of previous stage in a cascade of modules. A schematic of the concept used by the author has been shown in Figure 2.5. The authors have provided a theoretical analysis of countercurrent cascade of cross flow DCMD modules. Such cascades can be useful in improving the recovery and energy efficiency of the system. The authors have claimed a recovery of 60% and gain output ratio of more than 60% for appropriate configurations and temperature difference. Yang et al [68] have investigated the effect of various fiber geometries (Figure 2.6) on performance of DCMD both experimentally and theoretically. The flux enhancement as high as 300% has been claimed due to reduced thermal boundary layer resistance. Experimental and theoretical feasibility of roughened surface for DCMD process has been demonstrated by Ho et al [69].

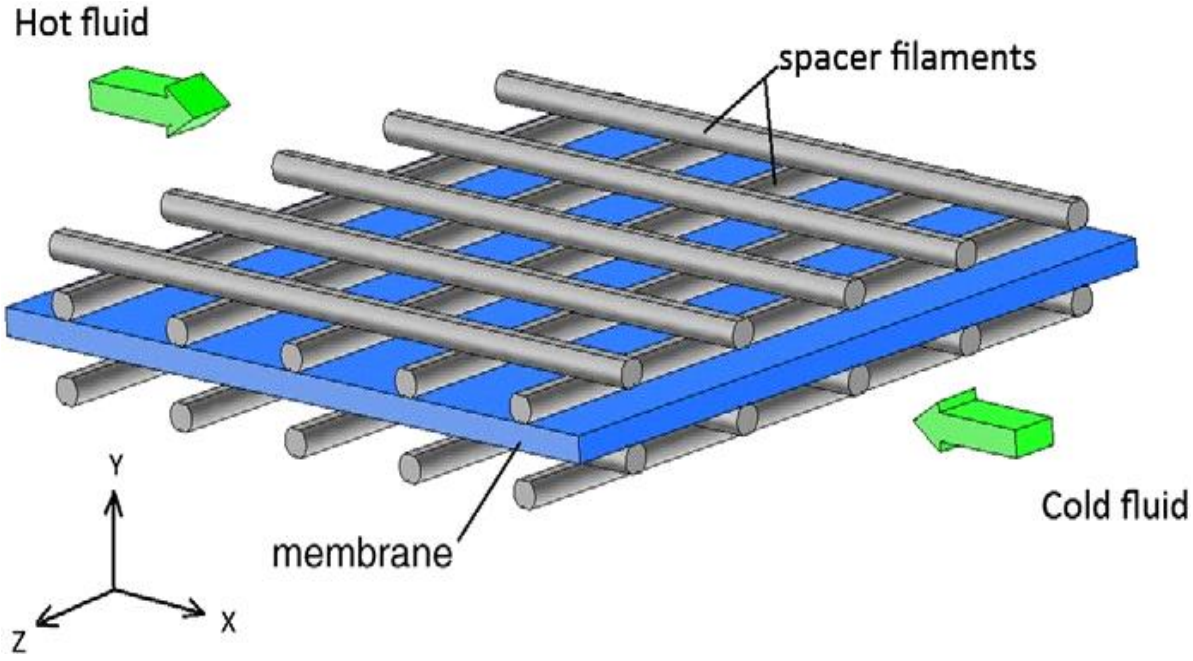

Figure 2.4: Space filled channels used to improve the hydrodynamic conditions at the membrane surface in MD [70]

Rotational and tangential to the membrane surface flow has been proven very affective in increasing the performance of the AGMD [71]. Such flow combined with the partial contact of membrane with condensing surface in AGMD has caused synergetic effects. The authors have claimed the permeate flux as high as 119 $kg/m^2.h$ at feed inlet temperature of 77^oC. The claimed flux is ~2.5 times higher than the flow observed in traditional AGMD studies carried out under the identical conditions. The authors have associated the improvement with improved heat and mass transfer due to the specific flow patter generated and due to the contact of membrane with the cooling plate. AGMD module designing involves bulky modules in order to incorporate the air gap, condensing plate and cooling channel. In their proposed configuration as illustrated

in Figure 2.7, Singh and Sirkar [72] have introduced porous and non-porous hollow fibers in the same lab scale modules to compact the module volume. The vapors from hot feed passing through the porous fibers are condensed at the outer wall of non-porous fiber which has been cooled by the circulation of a cold fluid inside the fiber. On the similar lines, Geng et al [73] have designed a module with the heat exchanging hollow fibers that collect the latent heat of vapors and transfer to the cold feed. The authors have claimed a thermal efficiency of 80% or higher in all the studied cases.

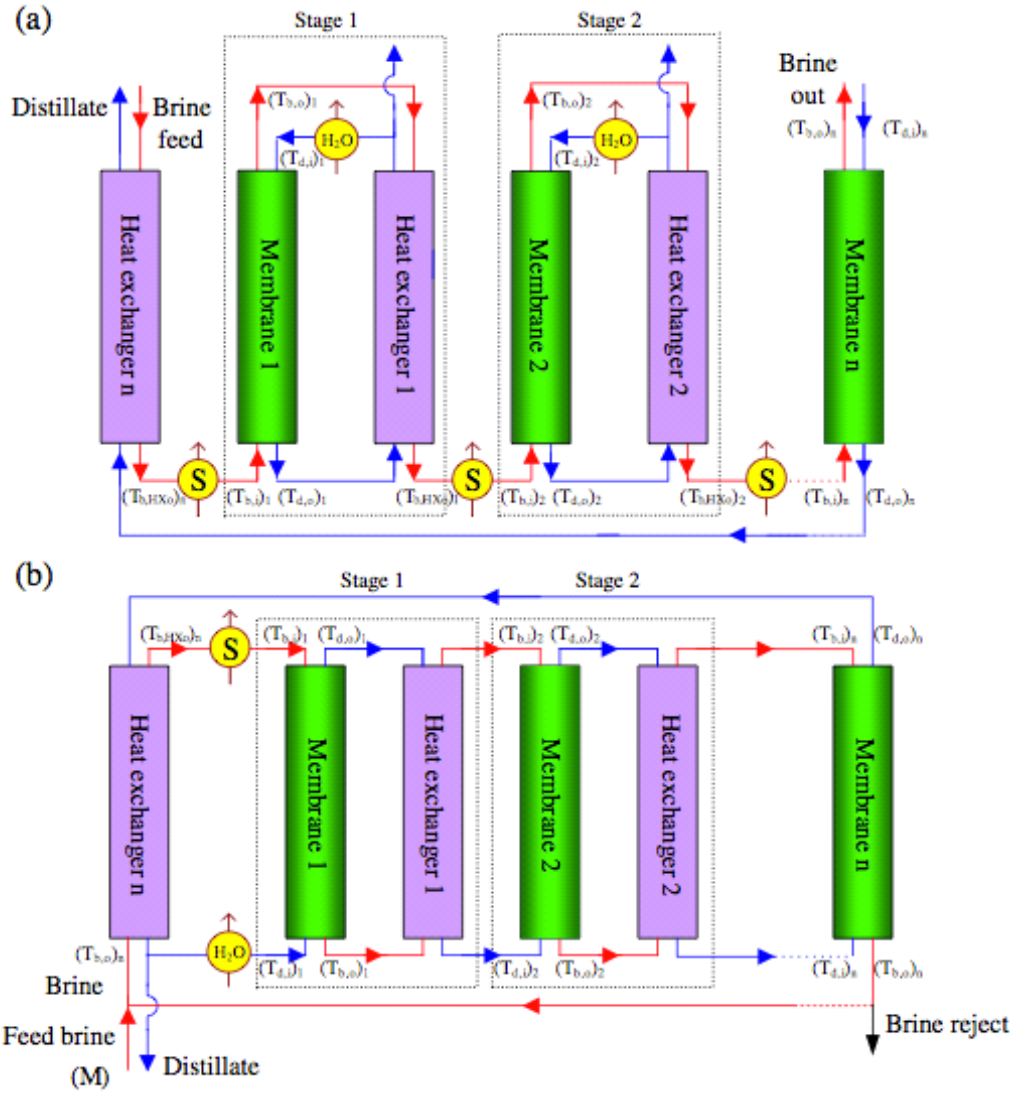

Figure 2.5: Cascade module design used by He et al. [67]

Zhao et al [8] have explored the performance of a V-MEMD module introduced by Memsys under solar and diesel heating arrangements. The authors have identified the number of stages and the size of each stage as the key parameter for optimizing the module performance for large scale applications. The module efficiency is mainly controlled by the hot and cooling fluid temperatures. Form optimization results, it was concluded that the module has a very attractive gain output ratio. Zhang et al [74] have explored the effect of fiber packing density and module length on their performance in VMD. The initial flux decay under constant operating conditions was attributed to the membrane compression that took place due to the hydraulic pressure. The shorter modules with compact packing have been recommended by the authors for a high yield per unit module volume. The authors have also pointed out that increase in flux at high feed flow rate is due

to increased average temperature instead of enhanced thermal polarization coefficient. The effect of liquid distributor on the performance of VMD process has been investigated theoretically by Wang et al [75]. The authors have claimed that the appropriate design of distributor plays a significant role in optimizing the performance of VMD process. The liquid distribution in dome-like and pyramidal distributor was better than plate-like distributor.

Figure 2.6: Various hollow fiber configurations used by Yang et al [68]

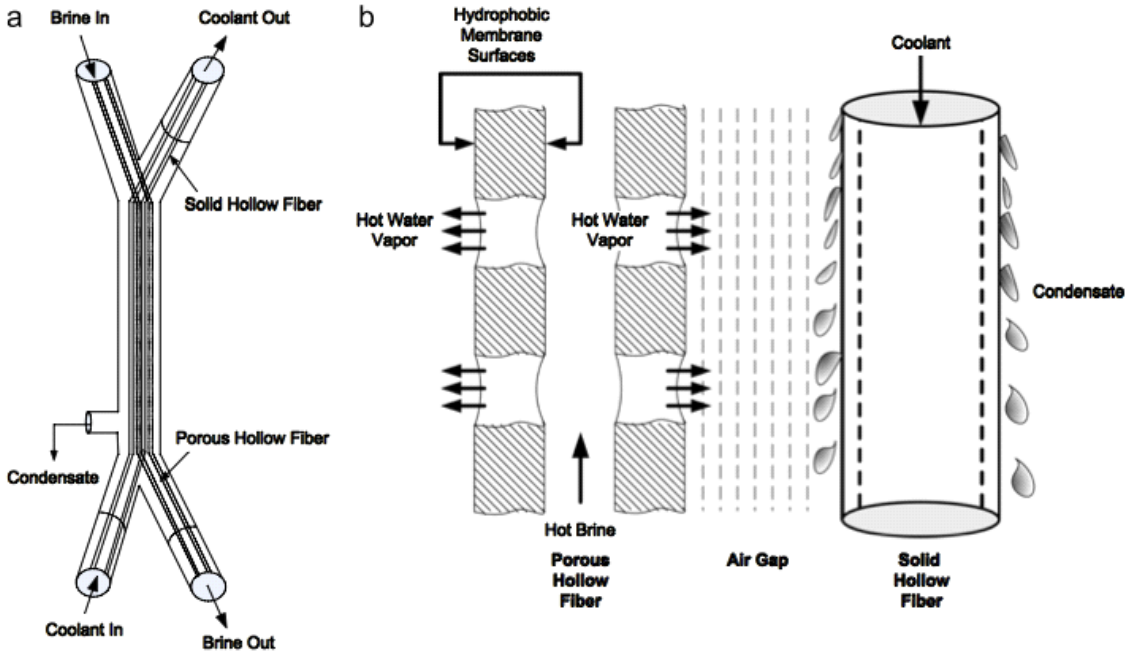

Figure 2.7: Conceptual mechanism of hollow and heat recovery fibers reported by Singh and Sirkar [72]

5. Fouling in MD

As discussed in Chapter 1, the fouling in MD differs in nature from low pressure membrane processes. A summary of various types of fouling observed in MD has been provided in Table 2.4. The salt solutions such as brine mainly induce surface scaling and pore wetting and precipitation inside the pores in certain cases. Fouling and wetting caused by organics and macromolecules such as protein has been observed in other

studies [76] [77]. Protein-type macromolecules have special tendency to adsorb at the membrane surface. The initial fouling layer in such cases can be associated with the adsorption of molecules at the hydrophobic surface. Once built, such layer will tend to accumulate more solute molecules at the membrane surface and ultimately, a thick cake layer can establish under high convective flux conditions. The initial adsorption at the membrane surface followed by the further buildup of fouling cake layer can decrease the flux due to increase in net resistance to heat and mass transfer [78].

In addition to the typical fouling, some other parameters also affect the MD performance. The mass transfer rate across microporous hydrophobic membrane in MD is driven by the temperature gradient across the membrane surfaces. The heat losses attributed to the conduction through the membrane and convection associated with the vapor transport reduce the surface temperature at the feed side and increase the corresponding temperature at the permeate side, thus inducing the thermal polarization at both sides. The effect of temperature polarization on flux reduction in membrane distillation has been well acknowledged in several studies [79] [80] [81]. For a well-designed system, the value of thermal polarization coefficient has been indicated in the range of 0.4 to 0.7 [79].

The scale formation at the membrane surface has been observed in the studies addressing the MD applied to solutions containing salts. Gryta [82] has investigated the membrane distillation performance in treating the spent solution from heparin production. The rapid flux declined was reported due to the fouling and scaling. The presence of salts deposits on distillate side confirms the occurrence of wetting as well. The removal of foulants by boiling the feed followed by the separation of the deposits was found to be an affective pretreatment to reduce the fouling during the membrane distillation process. The problem of scale formation at the distribution channel of the membrane modules and at the membrane surface was observed in a study conducted by Kullab and Martin [83] for production of water for cogeneration power plants. The permeate quality and the operation stability was dependent upon the nature of the feedstock. Ca and Mg were identified as the main scale forming salts. In another study, Gryta [84] has analyzed the performance of MD against several different types of feed solutions including brine, bilge water and water containing protein. The strength and nature of fouling was dependent upon the feed and operating conditions used. The formation of Ca and protein based deposits on the membrane surface was detected. The scale formation in MD was pointed out as one of the major responsible factors for wetting, flux reduction and damage to the membrane structure. The formation of porous deposits decreases the flux by lowering the heat transferred to the membrane surface while the non-porous deposits increase the resistance to the mass transfer. The scaling occurred at membrane surface and in distribution channels observed in various studies has been shown in Figure 2.8.

More recently, some further focus has been devoted for deeper understanding of scaling in MD process. Burrieza et al [85] have studied the effect of intermittent MD operation at the surface scaling. The intermittent operation has been simulated by exposing the PTFE and PVDF membranes to wet/dry cycles. A decrease in contact angle and scaling inside the pores was observed. The scaling inside the pores was more prominent for PVDF based membranes due to their low contact angle. The scaling reduced the surface roughness and promoted the calcium carbonate adhesion with the surface. The effect of coating on surface scaling of heat exchanger has been investigated by Al-Janabi et al [86]. The authors have developed and applied various coating at the surface of heat exchanger to be used in MD to minimize the surface energy and to impart anti scaling properties. The electron donor coating materials have shown the best performance. Ge et al [87] have investigated the surface scaling and wetting behavior of PVDF membrane under different operating conditions. The authors have observed that scaling and wetting increases with temperature. Chen et al [88] have demonstrated the efficacy of gas bubbling in controlling the surface scaling in DCMD process.

A significant increase in flux and delayed flux decline was observed under the gas bubbling conditions. Similarly, the use of polyphosphate has been proven effective in decreasing the $CaCO_3$ scaling at membrane surface in another study [89].

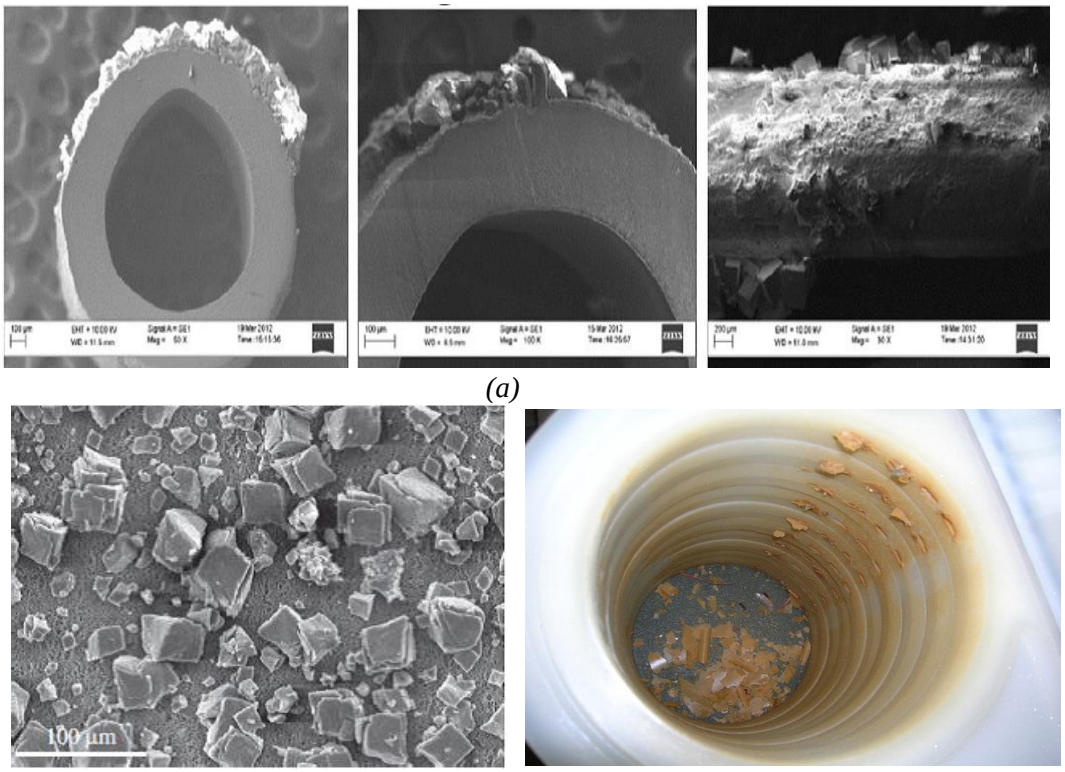

(a)

(b) *(c)*

Figure 2.8: Scale formation observed at the membrane surfaces and in distribution channels (a, b and c respectively, taken from [139], [140], [137]).

Table 2.4: Different types of fouling observed in MD studies

Feed type	*Membrane used*	*Type of fouling observed*	*Reference*
Wastewater from heparin production	PP capillary membranes	Wetting, deposition, scaling, biofouling	[82]
NaCl solution	Accurel PP S6/2 membrane	Wetting, surface scaling	[90]
Synthetic wastewater	PVDF flat sheet MILLIPORE® Durapore GVHP)	Wetting, thick layer of biofouling	[91]
Bilge water, saline water from meat processing industry, tap water	Accurel S6/2 PP, Membrana, Germany	Deposit layer formation at the surface, bio fouling, surface and internal crystallization	[84]
Skim milk and whey solution	PTFE flat sheet membranes with woven PP support, GE Osmonics, Minneapolis, MN, USA	Layer of deposits at the membrane surface	[92]
Municipal water and flu gas condensate	PTFE flat sheet, SCARAB AB.	Scale formation at the membrane surface	[83]

Due to the emerging use of MD process in membrane bio reactors, the importance of understanding and control of bio fouling in MD has gained more focus. Goh et al [76] have highlighted the importance of bio processes in controlling the membrane wetting of MD present at downstream. The authors have shown that biofouling formed at the membrane surface does not only cause membrane wetting but can also increase the resistance to heat and mass transfer. MD integrated at downstream of bioreactor is less prone to wetting and fouling due to removal of nutrient in the bioreactor. The effect of sludge hydrophilicity on biofouling and transport characteristics in membrane has been studied by Goh et al [93]. The microporous structure of the biofilm has been held responsible for vapor pressure depression and further addition of resistance to heat and mass transport. The membrane with high thermal resistance and a hydrophilic layer facing to the feed can mitigate the vapor pressure reduction. A detailed understanding of fouling of dairy products on hydrophobic membranes applied in MD can be found in work by Hausmann [77][92] (Figure 2.9).

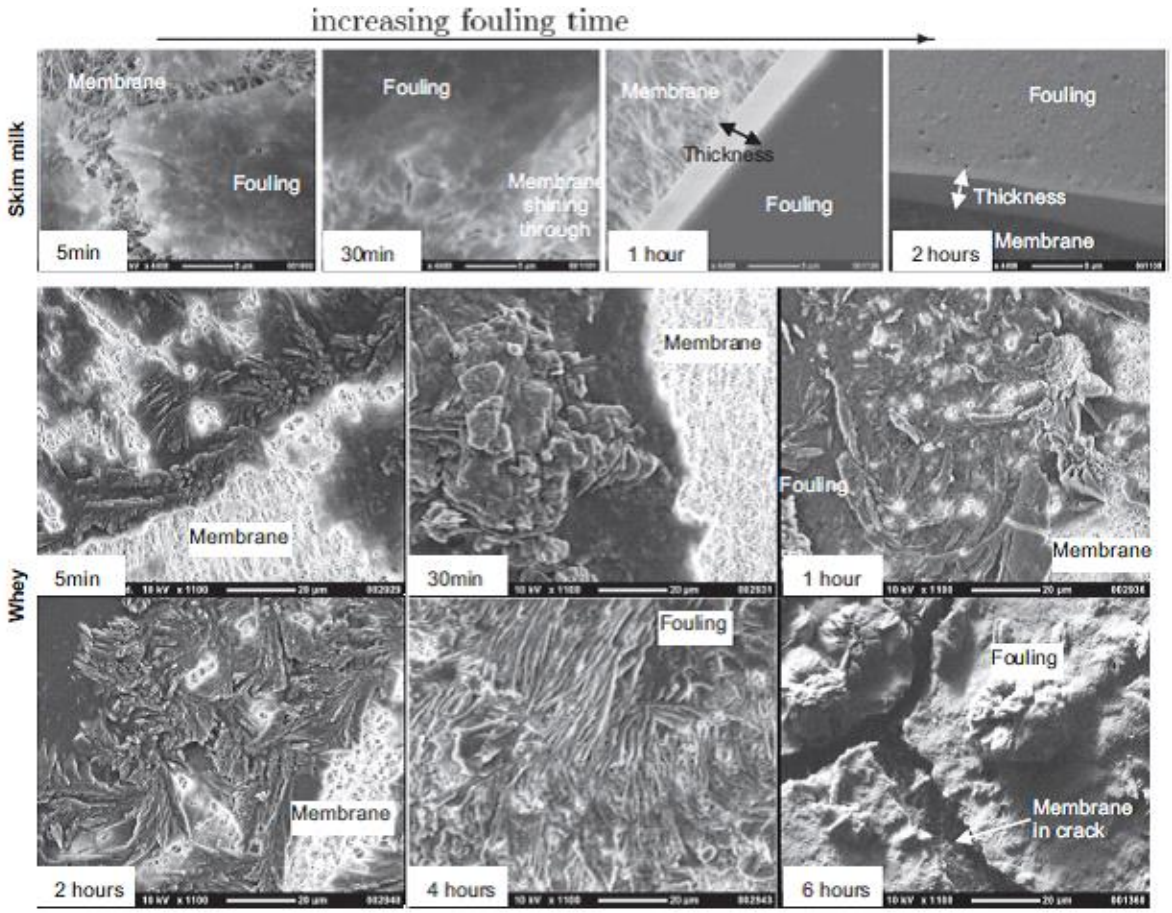

Figure 2.9: Fouling caused by skim milk (top) and whey solution (bottom) as function of time [77]

Recently, Gilron et al [94] have investigated the effect of silica scaling and membrane pore wetting on MD process. In case of partial wetting, it has been shown by the authors that the temperature at the pore mouth can be significantly less than that at the membrane surface and can decrease the temperature polarization coefficient. For a given feed and membrane combination, the wetting can be controlled by selecting the appropriate conditions of temperature and flow rate (hydraulic pressure). More comprehensively, feed temperature, feed composition, pore size and hydrophobic character of the membrane combined with the hydraulic pressure applied at the membrane surface will dictate the wetting phenomenon in MD.

6. Innovative and large scale applications

In addition to the traditional membrane based processes, new interesting applications of MD have been tried recently. MD has potential for temperature sensitive products such as pharmaceutical compounds, juices, dairy products, natural aromatic compounds and solutions of several chemicals. The process can be applied in the fields where a very high rejection of certain nonvolatile component is required such as the treatment of nuclear waste or radioactive water and water for semiconductor industry. In oil and gas sector, shale gas has been identified as the game changer due to its abundant availability in various regions across the world [95]. However, the detrimental environment impacts of shale gas exploration are big hindrance in its wide spread adaptation. The fracturing or produced water is one of the major causes responsible for the hazardous environmental impact of exploring shale gas. Produced water contains very high level of salts, various hydrocarbons and production chemicals. Treatment of such complex steam through state-of-the-practice processes is really challenging [96]. Moreover, high pressure and temperature of the produced water during

the production process provides additional complexity for its immediate treatment. MD has proven a feasible candidate for the treatment of this water after certain physical processes that remove hydrocarbons from the stream [30]. Similarly traditional MBRs suffer from the major fouling issues. MD as standalone process or in integration with some other processes (such as FO) has provided very interesting results [97]. Likewise the removal of heavy metals that acts as a micropollutant is challenging for existing RO plants. For example, due to its existence as boric acid under normal pH conditions, the boron can diffuse through the RO membrane and thus traditional RO cannot meet the required removal criteria (0.5-2.5 ppm). The current alternative techniques are either costly or not robust as the operating conditions change. MD has been applied successfully to remove the boron well below the set limits. Similarly, the removal of chromium has been successfully achieved to the desired level by using MD.

Another potentially interesting field for MD is the recovery/removal of phosphorous from agricultural, household and industrial runoffs. The presence of phosphorous in soil is essential for growth of crops. On the other hand, the access of phosphorous gives rise to the condition known as eutrophication, characterized by the excessive growth of algae inside the water thus reducing the oxygen level and causing an adverse effect on marine life. As the phosphorous reservoirs are limited, MD as standalone process or in integration with other membrane based processes can be utilized not only to control the level of phosphorous in water runoffs but also to recover phosphorous crystals from the phosphorous rich-streams [98]. Similarly, during protein crystallization and crystallization of pharmaceutical compounds via membrane crystallization, the level and rate of supersaturation can be finely tuned and membrane surface creates heterogeneous nucleation providing the opportunity to selectively crystalize various polymorphs [99]. Similarly, the recovery of various valuable components from waste streams and RO brine has been reported in several studies [100] [101] [102].The crystals recovered through MD process show better quality in terms of crystal size, crystal size distribution, coefficient of variance and nucleation kinetics. A list of innovative and potential uses of MD for various applications mentioned in the recent literature has been provided in Table 2.5.

Besides the lab scale applications, various activities can be seen at the commercial scales too. Jensen et al [15] have demonstrated the potential of membrane distillation modules at large scales for desalination purposes. The authors have used a total membrane area of 300m^2 and have observed no problem of scaling or biofouling over a period of 4-14 months. Burrieza et al [103] have compared the performance of two pilot scale AGMD modules over a period of two years for NaCl solution of 1 and 35 g/L. The modules have produced excellent and constant quality distillate throughout the process. On the similar lines, Raluy et al [104] have compiled the 5 years' experience and data analysis of a solar collector MD unit installed in Instituto Tecnológico de Canarias (ITC) in Playa de Pozo Izquierdo (Gran Canary Island-Spain). The authors have reported a specific thermal energy consumption in the range of 140–350 kWh/m^3 while the distillate quality was very good (20-200 µs/cm). Asadi et al [105] have demonstrated desalination of deoiled stream coming from the oil refinery by using a MD module with an area of 40 m^2. The water produced fulfills the loca irrigation standards.

Table 2.5: Applications of MD mentioned in different recent studies

Feed	*Target*	*Membranes used*	*Configuration*	*Ref*
Seawater	Boron removal	PVDF	DCMD	[106]
Simulated water	Chromium removal	PTFE	DCMD	[107]
Produced water	Desalination	PTFE	DCMD	[108]
Aqueous solution of N-methyl-2-pyrrolidone	concentration of N-methyl-2-pyrrolidone solution	PP	VMD	[109]
Cooling tower blow down water	Desalination	FS PP	DCMD	[110]
Aqueous ammonia solution	Removal of Ammonia	PVDF capillary	DCMD and MDCMD	[111]
Olive oil waste mill water	Concetration of phenolic compounds	FS PTEF	DCMD	[97]
Produced water	Desalination	FS PTFE	AGMD	[112]
Model lactose solution	Ethanol production	PP capillary membrane	DCMD	[113]
Synthetic solution of trace OC	Removal of complex trace organic compounds	FS PTFE	DCMD	[114]
Aqueous H_2SO_4 solution	Concentration of H_2SO_4 solution	PP hollow fiber	Multi effect MD	[115]
Retentate of NF and RO	Improvement of water RF and salt crystallization	PVDF hollow fibers	DCMD	[116]
Water from great salty lake	Recovery of minerals	FS PTFE and PP	DCMD	[117]
Zabłocka Thermal Brine	Brine concentration	PP hollow fiber Accrual	DCMD	[118]
Glycerol fermentation broth	Separation of acetic acid from the broth	Acuurel PP hollow fiber	DCMD	[119]
Synthetic radioactive wastewater	Removal of radioactive elements	Hydrophobic ally modified FS PS or PES	DCMD	[120]
Wastewater containing arsenic in different concentrations	Removal of arsenic	PP and FS PVDF	VMD	[121]
Dilute glycerol wastewater	Concentration of glycerol	FS PTFE	SGMD	[122]
Ethanol-water mixture	Ethanol separation	FS PTFE	SGMD	[123]

7. Recent commercial activities

The slow progress of membrane distillation has been related with the unavailability of appropriate membranes for MD applications, high energy consumption with respect to RO that boost the overall energy demand, membrane wetting, low flux and limited investigations carried out on module designing. However, thanks to the recent and growing extensive research activities carried out in various areas of MD, the process has become much more attractive due to the availability of better membranes, possibility to utilize alternative energy sources and uncertainty about the sustainability of fossil fuel. Furthermore, new rigorous separation requirements driven by the new regulations and needs have further highlighted the importance of the field. As a result, a ‘’research boom’’ has been observed in various aspects of MD since last one decade or so. Recently, some companies have been involved in commercialization efforts for MD (Table 2.6). Aquaver Company is an example that has recently commissioned the world’s first seawater MD based desalination plant in Maldives. The plant uses the waste grade heat available from a local power plant and has the capacity of 10,000L/day (http://www.aquaver.com).

Table 2.6: Main companies involved in commercialization efforts for MD

Membrane Trade Name/ Manufacturer	*Material*	*Application*	*Web address*
Fraunhofer Institute for Solar Energy Systems (ISE)			Fraunhofer Institute for Solar Energy Systems (ISE), Heidenhofstr.2, D 79110 Freiburg, Germany
OEM GE Nylon - Hydrophobic Membranes	Hydrophobic Nylon supported on an inert polyester web.	-Bag vents -Bioreactor venting applications -CO_2 monitors -Fermentation air applications -Filtering gasses to remove particulate -Insufflation filters -Lyophilizer venting or inlet air	
Donaldson Company Inc., Microelectronics Group	PTFE		e-mail: LeuvenRD@mail.donaldson.com Tetratec-Europe@mail.donaldson.com Website: www.donaldson.com
Liqui-Cel®		Degasification and deaeration	http://www.liqui-cel.com/
TNO			info-beno@tno.nl
Scarab Development		Development of Technology	

AB		for Water Purification, Solar Power, Poly-Generation, Recycling and Sustainable Systems	
S6/2 MD020CP2N/ AkzoNobel Microdyn	PP	Water and wastewater treatment, food and pharmaceutical industry.	e-mail: sales@microdyn-nadir.de Web site: www.microdyn-nadir.de
Membranes from PP (Membrana GmbH, Germany) with microfiltration properties.	PP,PE, PES	Generally for gas-liquid contactors	info@membrana.de http://www.membrana.com
Pall-Microza PVDF fibres	PVDF	VMD for water desalination.	http://www.pall.com/microe.asp
Celgard Inc. – Membrana Underlining Performance Industrial Separations (a Division of Celgard)		Membrane contactors SuperPhobic® e Liquicel®	Jschneid@celgard.net www.liquicell.com www.membrane.com
Memsys/MemDist module	PP	-Desalination -Wastewater treatment -Process water (Semi conductor , Boiler feed water, Food & beverage) -Aircon – desiccant cooling -Process engineering (Alcohol destillation) -Cooling towers	
Aquaver	PTFE	Seawater desalination Cogeneration Brine treatment Landfill leachate Industrial wastewater Difficult-to-treat waters	Aquaver info@aquaver.com
Aquastill			http://www.aquastill.nl/index.html

SolarSpring		Drinking water Process and industry Research	E-mail: contact@solarspring.de www.solarspring.de

Starting from the first article by Bodell in 1963, substantial growth in the field has been observed over time. The progress and advancements have been reviewed in different review articles [17][124][99][125][18][79]. The number of scientists and researchers working on MD has increased tremendously in the recent years and a lot of research articles are coming out each year. Advent of commercialization era for the process has also contributed significantly in fueling the research in MD. DCMD is still dominant field for recent research, despite the fact that most commercializing companies are adopting VMD or AGMD for their plants.

From the first MD patent in 1963, additional 12 more have been registered till the end of 2011, as documented by Drioli et al [126]. The total number of patents shows slow progress of MD. Nevertheless, the research momentum gained by the technology can be realized by the 8 patents published during 2013 and 2014. These patents cover membrane preparation methods, application of MD in integration with other processes to achieve complex separations, module designing, configurational modifications to improve process efficiency, oleophobic membranes, use of the process in steam production etc. A list of the patents published recently has been provided in Table 2.7.

Table 2.7: Recent patents in MD

Patent	*Inventor/s*	*Remarks*
Combined membrane-distillation-forward-osmosis systems and methods of use Publication number: US 8029671 B2 Publication date: Oct 4, 2011	T. Y. Cath, A.E. Childress, C.R. Martinetti	Embodiments of the present disclosure provide combined membrane-distillation/forward-osmosis systems and methods for purifying a liquid, such as reducing its solute or suspended solids load.
Membrane Distillation Apparatus and Methods Publication number: US 20110272354 A1 Publication date: Nov 10, 2011	S. Mitra, K. Gethard	Methods based on MD for solvent removal, sample preconcentration and desalination employing hollow fiber porous hydrophobic membranes with carbon nanotubes are disclosed
Composite membranes for membrane distillation and related methods of manufacture. Publication number: WO 2012100318 A1 Publication date: Aug 2, 2012 Applicant: Membrane Distillation Desalination Ltd. Co.	M. Khayet, T. Matsuura, M. R. Qtaishat	The present invention provides composite membranes for membrane distillation and related methods of manufacture.
MEMBRANE AND METHOD PRODUCING THE SAME Publication number:	M. M. TEOH, N. PENG, T.-S. Chung	The present disclosure relates to a membrane comprising a porous polymer body with a plurality of channels extending through the

US20120285882 A1 Publication date: Nov 15, 2012		polymer body, a method of producing the same and a water treatment system comprising the membrane
Forward osmotic desalination device using membrane distillation method Publication number: US 20130112603 A1 Publication date: May 9, 2013	S. M. Koo, S. Jin Lee, S. M. Shim	The present invention relates to a fresh water separator using a membrane distillation method and a forward osmotic desalination device comprising the fresh water separator
Solar membrane distillation system and method of use Publication number: US 8,460,551 B2 Publication date: Jun. 11, 2013	I. A. Al-Arifi, H.T.A. El-Dessouky	The invention relates to distillation systems and, more particularly, to a solar driven membrane distillation system and method of use.
Forward osmosis system comprising solvent separation by means of membrane distillation Publication number: US 20130264260 A1 Publication date: Oct 10, 2013	W. Heinzl	The invention relates to a system for separating a product contained as solvent in a solution to be processed, comprising at least one forward osmosis device through which the solution to be processed and a draw solution flow, and a device connected downstream thereof for obtaining the product.
Polyazole membrane for water purification Publication number: EPA 13155093.1 Publication date: 14.08.2013	P.S. Nunes, H. Maab, L. Francis	The method describes a membrane prepared for fluid purification comprising a polyazole polymer.
Method of converting thermal energy into mechanical energy, and an apparatus therefor Publication number: US 20140014583 A1 Publication date: Jan 16, 2014	J. H. Hanemaaijer	The invention relates to a method of converting thermal energy into mechanical energy wherein a working liquid such as is evaporated to generate a stream of a working fluid
Membrane distillation apparatus Publication number: US 20140138299 A1 Publication date: May 22, 2014	P. Nijskens, B. Kregersman, S. Puttemans, C. Dotremont, B. Cools	The present invention relates to membrane distillation apparatus and is more particularly, although not exclusively, concerned with the production of desalinated water from seawater
Membrane distillation modules using oleophobically and antimicrobially treated microporous membranes Publication number: US 20130068689 A1	V. Bansal, C. Keller	The present invention provides a system for liquid distillation which includes a vapor permeable-liquid impermeable microporous membrane having structures defining a plurality of

Publication date: Mar 21, 2013		pores, an oleophobic material that is applied to the structures of the vapor permeable-liquid impermeable microporous membrane
Membrane Distillation Device Publication number: 20140216916 Publication date: 2014-08-07	W. Heinzl	The invention describes a method to improve the efficiency of MD process by using the latent heat of condensation of the vapors to heat the feed during various stages.

References

[1] E. Drioli, A. Criscuoli, and E. Curcio, *Membrane contactors: fundamentals, applications and potentialities*, Membr. Sci. Elsevier, Amsterdam; Boston, 2006.

[2] E. K. Summers, H. a. Arafat, and J. H. Lienhard, "Energy efficiency comparison of single-stage membrane distillation (MD) desalination cycles in different configurations," *Desalination*, vol. 290, pp. 54–66, Mar. 2012.

[3] S. Cerneaux, I. Strużyńska, W. M. Kujawski, M. Persin, and A. Larbot, "Comparison of various membrane distillation methods for desalination using hydrophobic ceramic membranes," *J. Memb. Sci.*, vol. 337, no. 1–2, pp. 55–60, Jul. 2009.

[4] Z. Ding, L. Liu, Z. Li, R. Ma, and Z. Yang, "Experimental study of ammonia removal from water by membrane distillation (MD): The comparison of three configurations," *J. Memb. Sci.*, vol. 286, no. 1–2, pp. 93–103, Dec. 2006.

[5] L. Francis, N. Ghaffour, A. A. Alsaadi, and G. L. Amy, "Material gap membrane distillation : A new design for water vapor fl ux enhancement," *J. Memb. Sci.*, vol. 448, pp. 240–247, 2013.

[6] R. Liu, Y. Qin, X. Li, and L. Liu, "Concentrating aqueous hydrochloric acid by multiple-effect membrane distillation," *Front. Chem. Sci. Eng.*, vol. 6, no. 3, pp. 311–321, Jul. 2012.

[7] K. Zhao, W. Heinzl, M. Wenzel, S. Büttner, F. Bollen, G. Lange, S. Heinzl, and N. Sarda, "Experimental study of the memsys vacuum-multi-effect- membrane-distillation (V-MEMD) module," *Desalination*, vol. 323, pp. 150–160, 2013.

[8] K. Zhao, W. Heinzl, M. Wenzel, S. Büttner, F. Bollen, G. Lange, S. Heinzl, and N. Sarda, "Experimental study of the memsys vacuum-multi-effect-membrane-distillation (V-MEMD) module," *Desalination*, vol. 323, pp. 150–160, Aug. 2013.

[9] D. Winter, J. Koschikowski, and S. Ripperger, "Desalination using membrane distillation : Flux enhancement by feed water deaeration on spiral-wound modules," *J. Memb. Sci.*, vol. 423–424, pp. 215–224, 2012.

[10] S. Alobaidani, E. Curcio, F. Macedonio, G. Diprofio, H. Alhinai, and E. Drioli, "Potential of membrane distillation in seawater desalination: Thermal efficiency, sensitivity study and cost estimation," *J. Memb. Sci.*, vol. 323, no. 1, pp. 85–98, Oct. 2008.

[11] S. Bonyadi and T. S. Chung, “Flux enhancement in membrane distillation by fabrication of dual layer hydrophilic–hydrophobic hollow fiber membranes,” *J. Memb. Sci.*, vol. 306, no. 1–2, pp. 134–146, Dec. 2007.

[12] F. Laganà, G. Barbieri, and E. Drioli, “Direct contact membrane distillation: modelling and concentration experiments,” *J. Memb. Sci.*, vol. 166, no. 1, pp. 1–11, Feb. 2000.

[13] C. Gostoli, G. C. Sarti, and S. Matulli, “Low Temperature Distillation Through Hydrophobic Membranes,” *Sep. Sci. Technol.*, vol. 22, no. 2–3, pp. 855–872, Feb. 1987.

[14] H. Y. Wu, R. Wang, and R. W. Field, “Direct contact membrane distillation: An experimental and analytical investigation of the effect of membrane thickness upon transmembrane flux,” *J. Memb. Sci.*, vol. 470, pp. 257–265, Nov. 2014.

[15] a. E. Jansen, J. W. Assink, J. H. Hanemaaijer, J. van Medevoort, and E. van Sonsbeek, “Development and pilot testing of full-scale membrane distillation modules for deployment of waste heat,” *Desalination*, vol. 323, pp. 55–65, Aug. 2013.

[16] M. Khayet, K. Khulbe, and T. Matsuura, “Characterization of membranes for membrane distillation by atomic force microscopy and estimation of their water vapor transfer coefficients in vacuum membrane distillation process,” *J. Memb. Sci.*, vol. 238, no. 1–2, pp. 199–211, Jul. 2004.

[17] A. Alkhudhiri, N. Darwish, and N. Hilal, “Membrane distillation : A comprehensive review,” *Desalination*, vol. 287, pp. 2–18, 2012.

[18] M. Khayet, “Membranes and theoretical modeling of membrane distillation : A review,” *Adv. Colloid Interface Sci.*, vol. 164, no. 1–2, pp. 56–88, 2011.

[19] H. Fang, J. F. Gao, H. T. Wang, and C. S. Chen, “Hydrophobic porous alumina hollow fiber for water desalination via membrane distillation process,” *J. Memb. Sci.*, vol. 403–404, pp. 41–46, 2012.

[20] X. Wei, B. Zhao, X. Li, Z. Wang, B. He, T. He, and B. Jiang, “CF 4 plasma surface modification of asymmetric hydrophilic polyethersulfone membranes for direct contact membrane distillation,” *J. Memb. Sci.*, vol. 407–408, pp. 164–175, 2012.

[21] G. Zuo and R. Wang, “Novel membrane surface modi fi cation to enhance anti-oil fouling property for membrane distillation application,” *J. Memb. Sci.*, vol. 447, pp. 26–35, 2013.

[22] D. Hou, J. Wang, X. Sun, Z. Ji, and Z. Luan, “Preparation and properties of PVDF composite hollow fiber membranes for desalination through direct contact membrane distillation,” *J. Memb. Sci.*, vol. 405–406, pp. 185–200, 2012.

[23] M. Bhadra, S. Roy, and S. Mitra, “Nanodiamond immobilized membranes for enhanced desalination via membrane distillation,” *Desalination*, vol. 341, pp. 115–119, 2014.

[24] A. G. Fane, C. J. D. Fell, and A. G. Waters, “The relationship between membrane surface pore characteristics and flux for ultrafiltration membranes,” *J. Memb. Sci.*, vol. 9, pp. 245–262, 1981.

[25] U. MERIN and M. CHERYA, “Ultrastructure o f the Surface o f a Polysulfone Ultrafiltration Membrane,” *J. Appl. Polym. SceinceApplied Polym. Sceince*, vol. 25, pp. 2139–2142, 1980.

[26] G. Capannelli, F. Vigo, and S. Munari, “Ultrafiltration membranes —characterization methods,” *J. Memb. Sci.*, vol. 15, pp. 289–313, 1983.

[27] N. Mohammad, “Properties of Asymmetric Polyimide Ultrafiltration Membranes. I. Pore Size and Morphology Characterization,” *J. Appl. Polym. Sci.*, vol. 29, pp. 743–753, 1984.

[28] P. Dietz, P. K. Hansma, O. Inackerb, and H.-D. L. H. Karl-Heinz, “Surface pore structures of micro- and ultrafiltration membranes imaged with the atomic force microscope,” *J. Memb. Sci.*, vol. 65, pp. 101–111, 1992.

[29] W. R. BOWEN, N. HILAL, R. W. LOVITT, and A. P. M. WILLIAMS, “Atomic Force Microscope Studies of Membranes : Surface Pore Structures of Diaflo Ultrafiltration Membranes,” *J. Colloid Interface Sci.*, vol. 359, pp. 350–359, 1996.

[30] F. Macedonio, A. Ali, T. Poerio, E. El-sayed, E. Drioli, and M. Abdel-jawad, “Direct contact membrane distillation for treatment of oilfield produced water,” *Sep. Purif. Technol.*, vol. 126, pp. 69–81, 2014.

[31] P. Wang and T. Chung, “Design and fabrication of lotus-root-like multi-bore hollow fiber membrane for direct contact membrane distillation,” *J. Memb. Sci.*, vol. 421–422, pp. 361–374, 2012.

[32] F. Edwie and T. Chung, “Development of hollow fiber membranes for water and salt recovery from highly concentrated brine via direct contact membrane distillation and crystallization,” *J. Memb. Sci.*, vol. 421–422, pp. 111–123, 2012.

[33] N. Tang, Q. Jia, H. Zhang, J. Li, and S. Cao, “Preparation and morphological characterization of narrow pore size distributed polypropylene hydrophobic membranes for vacuum membrane distillation via thermally induced phase separation,” *Desalination*, vol. 256, no. 1–3, pp. 27–36, Jun. 2010.

[34] L. D. Tijing, J.-S. Choi, S. Lee, S.-H. Kim, and H. K. Shon, “Recent progress of membrane distillation using electrospun nanofibrous membrane,” *J. Memb. Sci.*, vol. 453, pp. 435–462, Mar. 2014.

[35] M. M. a. Shirazi, a. Kargari, S. Bazgir, M. Tabatabaei, M. J. a. Shirazi, M. S. Abdullah, T. Matsuura, and a. F. Ismail, “Characterization of electrospun polystyrene membrane for treatment of biodiesel’s water-washing effluent using atomic force microscopy,” *Desalination*, vol. 329, pp. 1–8, Nov. 2013.

[36] M. J. a. Shirazi, S. Bazgir, M. M. a. Shirazi, and S. Ramakrishna, “Coalescing filtration of oily wastewaters: characterization and application of thermal treated, electrospun polystyrene filters,” *Desalin. Water Treat.*, vol. 51, no. 31–33, pp. 5974–5986, Sep. 2013.

[37] S. Tabe, *Electrospun Nanofiber Membranes and Their Applications in Water and Wastewater Treatment. In A. Hu and A. Apblet, Nanotechnology for Water Treatment and Purification*. Springer International Publisher Switzerland, 2014.

[38] R. R. Nair, H. a Wu, P. N. Jayaram, I. V Grigorieva, and a K. Geim, “Unimpeded permeation of water through helium-leak-tight graphene-based membranes.,” *Science*, vol. 335, no. 6067, pp. 442–4, Jan. 2012.

[39] K. Huang, G. Liu, Y. Lou, Z. Dong, J. Shen, and W. Jin, “Graphene Oxide Membranes A Graphene Oxide Membrane with Highly Selective Molecular Separation of Aqueous Organic Solution,” *Angew. Chemie Int. Ed.*, vol. 53, no. 27, pp. 6929–6932, 2014.

[40] P. Sun, M. Zhu, K. Wang, M. Zhong, J. Wei, D. Wu, Z. Xu, and H. Zhu, “Selective Ion Penetration of Graphene,” *ACSNano*, no. 1, pp. 428–437, 2013.

[41] H. Du, J. Li, J. Zhang, G. Su, X. Li, and Y. Zhao, “Separation of Hydrogen and Nitrogen Gases with Porous Graphene Membrane,” *J. Phys. Chem.*, vol. 115, pp. 23261–23266, 2011.

[42] Y. Han, Z. Xu, and C. Gao, “Ultrathin Graphene Nanofiltration Membrane for Water Purification,” *Adv. Funct. Mater.*, vol. 23, no. 29, pp. 3693–3700, Aug. 2013.

[43] Y. L. F. Musico, C. M. Santos, M. L. P. Dalida, and D. F. Rodrigues, “Surface Modi fi cation of Membrane Filters Using Graphene and Graphene Oxide-Based Nanomaterials for Bacterial Inactivation and Removal,” *ACS Sustain. Chem. Eng.*, vol. 2, no. 7, pp. 1159–1565, 2014.

[44] J. Lee, H. Chae, Y. June, K. Lee, C. Lee, H. H. Lee, I. Kim, and J. Lee, “Graphene oxide nanoplatelets composite membrane with hydrophilic and antifouling properties for wastewater treatment,” *J. Memb. Sci.*, vol. 448, pp. 223–230, 2013.

[45] M. Kumar, M. Grzelakowski, J. Zilles, M. Clark, and W. Meier, “Highly permeable polymeric membranes based on the incorporation of the functional water channel protein Aquaporin Z,” vol. 104, no. 52, pp. 20719–20724, 2007.

[46] C. Y. Tang, Y. Zhao, R. Wang, C. Hélix-nielsen, and A. G. Fane, “Desalination by biomimetic aquaporin membranes : Review of status and prospects,” 2012.

[47] K. Gethard, O. Sae-khow, and S. Mitra, “Water Desalination Using Carbon-Nanotube-Enhanced Membrane Distillation,” *Appl. Mater. Interfaces*, vol. 3, pp. 110–114, 2011.

[48] L. Dumée, J. L. Campbell, K. Sears, J. Schütz, N. Finn, M. Duke, and S. Gray, “The impact of hydrophobic coating on the performance of carbon nanotube bucky-paper membranes in membrane distillation,” *Desalination*, vol. 283, pp. 64–67, 2011.

[49] L. F. Dumée, K. Sears, J. Schütz, N. Finn, C. Huynh, S. Hawkins, M. Duke, and S. Gray, “Characterization and evaluation of carbon nanotube Bucky-Paper membranes for direct contact membrane distillation,” *J. Memb. Sci.*, vol. 351, pp. 36–43, 2010.

[50] S. Roy, M. Bhadra, and S. Mitra, “Enhanced desalination via functionalized carbon nanotube immobilized membrane in direct contact membrane distillation,” *Sep. Purif. Technol.*, vol. 136, pp. 58–65, Nov. 2014.

[51] S. Al-Sharif, M. Albeirutty, A. Cipollina, and G. Micale, “Modelling flow and heat transfer in spacer-filled membrane distillation channels using open source CFD code,” *Desalination*, vol. 311, pp. 103–112, Feb. 2013.

[52] H. Yu, X. Yang, R. Wang, and A. G. Fane, “Numerical simulation of heat and mass transfer in direct membrane distillation in a hollow fiber module with laminar flow,” *J. Memb. Sci.*, vol. 384, no. 1–2, pp. 107–116, 2011.

[53] X. Yang, H. Yu, R. Wang, and A. G. Fane, “Optimization of microstructured hollow fiber design for membrane distillation applications using CFD modeling,” *J. Memb. Sci.*, vol. 421–422, pp. 258–270, 2012.

[54] Y. M. Manawi, M. Khraisheh, A. K. Fard, F. Benyahia, and S. Adham, “Effect of operational parameters on distillate flux in direct contact membrane distillation (DCMD): Comparison between experimental and model predicted performance,” *Desalination*, vol. 336, pp. 110–120, Mar. 2014.

[55] A. R. Kurdian, M. Bahreini, G. H. Montazeri, and S. Sadeghi, “Modeling of direct contact membrane distillation process : Flux prediction of sodium sulfate and sodium chloride solutions,” *Desalination*, vol. 323, pp. 75–82, 2013.

[56] A. Tamburini, P. Pitò, A. Cipollina, G. Micale, and M. Ciofalo, “A Thermochromic Liquid Crystals Image Analysis technique to investigate temperature polarization in spacer- fi lled channels for Membrane Distillation,” *J. Memb. Sci.*, vol. 447, pp. 260–273, 2013.

[57] a. Ali, F. Macedonio, E. Drioli, S. Aljlil, and O. a. Alharbi, “Experimental and theoretical evaluation of temperature polarization phenomenon in direct contact membrane distillation,” *Chem. Eng. Res. Des.*, vol. 91, no. 10, pp. 1966–1977, Oct. 2013.

[58] M. Gryta, M. Tomaszewska, and A. W. Morawski, “Membrane distillation with laminar flow,” *Sep. Purif. Technol.*, vol. 5866, no. 97, pp. 2–6, 1997.

[59] E. K. Summers and J. H. L. V, “Experimental study of thermal performance in air gap membrane distillation systems , including the direct solar heating of membranes,” *Desalination*, vol. 330, pp. 100–111, 2013.

[60] H. Geng, Q. He, H. Wu, P. Li, C. Zhang, and H. Chang, “Experimental study of hollow fiber AGMD modules with energy recovery for high saline water desalination,” *Desalination*, vol. 344, pp. 55–63, Jul. 2014.

[61] A. S. Alsaadi, N. Ghaffour, J. Li, S. Gray, L. Francis, H. Maab, and G. L. Amy, “Modeling of air-gap membrane distillation process : A theoretical and experimental study,” *J. Memb. Sci.*, vol. 445, pp. 53–65, 2013.

[62] J. Zhang, J. Li, M. Duke, M. Hoang, Z. Xie, A. Groth, C. Tun, and S. Gray, “Modelling of vacuum membrane distillation,” *J. Memb. Sci.*, vol. 434, pp. 1–9, 2013.

[63] G. Zuo, G. Guan, and R. Wang, “Numerical modeling and optimization of vacuum membrane distillation module for low-cost water production,” *Desalination*, vol. 339, pp. 1–9, 2014.

[64] J. Lee and W. Kim, “Numerical modeling of the vacuum membrane distillation process,” *Desalination*, vol. 331, pp. 46–55, 2013.

[65] A. S. Kim, “Cylindrical cell model for direct contact membrane distillation (DCMD) of densely packed hollow fibers,” *J. Memb. Sci.*, vol. 455, pp. 168–186, Apr. 2014.

[66] S. G. Lovineh, M. Asghari, and B. Rajaei, “Numerical simulation and theoretical study on simultaneous effects of operating parameters in vacuum membrane distillation,” *Desalination*, vol. 314, pp. 59–66, 2013.

[67] F. He, J. Gilron, and K. K. Sirkar, “High water recovery in direct contact membrane distillation using a series of cascades,” *Desalination*, vol. 323, pp. 48–54, 2013.

[68] X. Yang, R. Wang, and A. G. Fane, “Novel designs for improving the performance of hollow fiber membrane distillation modules,” *J. Memb. Sci.*, vol. 384, no. 1–2, pp. 52–62, 2011.

[69] C.-D. Ho, C.-H. Huang, F.-C. Tsai, and W.-T. Chen, “Performance improvement on distillate flux of countercurrent-flow direct contact membrane distillation systems,” *Desalination*, vol. 338, pp. 26–32, Apr. 2014.

[70] M. Shakaib, S. M. F. Hasani, I. Ahmed, and R. M. Yunus, “A CFD study on the effect of spacer orientation on temperature polarization in membrane distillation modules,” *Desalination*, vol. 284, pp. 332–340, 2012.

[71] R. Tian, H. Gao, X. H. Yang, S. Y. Yan, and S. Li, “A new enhancement technique on air gap membrane distillation,” *Desalination*, vol. 332, pp. 52–59, 2014.

[72] D. Singh and K. K. Sirkar, “Desalination by air gap membrane distillation using a two hollow-fiber-set membrane module,” *J. Memb. Sci.*, vol. 421–422, pp. 172–179, 2012.

[73] H. Geng, H. Wu, P. Li, and Q. He, “Study on a new air-gap membrane distillation module for desalination,” *Desalination*, vol. 334, no. 1, pp. 29–38, 2014.

[74] J. Zhang, J. Li, M. Duke, M. Hoang, Z. Xie, A. Groth, C. Tun, and S. Gray, “In fl uence of module design and membrane compressibility on VMD performance,” *J. Memb. Sci.*, vol. 442, pp. 31–38, 2013.

[75] L. Wang, H. Wang, B. Li, Y. Wang, and S. Wang, “Novel design of liquid distributors for VMD performance improvement based on cross- fl ow membrane module,” *Desalination*, vol. 336, pp. 80–86, 2014.

[76] S. Goh, J. Zhang, Y. Liu, and A. G. Fane, “Fouling and wetting in membrane distillation (MD) and MD-bioreactor (MDBR) for wastewater reclamation,” *Desalination*, vol. 323, pp. 39–47, 2013.

[77] A. Hausmann, P. Sanciolo, T. Vasiljevic, M. Weeks, K. Schroën, S. Gray, and M. Duke, “Fouling mechanisms of dairy streams during membrane distillation,” *J. Memb. Sci.*, vol. 441, pp. 102–111, 2013.

[78] Z. Ding, L. Liu, J. Yu, R. Ma, and Z. Yang, “Concentrating the extract of traditional Chinese medicine by direct contact membrane distillation,” *J. Memb. Sci.*, vol. 310, no. 1–2, pp. 539–549, Mar. 2008.

[79] K. W. Lawson and D. R. Lloyd, “Membrane distillation,” *J. Memb. Sci.*, vol. 124, 1997.

[80] R. W. Schofield and A. G. Fane, “Heat and mass transfer in membrane distillation,” *J. Memb. Sci.*, vol. 33, pp. 299–313, 1987.

[81] J. Phattaranawik, R. Jiraratananon, and a. . Fane, “Heat transport and membrane distillation coefficients in direct contact membrane distillation,” *J. Memb. Sci.*, vol. 212, no. 1–2, pp. 177–193, Feb. 2003.

[82] M. Gryta, “Concentration of saline wastewater from the production of heparin,” *Desalination*, vol. 129, pp. 35–44, 2000.

[83] A. Kullab and A. Martin, “Membrane distillation and applications for water purification in thermal cogeneration plants,” *Sep. Purif. Technol.*, vol. 76, no. 3, pp. 231–237, 2011.

[84] M. Gryta, “Fouling in direct contact membrane distillation process,” *J. Memb. Sci.*, vol. 325, no. 1, pp. 383–394, Nov. 2008.

[85] E. Guillen-burrieza, R. Thomas, B. Mansoor, D. Johnson, and N. Hilal, “Effect of dry-out on the fouling of PVDF and PTFE membranes under conditions simulating intermittent seawater membrane distillation (SWMD),” *J. Memb. Sci.*, vol. 438, pp. 126–139, 2013.

[86] A. Al-janabi, M. R. Malayeri, E. Guillén-burrieza, and J. Blanco, “Field evaluation of coated plates of a compact heat exchanger to mitigate crystallization deposit formation in an MD desalination plant,” *Desalination*, vol. 324, pp. 21–33, 2013.

[87] J. Ge, Y. Peng, Z. Li, P. Chen, and S. Wang, “Membrane fouling and wetting in a DCMD process for RO brine concentration,” *Desalination*, vol. 344, pp. 97–107, 2014.

[88] G. Chen, X. Yang, R. Wang, and A. G. Fane, “Performance enhancement and scaling control with gas bubbling in direct contact membrane distillation,” *Desalination*, vol. 308, pp. 47–55, 2013.

[89] M. Gryta, “Polyphosphates used for membrane scaling inhibition during water desalination by membrane distillation,” *Desalination*, vol. 285, pp. 170–176, 2012.

[90] M. Gryta, “Direct Contact Membrane Distillation with Crystallization Applied to NaCl Solutions,” *Chem. Pap.*, no. May 2001, pp. 14–19, 2002.

[91] S. Goh, J. Zhang, Y. Liu, and A. G. Fane, “Fouling and wetting in membrane distillation (MD) and MD-bioreactor (MDBR) for wastewater reclamation,” *Desalination*, vol. 323, pp. 39–47, 2013.

[92] A. Hausmann, P. Sanciolo, T. Vasiljevic, M. Weeks, K. Schroën, S. Gray, and M. Duke, “Fouling of dairy components on hydrophobic polytetrafluoroethylene (PTFE) membranes for membrane distillation,” *J. Memb. Sci.*, vol. 442, pp. 149–159, Sep. 2013.

[93] S. Goh, Q. Zhang, J. Zhang, D. Mcdougald, W. B. Krantz, Y. Liu, and A. G. Fane, “Impact of a biofouling layer on the vapor pressure driving force and performance of a membrane distillation process,” *J. Memb. Sci.*, vol. 438, pp. 140–152, 2013.

[94] J. Gilron, Y. Ladizansky, and E. Korin, “Silica Fouling in Direct Contact Membrane Distillation,” *Ind. Eng. Chem. Res.*, vol. 52, pp. 10521–10529, 2013.

[95] S. P. A. Brown and A. J. Krupnick, “Abundant Shale Gas Resources: Long-Term Implications for U.S. Natural Gas Markets,” *Resour. Futur.*, 2010.

[96] A. Fakhru’l-Razi, A. Pendashteh, L. C. Abdullah, D. R. A. Biak, S. S. Madaeni, and Z. Z. Abidin, “Review of technologies for oil and gas produced water treatment.,” *J. Hazard. Mater.*, vol. 170, no. 2–3, pp. 530–51, Oct. 2009.

[97] M. Xie, L. D. Nghiem, W. E. Price, and M. Elimelech, “A Forward Osmosis − Membrane Distillation Hybrid Process for Direct Sewer Mining: System Performance and Limitations,” *Environ. Sci. Technol.*, vol. 47, pp. 13486–13493, 2013.

[98] M. Xie, L. D. Nghiem, W. E. Price, and M. Elimelech, “Toward Resource Recovery from Wastewater: Extraction of Phosphorus from Digested Sludge Using a Hybrid Forward Osmosis − Membrane Distillation Process,” *Environ. Sci. Technol. Lett.*, vol. 1, pp. 191–195, 2014.

[99] E. Drioli, G. Di Profio, and E. Curcio, “Progress in membrane crystallization,” *Curr. Opin. Chem. Eng.*, vol. 1, no. 2, pp. 178–182, May 2012.

[100] E. Curcio, X. Ji, A. Matin, S. Barghi, G. Di, E. Fontananova, T. Macleod, and E. Drioli, “Hybrid nanofiltration – membrane crystallization system for the treatment of sulfate wastes,” *J. Memb. Sci.*, vol. 360, no. 1–2, pp. 493–498, 2010.

[101] X. Ji, E. Curcio, S. Al, G. Di, E. Fontananova, and E. Drioli, “Membrane distillation-crystallization of seawater reverse osmosis brines,” *Sep. Purif. Technol.*, vol. 71, pp. 76–82, 2010.

[102] F. Macedonio, C. A. Quist-jensen, O. Al-harbi, H. Alromaih, S. A. Al-jlil, F. Al Shabouna, and E. Drioli, “Thermodynamic modeling of brine and its use in membrane crystallizer,” *Desalination*, vol. 323, pp. 83–92, 2013.

[103] E. Guillén-burrieza, G. Zaragoza, S. Miralles-cuevas, and J. Blanco, “Experimental evaluation of two pilot-scale membrane distillation modules used for solar desalination,” *J. Memb. Sci.*, vol. 409–410, pp. 264–275, 2012.

[104] R. G. Raluy, R. Schwantes, V. J. Subiela, B. Peñate, G. Melián, and J. R. Betancort, “Operational experience of a solar membrane distillation demonstration plant in Pozo Izquierdo-Gran Canaria Island (Spain),” *Desalination*, vol. 290, pp. 1–13, Mar. 2012.

[105] R. Zarasvand Asadi, F. Suja, F. Tarkian, F. Mashhoon, S. Rahimi, and A. Atash Jameh, “Solar desalination of Gas Refinery wastewater using membrane distillation process,” *Desalination*, vol. 291, pp. 56–64, Apr. 2012.

[106] D. Hou, G. Dai, J. Wang, H. Fan, Z. Luan, and C. Fu, “Boron removal and desalination from seawater by PVDF fl at-sheet membrane through direct contact membrane distillation,” *Desalination*, vol. 326, pp. 115–124, 2013.

[107] M. Bhattacharya, S. K. Dutta, J. Sikder, and M. K. Mandal, “Computational and experimental study of chromium (VI) removal in direct contact membrane distillation,” *J. Memb. Sci.*, vol. 450, pp. 447–456, 2014.

[108] D. Singh and K. K. Sirkar, “Desalination of brine and produced water by direct contact membrane distillation at high temperatures and pressures,” *J. Memb. Sci.*, vol. 389, pp. 380–388, Feb. 2012.

[109] F. Shao, C. Hao, L. Ni, Y. Zhang, R. Du, and J. Meng, “Experimental and theoretical research on N-methyl-2-pyrrolidone concentration by vacuum membrane distillation using polypropylene hollow fi ber membrane,” *J. Memb. Sci.*, vol. 452, pp. 157–164, 2014.

[110] X. Yu, H. Yang, H. Lei, and A. Shapiro, “Experimental evaluation on concentrating cooling tower blowdown water by direct contact membrane distillation,” *Desalination*, vol. 323, pp. 134–141, 2013.

[111] D. Qu, D. Sun, H. Wang, and Y. Yun, “Experimental study of ammonia removal from water by modi fi ed direct contact membrane distillation,” *Desalination*, vol. 326, pp. 135–140, 2013.

[112] A. Alkhudhiri, N. Darwish, and N. Hilal, “Produced water treatment: Application of Air Gap Membrane Distillation,” *Desalination*, vol. 309, pp. 46–51, Jan. 2013.

[113] M. Tomaszewska and L. Bia, “Production of ethanol from lactose in a bioreactor integrated with membrane distillation,” *Desalination*, vol. 323, pp. 114–119, 2013.

[114] K. C. Wijekoon, F. I. Hai, J. Kang, W. E. Price, T. Y. Cath, and L. D. Nghiem, “Rejection and fate of trace organic compounds (TrOCs) during membrane distillation,” *J. Memb. Sci.*, vol. 453, pp. 636–642, 2014.

[115] X. Li, Y. Qin, R. Liu, Y. Zhang, and K. Yao, “Study on concentration of aqueous sulfuric acid solution by multiple-effect membrane distillation,” *Desalination*, vol. 307, pp. 34–41, 2012.

[116] C. M. Tun and A. M. Groth, “Sustainable integrated membrane contactor process for water reclamation , sodium sulfate salt and energy recovery from industrial ef fl uent,” *Dsalination*, vol. 283, pp. 187–192, 2011.

[117] K. L. Hickenbottom and T. Y. Cath, “Sustainable operation of membrane distillation for enhancement of mineral recovery from hypersaline solutions,” *J. Memb. Sci.*, vol. 454, pp. 426–435, 2014.

[118] M. Gryta, “The concentration of geothermal brines with iodine content by membrane distillation,” *Desalination*, vol. 325, pp. 16–24, 2013.

[119] M. Gryta, A. Markowska-szczupak, J. Bastrzyk, and W. Tomczak, “The study of membrane distillation used for separation of fermenting glycerol solutions,” *J. Memb. Sci.*, vol. 431, pp. 1–8, 2013.

[120] M. Khayet, “Treatment of radioactive wastewater solutions by direct contact membrane distillation using surface modi fi ed membranes,” *Desalination*, vol. 321, pp. 60–66, 2013.

[121] A. Criscuoli, P. Bafaro, and E. Drioli, “Vacuum membrane distillation for purifying waters containing arsenic,” *Desalination*, vol. 323, pp. 17–21, 2013.

[122] M. M. a. Shirazi, A. Kargari, M. Tabatabaei, A. F. Ismail, and T. Matsuura, “Concentration of glycerol from dilute glycerol wastewater using sweeping gas membrane distillation,” *Chem. Eng. Process. Process Intensif.*, vol. 78, pp. 58–66, Apr. 2014.

[123] M. M. a. Shirazi, A. Kargari, and M. Tabatabaei, “Sweeping Gas Membrane Distillation (SGMD) as an Alternative for Integration of Bioethanol Processing: Study on a Commercial Membrane and Operating Parameters,” *Chem. Eng. Commun.*, no. October 2014, p. 140917052218009, Jun. 2014.

[124] L. Camacho, L. Dumée, J. Zhang, J. Li, M. Duke, J. Gomez, and S. Gray, “Advances in Membrane Distillation for Water Desalination and Purification Applications,” *Water*, vol. 5, no. 1, pp. 94–196, Jan. 2013.

[125] M. S. El-bourawi, Z. Ding, R. Ma, and M. Khayet, “A framework for better understanding membrane distillation separation process,” *J. Memb. Sci.*, vol. 285, pp. 4–29, 2006.

[126] E. Drioli, F. Macedonio, and A. Ali, “Membrane Distillation: Basic aspects and applications,” *J. Memb. Sci.*, 2012.

[127] L. Mart, A. Hernández, and P. Prádanos, “Characterisation of three hydrophobic porous membranes used in membrane distillation Modelling and evaluation of their water vapour permeabilities,” J. Memb. Sci., vol. 203, pp. 15–27, 2002.

[128] M. A. Izquierdo-Gil, M. C. GarcõÂa-Payo, and C. FernaÂndez-Pineda, “Air gap membrane distillation of sucrose aqueous solutions,” J. Memb. Sci., vol. 155, pp. 291–307, 1999.

[129] M. Khayet, J. I. Mengual, and G. Zakrzewska-Trznadel, “Direct contact membrane distillation for nuclear desalination . Part I : Review of membranes used in membrane distillation and methods for their characterisation,” Int. J. Nucl. Desalin., vol. 1, no. 4, pp. 435–449, 2005.

CHAPTER 3

Membranes for membrane distillation

1. Introduction

One of the most crucial aspects of the membrane distillation is to have at disposal membranes with well controlled properties. Moreover, the final performance of a process is a direct consequence of the structural and physicochemical parameters of the utilized membranes. This aspect gains relevance when the proposed membrane technology is based on advanced systems where the use of well-structured and functionalized membranes becomes an imperative. Membrane distillation performance is intrinsically affected by the structure of the film in terms of thickness, porosity, mean pore size, pore distribution and geometry. Thus, the successful outcome of the process is reasonably expected to be depending upon the capability of the membrane to interface two media without dispersing one phase into another and to combine high volumetric mass transfer with high resistance to liquid intrusion in the pores. The membranes for membrane contactor application have to be porous, hydrophobic, with good thermal stability and excellent chemical resistance to feed solutions. In particular, the characteristics needed for membranes are as follows:

1. *High liquid entry pressure (*LEP*),* the minimum hydrostatic pressure that must be applied onto the feed solution before it overcomes the hydrophobic forces of the membrane and penetrates into the membrane pores. *LEP* is characteristic of each membrane and permits to prevent wetting of the membrane pores. High *LEP* may be achieved using a membrane material with high hydrophobicity and a small maximum pore size (see Equation 1)

$$LEP_w = \frac{B\ \gamma_L \cos\theta}{d_{max}} \quad (1)$$

where *B* is a geometric factor determined by pore structure, γ_L the liquid surface tension and θ is the liquid/solid contact angle.

However, as the maximum pore size decreases, the mean pore size of the membrane decreases and the permeability of the membrane becomes low.

2. *High permeability.* The flux will "*increase*" with an increase in the membrane pore size and porosity, and with a decrease of the membrane thickness and pore tortuosity. In fact, molar flux through a pore is related to the membrane's average pore size and other characteristic parameters by:

$$N \propto \frac{< r^{\alpha} > \cdot \varepsilon}{\tau \cdot \delta} \quad (2)$$

where ε is the membrane porosity, τ is the membrane tortuosity, δ is the membrane thickness, $< r^{\alpha} >$ is the average pore size (for Knudsen diffusion α=1 or the average squared pore size for viscous flux α=2).

Eq. (2) illustrates the importance (in terms of molar flux) of maximizing the membrane porosity and pore size, while minimizing the transport path length through the membrane, ($\tau\ \delta$). In other words, to obtain a high permeability, the surface layer that governs the membrane transport must be as thin as possible and its surface porosity as well as pore size must be as large as possible. However, a conflict exists between the requirements of high mass transfer associated with thinner membranes and low conductive heat losses achievable by using thicker membranes. In fact, as described in the following sections, thermal efficiency in MD increases gradually with

the growing of membrane thickness and on optimization between the two requirements has to be found.

3. *Low fouling problem*. Fouling is one of the major problems in the application of porous membranes. Fortunately, in the gas–liquid contactor applications, the contactors are less sensitive to fouling since there is no convection flow through the membrane pores. However, in industrial applications, gas and liquid streams with large content of suspended particles can cause plugging due to the small hollow fiber diameter. Pre-filtration is necessary in such a case [51].
4. *High chemical stability.* The chemical stability of the membrane material has a significant effect on its long-term stability. Any reaction between the solvent and membrane material could possibly affect the membrane matrix and surface structure. Liquid with high load of acid gases are corrosive in the nature, which make the membrane material less resistance to chemical attack.
5. *High thermal stability.* Under high temperatures, the membrane material may not be able to resist to degradation or decomposition. Changing in the nature of membrane depends on the glass transition temperature T_g for morphous polymers or the melting point T_m for crystalline polymers. Over these temperatures, the properties of the polymers change dramatically. In Table 3.1, the T_g for the polymers commonly used in membrane contactors is reported.

Table 3.1: Glass Transition temperature Tg of polymers [1][2]

Polymer	T_g *[°C]*
Polyethylene (PE)	−120
Polypropylene (PP)	−15
Polytetrafluoroethylene (PTFE)	126
Polysulfone	190
Polyether sulfone	230
Polyimide (Kapton)	300

The transition temperature of a polymer is determined largely by its chemical structure, which includes mainly the chain flexibility and chain interaction. As it can be seen from Table 3.1, polytetrafluoroethylene has a much higher T_g compared to polyethylene and polypropylene. This contributes to the higher stability and less flexible polyvinyl chain of PTFE with respect to PE and PP. In general, the factors that increase the T_g/T_m or the crystallinity of a membrane can enhance both its chemical and thermal stability. Therefore, in terms of long term stability membrane material with suitable T_g needs to be applied. For operations at high temperatures, fluorinated polymers are good candidates due to their high hydrophobicity and chemical stability [2].

As pointed out in chapter 1, the membranes prepared for MF/UF do not meet the exact requirements for MD. Limited porosity, broader pore size distribution, generally high thickness, and often unsufficient hydrophobicity need to be further addressed to make these membranes suitable for MD applications. Non solvent induced phase separation (NIPS) has appeared as the widely adopted technique for synthesizing the membranes for MD applications. PVDF is the most common polymer used for this purpose due to its easy processassibility during membrane synthesis process. There are several variables that affect the properties of membrane produced through NIPS. Both the composition-related variables and operating conditions affect the membrane properties greatly. It is important to understand the relationship between the various parameters that influence the membrane properties and then to further investigate the

correlation between membrane properties and their performance in MD. Furthermore, the membrane properties required for optimum performance in different configurations can be different.
The focus of the study presented in this chapter is to understand the effect of operating conditions and dope composition on membrane properties (morphology, pore size distribution, porosity, and mechanical strength) and to correlate the membrane features with their performance in direct contact and VMD. In particular, the effect of air gap, bore fluid, coagulation bath and dope composition on membrane properties has been further investigated. Two fiber types were obtained using water and high percentage of PVP in the dope, since their synergistic effect ensures reduction of macrovoids, porosity and pore sizes suitable for MD as observed in a previous work [3]. A third fiber type was obtained introducing another additive, maleic anhydride. The use of this additive, in combination with PVP (high Mw=1,300,000), for preparation of microfiltration PVDF hollow fibre membranes, was already reported in literature [4]. However, in this work, maleic anhydride was used in combination with low Mw PVP in order to facilitate PVP leaching by treatment with sodium hypochlorite, as suggested in literature [5] [6] [7] [8] [9], thus ensuring fibres hydrophobicity. Our aim was to obtain the fibers having very different properties and morphology, in order to compare different morphologies in different MD configurations.
The prepared membranes were used for carrying out both DCMD and VMD tests, to make a comparison of their performance in the two MD configurations. The obtained results were also compared to those obtained using commercial polypropylene (PP) hollow fiber membranes tested both in DCMD and VMD under the same conditions.

2. Experimental

2.1. Hollow fiber preparation

For preparation of polymeric dopes, the polymer poly(vinylidene fluoride) (PVDF Solef® 6012 or 1015 from Solvay chemical company) was dissolved in N-methyl pyrrolidone (NMP) or N,N-dimethylformamide (DMF) in concentration ranging from 15 to 18 wt.%. Double distilled water, Polyvinyl Pyrrolidone (PVP K-17) and Maleic Anhydride (AMAL) were used as pore forming additives, according to the compositions reported in Table 3.2. The solution was stirred at selected temperature (60-85°C) until a homogeneous dope was obtained. The dope was allowed to degas overnight before being transferred to the pressurized reservoir of the spinning set-up. Hollow fibers were spun by the dry/wet technique described elsewhere [3][10]. The most significant fiber-spinning-conditions are summarized in Table 3.2; further details on fibers preparation method can be found in [3].

2.2. Hollow fiber post treatment

The produced PVDF hollow fibers were rinsed completely with abundant water to ensure complete coagulation and total removal of residual solvent. PVP was leached out as suggested in literature [5] [6] [7] [8] [9] by washing the fibers with a solution of sodium hypochlorite 4000 ppm buffered to pH 7. Fibers were washed again and soaked in an aqueous solution of glycerol (30%) for 3-4 hours before drying to avoid collapse of their porous structure.

Table 3.2: The compositions and operating conditions applied in spinning experiments

Fiber	*Polymer PVDF*	*Additives*	*Solvent*	*T (°C)*	*Air gap (cm)*	*Spinning rate (g/min)*	*Bore fluid*
M1	6012-18%	PVP(K-17) 14%, H_2O 6%	NMP 62%	85	14	11	NMP 30%, 10 ml/min
M2	6012-18%	PVP(K-17) 14%, H_2O 6%	NMP 62%	85	25,5	11	H_2O 100%, 10 ml/min
M3	1015-15%	PVP(K-17) 15%, AMAL 10%	DMF 60%	60	25,5	11	IPA 30%, 17 ml/min

**Note: Fibers type M1 was prepared using Ethanol 30% as coagulation bath. In the other cases, tap water was used as other coagulant.*

Abbreviations list: PVDF = poly(vinylidene fluoride); PVP = poly (vinyl pyrrolidone); AMAL = maleic anhydride; NMP = N-methyl pyrrolidone; DMF = N,N-dimethyl formamide; IPA = isopropanol.

2.3. Hollow fiber modules

Hollow fiber modules were prepared in the lab, by coaxially inserting three hollow fibers in a glass device (length 20 cm). Both sides were potted by epoxy glue. Fibers part covered with glue was not considered in the calculation of active membrane area.

In order to remove glycerol, prior to use, modules were washed using double distilled water at 50°C and trans-membrane pressure of ~1 bar for at least 2 hours.

2.4. Scanning electron microscopy (SEM) characterization

The morphology of the PVDF hollow fibers prepared in this work was analyzed by SEM (Quanta FENG 200, FEI Company). For the cross sectional study, the samples were prepared by freeze fracturing the selected fibers into liquid nitrogen.

2.5. Mechanical properties

The mechanical properties of the produced fibers were measured by using ZWICK/ROELL Z 2.5 test unit. The stretching rate was adjusted at 5mm/min while maintaining the unidirectional stretching. The initial distance between the clamps was adjusted at 50 mm. For each type of fiber, 5 tests were performed and the results were reported as the average values of these tests.

2.6. Bubble point and pore size distribution

Fibers bubble points, largest pore size and pore size distribution were determined using a PMI Capillary Flow Porometer (CFP 1500 AEXL, Porous Materials Inc., USA). By this technique, only active pores are measured, that means pores interconnected and open on both surfaces. For each test, fiber samples not treated with glycerol were fully wetted using Porewick (16 dyne/cm). Samples were connected to the instrument and tests were performed according to the wet-up/dry-up mode using the software Capwin. The measurement of bubble point, largest pore size and pore size distribution is based on the Laplace's equation:

$$d_P = 4\gamma_L cos\theta / P$$

where d_P is the pore diameter, γ_L is the surface tension of the liquid, θ is the contact angle of the liquid (assumed to be 0 in case of full wetting, which means $cos\ \theta = 1$) and P is the external pressure.
The results of each test were imported as an excel file using the software Caprep for further processing.

2.7. Porosity measurement

The porosity of the fibers was measured according to the procedure described elsewhere [3]. The gravimetric method was used, which is based on measuring the weight of the liquid entrapped within the membrane pores. The overall porosity was calculated according to the following formula:

$$\varepsilon_m(\%) = [(w_1 - w_2)/D_k]/[(w_1 - w_2)/D_k + w_2/D_{pol}] \times 100$$

Where

w_1 Weight of the wet membrane

w_2 Weight of the dry membrane

D_k Density of kerosene oil (0.82 g/cm^3)

D_{pol} Density of PVDF (1.78 g/cm^3)

For each fiber type, five measurements were carried out; then, average and standard deviation were calculated.

2.8. Trans-membrane flux

Membrane characterization in terms of trans-membrane flux was carried out in vacuum and direct contact configuration.

2.8.1 Vacuum membrane distillation

The procedure and the set-up used for vacuum membrane distillation are described elsewhere [3] and shown in Figure 3.1a. Briefly, the feed is introduced in the lumen side of the fibers by using a peristaltic pump after heating. Vacuum is applied on the outer side (module shell side) by using a vacuum pump. The vapors transported through the membrane are condensed in the condensate tank by using liquid nitrogen. Double distilled water was used as feed. The feed temperature and flow-rate were adjusted at 50°C and 6 L/h, respectively, while the vacuum pressure applied was 40 mbar. The distillate collected (m) after specific interval of time was weighted and the flux was calculated according to the following relation.

$$J = \frac{m}{A.t}$$

Where J is the trans-membrane flux, A is the active membrane surface area calculated on the basis of membrane inner diameter, length of each fiber and the total number of fiber, and t is the time.

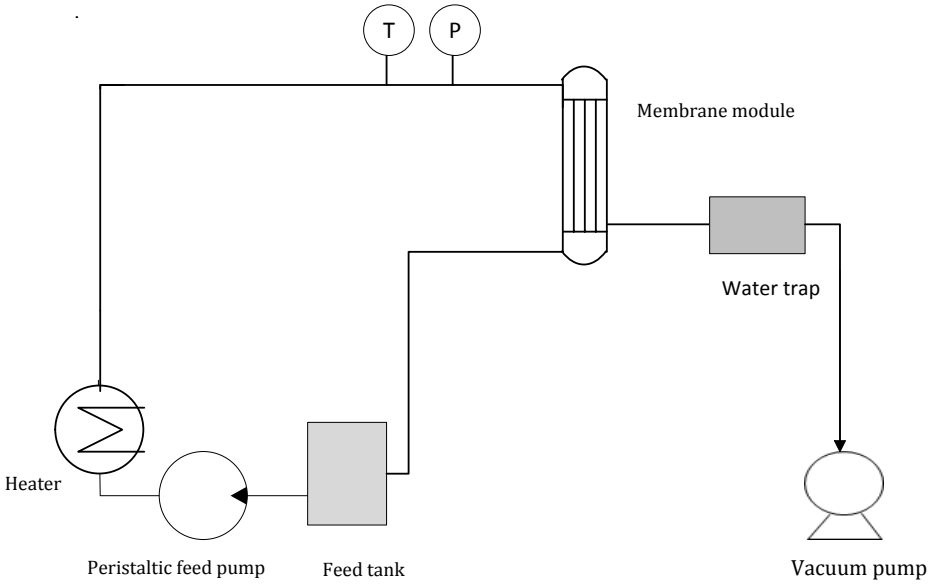

(a)

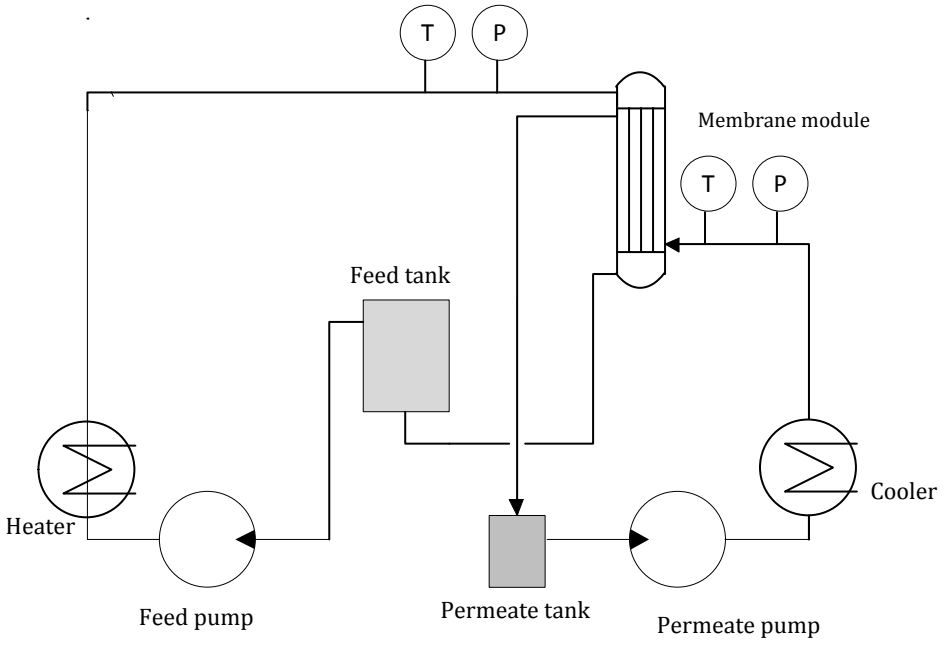

(b)

Figure 3.1: a) VMD set-up and b) DCMD set-up used in this work.

2.8.2 Direct contact membrane distillation

The set-up used for DCMD is shown in Figure 3.1b. Double distilled water was used on both feed and permeate sides. The feed is heated before entering into the membrane module and is introduced on the lumen side of the fibers while the distillate stream is sent at the shell side. The feed and permeate flow rates are controlled by using peristaltic pumps. The distillate tank was placed on a balance that registered the mass of permeate produced during the experiments. The trans-membrane flux was calculated as for the VMD operation.

DCMD tests were performed by varying temperature conditions on the feed side, while keeping the permeate temperature constant. The permeate temperature and flow-rate were fixed at 25°C and 6 L/h, respectively, while the feed temperature was changed from 50°C to 70°C with an interval of 10°C each. For each temperature condition, four different flow rates were applied, ranging from 6 L/h to 11.4 L/h, with an interval of 1.8 L/h each.

2.9. Commercial hollow fiber membranes

Commercial poly propylene hollow fiber membranes type ACCUREL® PP S6/2 were purchased from Membrana GmbH. The commercial hollow fibers were characterized using the same methods described for lab-produced PVDF hollow fibers. The results are reported in Table 3.3. The commercial PP fibers were assembled in modules and tested in both VMD and DCMD set-ups described in section 2.7.

3. Results and discussion

3.1. Membrane morphology

The scanning electron microscopy pictures of the fibers produced in the present work are shown in Figure 3.2 - Figure 3.4. Figure 3.2 reveals that the morphology of the fibers type M1 is dominated by sponge-like structure. In Figure 3.3, it can be noticed that fibers type M2 shows finger like macrovoids at both the inner and outer surface. Fibers type M3 shows tear-drop macrovoids at the inner surface and a thin sponge-like layer at the outer surface, as shown in Figure 3.4.

The morphology, properties and, subsequently, MD performance of hollow fiber membranes arise from interplay between different factors. For fibers produced by *Non-solvent or Diffusion Induced Phase Separation (NIPS or DIPS)* the main factors are: polymer molecular weight and concentration; type of solvent; temperature and viscosity of polymeric dope[11][12]; temperature and composition of outer coagulation bath [13] [14]; eventual use of additives such as polymers (PVP, PEG), small molecules (Glycerol, Ethanol, Water) or salts (LiCl, $LiClO_4$) [15][16]; mutual affinity between solvent and nonsolvent (Hildebrand solubility parameters) [16]; composition and injection rate of inner coagulant [17] [18]; typical spinning parameters such as dope extrusion rate, air gap and fiber take-up speed [17] [18].

In this study, the attention has been focused on the combined effect of dope composition (PVDF Mw and concentration, use of pore forming additives) and operating conditions used in the spinning experiments, i.e. the composition of the used bore fluid, the air gap and the composition of the outer coagulant. Indeed, coagulation media are among the most important factors affecting the final morphology of hollow fiber membranes prepared by NIPS, since they directly influence the coagulation rate. In general, while large finger-like macrovoids and cavities-like structures are usually produced by fast coagulation rate, slower coagulation gives rise to porous sponge-like structures, as reported in literature [12].

For fibers type M1, the presence of water and NMP, in both solvent and bore fluid, decreases the difference between the solubility parameters of solvent and coagulant and, thus, attributes a “soft”

character to the inner coagulant. Consequently, de-mixing between polymer rich and polymer lean phases is delayed and a dominant sponge-like structure is obtained. Formation of sponge-like structure is also promoted by the use of ethanol 30% as outer coagulant instead of tap water, in agreement to what reported in literature. Deshmukh and Li [19] examined the effect of coagulation bath composition on morphology of polyvinylidene fluoride (PVDF) hollow fiber membranes using ethanol and water mixtures with different ratio (from 10/90 to 50/50). They found that fibers morphology near the outer wall was changed from long finger-like structure, to short finger-like structure and, finally, to a sponge-like structure, by increasing ethanol concentration in outer coagulation medium.

Fibers morphology also depends on the pore forming additive used in the dope solution (PVP K-17). It has been observed in the previous studies [3] that the addition of PVP as pore forming additive interferes with thermodynamic stability of the solution and influences the de-mixing behavior of the solution during phase separation. At low concentration, the de-mixing is accelerated in presence of PVP. However, due to the compatibility of PVP with PVDF, dope viscosity increases and de-mixing is delayed at higher concentration of PVP into the solution; this leads towards the formation of a dominant macrovoids free, sponge like structure, as observed in case of fiber type M1.

The morphology of fiber type M2 is strongly affected by the use of water as both internal and external coagulant, which generates finger like macrovoids on both surfaces of the fiber. As widely accepted in literature [13][20][19][21], water is a non-solvent for PVDF. It causes instantaneous liquid-liquid de-mixing and leaves a structure containing finger-like macrovoids. The morphology of the inner surface seems to be more sensitive towards the composition of the bore fluid as compared to the dependence of outer surface on the composition of coagulant. In fact, as it can be noticed in Figure 3.2, finger-like structures are much more evident at the fiber inner wall. This is due to the different coagulation dynamics of fibers inner and outer walls. Coagulation of the inner layer starts immediately, due to the contact of the nascent fiber inner wall with the bore fluid, while the nascent fiber passes through an air gap of 25 cm before entering in the coagulation bath.

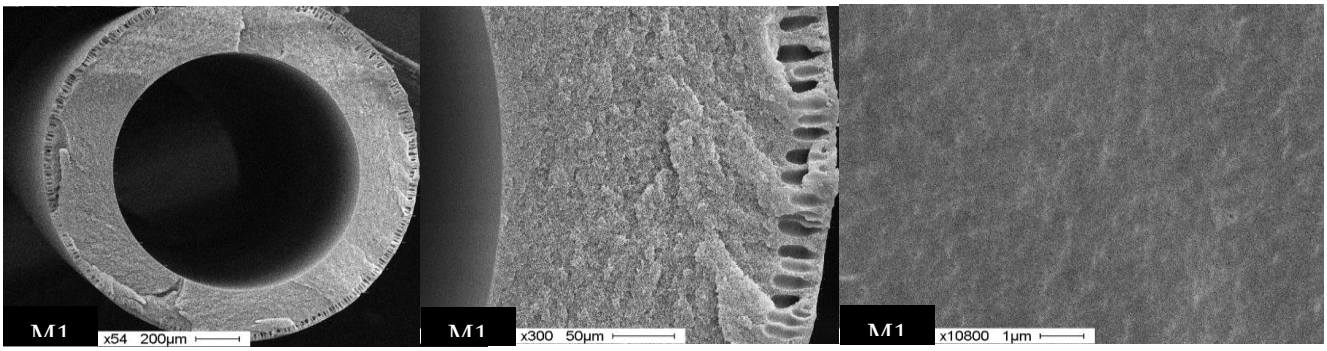

(a) (b) (c)

Figure 3.2: SEM pictures of fibers M1. a) Cross section (54X); b) Enlarged cross section (300X); c) Inner surface (10800X).

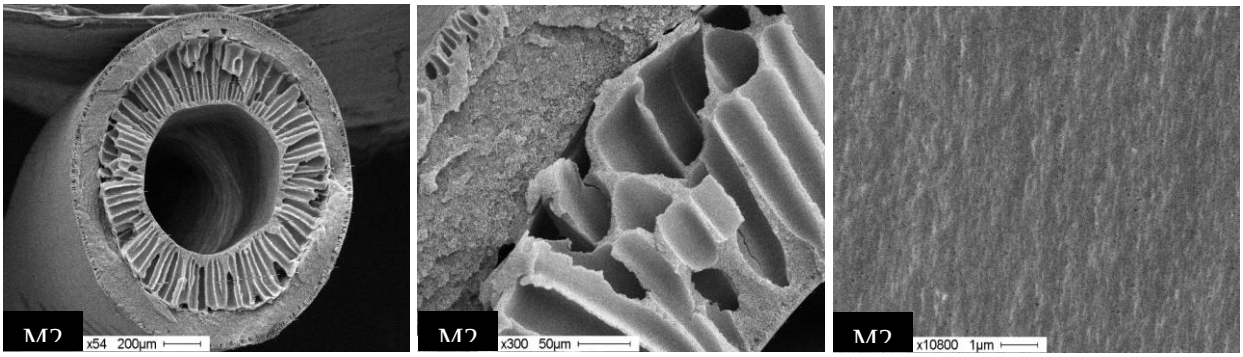

(a) (b) (c)

Figure 3.3: SEM pictures of fibers M2. a) Cross section (54X); b) Enlarged cross section (300X); c) Inner surface (10800X).

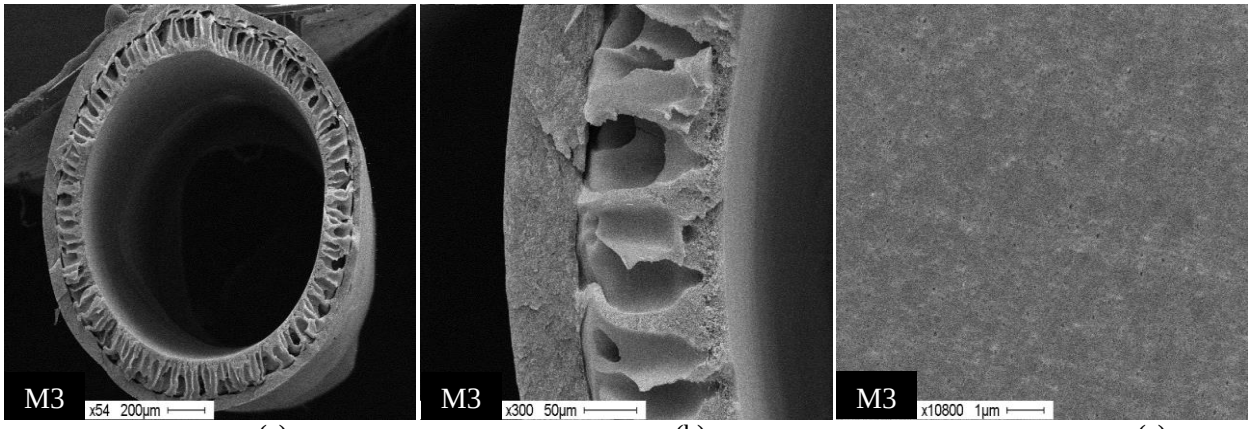

(a) (b) (c)

Figure 3.4: SEM pictures of fibers M3. a) Cross section (54X); b) Enlarged cross section (300X); c) Inner surface (10800X).

Fibers type M3 were produced using a different PVDF type (Solef 1015, which has higher Mw with respect to Solef 6012), lower polymer concentration (15 wt.%), and different additives (PVP K-17 and AMAL), with respect to fibers M1 and M2, as reported in Table 3.2. However, we added also this type of fibers in our analysis, to discuss the effect of different membrane structures on the membrane distillation performance. Regarding the fibers outer surface, also in this case, the used air gap distance of 25 cm resulted in reduction of macrovoids similarly to what observed for fibers type M2. Regarding fibers inner surface, even if IPA 30% is a softer coagulant for PVDF with respect to pure water [6][21], tear-drop macrovoids can be noticed. The development of this structure can be connected to the low polymer concentration in the dope (15%), in agreement to what reported by Smolders et al [22].

3.2. Mechanical properties

The mechanical properties of the PVDF hollow fibers produced are reported in Table 3.3. The fiber type M1 shows the best mechanical properties among the tested ones, in terms of Young's modulus/tensile strength and elongation at break. Fibers type M2 show the lowest Young's Modulus; while, fibers type M3 are characterized by lower tensile strength and elongation at break.

It is well known that the mechanical properties are strongly related with the microstructure developed during the fiber formation. Therefore, fibers mechanical properties can be explained taking into account the dope composition and coagulations conditions employed during spinning experiments.
Fibers M1 are characterized by sponge-like structure, which is consequence of dope and coagulants composition, as explained in Section 3.1. This structure imparts superior mechanical properties to the fibers.

Table 3.3: Properties of the PVDF hollow fibers produced in this work and commercial PP membrane used

Fiber type	*O.D. (mm)*	*I.D. (mm)*	*Thickness (mm)*	*Emod N/mm²*	*Rm N/mm²*	*ε_{break} %*	*W Nm*	*Bubble point (bar)*	*Largest pore size (µm)*	*Average pore size (µm)*	*Porosity (%)*
M1	1.80	1.04	0.38	70.34	3.43	251.97	0.60	2.093	0.219	0.191	80.90
M2	1.59	0.70	0.45	57.15	2.84	192.88	0.30	2.789	0.164	0.121	79.11
M3	1.60	1.15	0.23	63.71	2.62	163.82	0.19	1.267	0.362	0.318	83.39
PP Accurel®	2.70	1.80	0.45	103.75	4.16	174.40	1.11	0.672	0.682	0.2	70.00

Note: The relative standard error is less than 5% in all cases.

On the other hand, finger-like macrovoids represent weak points in the structure and, hence, the corresponding fibers show mediocre mechanical properties. The increased porosity also generates the fibers with weaker mechanical properties. Relatively substandard mechanical properties exhibited by M2 can be related with the application of water as both inner and outer coagulant, which produces a structure containing finger-like macrovoids at both the faces due to instantaneous de-mixing. The low graded mechanical character of M3 can be associated with the lower polymeric composition in the dope and, consequently, the higher porosity achieved.

3.3. Porosity

As shown in Table 3.3, the porosity of all the membranes obtained in current work is quite high, and ranges from 79% to 83%. As also observed in section 3.2, fibers properties can be explained taking into account dope composition and coagulation conditions, which influence de-mixing rate during coagulation and, hence, final fibers morphology. The porosity of fibers types M1 and M2 is similar. Therefore, in this case, fibers void fraction is mostly affected by dope composition, which is the same in the two cases; while, the bore fluid composition has less effect. Surprisingly, the finger-like macrovoids observed in fibers M2 structure do not contribute to increase the overall fibers void fraction. This let us to conclude that the sponge-like structure sandwiched between the two finger-like layers in fiber M2 (Figure 3.3) should be tighter, with respect to fibers type M1.

The higher porosity observed for M3 can be related to the reduced amount of polymer and the additional pore forming additive into the dope solution, which affect fibers morphology as explained in Section 3.1. Fibers porosity is enhanced by the presence of finger-like macrovoids, which are predominant with respect to the thin sponge-like layer in fibers structure, as shown in Figure 3.4.

3.4. Bubble point and pore size distribution

The results of the characterization procedures are reported in Table 3.3. In general, fibers pore size distributions are sharp, with bubble points ranging from 1.3 (Fiber M3) to 2.8 (Fiber M2) bar, corresponding to largest pore size of 0.36 and 0.16 μm respectively.

For fibers M1, the average pore size is about 0.2 μm. Fibers type M2 shows lower average pore size (about 0.12 μm). The observed average pore size values of fibers M1 and M2 can be explained taking into account the preparation procedure. For fiber M1, the use of "soft" coagulants, both as bore fluid and coagulation bath, delayed liquid/liquid demixing during coagulation and promoted the formation of larger pores with respect to M2. In agreement with what observed by Liu et al. [23], when only water is used as bore liquid, as for M2, fast solvent/nonsolvent exchange could result in small pores. Also in [17] it is observed that the rapid phase inversion and polymer solidification in the case of strong nonsolvents, such as water, does not allow a significant pore growth.
Fibers type M3 show larger average pore size, with respect to M1 and M2, and pore size distribution located between 0.36 and 0.32 μm.
The use of lower polymer concentration in the dope, together with two pore forming additives (PVP and Maleic anhydride), and, also, use of "soft" inner coagulant (IPA 30%) resulted in the development of porous structure. As widely accepted, lower polymer concentration results, in general, in enhanced coalescence of the polymer lean phase during phase inversion. Moreover, Liu et al. [23] observed that, when solvent/non solvent exchange takes place with slower rate, the initiated nuclei get the chance to grow before phase separation occurs. Therefore, the dope composition and the coagulation conditions used during fibers M3 spinning resulted in larger pore size.

3.5. Membrane distillation

The PVDF hollow fibers produced in this study were assembled in modules to be tested in MD working both under vacuum and direct contact mode. In this section, the results obtained in both configurations will be illustrated and discussed.

Before any VMD test, fibers were checked to verify that, after vacuum application, no liquid water passed from the fibers lumen (feed side) to the shell side of the module. For all the tested modules, no liquid droplets were evidenced on fibers outer surface, therefore all fibers were used for VMD experiments.

3.5.1 VMD results

Looking at the results reported in Table 3.4, it can be noticed that fibers type M1 shows lower trans-membrane water vapor flux with respect to fibers M2 (15.06 kg/m^2h vs. 22.37 kg/m^2h) and that fibers type M3 shows the highest fluxes 41.78 kg/m^2h.

As widely accepted in literature, the MD trans-membrane water vapor flux is strongly associated with the membranes porosity and thickness [24]. The amount of vapor transported through the membrane increases by increasing the membrane porosity. Similarly, reduced membrane thickness offers less resistance to the vapor transport through the membrane.

Table 3.4: Results of the VMD tests performed using double distilled water as feed (P_{vacuum} 40 mbar, T_f 50°C, Q_f 6 L/h).

Fiber	*VMD flux (H_2O) ($kg/h \cdot m^2$)*
M1	15.06
M2	22.37
M3	41.78
PP	22.00

The morphology of fibers M1 is dominated by the sponge-like structure with an average pore size of 0.19 μm. The limited flux is connected to both its thickness (0.38 mm) and structure. Fibers type M2 have an average pore size of 0.12 μm and are thicker (0.45 mm), but present a sponge-like structure only 0.1 mm thick, and have finger-like layers (which can be noticed in Figure 3.3) that offer a reduced resistance to the transport. Therefore, these fibers show higher VMD flux.
Fibers M3 show typical dual layer structure, with reduced thickness (0.23 mm) and a very thin sponge-like layer (about 0.055 mm) at the outer surface, and finger-like elements close to the inner surface, as evidenced in Figure 3.4. As pointed out in Section 3.3, this morphology results in higher porosity with respect to the other fibers and, as also discussed above, finger-like structures offer reduced resistance to transport. Both factors, together with the reduced thickness and higher average pore size (of about 0.32 μm), lead to a high trans-membrane flux.

3.5.2 DCMD results

The results obtained in the DCMD tests performed using fibers type M1-M3 are shown in Figure 3.5a-c, respectively.

In all cases, it can be noticed that the trans-membrane flux increases by increasing feed flow rates for all the temperatures investigated. The increase in flow rate decreases the boundary layer thickness and thus the flux increases due to more effective heat transfer from the bulk to the membrane surface. For each flow rate, trans-membrane flux increases when increasing the temperature at the feed side. This behavior can be related to the higher vapor pressure at the feed side that leads to higher partial pressure gradient between the two phases (higher driving force).
As discussed in Section 3.1, the structure of fibers M1 is dominated by the sponge-like morphology, which offers more resistance to the mass transfer and, hence, limits the vapor transport across the membrane. Additionally, Table 3.3 indicates that fiber type M1 possesses high thickness, which also contributes in decreasing the value of the trans-membrane flux. Moreover, the presence of some fingers at the outer surface could lead to a partial wetting by the distillate stream that flows at the shell side. This would imply that not all the membrane cross section is available for the vapor transport and that the overall membrane resistance increases. The maximum flux attained reached the value of 14 kg/m^2h.

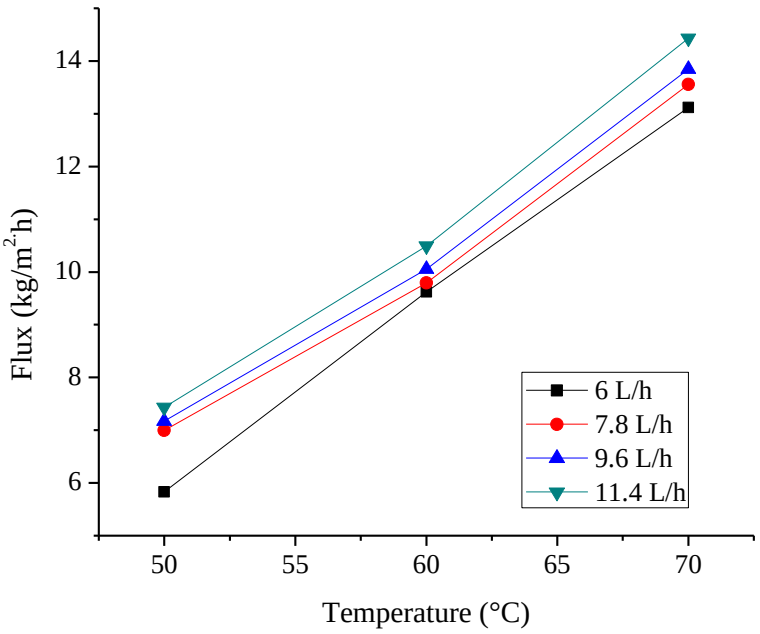
Flux (kg/m2.h)
14
12
10
8
6
50
55
60
65
70
Temperature (°C)
6 L/h
7.8 L/h
9.6 L/h
11.4 L/h

(a)

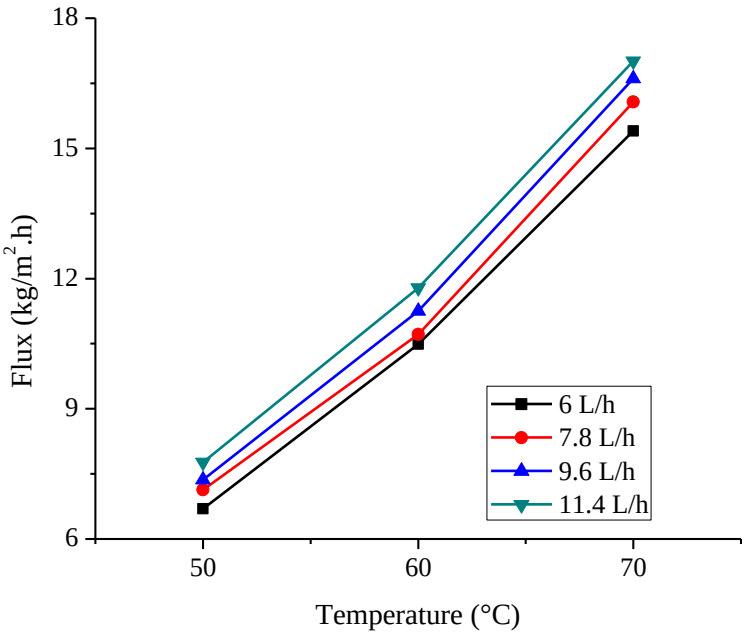
Flux (kg/m2.h)
18
15
12
9
6
50
60
70
Temperature (°C)
6 L/h
7.8 L/h
9.6 L/h
11.4 L/h

(b)

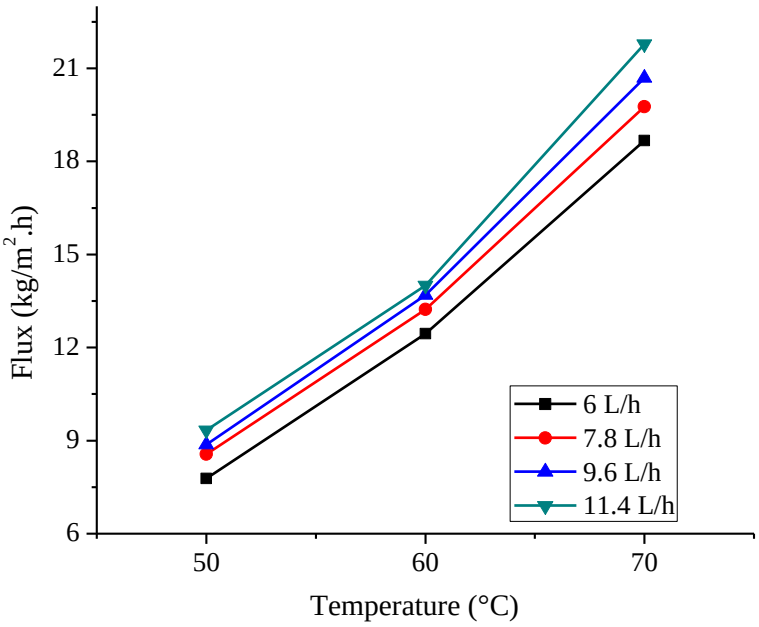

(c)

Figure 3.5: Asymptotic flux obtained at various temperatures and flow-rates for fibers type (a) M1, (b) M2, (c) M3

Fibers type M2 show trans-membrane water vapor fluxes higher than that for M1. As discussed in Section 3.1, and evidenced in MD tests carried out under vacuum, these fibers have finger-like structures on both inner and outer surface. The presence of finger-like structure reduces the resistance to vapor transport and effective tortuosity along the membrane thickness, as well as the heat loss by conduction. However, significant increase of the trans-membrane flux with respect to fibers dominated by the sponge-like structure was not observed when working under the direct contact mode, on the contrary of what observed during VMD tests. This result could be probably due to the partial wetting of the finger-like structure at the outer surface of the fibers, present in both membrane types (M1 and M2). As reported above, in partially wetted membranes, the cross section dry and available for the vapor transport is reduced and the overall resistance offered by the membrane increases. Therefore, the gain in membrane flux, that could be obtained with fibers type M2 thanks to the presence of the finger-like structure (characterized by a lower membrane resistance), is, in fact, reduced because of the higher resistance offered by the wetted portion of the membrane.

Similarly to what observed in VMD tests, the obtained flux is the maximum for fibers type M3 among all the tested ones. As already explained above, this can be related with the higher porosity and pore size, presence of the fingers and the lowest thickness of these fibers among all the used ones. In this case, a spongy structure is observed on the outer surface and, thus, no wetting phenomena by the distillate stream can occur. The maximum flux achieved approaches the value of 22 kg/m^{2}h, as shown in Figure 3.5c. Again, the gain in flux is not as high as for VMD, due to the increase of the heat loss by conduction at lower membrane thickness.

As discussed in literature [16], sponge-like structure narrows down the difference between DCMD and VMD flux. As the structure changes from spongy to the one containing macrovoids, the difference in flux becomes more and more significant.

The results obtained for all the investigated fibers and that for commercial polypropylene (PP Accurel® S6/2) are compared in Figure 3.6, which shows the average flux obtained for each fiber at

different feed temperatures. The flux obtained for each type of fiber at various flow rates and at a specific temperature was averaged. It can be noticed that the maximum flux is obtained with the fibers type M3 at all the tested temperatures.

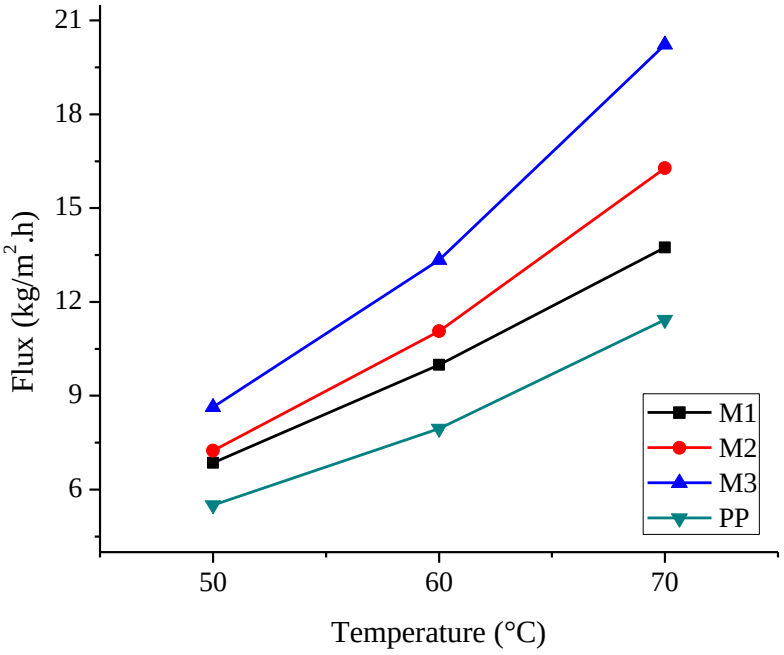

Figure 3.6: Average asymptotic flux obtained for various types of fibers at different temperatures

3.5.3 Comparison between VMD and DCMD

Looking at the results obtained in VMD and DCMD experiments, it can be noticed that the trend of trans-membrane flux for various types of fibers is same in both configurations i.e. the highest flux is exhibited by fiber type M3 while M1 shows the limited values of flux, flux for M2 lays between M3 and M1.

The heat transferred through the membrane is governed by the following equation

$$Q_m = k_m / d(T_{Fm} - T_{Pm}) + J/$$

Where k_m is the thermal conductivity of the membrane, δ is the membrane thickness and λ is the latent heat of vaporization. Hot and cold phases separated by thin membranes in DCMD cause the thermal losses through the membrane. Moreover, the vapors transported from the hot to the cold side produce the local increase in temperature at the distillate side. Consequently, the effective vapor pressure gradient between the two phases decreases. In VMD, the conductive losses can be neglected due to the high vacuum applied at the other side of the membrane. Thus, no temperature profile is present at the permeate side.

As already reported, the mass transfer flux through the membrane is proportional to the vapor pressure gradient across the membrane, which is a function of the membrane surface temperatures.

$$\Delta P_m = \exp\left(A - \frac{B}{T_{Fm} - C}\right) - \exp\left(A - \frac{B}{T_{Pm} - C}\right) \qquad (1)$$

In case of vacuum membrane distillation, the second term in above equation equals the vacuum pressure applied and therefore, the effective pressure gradient across the membrane increases. Due to the lower driving force and the heat loss by conduction, trans-membrane water vapor fluxes obtained while working in the direct contact mode are lower with respect to those obtained working under vacuum for the same feed temperature and flow-rate.

The comparison of the fluxes obtained for the two configurations at the same feed inlet temperatures and flow rates (50°C and 6L/h) is given in Figure 3.7. The general trend observed for trans-membrane water vapor flux among the tested fibers is the same working under both MD configuration, i.e. M3>M2>M1. However, the difference between the VMD and DCMD performance becomes much more evident going from M1 to M3. As already discussed, this could be attributed to the different fibers morphology and properties (M1 mainly characterized by a sponge-like structure; M2 and M3 asymmetric type: M2, sponge structure "sandwiched" between finger-type structures at inner and outer surfaces; M3, thin sponge layer at the outer surface and finger elements at the inner surface, together with higher porosity and pore size and lower thickness than M1 and M2). In the case of M1, the high thickness of the dominant sponge-like structure increases the resistance to the vapor transport while reducing the heat loss across the membrane. Therefore, the difference between VMD and DCMD fluxes is reduced. Due to the same reasons, when reducing the membrane thickness and increasing the percentage of macrovoids in the fibers structure, i.e. going to M2 and, especially, to M3, the difference between DCMD and VMD performance becomes much more evident. The highest difference observed between the two MD configurations, achieved for fibers type M3, can be explained taking into account that, due to the fibers reduced thickness, the heat losses by conduction increase and affect the DCMD flux, whereas the VMD flux benefits of the reduced resistance to the transport.

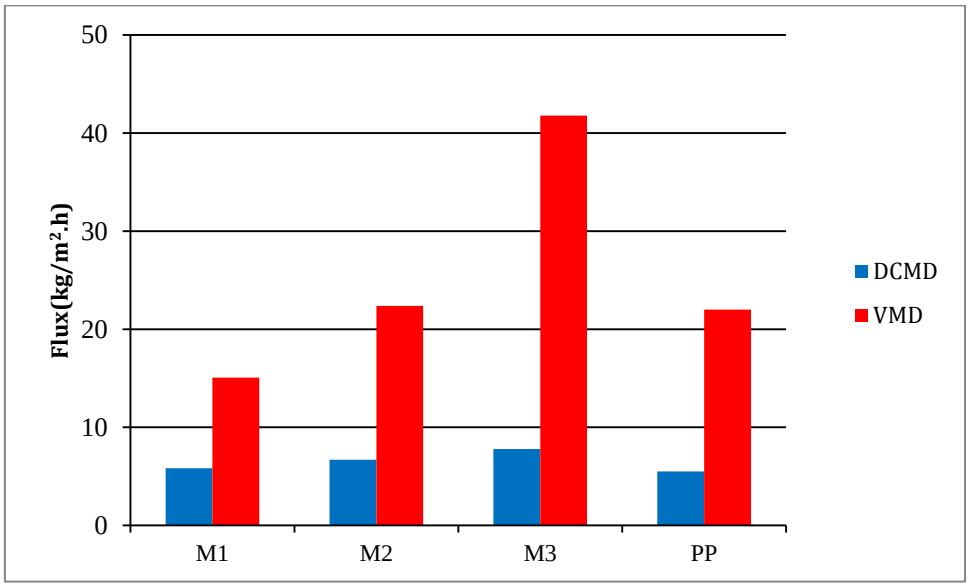

Figure 3.7: Comparison of flux obtained at the same feed conditions (50°C, 6 L/h) for different types of membranes used in DCMD and VMD tests

3.5.4. Comparison of VMD performance with literature data

As described in the Introduction, the aim of the present work was to investigate the behaviour of different fiber morphologies in membrane distillation. PVDF hollow fibers were produced changing

dope composition and spinning conditions on the basis of what already obtained in a previous work [3]. In order to facilitate comparison between fiber properties and VMD performance we resume here the similarities and differences between the preparation conditions of fibers produced in this and in the previous work. The comparison with previous results is shown in Figure 3.8.

1) The dope composition of fibers M1 and M2 contains water and high percentage of PVP K-17 as reported in the previous work [3].

2) For Fiber M1: NMP 30% was used as bore fluid. Since dope and bore fluid compositions were already optimized in the previous work, we changed the coagulation bath composition (from pure water to ethanol 30%). Consequently to this change and connected to the use of a different coagulation bath tank in the hollow fiber spinning plant, it was necessary to change also the air gap (from 25 to 14 cm).

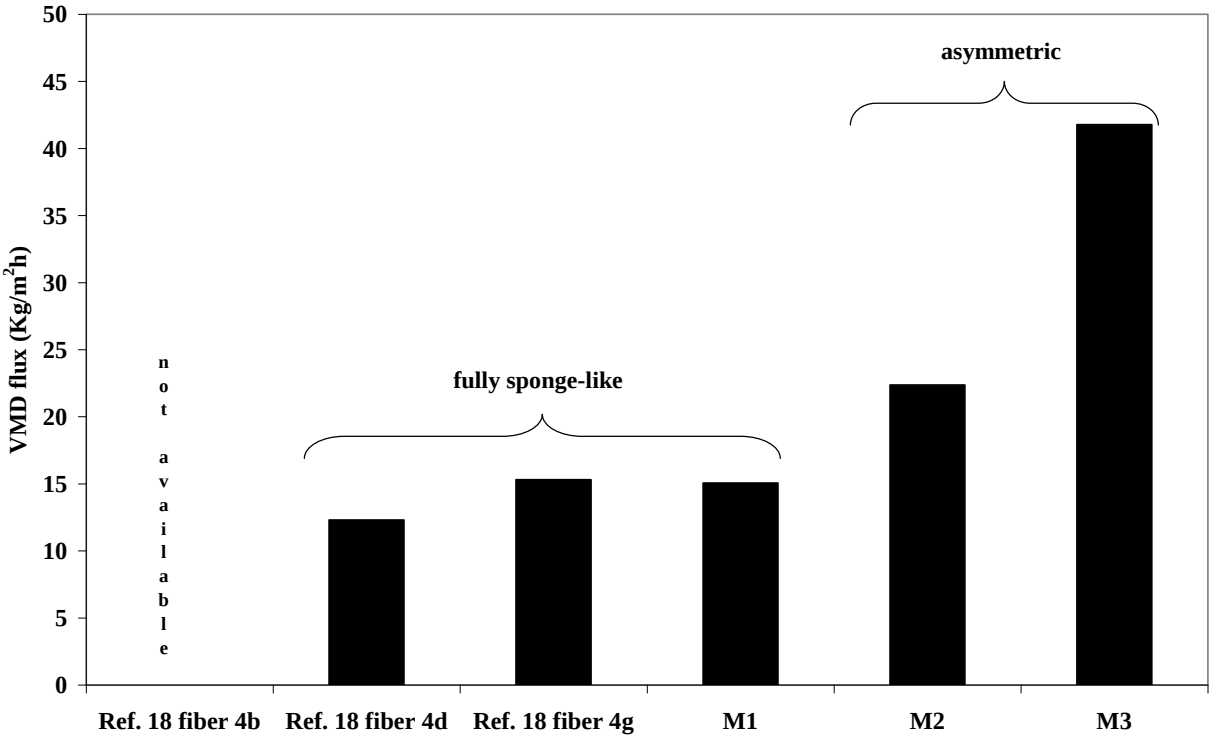

Figure 3.8: Comparison of VMD fluxes of fibers produced in this work and in [3]. Fibers morphologies are highlighted

3) For Fiber M2: The dope composition and spinning conditions are similar to that of M1 and were already optimized [3]. The coagulation bath was H_2O 100% as also in a previous work [3]. Therefore, we have chosen to investigate the effect of H_2O 100% as a bore fluid (not used in [3]) in order to obtain different fiber morphology.

4) For Fiber M3: A further additive, maleic anhydride, was tested as pore former. As described in the Introduction, this additive was already used, in combination with high Mw PVP, for preparation of microfiltration PVDF hollow fibre membranes [4]. This additive was, then, selected and used in the dope composition, since, as reported by many authors, fibers with microfiltration properties can be used in MD. High Mw PVP was replaced by PVP K-17 (with the same concentration used in [3]) in order to facilitate its removal by sodium hypoclorite, as suggested in literature [20-24]. The PVDF

type Solef 1015 and its concentration (15%) were chosen on the basis of what reported in literature, as well as the dope temperature [4]. The bore fluid composition and all the other spinning parameters were also chosen on the basis of our experience [3].

The Comparison of the morphology, properties and performance of the fibers produced in the present work and the reported in [3] is shown in Figure 3.8.

4. Conclusions

In this work, microporous hydrophobic PVDF hollow fibers were produced by the phase inversion method, varying polymer MW and concentration, type and concentration of different additives (H_2O, PVP and AMAL) in the polymeric dope, composition of inner and outer coagulants.
The effect of all these parameters on the morphology of the produced hollow fiber membranes was analyzed. A correlation between the developed morphology, fibers characteristics in terms of thickness and porosity, and the trans-membrane water vapor flux in MD was observed.
In general, fibers showing macrovoids in the structure possess higher porosity, reduced mechanical strength and enhanced flux. The best mechanical properties are obtained when a weak non-solvent, like NMP or EtOH solution, is used as the bore fluid and external coagulant.
It has been shown that the introduction of further pore forming additive (AMAL), combined with the relatively lower composition of polymer into the dope solution (Fiber type M3), leads to the structures exhibiting maximum trans-membrane flux working under both MD configurations (J_{VMD} (50°C)= 41.78 kg/m^{2}h, J_{DCMD} (70°C)= 21.78 kg/m^{2}h). Furthermore, the fluxes obtained are higher or comparable to that mentioned in literature. In particular, the VMD flux is 90% higher than that obtained with the commercial membranes (PP Accurel) when using the M3 membrane. This interesting result can be attributed to the asymmetric structure of the produced (M3) membrane where the spongy layer has a reduced thickness and is supported by a very open finger type structure.

References

[1] A. Mansourizadeh and A. F. Ismail, “Hollow fiber gas – liquid membrane contactors for acid gas capture : A review,” J. Hazard. Mater., vol. 171, pp. 38–53, 2009.

[2] J. C. Jansen, M. Macchione, and E. Drioli, “High flux asymmetric gas separation membranes of modified poly (ether ether ketone) prepared by the dry phase inversion technique,” J. Memb. Sci., vol. 255, pp. 167–180, 2005.

[3] S. Simone, A. Figoli, A. Criscuoli, M. C. Carnevale, A. Rosselli, and E. Drioli, “Preparation of hollow fibre membranes from PVDF / PVP blends and their application in VMD,” J. Memb. Sci., vol. 364, no. 1–2, pp. 219–232, 2010.

[4]] J. Ji, C. Di Cecca, E. M. Schulz, M. Mehta, D. Stead, D. McKinley, and D. H. Koch, “Hollow fibre microfiltration membranes and a method of making these membranes,” Patent N° US 6,890.435 B22005.

[5] J. J. Qin, Y. M. Cao, Y. Q. Li, Y. Li, M. H. Oo, and H. Lee, “Hollow fibre ultrafiltration membranes made from blends of PAN and PVP,” Sep. Purif. Technol., vol. 36, pp. 149–155, 2004.

[6] B. Jung, J. Ki, B. Kim, and H. Rhee, “Effect of molecular weight of polymeric additives on formation , permeation properties and hypochlorite treatment of asymmetric polyacrylonitrile membranes,” J. Memb. Sci., vol. 243, pp. 45–57, 2004.

[7] J. Qin, M. Htun, and Y. Li, “Development of high flux polyethersulfone hollow fiber ultrafiltration membranes from a low critical solution temperature dope via hypochlorite treatment,” J. Memb. Sci., vol. 247, pp. 137–142, 2005.

[8] L. Wan, Z. Xu, and Z. Wang, “Leaching of PVP from Polyacrylonitrile / PVP Blending Membranes : A Comparative Study of Asymmetric and Dense Membranes,” J. Polym. Sceince Part B Polym. Phys., vol. 44, pp. 1490–1498, 2006.

[9] S. Rouaix, C. Causserand, and P. Aimar, “Experimental study of the effects of hypochlorite on polysulfone membrane properties,” J. Memb. Sci., vol. 277, pp. 137–147, 2006.

[10] F. Tasselli, J. C. Jansen, F. Sidari, and E. Drioli, “Morphology and transport property control of modified poly (ether ether ketone) (PEEKWC) hollow fiber membranes prepared from PEEKWC / PVP blends : influence of the relative humidity in the air gap,” J. Appl. Polm. Sci., vol. 255, pp. 13–22, 2005.

[11] Q. Li, Z. Xu, and L. Yu, “Effects of Mixed Solvents and PVDF Types on Performances of PVDF Microporous Membranes,” J. Memb. Sci., 2009.

[12] M. L. Yeow, Y. T. Liu, and K. Li, “Morphological Study of Poly (vinylidene fluoride) Asymmetric Membranes : Effects of the Solvent , Additive , and Dope Temperature,” J. Appl. Polm. Sci 92 (2004) pp.1782-1789.

[13] M. G. Buonomenna, “POLYMER Poly (vinylidene fluoride) membranes by phase inversion : the role the casting and coagulation conditions play in their morphology , crystalline structure and properties,” Eur. Polym. J., vol. 43, pp. 1557–1572, 2007.

[14] E. Drioli, a. Ali, S. Simone, F. Macedonio, S. a. AL-Jlil, F. S. Al Shabonah, H. S. Al-Romaih, O. Al-Harbi, a. Figoli, and a. Criscuoli, “Novel PVDF hollow fiber membranes for vacuum and direct contact membrane distillation applications,” Sep. Purif. Technol., vol. 115, pp. 27–38, Aug. 2013.

[15] E. Fontananova, J. C. Jansen, A. Cristiano, E. Curcio, and E. Drioli, “Effect of additives in the casting solution on the formation of PVDF membranes,” Desalination, vol. 192, no. August 2005, pp. 190–197, 2006.

[16] J. Kim and K. Lee, “Effect of PEG additive on membrane formation by phase inversion,” J. Appl. Polm. Sci., vol. 138, pp. 153–163, 1998.

[17] F. Tasselli, J. C. Jansen, and E. Drioli, “PEEKWC Ultrafiltration Hollow-Fiber Membranes : Preparation , Morphology , and Transport Properties,” J. Appl. Polym. Sci., vol. 91, pp. 841–853, 2004.

[18] F. Tasselli and E. Drioli, “Tuning of hollow fiber membrane properties using different bore fluids,” J. Memb. Sci., vol. 301, pp. 11–18, 2007.

[19] S. P. Deshmukh and K. Li, “Effect of ethanol composition in water coagulation bath on morphology of PVDF hollow ® bre membranes,” J. Memb. Sci., vol. 150, pp. 75–85, 1998.

[20] A. Xu, A. Yang, and S. Young, “Effect of internal coagulant on effectiveness of polyvinylidene fluoride membrane for carbon dioxide separation and absorption,” J. Memb. Sci., vol. 311, pp. 153–158, 2008.

[21] P. Sukitpaneenit and T. Chung, “Molecular elucidation of morphology and mechanical properties of PVDF hollow fiber membranes from aspects of phase inversion , crystallization and rheology,” J. Memb. Sci., vol. 340, pp. 192–205, 2009. Tasselli, F. et al., 2005.

[22] C. A. Smolders, A. J. Reuvers, R. . Boom, and I. M. Wienk, “Microstructures in phase-inversion membranes. Part I. Formation of macrovoids,” J. Memb. Sci., vol. 73, pp. 259–275, 1992.

[23] Y. Liu, G. H. Koops, and H. Strathmann, “Characterization of morphology controlled polyethersulfone hollow fiber membranes by the addition of polyethylene glycol to the dope and bore liquid solution,” J. Memb. Sci., vol. 223, pp. 187–199, 2003.

[24] S. Alobaidani, E. Curcio, F. Macedonio, G. Diprofio, H. Alhinai, and E. Drioli, “Potential of membrane distillation in seawater desalination: Thermal efficiency, sensitivity study and cost estimation,” J. Memb. Sci., vol. 323, no. 1, pp. 85–98, Oct. 2008.

[25] A. Noori, S. Simone, A. Figoli, E. Drioli, Q. F. Alsalhy, and K. T. Rashid, “Poly (vinyl chloride) Hollow-Fiber Membranes for Ultrafiltration Applications : Effects of the Internal Coagulant Composition,” J. Appl. Polym. Sci., vol. 124, pp. 2087–2099, 2011.

CHAPTER 4

Experimental and theoretical evaluation of temperature polarization coefficient in direct contact membrane distillation

1. Introduction

A significant amount of heat is wasted in MD process due to thermal polarization associated with conduction and convection of heat from feed to the permeate side. The problem of thermal polarization becomes worse in DCMD due to direct contact of hot feed and cold distillate with opposite sides of the membrane. Under inappropriate operating conditions and for membrane with high thermal conductivity, the major contribution to heat transfer comes from the conduction through the membrane. The vapors transported from hot feed to the cold distillate side also play their role in inducing thermal polarization. Thermal polarization coefficient (TPC) defined by equation (a) has been established to quantify the thermal losses in MD.

$$TPC = \frac{T_{fm} - T_{pm}}{T_f - T_p} \qquad \text{(a)}$$

Where T_f and T_p are the feed and permeate temperature, respectively in the bulk and subscript m denotes their corresponding values at the membrane surface. The value of temperature polarization coefficient approaching to unity describes a thermally efficient process.

Temperature polarization plays a key role in correctly elaborating heat and mass transfer analysis in DCMD and a lot of studies have been carried out in this context. The significance of temperature polarization was initially underlined quantitatively by Schofield et al [1]. They developed the basic equations to describe heat and mass transfer in MD and highlighted the importance of temperature polarization in designing and operation of large scale MD modules. Martinez-Diez and Vázquez-González [2] proposed a method to evaluate heat and mass transfer coefficients of membrane and the boundary layer heat transfer coefficients on the basis of the measurements of mass flux and evaporation efficiency. The effect of concentration and temperature polarization on the effective pressure gradient across the membrane was quantified by using an overall coefficient that coincides with thermal polarization coefficient when pure water is used as feed. Phattaranawik et al [3] analyzed the effect of spacers on mass flux enhancement in direct contact membrane distillation. It was observed that in presence of spacers, the value of temperature polarization approaches to unity and thus the flux increases.

Effect of operational parameters including the hydrodynamic and thermal conditions and feed concentration on heat and mass transport in MD has been interesting to investigate. Yun et al [4] studied the effect of feed concentration, feed temperature and feed flow rates on mass transfer by using highly concentrated NaCl solutions as feed in DCMD. The authors proved that the increase of NaCl in solution results in flux decline due to decrease in driving force. However, another phenomenon has to be taken into account: during the process, the concentration of the solution changes continuously due

to the migration of the solvent from feed to the permeate side. The concentration affects not only the vapor pressure of the feed (i.e., the driving force) but also the solution properties including viscosity, density, thermal conductivity etc. These properties consequently affect the other key parameters including solution hydrodynamic and diffusion properties. The changes in hydrodynamic of the solution and diffusion of the solvent can affect the temperature polarization coefficient and mass transfer coefficient.

In this work, heat and mass transfer in direct contact membrane distillation has been analyzed by using a cell specifically designed for this purpose. The effect of hydrodynamic and thermal conditions on heat and mass transport phenomenon in DCMD using pure water as feed solution has been investigated. Finally, the effect of NaCl solution concentration on heat and mass transfer has also been incorporated in the analysis.

2. Theory

Flux in membrane distillation is proportional to the vapor pressure gradient created across a microporous hydrophobic membrane. The Antoine equation can be applied to calculate the vapor pressure P at any temperature T.

$$P = \exp\left(A - \frac{B}{T - C}\right) \tag{1}$$

where 23.238, 3841.273 and 42 have been used as the values of the constants A, B, C respectively, for water [5].

The theoretical flux (J) can be calculated by the following relation [4].

$$J = \frac{P_{fm} - P_{pm}}{R_m(t) + R_f(t) + R_c(t)} \tag{2}$$

where P_{fm} and P_{pm} are the vapor pressures at the membrane surface on feed and permeate side respectively, R_m, R_c and R_f are the resistances due to the membrane, solution concentration and fouling, respectively. For a clean membrane using distilled water as feed and permeate, R_c and R_f are zero. R_m can be estimated by Knudsen and molecular diffusion model or the combination of both. If the Knudsen model is utilized, R_m can be described according to Mart and Rodr [6].

$$R_m(t) = \frac{\delta \tau RT}{\varepsilon M_w D_{kA}} \tag{3}$$

where δ is the membrane thickness, τ is the tortuosity factor, ε is the porosity, T is the absolute temperature, M_w is the molecular weight of water and D_{KA} is the Knudsen diffusion coefficient.

D_{KA} can be calculated by the following expression [4].

$$D_{KA} = 97r\left(\frac{T}{M_w}\right)^{0.5} \tag{4}$$

where r is the mean pore size.

For molecular diffusion model, the following representative expression is used [4].

$$R_m(t) = \frac{\delta \tau R Y_{\ln} T}{\varepsilon M_w P D_{WA}} \quad (5)$$

where Y_{ln} is the log mean partial pressure of air, P is total pressure and D_{WA} is the molecular diffusion coefficient which can be calculated by using the following expression.

$$D_{wA} = 1.19 \times 10^{-4} \left(\frac{T^{1.75}}{P} \right) \quad (6)$$

The resistance to the mass transport can also be expressed in terms of combined Knudsen and molecular diffusion model.

$$R_m(t) = \frac{\delta \tau R T}{\varepsilon M_w D_{kA}} + \frac{\delta \tau R Y_{\ln} T}{\varepsilon M_w P D_{WA}} \quad (7)$$

Experimentally, feed side boundary layers resistances and membrane resistance to mass transfer can be calculated by the following expressions [7].

$$R_{fb} = \frac{P_{fm} - P_{fb}}{J} \quad (8)$$

$$R_m = \frac{P_{fm} - P_{pm}}{J} \quad (9)$$

$$R_{pb} = \frac{P_{pm} - P_{pb}}{J} \quad (10)$$

where R_{fb} and R_{Pb} are the feed and permeate boundary layer resistances, respectively.

The heat transfer in membrane distillation takes place in three steps: the heat transfer from the bulk feed side to the membrane surface, the transfer of the heat through the membrane and heat transferred from the membrane surface to the bulk of the permeate. These steps can be expressed by the following relations.

$$Q_f = h_f (T_f - T_{fm}) \quad (11)$$

$$Q_p = h_p (T_{pm} - T_p) \quad (12)$$

$$Q_m = \frac{K_m}{\delta} (T_{fm} - T_{pm}) + JH\{T\} \quad (13)$$

where h_f and h_p represent the heat transfer coefficients for the feed and permeate side respectively, K_m is the thermal conductivity of the membrane and H is the enthalpy at temperature T.

K_m has been calculated by using the widely accepted isostrain model.

$$K_m = \varepsilon K_g + (1 - \varepsilon) K_p \quad (14)$$

where K_g and K_p are the thermal conductivities of air and membrane material (polymer), respectively.

At steady state,

$$Q_F = Q_p = Q_m \tag{15}$$

$$h_p(T_{pm} - T_p) = h_f(T_f - T_{fm}) = \frac{k_m}{\delta}(T_{fm} - T_{pm}) + JH\{T\} \tag{16}$$

Theoretically, heat transfer coefficients can be calculated by the following general expression.

$$hi = Nu_i K_i / D_h \tag{17}$$

where

Nu Nusselt number

D_h hydraulic diameter

K Thermal conductivity

Nusselt number can be calculated according to the type of the flow (laminar or turbulent).

Different expressions are available in literature for determination of Nusselt number for both laminar and turbulent flow conditions. A list of the commonly used relationships for laminar flow has been provided in Table 4.1.

Table 4.1: Heat transfer correlations used in the literature for laminar flow

$Nu = 1.86\left(\frac{\mathrm{Re\,Pr}}{L/D}\right)^{1/3}$	(18)	[8]
$Nu = 4.36 + \frac{0.036\,\mathrm{Re\,Pr}(D/L)}{1 + 0.0011(\mathrm{Re\,Pr}(D/L)^{0.8}}$	(19)	[9]
$Nu_{cooling} = 11.5(\mathrm{Re\,Pr})^{0.23}(D/L)^{0.5}$	(20)	[5]
$Nu_{heating} = 15(\mathrm{Re\,Pr})^{0.23}(D/L)^{0.5}$	(21)	[5]
$Nu = 0.13(\mathrm{Re})^{0.64}(\mathrm{Pr})^{0.38}$	(22)	[5]
$Nu = 1.95\left(\frac{\mathrm{Re\,Pr}}{L/D}\right)^{1/3}$	(23)	[10]
$Nu = 0.097(\mathrm{Re})^{0.73}(\mathrm{Pr})^{0.13}$	(24)	[5]
$Nu = 3.66 + \frac{0.104\,\mathrm{Re\,Pr}(D/L)}{1 + 0.0106(\mathrm{Re\,Pr}(D/L))^{0.8}}$	(25)	[10]

Re and *Pr* in Table 4.1 are the Reynolds and Prandtl numbers respectively, *D* is the diameter and *L* is the length of the channel.

Once heat transfer coefficients (h_i) are known, the corresponding temperatures at the membrane surfaces can be calculated by the following equations [11].

$$T_{fm} = T_f - (T_f - T_p)\frac{(1/h_f)}{1/(h_v + k_m/\delta) + 1/h_p + 1/h_f}) \qquad (26)$$

where

$$h_v = \frac{J\Delta H_v}{T_{fm} - T_{pm}} \qquad (27)$$

where H_v is the vapor enthalpy and can be calculated by using the following thermodynamic relationship at any temperature *T*.

$$H_v\{T\} = 1.7535T + 2024.3 \qquad (28)\ [12]$$

where *T* is in K and H_v is in kJ/kg.

For theoretical analysis, equations (26) and (27) were solved by using iterative method.

Thermal efficiency (*TE*) can be defined as the ratio between the heat transported with the vapors to the total heat transported across the membrane.

$$TE(\%) = \frac{JH_v\{T\}}{JH_v\{T\} + \frac{K_m}{\delta}\left(T_{fm} - T_{pm}\right)} \times 100 \qquad (29)$$

3. Experimental

The experimentation was performed by using a specifically designed cell that contains the sensors positioned at specific locations within the cell to measure the bulk and surface temperatures at both feed and permeate sides. The detailed cell description is given in Figure 4.1. The cell consists of two halves made of Teflon with the temperature sensors located at specific points. Two halves can be clamped together to hold the flat sheet membrane between them. An aluminum mesh has been incorporated on distillate side to support the membrane. There are eight sensors on each side of the cell. Four sensors on each side are located on the membrane surface and the remaining four are devoted to measure the bulk temperature. For simplicity, the average of the temperatures measured at the membrane surface and in the bulk phases has been taken as the representative temperature of the corresponding phases. Temperatures were monitored by platinum thermocouples (Pt100) with sensitivity ±0.1 °C. The local interruption in flow dynamic caused by the sensors within the cell has been neglected due to very small diameter of the sensors as compared to the active dimensions of the cell.

The microporous hydrophobic PVDF commercial membranes used (M09G002OH500E) were kindly supplied by GVS S.P.A. The membranes have 0.2 µm as mean pore size, 192 µm as thickness and 56% as overall porosity. The porosity measurements were carried out by using the gravimetric method according to the procedure described by Simone et al [13]. The method relies on measuring the weight

of liquid entrapped within the membrane pores. Porosity measurements were performed twice; each time on 3 pieces of membrane with different dimensions and the average of the six specimens was considered as the final value. The effective area of the membrane clamped between two halves of the cell is 24.9 x 9.85 cm^2 while the depth of the channel on each side is 1.3 cm. The temperature measured by the sensors at different locations can be recorded and displayed in real time in the form of graphs with the aid of Lab view software. The software allows importing of data in some other software like MS Excel for the further data processing.

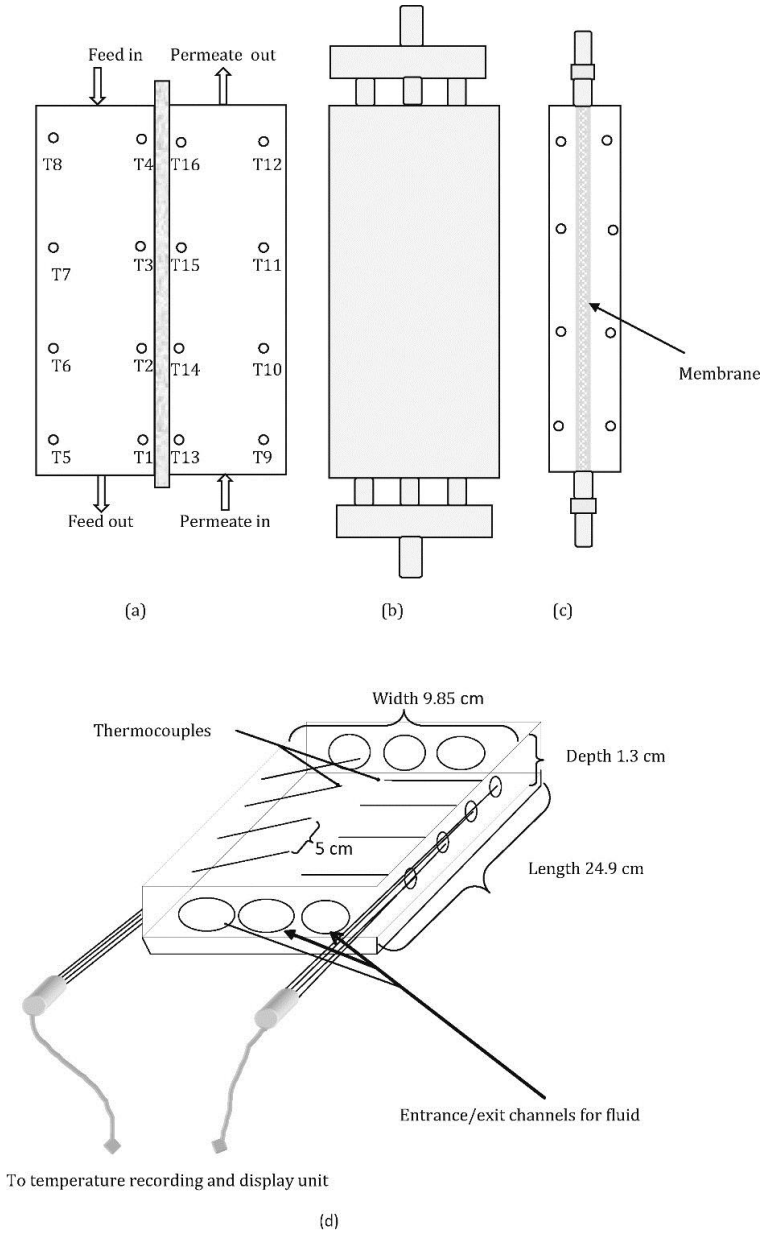

Figure 4.1: (a) Insight of the cell. Sensors1-4 are located in the bulk whereas sensors 5-8 measure the temperature at the membrane surface on the feed side. Sensors 13-16 are located at membrane surface whereas sensors 9-12 measure the bulk temperature on permeate side. (b) Front view of the cell (c) side view of the cell (d) geometrical features of one half of the cell

During the first phase, the experimentation has been performed by using double distilled water as feed and permeate. The experimentation has been performed at various hydrodynamic conditions varying the feed flow rate from 30 L/h to 150 L/h (corresponding to *Re* of 272 to 1360) while keeping the

permeate flow rate constant at 50L/h. The feed inlet temperature has been kept constant at 55±0.5 ^{o}C while the permeate inlet temperature has been set at 10^{o}C. Schematic of the set-up used for MD has been given in Figure 4.2. The effect of feed inlet temperature has been explored by using the fixed feed flow rate of 70L/h and feed inlet temperature ranging from 45^{o}C to 75^{o}C with an interval of 10^{o}C each. In second phase, the effect of solution concentration has been explored by using NaCl solution with initial concentration of 1 M and feed flow rate of 70L/h.

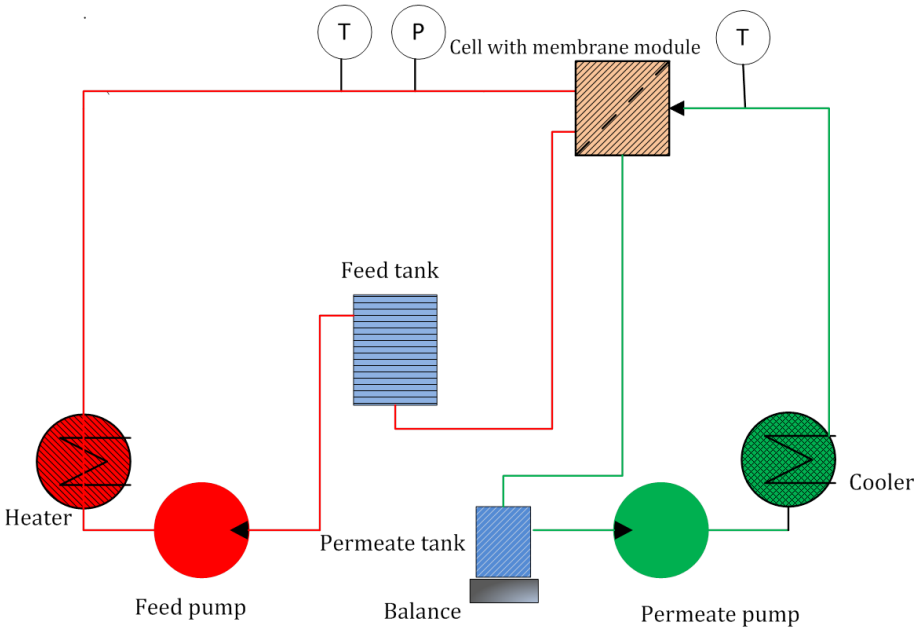

Figure 4.2: Set-up used in the experimentation

4. Results and discussion

4.1 Effect of hydrodynamic conditions

The trans-membrane flux measured at various *Re* and the corresponding feed side boundary layer resistance (R_{fb}) calculated according to equation 8 are shown in Figure 4.3. The figure indicates that the trans-membrane flux increases by increasing the *Re*. By increasing the *Re*, the resistance to the mass transfer offered by the feed side boundary layer decreases and the heat transfer from the bulk to the membrane surface becomes more efficient. Consequently, the trans-membrane flux increases.

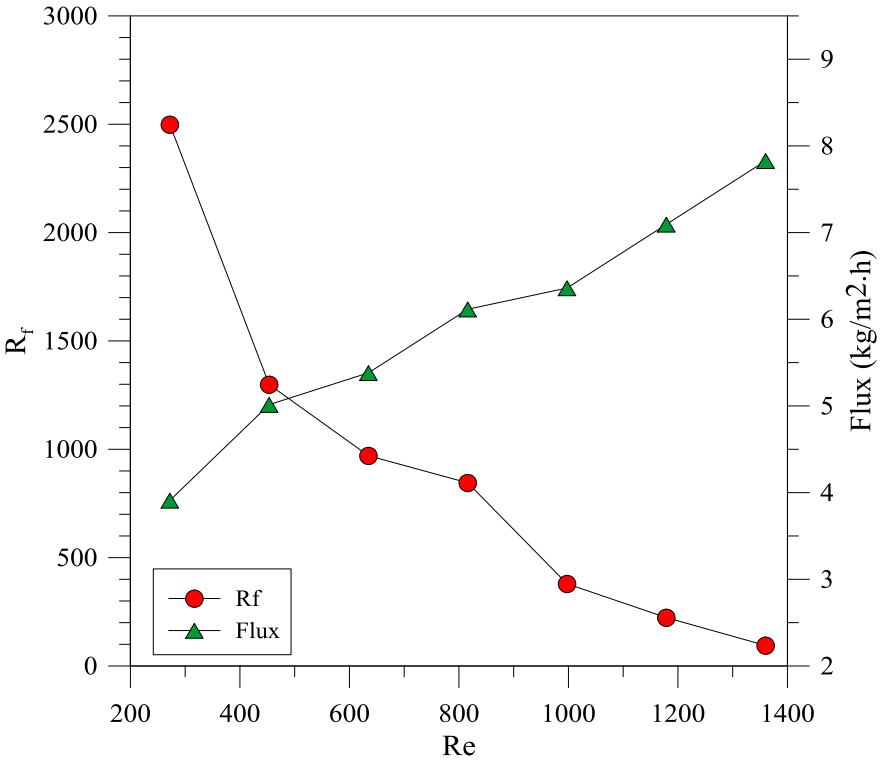

Figure 4.3: Flux and feed side boundary layer resistance as function of Re

The flux observed during the experimentation is also dependent on the resistance offered by the membrane. The experimental feed side boundary layer and membrane resistance determined experimentally and calculated theoretically under the hydrodynamic conditions studied are compared in Table 4.2. It is apparent from the table that at *Re* of 272, the resistance to mass transfer offered by the feed side boundary layer is similar to that for the membrane. However, R_{fb} drops dramatically when the feed flow rate is increased. The membrane resistances shown in the table indicate that the molecular diffusion model and the transition model describe the resistance realistically well while the resistance predicted by Knudsen diffusion model is too low than the experimental value.

The theoretical value of the membrane resistance for various hydrodynamic conditions was calculated by using the Knudsen diffusion model, molecular diffusion model and the combined Knudsen and molecular diffusion model. It is widely accepted in the literature that the mode of vapor transport through the membrane depends upon the pore size and feed temperature. If the mean free path of the water vapors is greater than the pore diameter, the collision of the vapors with the pore wall would be dominant and the mass transfer would be described by Knudsen diffusion model. On the other hand, when the mean free path of water vapors is shorter than the pore size, the collision of vapors with each other would be dominant and molecular diffusion model would characterize the mass transport through the membrane. However, in most cases of the practical interest, the pore size of the membrane is comparable to the mean free path of water molecules and the mass transport is described by the combined Knudsen and molecular diffusion model. The flux calculated on the basis of Knudsen diffusion model is greater than that for the other two models.

The value of membrane resistances calculated on the basis of various models have also been illustrated in Table 4.2 and compared to those obtained experimentally. It is evident from the table that Knudsen diffusion model predicts the values of the resistance much lower than the ones obtained experimentally under all the hydrodynamic conditions investigated. However, at lower Reynolds

number the both molecular and combined Knudsen and molecular diffusion models are adequate to describe the mass transport through the membrane. As the Reynolds number increases, the experimentally determined resistance follows more closely to the prediction of combined Knudsen and molecular diffusion model.

Table 4.2: Feed side boundary layer resistance and membrane resistance to the mass transfer measured experimentally and calculated on the basis of different models

Re	R_{fb}*(eq. 8)*	R_{mexp} *(eq.9)*	R_{mk}*(eq.3)*	D_{mk}*(%)*	R_{mm}*(eq.5)*	D_{mm}*(%)*	R_{mcom}*(eq.7)*	D_{mcom}*(%)*
272	2498	2225	22.6	98.98	2165	2.68	2269	-1.98
453	1298	2404	22.7	98.98	2233	-0.38	2249	-1.08
635	970	2355	22.8	98.98	2256	-1.40	2241	-0.74
816	845	2327	22.8	98.98	2233	-0.38	2246	-0.97
997	379	2262	22.9	98.97	2302	-3.47	2228	-0.13
1179	223	2218	23	98.97	2334	-4.89	2219	0.24
1360	95	2183	23	98.97	2363	-6.20	2212	0.57

Maximum standard deviation for R_{mexp} 10.12%

R_{fb} Feed side boundary layer resistance (experimental)
R_{mexp} Experimental membrane resistance
R_{mk} Membrane resistance calculated by using Knudsen diffusion model
R_{mm} Membrane resistance calculated by using molecular diffusion model
R_{mcom} Membrane resistance predicted by combined Knudsen-molecular diffusion model
D Difference from experimental value

Among all the membrane characteristics, tortuosity is the most controversial in the sense that its different values have been used by the researchers to predict the flux. Lower value of tortuosity factor favors the high mass transfer flux through the membrane. The value of the tortuosity factor for the membranes prepared through the phase inversion can be determined by the following relationship [14].

$$\tau = \frac{(2-\varepsilon)^2}{\varepsilon} \qquad (30)$$

For overall porosity of 56% of the membrane used in the current study, the value of τ comes out to be 3.7. Many researchers used 2 as the value of the tortuosity factor [15], [16]. Khayet et al [17] performed the gas permeation tests to calculate the value of tortuosity factor of 2.1. In the current study, both 2.1 and 3.7 have been used as values of τ to calculate the theoretical flux.

The values of the flux obtained by using Knudsen diffusion model (J_k), molecular diffusion model (J_m) and the combined Knudsen and molecular diffusion model (J_{com}) for tortuosity factors applied are given in Table 4.3. It can be observed that the experimental data follows closely to the molecular diffusion model and the combined Knudsen and molecular diffusion model when the value of τ is equal to 3.7 and 2.1, respectively.

Table 4.3: Experimental and theoretical flux for various values of τ by using Knudsen diffusion model, molecular diffusion model and the combined Knudsen and molecular diffusion model

Re	J_{exp}	*τ=2.1*			*τ=3.7*		
		J_k	J_m	J_{com}	J_k	J_m	J_{com}
272	3.91	21.59	7.21	5.40	9.45	3.15	2.36
453	5.01	27.33	9.17	6.87	11.96	4.01	3.00
635	5.38	27.82	9.42	7.04	12.17	4.12	3.08
816	6.12	29.73	9.97	7.47	13.01	4.36	3.27
997	6.36	35.25	11.91	8.90	15.42	5.21	3.89
1179	7.09	38.46	13.03	9.73	16.83	5.70	4.26
1360	7.83	41.36	13.92	10.42	18.09	6.09	4.56

Temperature polarization coefficient can be quantified by equation (a) and describes the effective temperature gradient across the membrane. The transfer of heat from the hot feed side through conduction and latent heat of vaporization associated with the transport of vapors causes a decrease in temperature at the membrane surface on feed side and increases the corresponding temperature at permeate side. Thus the effective driving force between the two phases reduces. When the fluid velocity at the fluid-membrane interface is low, the transfer of heat from the bulk to the membrane surface is hindered by the boundary layer and favors the reduction in temperature polarization coefficient. On the other hand, an increase in fluid velocity improves the Reynolds number of the fluid and decreases the thickness of the boundary layer. Consequently, the difference between the temperature at the membrane surface and the bulk decreases and imparts a positive impact to temperature polarization coefficient.

When the heat transfer coefficients, bulk temperatures for feed and permeate sides and overall trans-membrane flux are known, the corresponding temperature polarization coefficient can be calculated by using the following relation [3].

$$TPC = 1 - \left(\frac{JH_v\{(T_{fm} + T_{pm})/2\}}{T_f - T_p} \left(\frac{1}{h_f} + \frac{1}{h_p} \right) \right) \qquad (31)$$

The experimentally measured flux and bulk temperature and theoretically calculated heat transfer coefficients were used in equation (31) to estimate the theoretical value of TPC at different conditions. The values of temperature polarization coefficients determined experimentally and those obtained by using equation (31) under various hydrodynamic conditions have been shown in Figure 4.4. The figure indicates that the increase in TPC with *Re* is quite significant at low values of *Re*. With further increase in *Re*, the temperature polarization coefficient increases but the slope of the curve decreases. The increase in temperature polarization coefficient with *Re* is quite rational as the flow pattern developed within the cell by increasing *Re* favors the mixing of the fluid present at the membrane surface and in the bulk. Consequently, the temperature distribution within the cell becomes more

homogeneous and attributes a positive impact to TPC. The effect is more pronounced at low *Re*, as smaller increase will enhance the mixing significantly. Significantly different values of experimental and theoretical TPC can be attributed with higher uncertainty in experimental temperature at high *Re*. At high *Re*, the membrane support starts to bend and temperature sensors do not measure the surface temperature accurately. Furthermore, the disturbance caused by the sensors start to interfere with the normal flow patterns.

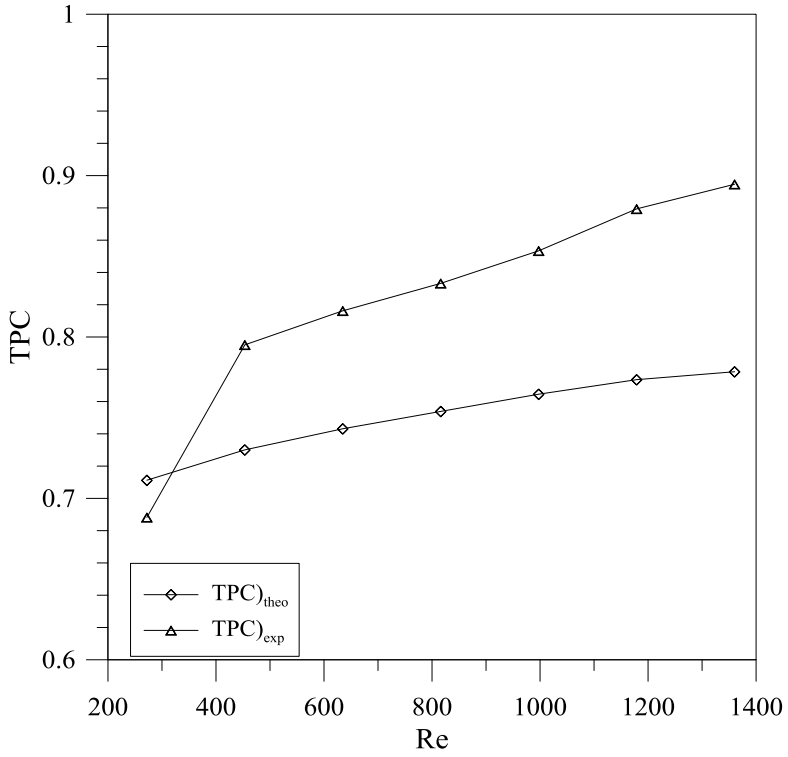

Figure 4.4: Theoretical and experimental temperature polarization coefficient as function of Re

Thermal efficiency (eq. 29) can be used as an indicator of the efficient utilization of the heat in the process. The dependence of thermal efficiency on hydrodynamic conditions is illustrated in Figure 4.5 along with feed side heat transfer coefficient. Thermal efficiency improves from ~13.5% to ~19.5% as the Reynolds number increases from 272 to 1360. This observation is essentially coherent with the trend observed for trans-membrane flux (Figure 4.3). The increased trans-membrane flux implies higher fraction of heat transported through the membrane via convection and as a result, the thermal efficiency of the system improves. The same trend can be seen for heat transfer coefficient which indicates the efficiency of heat transfer from bulk to the membrane surface. The resistance to the mass and associated heat transfer decreases sharply as the feed flow rate is increased. Consequently, the heat transferred from the bulk to the membrane surface becomes more efficient and a higher value of heat transfer coefficient is observed.

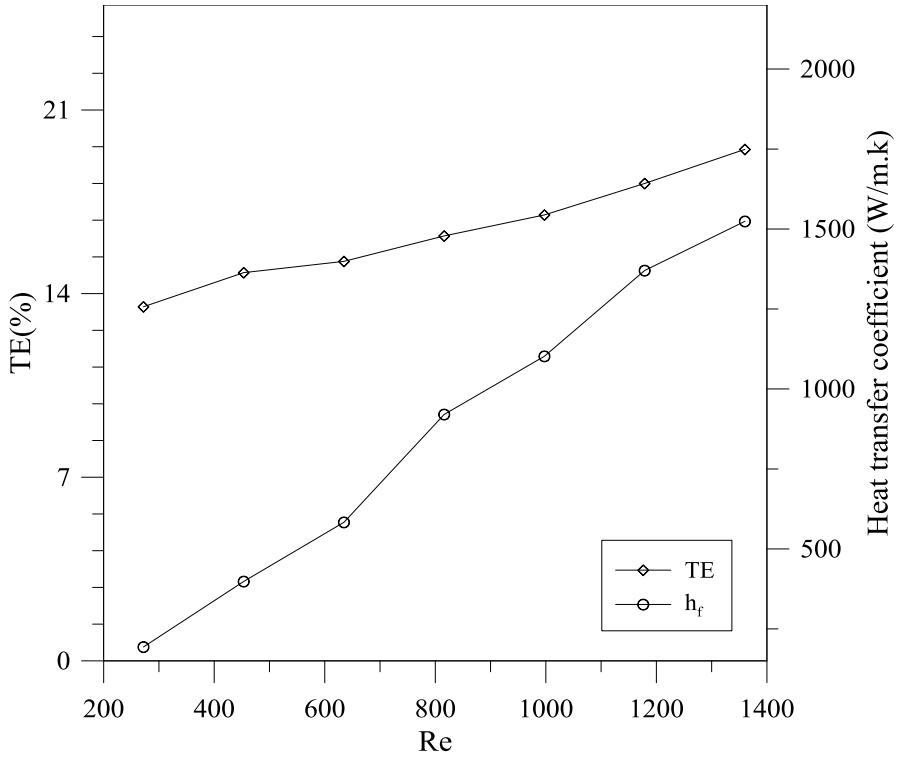

Figure 4.5: Effect of Reynolds number on thermal efficiency and heat transfer coefficient

The dependence of trans-membrane flux on feed side heat transfer coefficient has been shown in Figure 4.6. Flux shows a strong dependence on heat transfer coefficient for low *Re* ranges and starts to be level off at high *Re*.

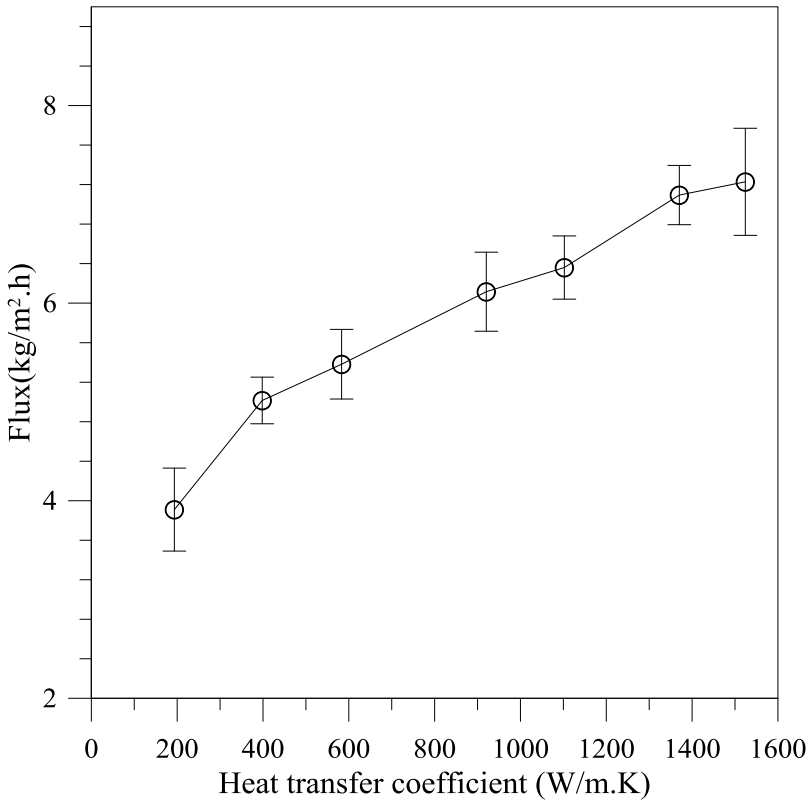

Figure 4.6: Dependence of trans-membrane flux on heat transfer coefficient of feed side

As illustrated by equation (16), at steady state the heat transferred from bulk of feed to the membrane surface is equal to the heat transferred through the membrane through convection and conduction and the heat transferred from the membrane to the permeate. This assumption allows calculating the feed and permeating heat transfer coefficients, once the bulk and interfacial temperatures are known (eq. 16). At steady state, neglecting the conductive heat flux, equation (16) can be written as [3].

$$h_p(T_{pm}-T_p) = h_f(T_f-T_{fm}) = JH\{T\} \qquad (32)$$

While equation (32) has been used to calculate experimental heat transfer coefficient, in literature, different expressions are available to calculate theoretical heat transfer coefficient based on the fluid properties and the geometry of the system. The heat transfer correlations for laminar flow are described by equations 18-25. The values of theoretically calculated heat transfer coefficients were in similar rages of those calculated experimentally for weak hydrodynamic conditions applied as shown in Table 4.4. However, experimental heat transfer coefficient deviates more strongly from theoretical predictions at high *Re*. The most probable reason for this behavior can be the geometry of the cell. As shown in Figure 4.1, the cell has three entrance and exit channels. At high *Re*, the entrance and exit effects can interrupt the normal flow pattern developed at low *Re*. Secondly, the membrane has been supported by using an aluminum mesh. At high *Re*, aluminum mesh can bend and contact of thermal sensors with the membrane may not remain very precise. Both these factors are the possible responsible for high deviation of experimental heat transfer coefficient from the experimental one at *Re*.

Table 4.4: Experimental and theoretical feed side heat transfer coefficients calculated for various hydrodynamic conditions

Re	*Eq. 21*	*Eq. 23*	*Eq. 18*	*Eq. 19*	*Eq. 22*	*Eq.24*	*Eq. 25*	*Exp.*
272	472	241	229	205	210	190	284	193
453	531	285	272	258	291	277	369	398
634	575	319	304	310	361	354	439	583
816	609	347	331	360	424	425	497	920
997	638	371	354	408	482	492	549	1185
1178	664	392	374	456	537	556	594	1782
1360	686	412	393	502	588	617	634	1838

4.2 Effect of feed inlet temperature

The effect of feed temperature on heat and mass transfer has been scrutinized by varying the feed inlet temperature from 45^{o}C to 75^{o}C with an interval of 10^{o}C each. The experimental flux compared with theoretical predictions has been shown in Figure 4.7. The flux increases exponentially by increasing the feed inlet temperature, as commonly accepted in the literature. The figure discloses that the experimental flux can be simulated reasonably well by using combined Knudsen and molecular diffusion model.

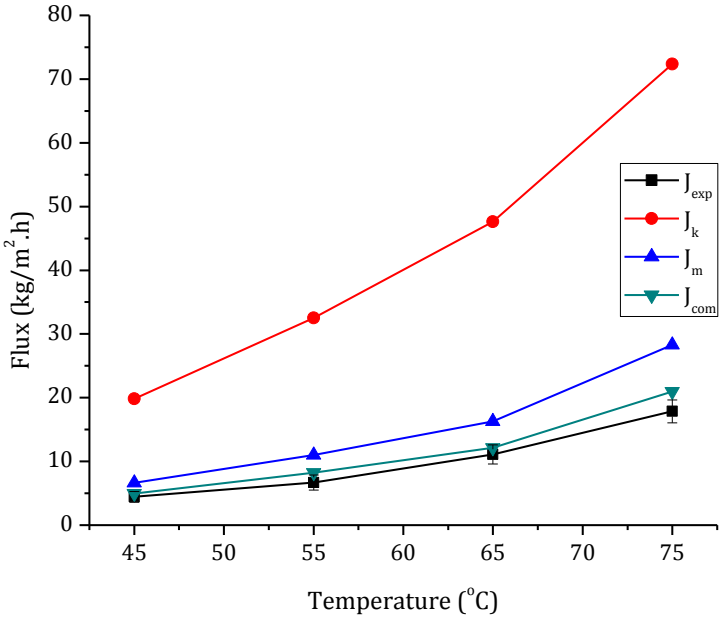

Figure 4.7: Effect of feed inlet temperature on trans-membrane flux. J_{exp}, J_k, J_m and J_{com} represent the experimental flux and that calculated on the basis of Knudsen diffusion model, molecular diffusion model and combined Knudsen and molecular diffusion models, respectively.

The feed side boundary layer resistance calculated at temperature conditions investigated has been shown in Table 4.5. The table shows that the feed side boundary layer resistance increases with rise in temperature. It can be related with increased convective and conductive heat flux through the membrane at higher temperature which induces a higher temperature gradient between the bulk and the membrane surface. Additionally, the increased evaporation at the membrane surface at high temperature induces a cooling effect, leading towards increased boundary layer resistance.

Table 4.5: Resistance to mass transfer offered by feed side boundary layer at various feed inlet temperatures

Temperature (^{o}C)	*R_f(eq.8)*	*Experimental S.D%*
45	401	6.9
55	450	9.4
65	505	8.4
75	534	11.2

Temperature polarization coefficient as function of feed inlet temperature has been shown in Figure 4.8. In the same figure, the total heat flux transported across the membrane and the Reynolds numbers corresponding to each temperature condition applied have been shown. The figure indicates that temperature polarization coefficient decreases when feed inlet temperature increases from 45^{o}C to 75^{o}C. As said in the above paragraph, rise in feed temperature increases the rate of heat transport from the feed to the permeate side and decreases the temperature at the membrane surface on feed side. The

transfer of heat from feed to the permeate side causes an increase of the surface temperature on the permeate side, as compared to its value in the bulk. The net result of the increased transport of heat via convection and conduction through membrane combined with the cooling effect caused by the evaporation at the feed side on membrane surface appears as a decrease in the observed TPC. On the other hand, the increase in temperature at the feed side improves the hydrodynamic of the system and *Re* increases. Contrary to the effect of increased heat transfer, the increase in *Re* tends to increase the temperature polarization coefficient. However, the impact of heat transfer plays the decisive role in dictating the overall trend of temperature polarization coefficient with respect to feed temperature.

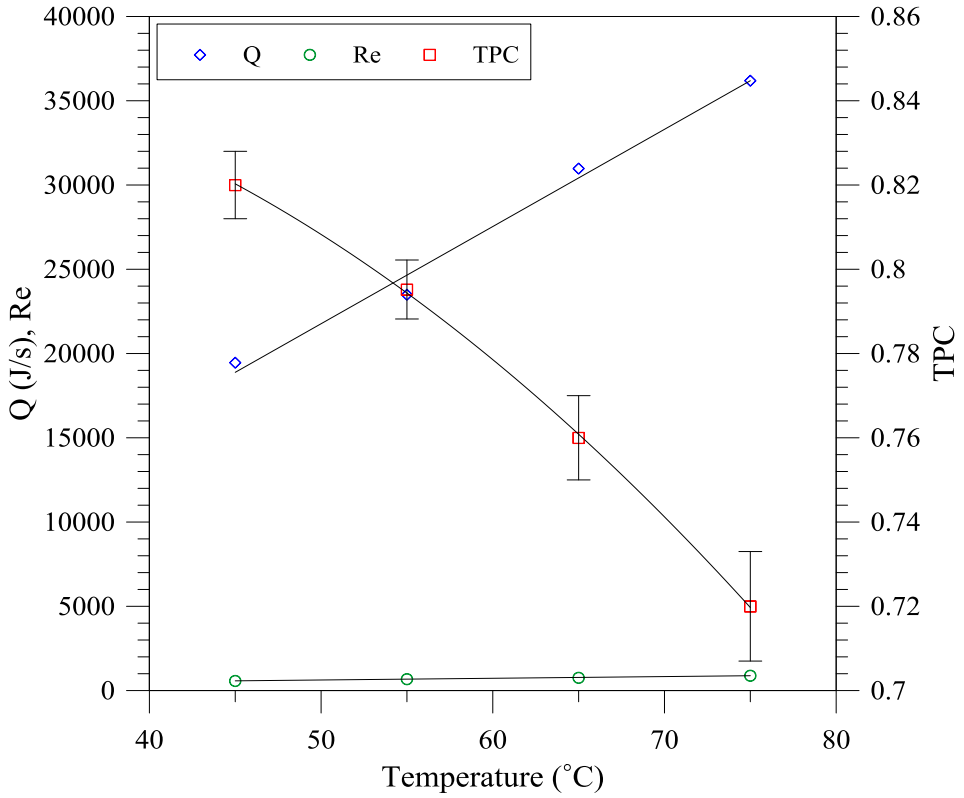

Figure 4.8: Total heat flux, Reynolds number and temperature polarization coefficient as function of feed inlet temperatures

The total heat flux, convective heat flux across the membrane and thermal efficiency for various feed inlet temperatures have been shown in Figure 4.9 which points out that thermal efficiency increases linearly with feed inlet temperature. The conductive heat flux increases linearly with temperature while the increase in convective flux with temperature is exponential. The net effect is an increase in thermal efficiency with feed inlet temperature. The relatively low values of thermal efficiency observed in this study are due to low overall porosity of the membrane that favors the conductive heat transfer across the membrane while limits the transport of vapors.

The theoretical heat transfer coefficients calculated according to the heat transfer models proposed by [5] are compared with those based on experimental data in Table 4.6. Generally a good agreement between experimental and theoretical values can be observed. Similarly, the corresponding temperatures calculated according to equation (26) are shown in Table 4.7 and agree well with the experimental values. However, similar to the observation made in section 4.1, no single correlation was found to fit the results well.

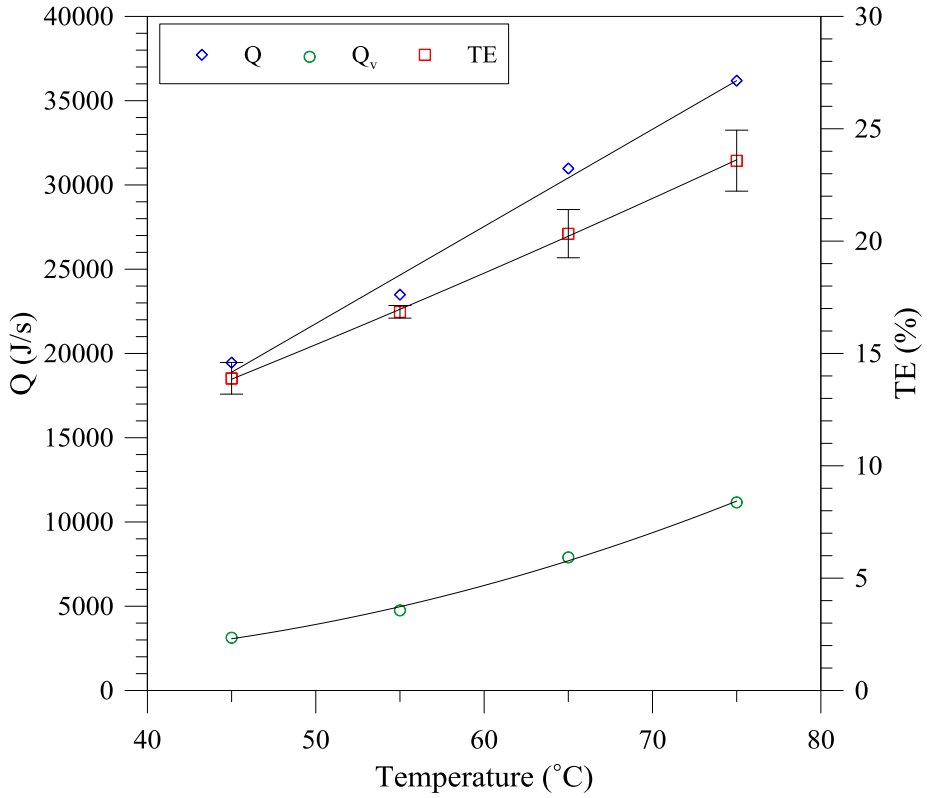

Figure 4.9: Total heat transfer flux (Q), convective heat transfer flux (Q_v) and thermal efficiency as function of feed inlet temperature

Table 4.6: Theoretical and experimental heat transfer coefficients for feed side

Temperature (^oC)	*h_f ($W/m^2.K$)*		
	On the basis of [5] (equation 24)	*Exp.*	*S.D (%)*
45	756.6	679	8
55	855.9	774	9
65	912.8	846	6
75	920.5	886	10

Table 4.7: Feed side membrane surface temperatures calculated by using heat transfer coefficients given in Table 4.6

Feed inlet temperature (^oC)	T_{fm} *(^oC)*		
	On the basis of [5]	*Exp.*	*S.D (%)*
45	42.2	42.0	2.4
55	51.4	50.1	3.5
65	57.8	57.5	1.2
75	63.9	65.2	2.8

4.3 Effect of feed concentration

The effect of feed concentration on mass and heat transfer has been investigated at various feed inlet temperatures by using the initial feed concentration of 1M. The flux obtained at applied feed inlet temperature as function of concentration is shown in Figure 4.10. The figure indicates a decreasing trend of flux with increase in concentration for all the temperatures investigated. It has been well accredited that the flux in membrane distillation is a function of both feed temperature and its concentration. The former has the exponential effect on the flux while the later changes the flux marginally, especially at lower concentrations. The effect of feed concentration on vapor pressure of the solution can be determined by using the relationship [4].

$$P = P^o(1-x)(1-0.5x-10x) \qquad (33)$$

where P is the partial pressure of the solvent in the solution, P^o is the vapor pressure of pure solvent and x is the mole fraction of solute in the solution.

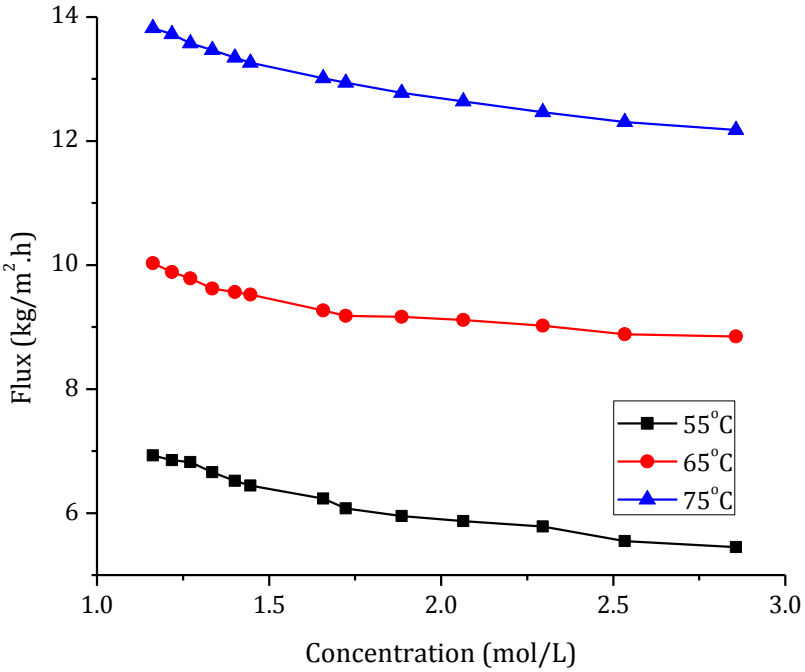

Figure 4.10: The effect of feed solution concentration on trans-membrane flux observed at different feed inlet temperatures

The effect of temperature polarization on flux has been realized by considering the difference in measured temperatures in the bulk phases and at the membrane surfaces and is shown in Figure 4.11. The quantitative role of solution concentration in flux reduction has been illustrated in the same figure. It can be noticed from the figure that the major contribution in flux reduction comes from thermal polarization effect (~24-29%, as the feed concentration rises from 1 M to 2.85 M) while the effect of feed concentration becomes prominent only at higher feed concentrations (~1.5-6% for the concentration of 1M to 2.85 M).

An important observation that can be made from the Figure 4.11 is the dependence of flux reduction due to thermal polarization effects on the feed concentration. This effect can be attributed towards the increase in solution viscosity and density with concentration. The increased solution viscosity hinders diffusion of vapors and associated heat transfer from the bulk of the feed to the membrane surface while both viscosity and density also negatively influence the *Re* which further decreases the heat and mass transfer from bulk to the membrane-solution interface. The change in solution concentration and the corresponding Reynolds number as function of experimental time for different solution temperature has been shown in Figure 4.12. *Re* decreases due to increase in solution viscosity and density as the concentration increases.

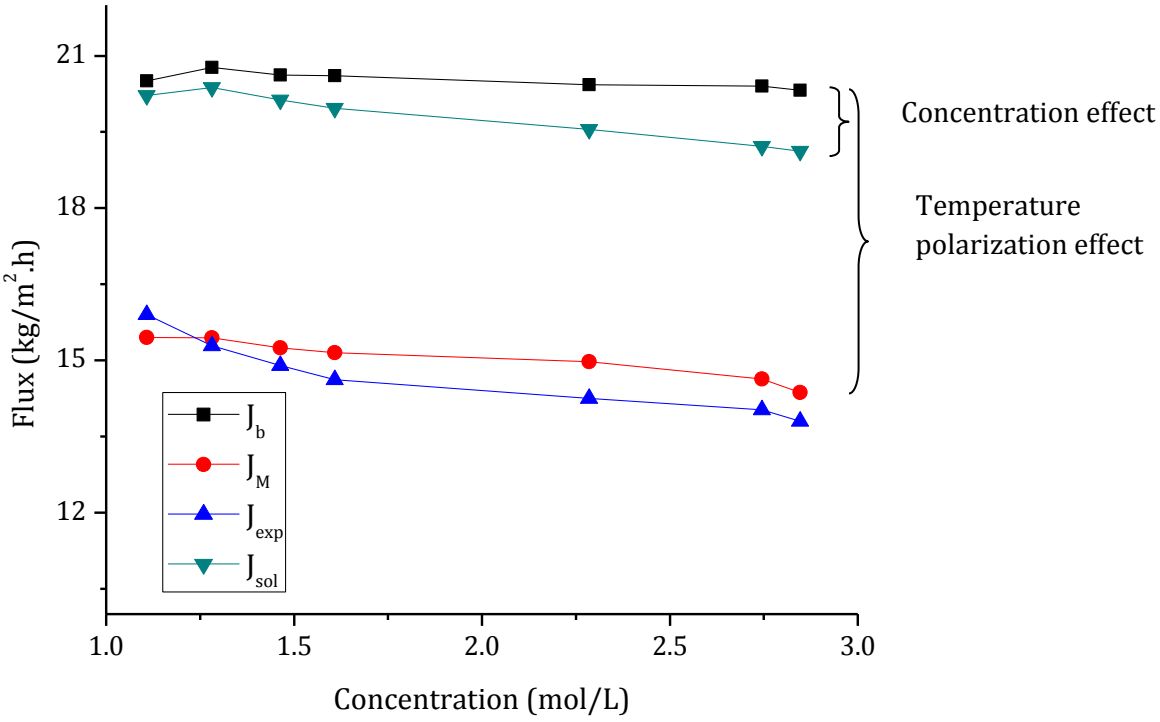

Figure 4.11: Flux calculated on the basis of different considerations and the effect of feed solution concentration and temperature polarization on reduction in flux. J_b, J_M, J_{sol} and J_{exp} represent the flux calculated on the basis of bulk temperatures, temperature at the membrane surface, on the basis of bulk temperatures combined with solution concentration effects and experimental flux, respectively.Feed inlet temperature was 77°C

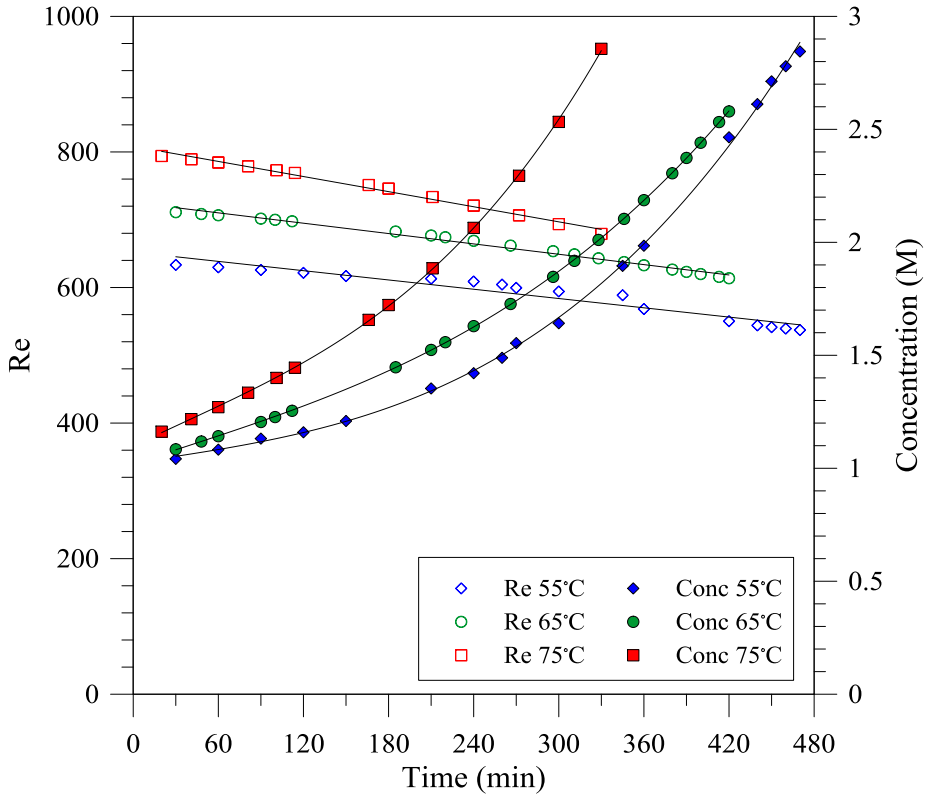

Figure 4.12: Change in feed solution concentration and the corresponding Reynolds number with experimental time

The effect of feed concentration on heat transfer coefficient has been illustrated in Figure 4.13 which shows a reduction in heat transfer coefficient and the corresponding Reynolds number as the solution concentration rises. It is attributed towards the retarded heat and mass flux from bulk to the membrane surface. This argument is further supported by Figure 4.14 that shows the temperature difference between the bulk and membrane surface as a function of feed concentration for various feed inlet temperatures. The figure clearly designates that the difference increases with feed concentration, thus indicating the coupling of thermal polarization with solution concentration.

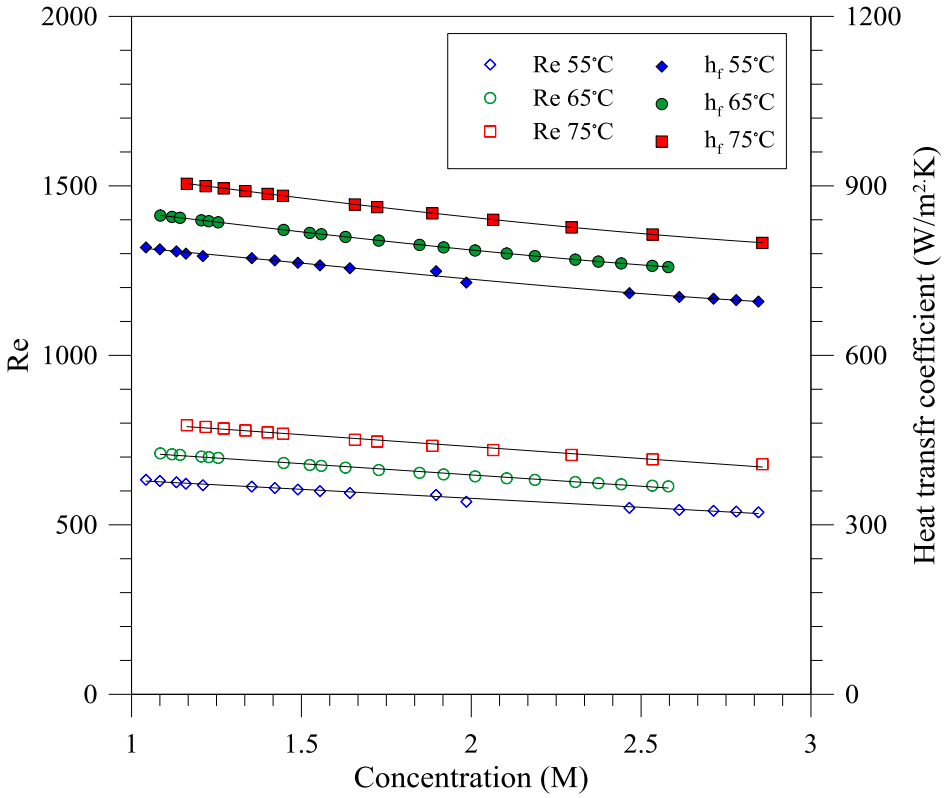

Figure 4.13: Dependence of heat transfer coefficient and Re on feed solution concentration

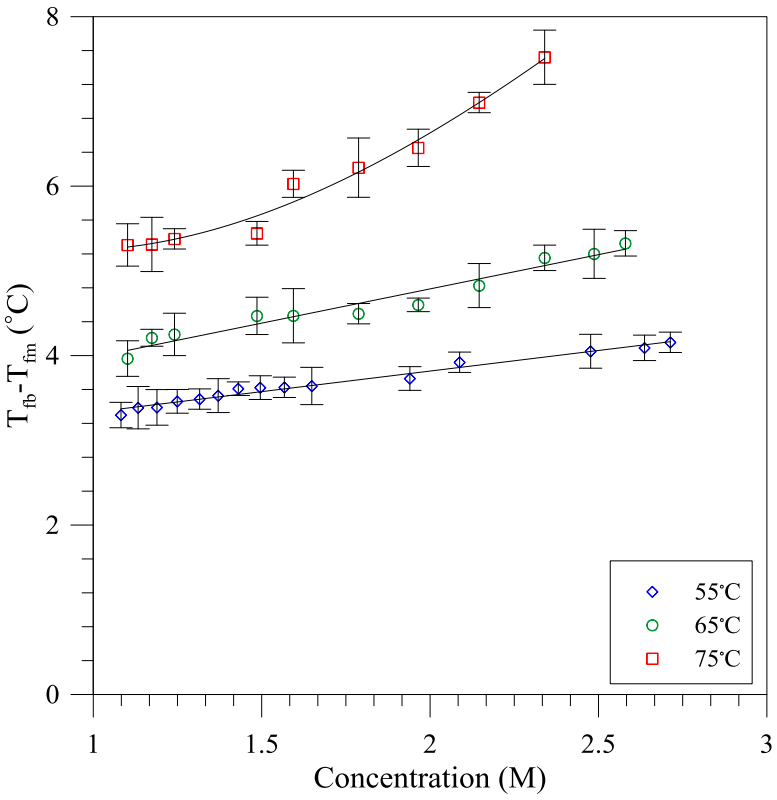

Figure 4.14: Temperature gradient between bulk and membrane surface on feed side as function of feed solution concentration at different temperatures

5. Conclusions

The effect of hydrodynamic conditions and feed inlet temperature on heat and mass transfer in DCMD has been investigated by using a specifically designed cell. It has been concluded that boundary layer resistance to the mass transfer is similar in magnitude to the membrane resistance at low feed flow rates (*Re*=272) while it decreases drastically by increasing the feed flow rate. The temperature polarization coefficient increases by increasing the feed flow rate. The membrane resistance at different hydrodynamic conditions can be described well by using either combined Knudsen diffusion and molecular diffusion models or simple molecular diffusion model. The temperature polarization coefficient increased from ~0.68 to ~0.89, value of heat transfer coefficient changed from ~200 $W/m^{2}.K$ to ~1500 $W/m^{2}.K$, while the thermal efficiency of the system improved from ~13 to 20% when the Reynolds number was increased from 272 to 1360. Experimental heat transfer coefficient lays within the range of theoretical predictions at low feed flow rates, though the values cannot be represented precisely with a single existing theoretical correlation.

At various feed inlet temperatures, the mass transfer can be best explained by using combined Knudsen and molecular diffusion model. The temperature polarization coefficient decreases as the feed inlet temperature is increased from $45^{o}C$ to $75^{o}C$. On the other hand, the boundary layer resistance to the mass transfer shows opposite trend. Thermal efficiency is the maximum at the highest temperature used in the experiment.

The increased solution concentration decreases the transfer of heat and mass from the bulk feed side to the membrane surface due to increase in solution viscosity and density which adversely affect the *Re* and heat transfer coefficient. The net effect is an increase in temperature gradient between the bulk feed phase and the membrane surface on feed side with solution concentration. The solution concentration has very limited role in flux reduction as compared to thermal polarization (1.5:24) at low feed concentration while the flux reduction due to concentration becomes important only at high feed concentration (6:29). Thermal polarization becomes worse at high solution concentrations, indicating a coupling of heat and mass transfer with the solution concentration.

Nomenclature

D_h Hydraulic diameter (m)

D_{KA} Knudsen diffusion coefficient

D_{WA} Molecular diffusion coefficient

h_f Feed side heat transfer coefficient ($W/m^2.K$)

H_v Enthalpy of vapor

J Flux ($kg/m^2.h$)

K Thermal conductivity (W/m.K)

L Length (m)

M_w Molecular weight (kg/mol)

Nu Nusselt number

P Pressure (Pa)

Pr Prandtl number

Q Heat flux (J/s)

R Universal gas constant (8.3143 J/K.mol)

R_c Resistance due to concentration

Re Reynolds number

R_f Resistance due to fouling

R_{fb} Feed side boundary layer resistance

R_m Resistance due to membrane

R_{pb} Permeate side boundary layer resistance

T_f Feed side bulk temperature (^oC)

T_{fm} Feed side membrane surface temperature (^oC)

T_p Permeate side bulk temperature (^oC)

TPC Temperature polarization coefficient

T_{pm} Permeate/distillate side membrane surface temperature (^oC)

r Mean pore size

Y_{ln} Log mean average pressure (Pa)

x Mole fraction of NaCl

ε Porosity

τ Tortuosity

δ Membrane thickness (m)

References

[1] R. W. Schofield and A. G. Fane, "Heat and mass transfer in membrane distillation," J. Memb. Sci., vol. 33, pp. 299–313, 1987.

[2] L. Martınez-Diez and M. I. Vázquez-González, "A method to evaluate coefficients affecting flux in membrane distillation," J. Memb. Sci., vol. 173, pp. 225–234, 2000.

[3] J. Phattaranawik, R. Jiraratananon, A. G. Fane, and C. Halim, "Mass flux enhancement using spacer filled channels in direct contact membrane distillation," J. Memb. Sci., vol. 187, pp. 193–201, 2001.

[4] Y. Yun, R. Ma, W. Zhang, A. G. Fane, and J. Li, "Direct contact membrane distillation mechanism for high concentration NaCl solutions," Desalination, vol. 188, no. February 2005, pp. 251–262, 2006.

[5] M. Gryta, M. Tomaszewska, and A. W. Morawski, “Membrane distillation with laminar flow,” Sep. Purif. Technol., vol. 5866, no. 97, pp. 2–6, 1997.

[6] L. Mart and J. M. Rodr, “On transport resistances in direct contact membrane distillation,” J. Memb. Sci., vol. 295, pp. 28–39, 2007.

[7] S. Srisurichan, R. Jiraratananon, and A. G. Fane, “Mass transfer mechanisms and transport resistances in direct contact membrane distillation process,” J. Memb. Sci., vol. 277, pp. 186–194, 2006.

[8] E. N. Sieder and G. . Tate, “Heat transfer and pressure drop of liquid in tubes,” Ind. Eng. Chem., vol. 28, pp. 1429–1435, 1936.

[9] M. Gryta and M. Tomaszewska, “Heat transport in the membrane distillation process,” J. Memb. Sci., vol. 144, no. February, 1998.

[10] L. C. Thomas, Heat Transfer. Prentice-Hall, Englewood Cliffs, NJ., 1992.

[11] M. MartõÂnez-DõÂez, L, VaÂzquez-GonzaÂlez, “Temperature and concentration polarization in membrane distillation of aqueous salt solutions,” J. Memb. Sci., vol. 156, pp. 265–273, 1999.

[12] J. Phattaranawik, R. Jiraratananon, and a. . Fane, “Heat transport and membrane distillation coefficients in direct contact membrane distillation,” J. Memb. Sci., vol. 212, no. 1–2, pp. 177–193, Feb. 2003.

[13] S. Simone, A. Figoli, A. Criscuoli, M. C. Carnevale, A. Rosselli, and E. Drioli, “Preparation of hollow fibre membranes from PVDF / PVP blends and their application in VMD,” J. Memb. Sci., vol. 364, no. 1–2, pp. 219–232, 2010.

[14] S. B. Iversen, V. K. Bhatia, K. Dam-Johansen, and G. Jonsson, “Characterization of microporous membranes for use in membrane contactors,” J. Memb. Sci., vol. 130, pp. 205–217, 1997.

[15] R. W. Schofield, a. G. Fane, C. J. D. Fell, and R. Macoun, “Factors affecting flux in membrane distillation,” Desalination, vol. 77, pp. 279–294, Mar. 1990.

[16] J. Phattaranawik, R. Jiraratananon, and A. G. Fane, “Heat transport and membrane distillation coefficients in direct contact membrane distillation,” J. Memb. Sci., vol. 212, pp. 177–193, 2003.

[17] M. Khayet, K. Khulbe, and T. Matsuura, “Characterization of membranes for membrane distillation by atomic force microscopy and estimation of their water vapor transfer coefficients in vacuum membrane distillation process,” J. Memb. Sci., vol. 238, no. 1–2, pp. 199–211, Jul. 2004.

CHAPTER 5

Active and passive techniques for controlling thermal polarization in membrane distillation

1. Introduction

Fouling has been indicated as a big hindrance in application of membrane based processes for several potential applications. For low pressure processes, several techniques have been practiced including the use of cross flow instead of dead end filtration, application of turbulent promoters (spacers or screens), implementation of periodic pulsing of the permeate, back washing etc. During last three decades or so, the application of rotating equipment and the induction of controlled secondary flows have gained popularity [1]. However, most of these techniques suffer from many drawbacks including the blockage of the screens due to suspended aggregates, cleaning difficulties and problem of sealing due to moving parts. Besides that, the relatively high energy consumption and scale-up might be the additional problems [2].

In membrane distillation (MD), the process performance is less altered by fouling or concentration polarization than thermal polarization characterized by the difference in temperatures at the membrane surfaces and in bulk phases [3]. While these observations about fouling and very less effect of concentration polarization are very much true for conventional salt solutions, the former can have significant effect on process performance for the solution containing macromolecules such as dairy streams and other solutions containing proteins [4]. For certain types of feed solutions, the initial fouling layer can be associated with the adsorption of molecules at the hydrophobic surface of the membrane. Once built, such layer may tend to accumulate more solute molecules at the membrane surface and ultimately, a thick cake layer can establish under high convection and low shear conditions. The formation of cake layer can hinder both heat and mass transfer to the membrane surface. The thickness of the fouling layer can play a decisive role in controlling the heat and mass transfer across the membrane. In addition to the fouling, flux reduction in MD can also be attributed to temperature polarization as well acknowledged in the numerous investigations:[5][6][7].
Membrane distillation can benefit from solutions developed by process engineers for increasing heat transfer in heat exchanging application and to mitigate fouling in conventional membrane operations. However, due to different nature and time scale of fouling in MD, most of the conventional techniques applied for fouling and concentration polarization reduction in pressure driven membrane processes may not be appropriate for MD. Moreover, due to limited flux (and therefore products), the techniques that consume too much energy may not be suitable for MD. After considering these factors, the most interesting techniques for MD are limited to only a few candidates. A pros and cons comparison of different state-of-the-art hydraulic techniques practiced for conventional membrane processes with application potential for MD has been provided in Table 5.1. Most of these techniques cannot only reduce the fouling in MD but they can also improve temperature distribution within the membrane module. The techniques can also have ‘’wash away’’ effect on surface scales/crystals.

Table 5.1 : A brief analysis of possible hydraulic techniques for fouling and thermal polarization reduction in MD

Technique	*Potential benefits*	*Potential challenges*
Induction of secondary flow	No extra equipment required, easy to adopt, strong effect on temperature polarization on up and down stream sides, high shear acting on the surface can remove the attached particles and fouling layer built up, the performance can be tuned simply by changing the coil diameter and pitch.	Although for heat exchangers and low pressure membrane processes, the process has been well studied yet further studies are required to establish the effects for MD
Pulsation flow	Reduction in concentration and thermal polarization, relatively simple to incorporate	Additional operational and capital cost associated with pulsating generating equipment
Air sparging	Can reduce the fouling in MD when treating complex mixtures	Additional cost related with air sparging equipment, air can occupy the part of membrane modules thus reducing the contact area, the pores can be occupied by the injected air leading towards reduced vapor pressure [8]
Backwashing	The crystallization, scaling and deposits partially wetting the pores can be removed	The pore wetting will occur leading to the post drying requirement, the effectiveness of the technique will be limited to remove deposition, scaling occurred within the pore or at pore mouth, no effect on thermal polarization
Rotating membranes	Reduction in concentration and thermal polarization,	High energy consumption, design modification for MD can be complicated, may not be suitable for hollow fibers

Some more potential techniques appropriate for reduction of fouling and/or thermal polarization phenomenon in MD have been given below. Most of these techniques are well known in process engineering to increase heat transfer coefficient of different systems.

1. Surface treatment: It can be applied to incorporate a continuous or discontinuous fine scale alteration or modification to the surface to enhance the turbulence.
2. Displace enhancement devices: The application of such insert to the forced convection makes the temperature distribution more homogenous. The technique can be suitable for flat sheet membranes.
3. External additives: Such technique are based on addition of trace of soluble additives, solid particles and gas bubbles to decrease the surface tension of the liquid and thus increasing the volatility of the liquid.
4. Swirl flow: Such flow pattern can be induced by twisted tapes, tube inserts and cored screw type tube inserts to introduce swirl flow superimposing the axial flow.
5. Mechanical aids: One application of this technique includes rotating tube heat exchanger. The background idea is to stir the fluid by mechanical means or by rotating surface.
6. Surface or fluid vibration: Such techniques are well known for increasing heat transfer coefficient.

As pointed out in Table 5.1 one passive approach for improving heat transfer and reducing fouling in MD can be based on inducing the secondary flows. The generation of secondary flows can be conveniently realized by using the undulating geometries. When a fluid flows in such channels, the centrifugal force caused by the geometry of the channel forces the fluid to flow toward the outer wall,

thus creating a secondary flow or counter rotating vortices also referred as Dean Vortices. The phenomenon was first studied systematically by Dean [9] and was applied to pressure driven membrane operations by some groups later on. A good review of the concept as applied to the membrane processes can be found in [10]. Helically coiled membrane modules have been effectively used to create such vortices inside the hollow fiber membranes to reduce the fouling in pressure driven processes [11][12][13][14]. The secondary flows direct the foulants away from the membrane surface. While the benefits of helical geometries have been relatively less explored for membrane processes, the use of such geometries has been adopted well to increase the performance of heat exchangers [15][16]. The approach can be very promising for membrane distillation, not only to reduce the fouling but also to improve the temperature polarization coefficient of the process both at upstream and downstream. Similar to helical geometries, crimped or wavy fibers have been used in membrane contactor and heat exchanger applications to increase mass and heat transfer coefficients [17][18]. The use of such geometries for MD applications, however, still needs further investigation.

An interesting active approach to reduce concentration and thermal polarization can be realized by changing the flow pattern of the fluid flowing in a channel. Intermittent flow and pulsating flow are two common approaches used to realize this objective. The use of intermittent flow has been proven effective in increasing heat and mass transfer for separation and heat transfer applications [19][20]. On the other hand, pulsatile flow has gained more attention for medical and biological applications [21][22]. Some studies have shown an improved heat transfer for pulsating flow [23][24][25]. Moreover, significant improvement in performance of ultrafiltration has been claimed in some other investigations [26].

The objective of the present study is to investigate the effect of secondary flows induced through helical and wavy shaped modules and flow patterns including intermittent and pulsatile flows on performance of direct contact membrane distillation process. In first part, the effective ranges of flow rate and heat transfer coefficient for applied systems have been simulated by using the simple existing relations. The parametric analysis of heat transfer in helical modules has also been performed. Helical and wavy shaped fibers have been tested experimentally under different hydrodynamic conditions. The pulsatile and intermittent flows have been generated by using simple mechanical modifications of the conventional set-ups for MD. The comparative performance analysis for each scheme has been provided.

2. Mathematical background and modelling

The state-of-the-art mathematical calculations for secondary flow induced through helical geometries have been based on a tube (which can be considered as a hollow fiber membrane) wrapped around a rod as shown in Figure 5.1. The geometrical terminologies of the system have been described in the same figure.

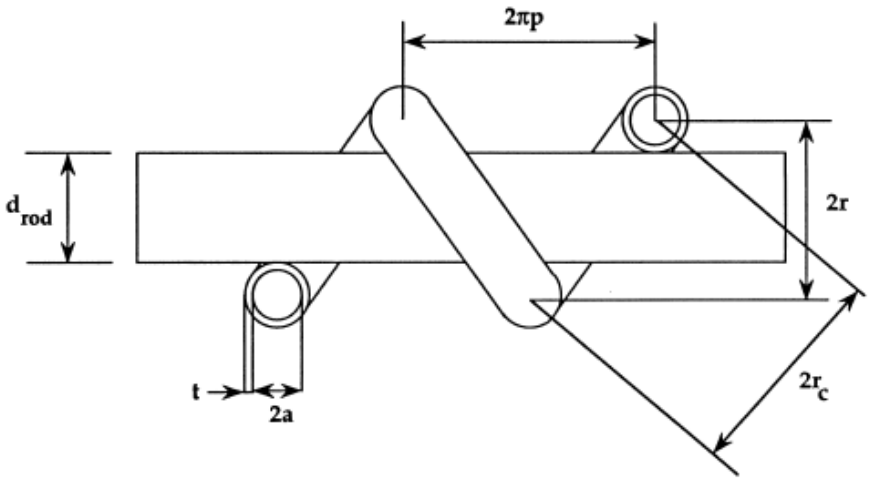

Figure 5.1: A tube helically wrapped around a rod

Dean [16] showed that flow in the coiled channels can be characterized by a dynamic parameter (named Dean number) defined as

$$De = \mathrm{Re}\sqrt{\frac{a}{r_c}} \qquad (1)$$

For a helical tube, a modified Dean number is used to incorporate the torsional effects.

$$De' = \mathrm{Re}\sqrt{\frac{a}{r_c'}} \qquad (2)$$

$$r_c' = r_c\left(1+\left(\frac{p}{\pi r_c}\right)^2\right) \qquad (3)$$

Where *Re*, *a* and r_c represent the Reynolds number, tube radius and radius of curvature, respectively. r_c can be defined as following

$$r_c = \frac{r^2 + p^2}{r} \qquad (4)$$

Where *r* is the radius of curvature of the tube coiled in a single plane and p is the pitch defined as

$$p = \frac{m}{2\pi} d_o \qquad (5)$$

Where d_o denotes the outer diameter of the tube and *m* is the number of tubes lying next to each other, *r* can be defined as

$$r = \frac{d_{rod}}{2} + t + a \qquad (6)$$

Where d_{rod} is the diameter of the rod and *t* is the tube thickness.

As evident from equation 2, for a given tube (membrane) diameter, Dean flow in helical tubes can be characterized by three main parameters including *Re*, coil diameter and pitch of the helical coil. For a constant Dean number, the effect of any of the above parameters can be compensated by adjusting the other two.

Table 5.2: Parameters used for the calculation and module fabrication

Membrane used	PP Accrual
Inner diameter of the fiber (mm)	1.8
Outer diameter of the fiber (mm)	2.25
Thickness of the membrane (mm)	0.225
Diameter of the rod (mm)	10
Length of the fiber (mm)	200
Pitch (mm)	40
No. of fibers in one module	4
No. of turn	4.5

As far as the heat transfer in straight fibers is concerned, several correlations exist in the literature to determine the Nusselt number under both laminar and turbulent conditions for MD using simple modules [27][28][29].

For the flow characterized with the presence of Dean vortices, several expressions have been proposed to calculate the Nusselt number of the system, however, most of the correlations do not hold true for the flow conditions applied and the fluid used in the present work. A summary of various correlations used by different authors have been described in Table 5.3. In present study, the expression used by Dravid et al [30] and Kalb and Seader [31] have been applied due to their close proximity with the conditions used in the current study.

Once the Nusselt number is known, the corresponding heat transfer coefficient can be calculated by using the relation.

$$h = \frac{Nuk}{D_h} \qquad (15)$$

Where k is the thermal conductivity of the fluid and D_h is the hydraulic diameter of the channel.

The heat transfer coefficients calculated for straight and coiled fiber modules for different Reynolds numbers according to relations proposed by different authors have been shown in Figure 5.2. The effect of *Re* on heat transfer coefficients according to the correlations defined by Kalb and Dravid et al is more sensitive to flow rate at low *Re*. Heat transfer coefficient increases by 41.4% when *Re* is increased from 50 to 100 while further increase of 50 in *Re* incorporates only 22.47% increase in heat transfer coefficient. Furthermore, as it would be explained in subsequent discussion, the decrease in boundary layer resistance is more effective in increasing the flux only at low *Re* where the role of membrane resistance in dictating flux is less significant than the boundary layer resistance.

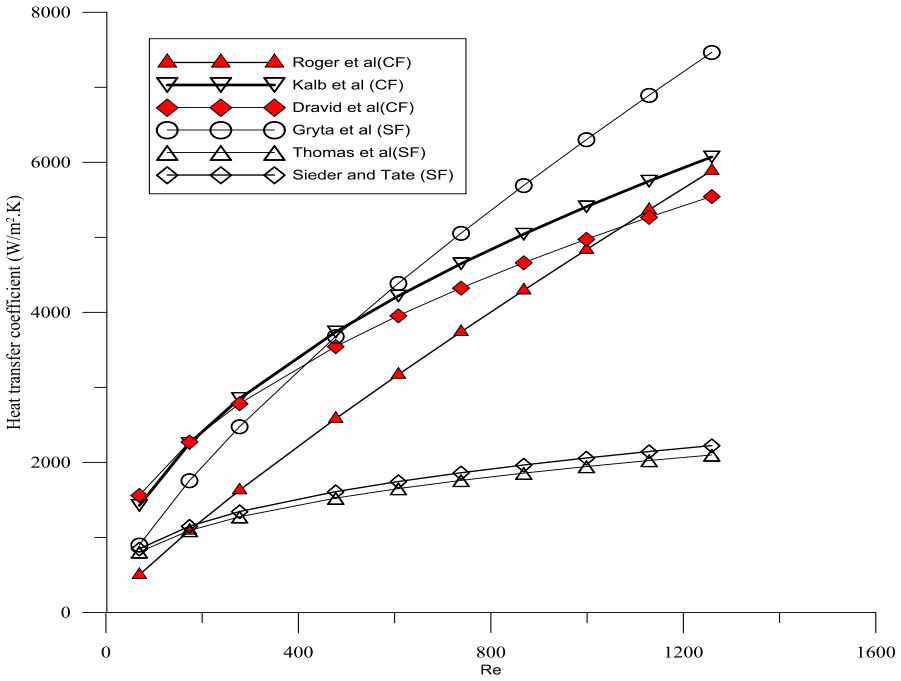

Figure 5.2: Nusselt number as function of Reynolds number for straight fibers (SF) and coiled fibers (CF) according to different correlations

In order to establish effective and feasible ranges of heat transfer coefficients and corresponding *Re*, a simple modeling was performed. The membrane temperatures at the feed side were assumed and the corresponding temperature at the membrane surface at permeate side was calculated according to the algorithm given in Figure 5.3. *Re*, feed side heat transfer coefficient and flux corresponding to each *Re* were calculated. The following main assumptions have been made during the calculations.

1. The flux can be described using the Knudsen molecular diffusion (transition) model.
2. The heat transfer on distillate side follows the correlations proposed by [31].
3. At steady state, heat transferred through the membrane is equal to the heat transferred from the bulk feed phase to the membrane surface.

Table 5.3: Heat transfer correlations for helical channels

$$Nu = (0.65\sqrt{De} + 0.76)\,\mathrm{Pr}^{0.175} \qquad [30]$$

$$Nu = 0.0551 De^{0.864}\,\mathrm{Pr}^{0.4} \qquad [32]$$

$$Nu = (2.153 + 0.318 De^{0.643})\,\mathrm{Pr}^{0.177} \qquad [33]$$

$$Nu = 0.67\delta^{0.13}\,\mathrm{Re}^{0.5}\,\mathrm{Pr}^{0.21} \qquad [34]$$

$$Nu = 0.83 De^{0.5}\,\mathrm{Pr}^{0.1} \qquad [31]$$

$$Nu = 0.023\,\mathrm{Re}^{0.85}\,\mathrm{Pr}^{0.4}\,\delta^{0.1} \qquad [35]$$

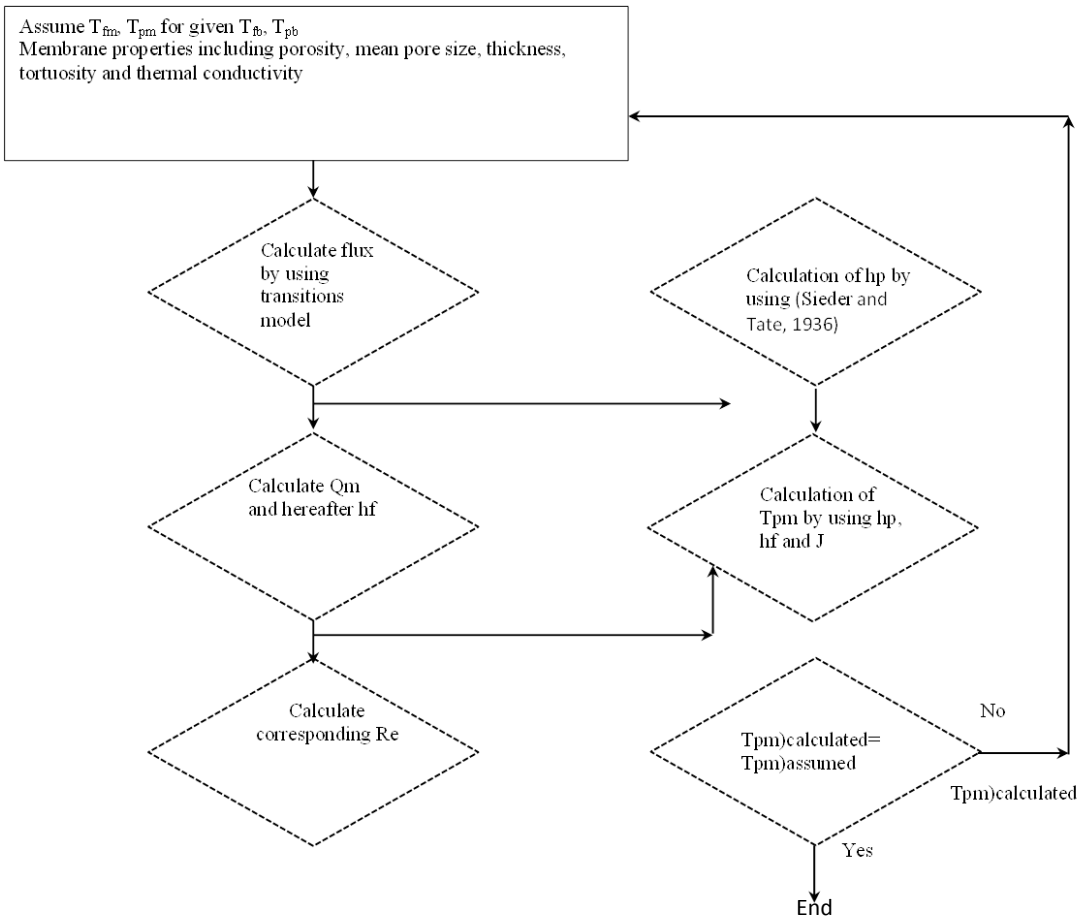

Figure 5.3: Algorithm used to calculate T_{pm} for a known T_{fm}

Re calculated according to different correlations to achieve a particular temperature at the membrane surface corresponding to a bulk feed temperatureof 55^{o}C and bulk permeate temperature of 25^{o}C has been shown in Figure 5.4. It can be seen from the figure that for all correlations mentioned, the membrane surface temperature of 52-53^{o}C can be reached at moderate values of *Re*, however, after that even to achieve a minor increase in surface temperature, *Re* has to be increased tremendously. Mathematically, it is due to the fractional power of *Re* involved in all correlations predicting the dependence of heat transfer coefficent on *Re* while physically, it is due to very high feed flow rate required in order to immediately mitigate the cooling effects arising due to the heat conduction through the membrane and evaporation taking place at the membrane surface. It somehow gives an indication of optimum *Re* value that should not be exceeded to achieve an optimum process performance. It should be noted however that such analysis does not apply if the membrane features such as thickness and pore wetting change due to the increase in hydraulic pressure.

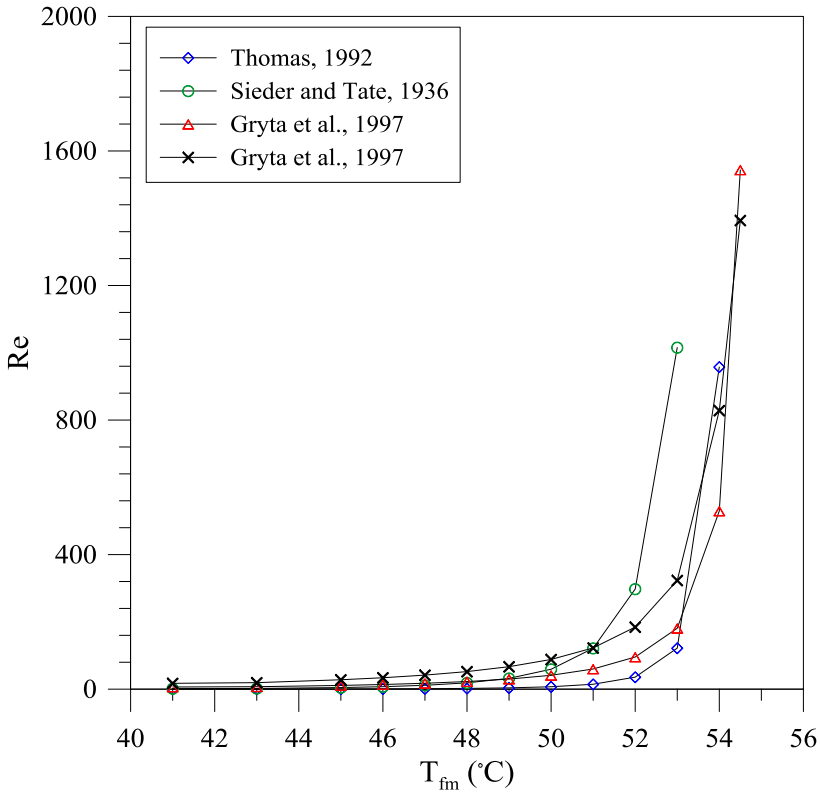

Figure 5.4: Re required to achieve a particular membrane surface temperature at feed side under the assumption 1-3 mentioned above

Dependence of flux on heat transfer coefficient has been illustrated in Figure 5.5. It can be infered from the figure that heat transfer coefficient exceeding ~1500W/m^{2}·K is not significantly important in increasing the performance of this particular system. After a certain value of heat transfer coefficient, the flux stays almost constant as the major resistance to mass transfer arises from the membrane itself instead of the feed side boundary layer. Also beyond this point, it becomes practically unfeasible to increase further the value of TPC as even a minor change in temperature at the membrane surface requires a huge increase in *Re*. Effective upper limit of heat transfer coefficent increases with increase in feed temperature. The heat transfer coefficient as function of *Re* has been shown in Figure 5.6. The figure indicates that upper limit of effective heat transfer coefficient can be reached at *Re* of ~600 for this particular system.

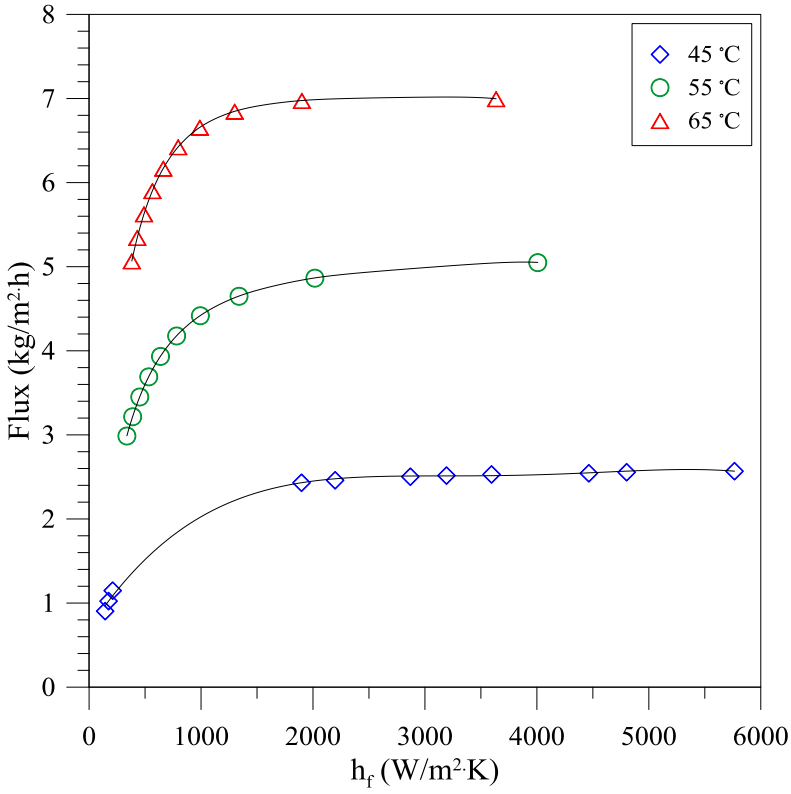

Figure 5.5: Variation of flux with heat transfer coefficient

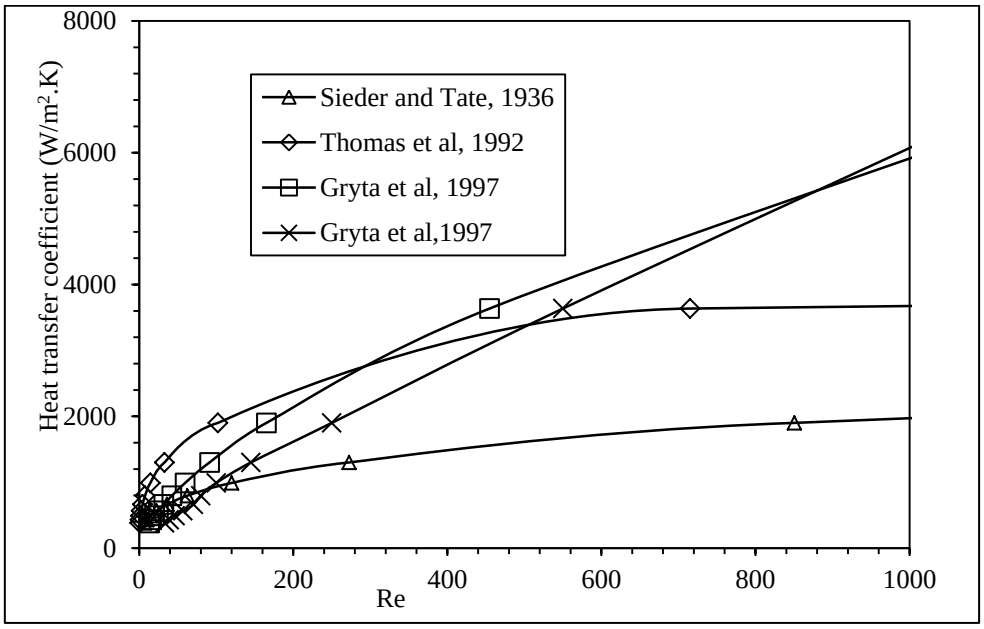

Figure 5.6: Heat transfer coefficient as function of Re according to different correlations

The dependence of various resistances on *Re* for feed bulk temperature of 54^{o}C has been shown in Figure 5.7. It can be seen that the feed side boundary layer resistance (R_f) is higher than the membrane resistance (R_m) below heat transfer coefficient of ~500 W/m^{2}.K. Below these conditions, the process is

dominanatly controlled by the heat transfer through the feed side boundary layer and beyond this point, the membrane resistance becomes higher than the boundary layer resistance and further decrease in feed side boundary layer resistance does not remain as effective as before this point. The conditions applied in the current study also indicate that at high heat transfer coefficent, the permeate side boundary layer resistance increases slightly by increasing the heat transfer coefficient that has been realized by increasing feed flow flow rate. This is a direct consequence of more heat transferred across the membrane through conduction and convection as the membrane surface temperature at feed side increases due to reduction in thermal polarization at high feed flow rates. At heat transfer coefficient ~2000 $W/m^2 \cdot K$, the permeate side boundary layer resistance becomes almost equal to the membrane resistance. In summary, the reduction in resistance offered by feed side boundary layer is useful only at low heat transfer coefficients (corresponding to low *Re*) as at high heat transfer coefficients, membrane and permeate side bonndary layer resistances dominate the process.
The results described above combined with Figure 5.2 indicate that the helically coiled modules are expected to give superior performance than their straight counterpart at low feed flow rates and high temperatures.

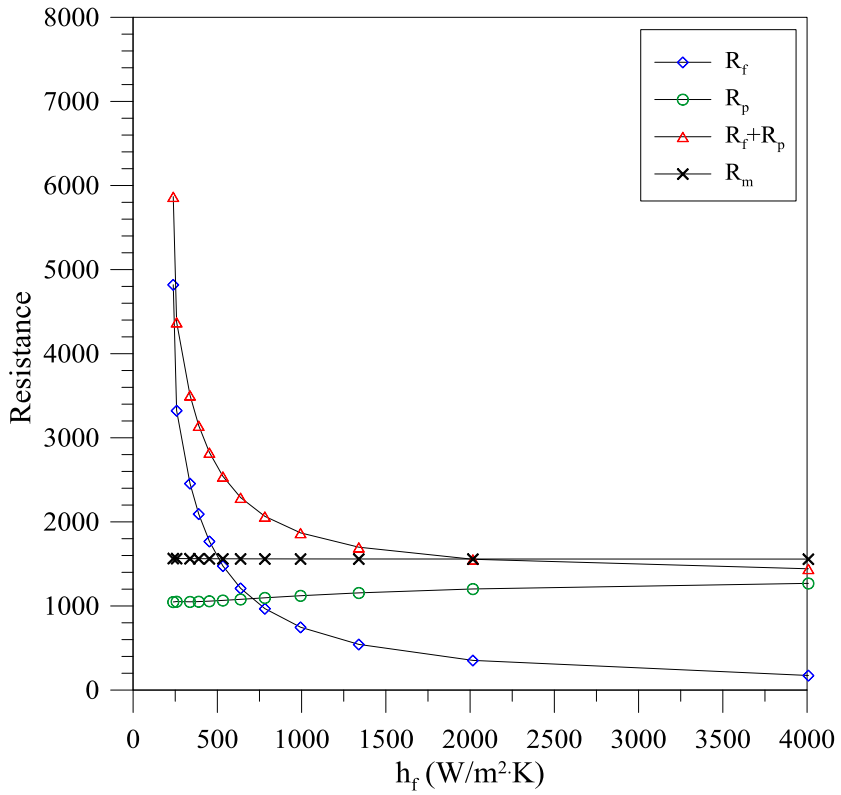

R_f feed side boundary layer resistance
R_p Permeate side boundary layer resistance
R_m Membrane resistance

Figure 5.7: Resistance analysis as function of heat transfer coefficient

3. Parametric analysis

For a given tube (membrane) diameter, Dean flow in helical tubes can be characterized by three main parameters including Reynolds number (*Re*), coil diameter and pitch of the helical coil.

The effect of *Re* on heat transfer coefficients according to the correlations defined by Kalb and Dravid et al has been illustrated in Figure 5.8. The figure indicates that the increase in heat transfer coefficient

is the most significant at low *Re*. The heat transfer coefficient increases by almost 144% when *Re* is increased from 50 to 250 while only a 41% increase can be noticed when the *Re* is further increased from 300 to 600. Further increase in flow rate might not be very fruitful due to membrane resistance dominating the mass transfer mechanism (see Figure 5.7).

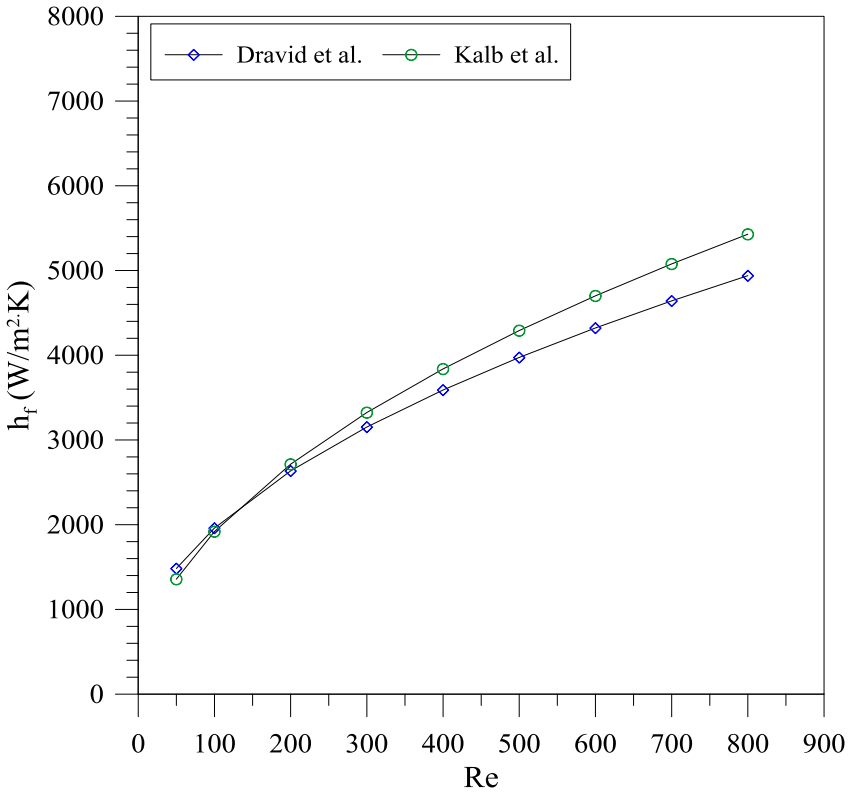

Figure 5.8: Effect of Re on heat transfer coefficient according to various correlations

The heat transfer in a helical coil is influenced by the coil diameter too. The coil diameter is a determining factor for the centrifugal forces acting on the moving fluid which influence the secondary flow along the cross section of the tube. With increase in coil diameter, the influence of curvature on flow characteristics (secondary flow) becomes weaker and therefore, the heat transfer coefficient decreases. The entrance effect prevails to a longer distance for the smaller coil diameter. The difference between inner and outer wall Nusselts number narrows down with increase in coil diameter [36]. The smaller diameter coil improves the heat transfer under the same conditions as compared to the larger diameter. The effect has been shown in Figure 5.9.

The effect of pitch on heat transfer coefficient has been illustrated in Figure 5.10. It can be seen from the figure that coil pitch does not affect the heat transfer coefficient significantly. With an 8 fold increase in pitch, the heat transfer coefficient decreases only by 6.16%. It could be particularly good news for polymeric membranes with relatively high elastic modulus as bending the membranes for a very small pitch could damage their structure at the bent points. However, the other studies indicate that the difference in Nu between the top and bottom points of the tube periphery increases with increase in coil pitch [36].

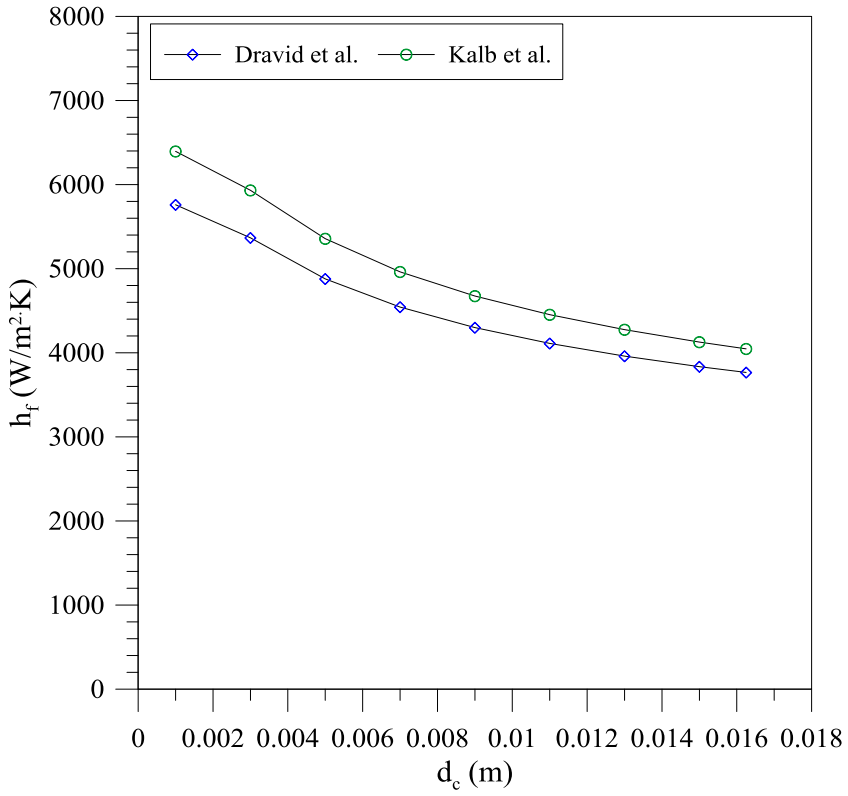

Figure 5.9: Effect of coil diameter on feed side heat transfer coefficient at Re=444 and pitch of 4mm

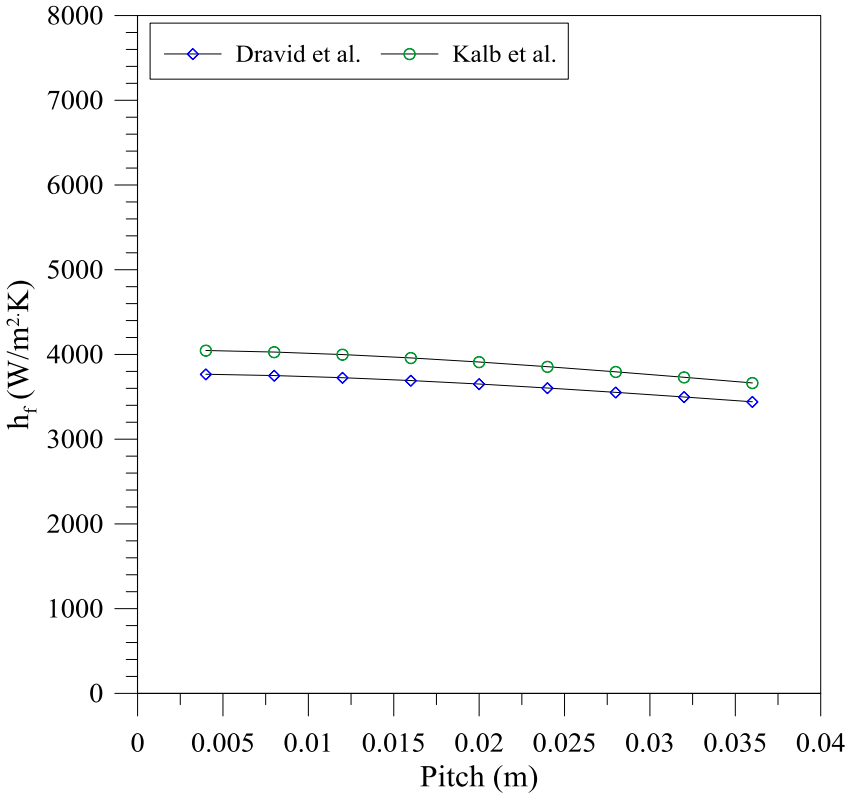

Figure 5.10: The effect of pitch on Nusselts number inside the membrane at Re of 444 and coil diameter of 16 mm

4. Experimental

4.1 Membrane applied

The membrane used in the experimentation was a hollow fiber PP membrane (Acuurel S6/2 PP, Membrana, Germany). The membrane has internal and external diameters of 1.80 mm and 2.25 mm, respectively. The porosity of the membrane has been reported as 73% by the manufacturer.

4.2 Formation of helical and wavy fibers

The helical fibers used in the study were prepared by simply winding the fibers around a rod of particular diameter as shown in Figure 5.11. The coil used had outer diameter of 10 mm while the pitch was adjusted at 40 mm. The supports were provided at four different locations on the rod in order to avoid the contact of fiber with the pipe, as the contact area can reduce the flux. The wrapped fibers were enclosed in a glass module and the ends of the module were sealed so that the feed can pass only through the fibers. In parallel to the helical module, a wavy fiber module was also prepared by using the same PP membrane. The formation of wavy fiber was realized by heat treatment of the twisted fibers. After knitting the fibers in wave type pattern, the heat treatment process was carried out in an oven at a temperature of 80oC for 30 min. The heat treatment sets the membranes in their knitted configuration even after removing the knitting supports. Wave length and amplitude of the fiber were set at 40 mm and 5 mm, respectively. A further decrease in wave length at this amplitude was not possible due to rigidity of the membrane. The fibers were assembled in glass modules for further testing.

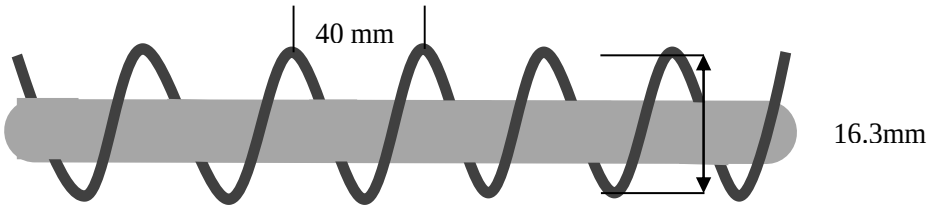

Figure 5.11: Schematic diagram of the helical module prepared in the lab

4.3 Induction of intermittent and pulsating flow

The flow generated through peristaltic pump is intermittent at very low rotational speed; however the degree of intermittency is low if a large number (≥4) of cylindrical rollers to squeeze the flexible plastic tube are used. An easy way to generate an intermittent flow is to modify the head structure of peristaltic pumps according to the explanation provided in Figure 5.12. The flow generated according to this procedure also follows forward and backward flow pattern that can be very useful in reducing concentration and thermal polarization in membrane processes. The relative magnitude of forward and backward components can be controlled by adjusting the frequency through rotational speed of the pump. At very low speed, the magnitude of both components is equal and no net flow is observed (pure oscillatory flow). With increase in rotational speed, the magnitude of forward component increase and a net flow is observed. Under intermittent-oscillatory condition with net flow, a better mixing of boundary layer and bulk fluid takes place that can be utilized to mitigate thermal or concentration polarization in membrane operations. A simple arrangement was used to create the pulsating flow in the current study by applying two pumps: the one that can deliver a constant flow

and the other one that delivers an intermittent flow as described above. Both these flows were combined in a tube to get the exact pulsating flow according to the scheme illustrated in Figure 5.13. *Re* for pulsatile flow was changed by changing the flow rate of intermittent component while keeping the steady component at a fixed value.

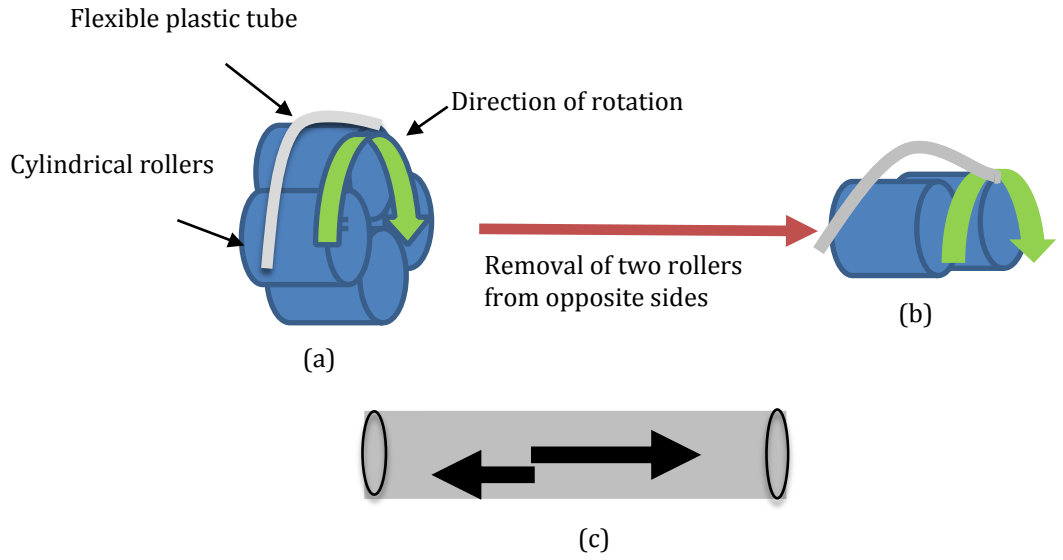

Figure 5.12: Simple procedure of inducing intermittent flow through a peristaltic pump and flow pattern created (a) Normal arrangement of cylindrical rollers present in a peristaltic pump (b) Two opposite sided rollers have been removed to generate intermittent flow (c) Oscillations of flow generated within the tube after removing two rollers

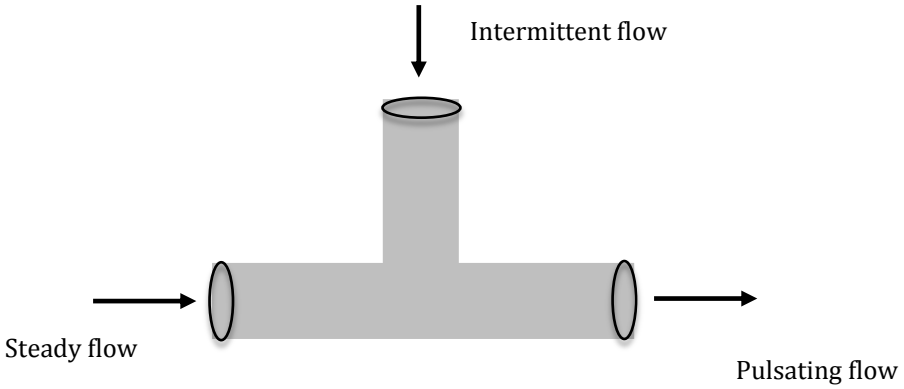

Figure 5.13: A simple arrangement applied to create pulsating flow

4.4 MD tests

MD tests were performed at different feed flow rates and at fixed feed temperature of 54±0.3°C, except in one case where the experimentation was performed at 45°C and feed side *Re* of ~860-3900 to test the behavior of the system under the conditions of low thermal polarization. For helical, wavy and straight fibers, the minimum feed side *Re* was 152 while for the intermittent flows, it was possible to use an average *Re* as low as ~76. *Re* for pulsating and intermittent flow was based on time average value of flow. The performance of helical module was also tested with the whey solution.

5. Results and discussion

5.1 Helical modules

(a) Pure water as feed

The flux of helical module under low thermal polarization conditions characterized by *Re*=1086 to 3908 that corresponds to a Dean number of 339 to 1219 and feed temperature of 45°C is shown in Figure 5.14. It is clear from the figure that flux is not significantly sensitive to the flow rate. Increased feed flow rate reduces the residence time of the fluid in the membrane and therefore the average temperature gradient between the feed and permeate sides along the membrane tends to rise causing an improvement in temperature polarization coefficient that enhances the flux under most of the circumstances. Very marginal increase in flux can be associated with the corresponding increase in temperature polarization coefficient as explained in section 2.1. At high Reynolds number, the process is not limited by the boundary layer resistance on the feed side, rather by the temperature of the feed stream. This observation is qualitatively consistent with the explanations given in section 2.1. The presence of secondary flows makes the temperature homogeneous even at lower Reynolds number due to better mixing of the fluid present in the bulk and at the membrane surface. Therefore, in case of helical modules the flux remains almost insensitive towards feed velocity.

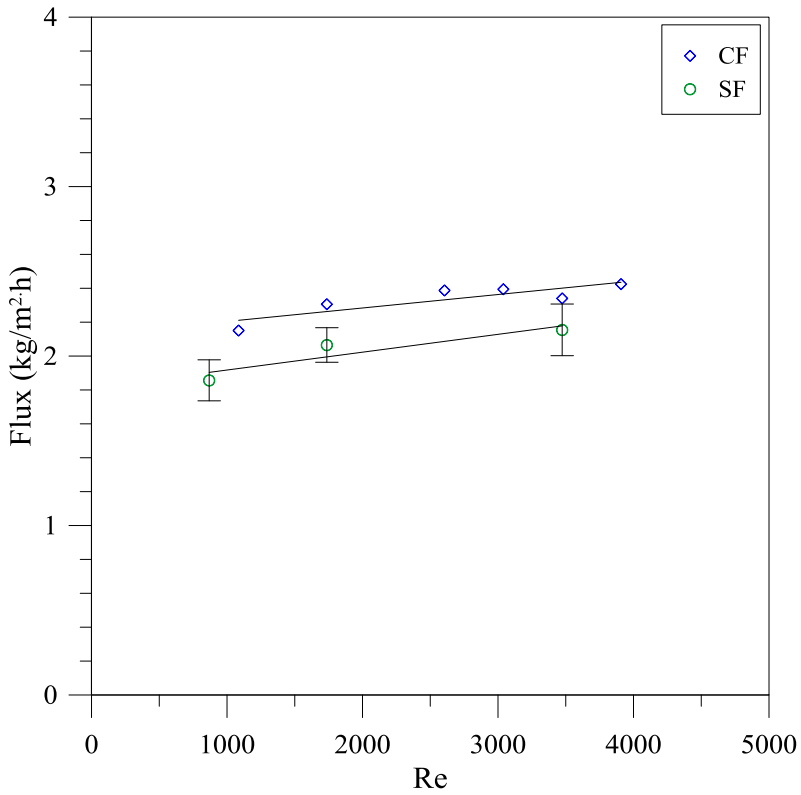

Figure 5.14: Comparison of flux observed for the module with straight fiber (SF) and coiled fibers (CF)

Figure 5.14 also illustrates a comparison of the flux observed for the straight fiber module and coiled fiber module under the same thermal and flow conditions. The observed flux varies slightly with flow rate. The dependence of the flux on flow rate for the modules with straight fibers is the common trend observed in the literature. Generally, the dependence of heat transfer coefficient on *Re* has been represented with a power law with an exponent of 1/3. The maximum difference observed in the flux

of straight and coiled fibers is 10% which is expected to raise at lower feed flow rates. This observation is qualitatively consistent with Figure 5.5 and Figure 5.7, which show that beyond a certain range of heat transfer coefficient or *Re*, the further increase in feed side flow rate is not effective in increasing the flux of the system, as membrane and permeate side resistances become the bottle necking. The difference in flux observed for the two configurations considered can be attributed mainly to improvement of heat transfer coefficient on permeates side for helical modules.

(b) Whey solution as feed

The performance of helical and straight fiber was also compared by using whey solution as feed. The experimentation was carried out at feed temperature of 54^{o}C and feed side *Re* of ~880. Due to its rapid fouling nature, whey was used as the feed solution. The flux obtained and the corresponding concentrations for inside-out configuration for helical and straight fiber modules have been shown in Figure 5.15. As illustrated in the figure, the flux exhibited by the coiled modules is higher than its straight counterpart throughout the experimental run.

Another interesting results obtained through the helically coiled module is the high flux even at high feed concentration. As shown in Figure 5.15, the concentrations achieved with helical and straight modules are 18.6% and 13.7%, respectively. The solute present in the feed can affect the MD flux in several possible ways: by building up the fouling layer at the membrane surface that offers an additional resistance to mass and heat transfer, by lowering the vapor pressure of feed solution, by adsorbing on the membrane surface and by introducing concentration polarization if the convective flux is high. Relatively higher flux for helical module can be associated with decreased thermal polarization for this module.
When comparing the flux obtained through straight and coiled fiber modules, it should also be noted that residence time of the solution inside the coiled module is high as compared to straight modules due to more resistance offered to the fluid flowing inside the module and total length of the fiber which is almost 21% longer than that of the straight one. Higher residence time combined with the relatively longer dimension tend to reduce more the overall driving force along the helical module under the same thermal and hydrodynamic conditions applied at inlet of the two module configurations used. The comparative results can be further attractive if the length of fibers in both modules is kept equal.

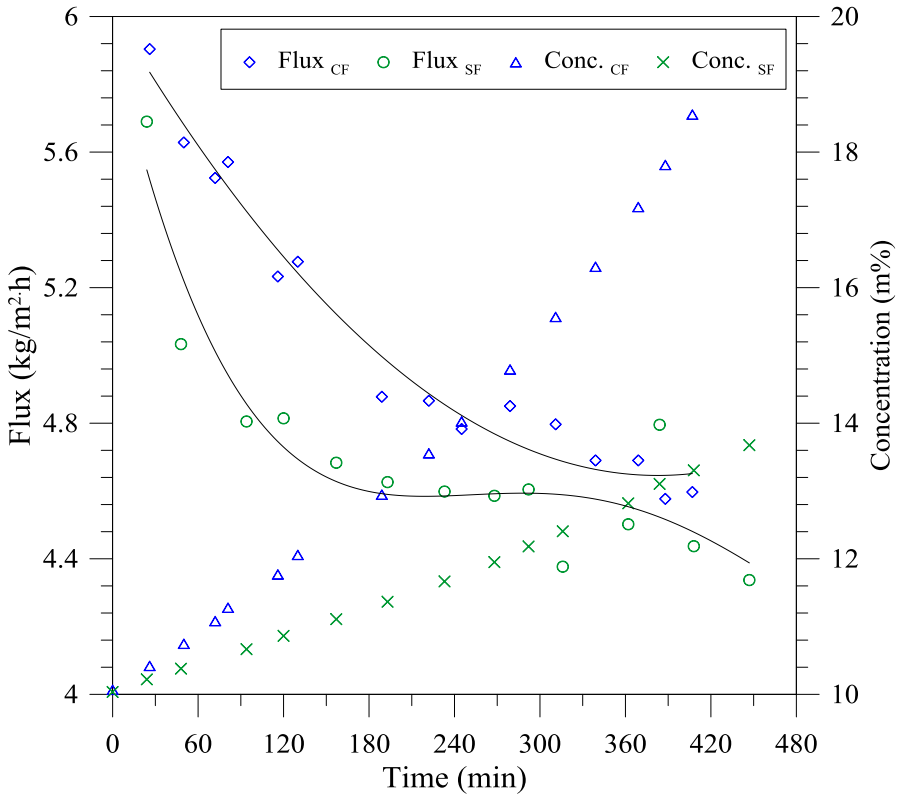

Figure 5.15: Flux achieved for straight (FS) and helical coiled (FC) modules with whey solution as feed

5.2 Wavy and helical fibers

In order to establish the performance of helical module under low *Re* and relatively high feed temperature, the experimentation was carried out at *Re*~180-1680 at feed inlet temperature of 54^{o}C. The results are shown in Figure 5.16 in form of normalized flux defined as the ratio of flux for helical/wavy module to the flux for their straight counterpart under the same hydrodynamic and thermal conditions. The figure confirms that the normalized flux is highest at low feed flow rates. At feed side *Re* of ~180, the flux for helical fibers is ~47 % more than straight fibers and this number decreases to ~11% at high feed flow rate. For wavy fibers, the highest value of normalized flux observed is 1.52 indicating a 52% increase in flux over its straight counterpart. The increase in flux for helical and wavy fibers can be associated with improvement in thermal polarization at both feed and permeate side. Again the relative insensitiveness of the flux at high *Re* is consistent with the modeling results presented in section 2.1.

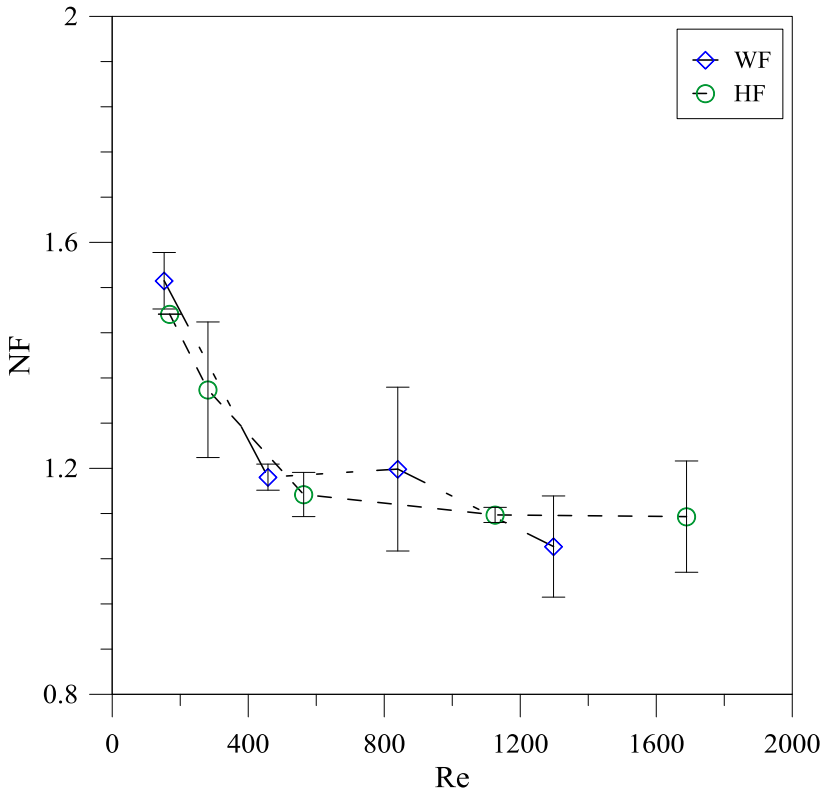

Figure 5.16: Normalized flux for wavy (WF) and helical fibers (HF) as function of feed side Re

5.3 Intermittent and pulsatile flow

The flux for intermittent and pulsatile flow has been compared with that obtained by using steady flow in Figure 5.17 and shows very interesting pattern. Even at very low *Re* (76), the flux obtained for intermittent flow is significantly higher than that observed for the steady flow. The maximum difference in flux between intermittent and steady flow is 28%. The pulsation frequency (more precisely back and forth flow frequency) is very low at lower flow rates but still it is effective to improve the mixing of fluid present at the membrane surface with the bulk. Moreover, due to high amplitude of back and forth movement at low frequencies, the residence time of the fluid in the module becomes high, leading towards more cooling. More increase in frequency further improves mixing and at the same time, decreases the residence time of fluid in the module. As the flow rate is increased further, the forward component of back and forth flow increases and the effectiveness of pulsatile flow starts to diminish. At high *Re*, the flux behavior resembles with that of steady flow.

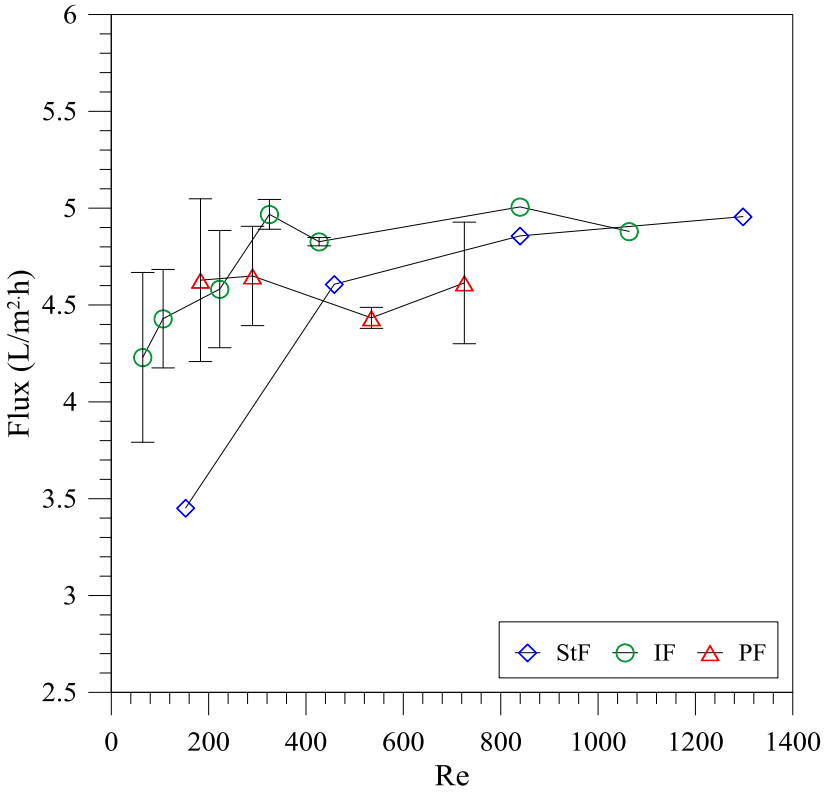

Figure 5.17: Flux for intermittent (IF), pulsatile (PF) and steady flow (SF) under the same thermal conditions

5.4 Performance ratio analysis

Performance ratio (PR) is an important parameter to assess the effectiveness of utilized energy for a module. Generally, the process performance in MD is based on the energy associated with its convective and conductive components transported through the membrane. In the present study, the total energy transported through the system is calculated by applying the enthalpy balance on entrance and exit of feed stream. PR has been calculated by using the following expression.

$$PR = \frac{J\lambda}{J\lambda + \frac{\dot{m} C_p \Delta T}{A_m}} \qquad (16)$$

Where A_m is the active membrane area through which heat transfer takes place while λ is latent heat of vaporization of water.

The flux data mentioned in Figure 5.16 and Figure 5.17 was used to calculate PR. A comparison of PR for helical and wavy modules with straight fiber modules has been provided in Figure 5.18 which indicates that PR for helical modules is ~64% higher than the module containing straight fibers at intermediate flow rates. At high feed flow rates, however, the difference in PR for both modules narrows down to 32%. With initial small increase in flow rate, the flux for helical fibers increases rapidly and then reaches a steady state range abruptly. At high feed flow rates, the flux does not increase significantly and overall impact reduces the PR of the system. Similarly for wavy fiber, a maximum increase of 90% in PR has been observed which reduces at high flow rates.

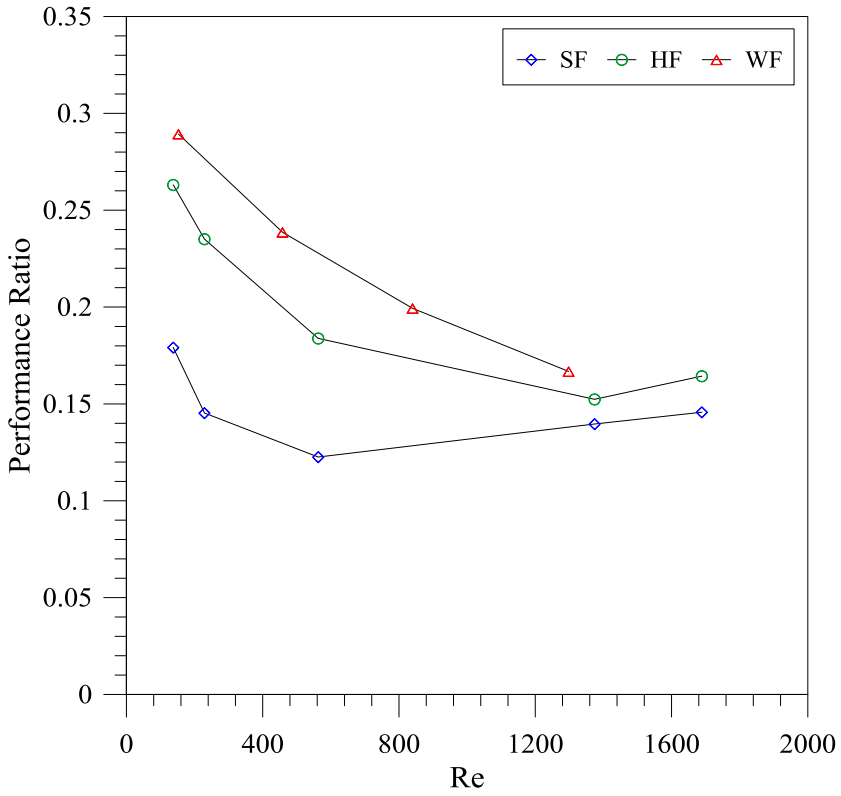

Figure 5.18: Performance ratio for helical (HM), wavy (WM) and straight fiber (SM) modules as function of feed side Re

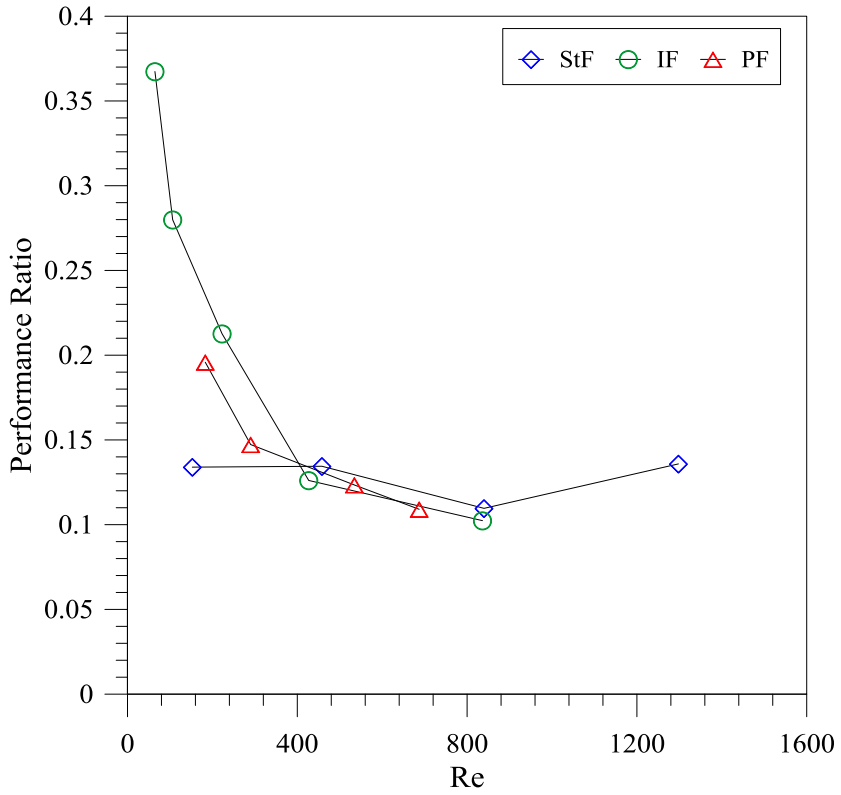

Figure 5.19: Comparison of PR for steady, intermittent and pulsatile flows

Similarly, a comparison of PR for intermittent and pulsatile flows with steady flow has been provided in Figure 5.19. It is evident from the figure that the highest PR is achieved for intermittent flow mode within the experimental flow conditions studied. The maximum difference observed between the PR of steady and intermittent flow is 175% (even at much low *Re* of intermittent flow) and it starts to approach to that of the steady flow with increase in flow. As evident from Figure 5.17, a significantly high value of flux is achieved at very low feed flow rates for intermittent flow which causes a high PR for this flow pattern. PR for pulsatile flow follows the similar trend to that of intermittent flow. However, it was not possible to operate the system used in present study below a certain value of *Re* for pulsatile flow, therefore, PR for pulsatile flow at low *Re* has not been mentioned in the current study.

5.5 Packing density

One of the major advantages of the membrane operations is their very high surface to volume ratio that is dictated by the high packing density of the module. Packing density for hexagonal lattice of straight module is 90.7% [37], although very high values can negatively disturb the heat and mass transfer on the shell side. For helical and wavy configurations, packing density varies with membrane outer diameter and coil diameter of the helix. In case of helical fiber, the space present inside the helix restricts the further increase in packing density. In case of wavy fibers, for a given membrane, it is function of wave length and outer diameter of the membrane. Packing density for different configurations has been calculated according to the correlation provided in [37]. The packing density plays a crucial role in dictating the overall module volume which can be important for certain applications. On the other hand, an area based enhancement factor (ABEF) gives an indication of the membrane area in comparison to the straight configuration to achieve a particular separation volume[37]. ABEF affects both membrane cost and operational cost. Similarly, VBEF gives an indication of the improvement in flux per unit change in module volume with respect to straight fibers.

Packing densities along with ABEF and VBEF for different configurations applied have been shown in Figure 5.20. Obviously, the best packing density can be expected for straight module. Since the straight fibers have been used for intermittent and pulsatile flow experimentation, their packing density is the same as that for the straight fiber in steady flow. The packing densities are significantly lower for helical and wavy configurations (59% and 57%, respectively). ABEF and VBEF were calculated at *Re*~230 for all flow pattern and module configurations used according to correlations used in [37]. ABEF is maximum for wavy shaped geometries which somehow indicates a lower operational and capital cost for such modules, although the low packing density and VBEF [37] are the drawback of this configuration. Similarly, EBEF for helical geometry is attractive (1.28) but packing density and VBEF are lower. Intermittent and pulsatile flow modes seem to be the best optimum due to their reasonable ABEF (1.32), high packing density and VBEF.

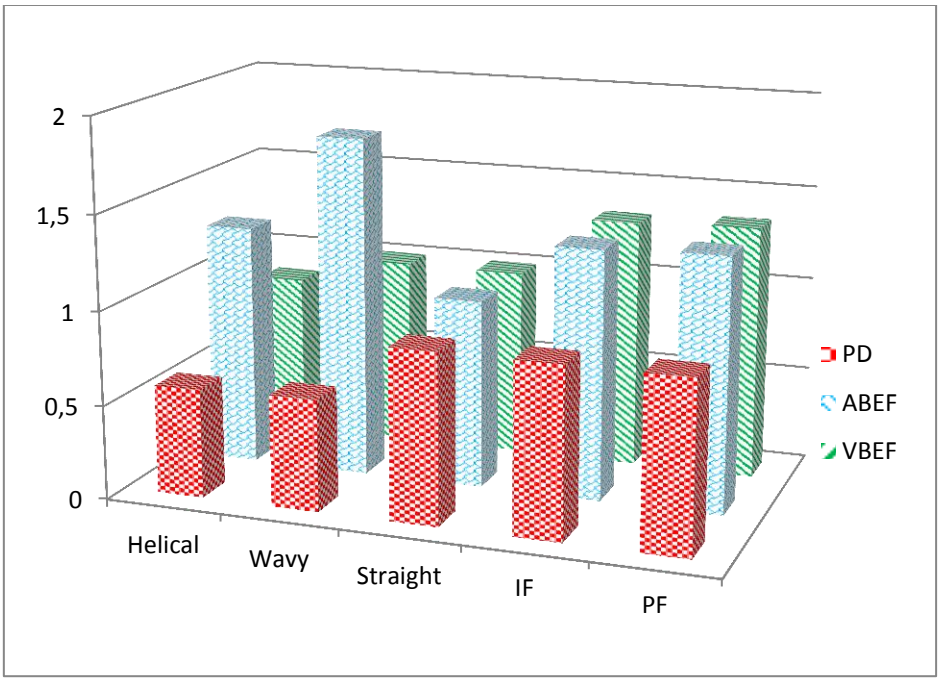

Figure 5.20: Packing density (PD), area based enhancement factor (ABEF) and volume based enhancement factor (VBEF) for different configurations and flow patterns

6. Conclusions

The performance of MD by using traditional straight fibers and steady flow is severely affected due to temperature polarization, especially at low feed flow rates. Active and passive techniques used to augment heat transfer in heat exchanger applications and to reduce concentration polarization in traditional membrane processes are promising candidates to reduce thermal polarization in MD. In current work, the effect of different module designs and flow pattern on performance of membrane distillation process has been investigated. The improvement in performance through both the techniques can be realized only at low feed flow rate where the system is controlled by the boundary layer resistance. At low feed flow rates, the highest mass transfer rate has been observed for wavy shaped fibers followed by the helically wounded fibers. On the other hand, intermittent flow shows the best performance ratio. In terms of surface and volume based enhancement factor and packing density, intermittent and pulsatile flows displayed most optimal performance. Further investigation to explore the effect of membrane features, configurational parameters of fibers and optimization of steady and unsteady components of pulsatile flow can be interesting to explore.

References

[1] M. Y. Jaffrin, "Hydrodynamic Techniques to Enhance Membrane Filtration," *Annu. Rev. Fluid Mech.*, vol. 44, no. 77–96, 2012.

[2] S. Luque, H. Mallubhotla, G. Gehlert, R. Kuriyel, S. Dzengeleski, S. Pearl, and G. Belfort, "A new coiled hollow-fiber module design for enhanced microfiltration performance in biotechnology.," *Biotechnol. Bioeng.*, vol. 65, no. 3, pp. 247–57, Nov. 1999.

[3] A. Ali, F. Macedonio, E. Drioli, S. Aljlil, and O. a. Alharbi, "Experimental and theoretical evaluation of temperature polarization phenomenon in direct contact membrane distillation," *Chem. Eng. Res. Des.*, vol. 91, no. 10, pp. 1966–1977, Oct. 2013.

[4] A. Hausmann, P. Sanciolo, T. Vasiljevic, M. Weeks, K. Schroën, S. Gray, and M. Duke, “Fouling mechanisms of dairy streams during membrane distillation,” *J. Memb. Sci.*, vol. 441, pp. 102–111, 2013.

[5] *K.* W. Lawson and D. R. Lloyd, “Membrane distillation,” *J. Memb. Sci.*, vol. 124, 1997.

[6] R. W. Schofield and A. G. Fane, “Heat and mass transfer in membrane distillation,” *J. Memb. Sci.*, vol. 33, pp. 299–313, 1987.

[7] *J.* Phattaranawik, R. Jiraratananon, and a. . Fane, “Heat transport and membrane distillation coefficients in direct contact membrane distillation,” *J. Memb. Sci.*, vol. 212, no. 1–2, pp. 177–193, Feb. 2003.

[8] Z. Ding, L. Liu, Z. Liu, and R. Ma, “The use of intermittent gas bubbling to control membrane fouling in concentrating TCM extract by membrane distillation,” *J. Memb. Sci.*, vol. 372, no. 1–2, pp. 172–181, 2011.

[9] W R Dean, “The stream-line motion of fluid in a curved pipe,” Philos. Mag. Ser. 7, vol. 5, no. 30, pp. 673–695, 1928.

[10] M. E. Brewster, K. Chung, and G. Belfort, “Dean vortices with wall flux in a curved channel membrane system A new approach to membrane module design,” *J. Memb. Sci.*, vol. 81, pp. 127–137, 1993.

[11] *P.* Moulin, J. C. Rouch, C. Serra, M. J. Clifton, and P. Aptel, “Mass transfer improvement by secondary flows: Dean vortices in coiled tubular membranes,” *J. Memb. Sci.*, vol. 114, no. 2, pp. 235–244, Jun. 1996.

[12] P. Moulin, P. Manno, J. C. Rouch, C. Serra, M. J. Clifton, and P. Aptel, “Flux improvement by Dean vortices : ultra ® ltration of colloidal suspensions and macromolecular solutions,” *J. Memb. Sci.*, vol. 156, pp. 109–130, 1999.

[13] *P.* Manno, J. C. Rouch, M. Clifton, and P. Aptel, “Mass transfer improvement in helically wound hollow fibre ultrafiltration modules Yeast suspensions,” *Sep. Purif. Technol.*, vol. 14, pp. 175–182, 1998.

[14] H. Mallubhotla, S. Hoffmann, M. Schmidt, J. Vente, and G. Belfort, “Flux enhancement during d*ean vortex tubular membrane nano ® ltration .,” J. Memb. Sci.,* vol. 141, pp. 183–195, 1998.

[15] *P.* Coronel and K. P. Sandeep, “Heat Transfer Coefficient in Helical Heat Exchangers under Turbulent Flow Conditions Heat Transfer Coefficient in Helical Heat Exchangers under Turbulent Flow Conditions ⇤,” *Int. J. Food Eng.*, vol. 4, no. 1, 2008.

[16] A. M. Elsayed, “Heat Transfer in Helically Coiled Small Diameter Tubes for Miniature *Cooling Systems By,”* University of Birmingham Edgbaston, Birmingham, B15 2TT, 2011.

[17] *M.* M. Teoh, S. Bonyadi, and T. Chung, “Investigation of different hollow fiber module designs for flux enhancement in the membrane distillation process,” *J. Memb. Sci.*, vol. 311, pp. 371–379, 2008.

[18] K. Tatebe and M. Yamazaki, “OXYGENATOR USING POROUS HOLLOW FIBER MEMBRANE,” US 54893821996.

[19] M. D. Karl E. Karlson, M.D., Ph.D., Ronald J. Massimino, B.S., C.C.P., Arun K. Singh and M. D. and George N. Cooper, Jr., “Laboratory and Clinical Evaluation of a Membrane Oxygenator with Secondary Flows in the Blood Channels,” World Journa Surg., vol. 6, pp. 358–361, 1982.

[20] *M*.-A. Hessami and N. W. Zulfiki, “EXPERIMENTAL STUDY OF PULSATILE FLOWS IN A HEATED HORIZONTAL TUBE FOR VARIOUS FLOW ρ,” in *ICET07*, 2007, pp. 11–13.

[21] K. M. Lim, J. Y. Park, J. C. Lee, J. C. Kim, B. G. Min, E. T. Kang, and E. B. Shim, “Quantitative Analysis of Pulsatile Flow Contribution to Ultrafiltration,” *Artif. Organs*, vol. 33, no. 1, pp. 69–73, 2009.

[22] *K*. M. Lim and E. B. Shim, “Computational assessment of the effects of a pulsatile pump on toxin removal in blood purification,” *BioMediacl Enginnering Online*, pp. 1–16, 2010.

[23] A. Faghri, M. Faghri, and K. Javdani, “Effect of Flow Pulsation on Laminar Heat Transfer Between Two Parallel Plates,” *Warme- und Stoffiibertragung*, vol. 13, pp. 97–103, 1980.

[24] *Z*. GUO, S. Y. KIM, and H. J. SUNG, “Pulsating flow and heat transfer in a pipe partially filled with a porous medium,” *J. Heat Transfer*, vol. 40, no. 17, pp. 4209–4218, 1997.

[25] M. Jafari, M. Farhadi, and K. Sedighi, “Pulsating fl ow effects on convection heat transfer in a corrugated channel : A LBM approach ☆,” *Int. Commun. Heat Mass Transf.*, vol. 45, pp. 146–154, 2013.

[26] *C*. Huang and H.-S. Chen, “The characteristic analysis of interrupted flow pulsation on ultrafiltration system,” *Appl. Mech. Mater.*, vol. 479–480, pp. 373–379, 2014.

[27] E. N. SIEDER and G. E. Tate, “Heat Transfer and Pressure Drop of Liquids in Tubes,” *Ind. Eng. Chem.*, vol. 28, pp. 1429–1435, 1936.

[28] *M*. Gryta, M. Tomaszewska, and A. W. Morawski, “Membrane distillation with laminar flow,” *Sep. Purif. Technol.*, vol. 5866, no. 97, pp. 2–6, 1997.

[29] L. C. Thomas, *Heat Transfer*. Prentice-Hall, Englewood Cliffs, NJ., 1992.

[30] A. N. Dravid, K. A. Smith, E. W. Merrill, and P. L. T. Brian, “Effect of Secondary Fluid Motion on Laminar Flow Heat Transfer in Helically Coiled Tubes,” *J. Heat Transfer*, vol. 17, no. 5, pp. 1114–1122, 1971.

[31] C. E. Kalb and J. D. Seader, “Fully Developed Viscous-Flow Heat Transfer in Curved Circular Tubes with Uniform WaII Temperature,” *AIChE J.*, vol. 20, no. 2, pp. 340–346, 1974.

[32] C. Yildiz and D. Pehlivan, “HEAT TRANSFER AND PRESSURE DROP IN A HEAT EXCHANGER WITH A HELICAL PIPE CONTAINING INSIDE SPRINGS,” *Energy Convers. Mgmi*, vol. 38, no. 6, pp. 619–624, 1997.

[33] R. C. Xin and M. A. Ebadian, “The Effects of Prandtl Numbers on Local and Average Convective Heat Transfer Characteristics in Helical Pipes,” *J. Heat Transfer*, vol. 119, pp. 467–473, 1997.

[34] N. Acharya, M. Sen, and H. Chang, “Analysis of heat transfer enhancement in coiled-tube heat exchangers,” *Int. J. Heat Mass Transf.*, vol. 44, pp. 3189–3199, 2001.

[35] G. F. C. Rogers and Y. . Mayhew, “Heat transfer and pressure loss in helically coiled tubes with turbulent flow,” *Int. J. Heat Mass Transf.*, vol. 7, pp. 1207–1216, 1964.

[36] J. S. Jayakumar, “Helically Coiled Heat Exchangers,” no. 1983, 2006.

[37] D. Kaufhold, F. Kopf, C. Wolff, S. Beutel, L. Hilterhaus, and M. Hoffmann, “Generation of Dean vortices and enhancement of oxygen transfer rates in membrane contactors for different hollow fiber geometries,” *J. Memb. Sci.*, vol. 424, pp. 342–347, 2012.

CHAPTER 6

Membrane based processes for treatment of produced water: application of MD

1. Introduction

The role of oil and gas industry in progress of modern civilization cannot be challenged. Despite of the increasing emphasis on the use of alternative and renewable resources for energy, the demand of oil and gas has even accelerated. It has been estimated that the daily consumption of petroleum would increase to 106.6 million barrels by 2030. However, likewise all other industrial activities, production of oil and gas is also associated with the generation of waste streams mainly entailing waste water that accounts for 80% of the wastes for newly drilled oilfield wells and up to 95% for the mature wells [1]. The waste water produced by oil and gas industry is referred as oilfield water or produced water (the modified terminology for co-produced water). The main sources of its production in petroleum exploration processes have been highlighted in Figure 6.1.

In US, the main contribution to increased production of natural gas is coming from unconventional sources including coal bed methane gas, shale gas, mine gas and tight gas. It has been estimated that technically recoverable gas reservoirs have increased by 48% from 2006 to 2010 [2]. Inspired from these figures, International Energy Agency (IEA) has speculated about ‘’Golden Age of Gas’’ that will be described by the abundant availability of natural gas at very economical cost in the urban regions with high energy demands. According to the predictions of U.S. Energy Information Administration (EIA), shale gas and CBM will contribute 34% to the total production by 2034 [3], [4]. Moreover, EIA also claims that global shale gas resources are approximately 716 trillion cubic meters which are sufficient to fulfill the energy demand for next 100 years. Significant developments in shale gas exploration are being carried out in Argentina, Canada, China, Poland and many new players. Therefore, in the case of shale gas, the production of produced water is obvious to increase even more swiftly and has become the main argument against the further developments in the field.

Hydraulic fracture is the main technique behind the rapid increase in production of the shale gas. During hydraulic fracture, in order to liberate the shale gas, huge amounts of produced water or flow back water are produced and brought to the surface (15-80%). This water can contain as much TDS as 5 times of the seawater. Besides that, elevated concentrations of heavy metals including beryllium, cadmium, chromium, copper, iron, lead, nickel, silver and zinc along with the natural radioactive radionuclides and until several hundred ppm of organic matters speak fairly about the toxic nature of the produced water. Treatment of this water is of particular importance for onshore shale gas reservoirs. The most practiced method for handling this type of wastewater is injection into deep wells, however, this methodology does not solve the problem in the area with ample shale gas production [5]. Besides the formation water, the water condensed from the gas is also a constituent of the produced water. Increasingly stringent regulations on the produced water disposal and eventual shrinking opportunities to reuse within the shale gas facilities will compel the industry to desalinate the produced water. Besides the increase in demand of energy from natural gas and oil, in future the oil supply will come mostly from the mature wells that will further boost the production of produced

water. Sustainable production of shale gas and oil, therefore, is associated with the technological advancements in desalination.

The enhanced production of the produced water forces to compromise either on the production volumes or the regulations about controlling the quality of the discharge. The generally accepted figure for oil to produced water ratio during initial stages of production activities is 1:3 [6] and its daily production volume is 240 million barrels. In United States (US), the reported average production of produced water is 10bbl/bbl of oil [7]. By 2030, an investment of 1trillion dollar will be required to maintain the production of oil and major part of this investment will be spent on handling the produced water [8].

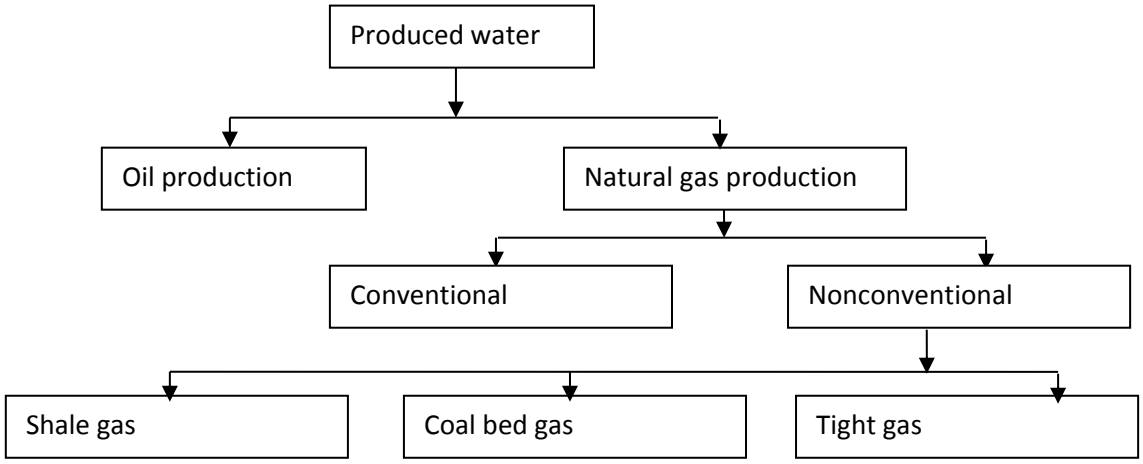

Figure 6.1: Main sources of produced water

The state-of-the-art practice for wastewater treatment includes gravity-based separation followed by discharge into the environment. However, these techniques suffer from several demerits mainly related with environmental issues; the discharge of the produced water can pollute the soil water, fresh water and underground water. The more severe affects can be attributed to the dissolved organic compounds, heavy metals present in the produced water and the production chemicals; however, their long term effects on the environment are not fully documented and understood so far. On the other hand, the new stringent rules and regulations put emphasis on more effective treatment. Both for the reuse and treatment, there are certain critical parameters that have to be considered and analyzed in order to proceed in anyway. TDS is crucial not only to determine the treatment technique but also to adjust the blending ratio with the fresh water, as excessive TDS create undesirable high friction during hydraulic fracturing process. Similarly the removal of suspended solids is important prior to reuse because high solids can plug the well. On the other hand, their characterization determines the filter characteristics required for the treatment. Likewise, the presence of hardness creating species, the amount of sulphate, barium, iron and bacteria needs to be characterized.

2. Membrane based treatments for produced water

The conventional treatment methods employed for the produced water treatment have certain limitations including the usage of toxic chemicals, high cost of treatment, large footprint and the creation of secondary pollution. Moreover, the conventional treatment methods may not sufficient to fulfill the new tight environment regulations. Due to these problems, membrane based operations have been declared the promising candidates for wastewater treatment in 21st century. A summary of membrane based treatment options has been provided in Figure 6.2.

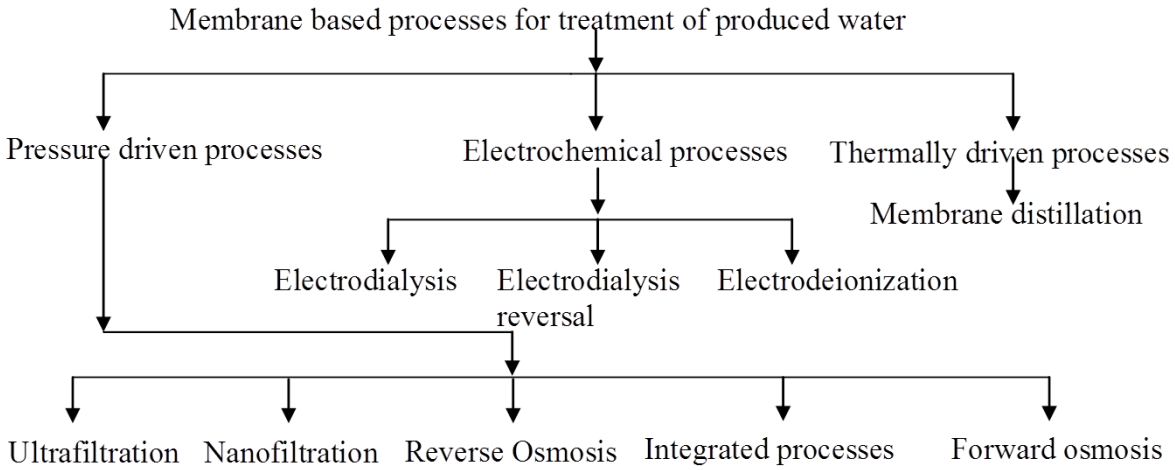

Figure 6.2: Schematic of membrane processes for produced water treatment

2.1 Pressure driven membrane processes

Microfiltration (MF), ultrafiltration (UF), nanofiltration (NF) and reverse osmosis (RO) are well-established membrane based operations and can be applied for the removal of the species with specific range of sizes. MF is generally applied for the removal of suspended solids and to reduce the turbidity while UF can be used to remove color, odor, viruses and colloidal organic matters. The effectiveness of UF in removing oil from the produced water is well established in comparison with traditional methods. Both ceramic and polymeric membranes can be used for MF and UF. All these processes can be used either as pretreatment or as the final treatment step.

Reverse osmosis and nanofiltration are high-pressure driven processes and can be used to remove the dissolved salts and other species with the size as small as 0.0001 µm. However, in case of RO, there are certain challenges which limit the efficiency of the process: the fouling and scaling of the membrane, the inability to operate the process at high solution concentrations and the problem of brine disposal. These problems can be minimized by using appropriate pre-treatment and post-treatment for the process. An integration of the different processes can be an efficient tool to deal with these problems.

A membrane operation suitable both as NF/RO pre-treatment and for produced water treatment is the membrane bioreactor (MBR). It combines the properties of a membrane with that of a biological catalyst providing a considerable high level of physical disinfection. This makes MBR especially suitable for reuse and recycling of wastewater.

2.2 Electrochemical processes

Besides the pressure driven membrane based processes, electrochemical membrane based processes have been applied to treat the produced water. Electrodialysis and electrodialysis reversal are two main examples in this context which involve the separation of ions by using an ion permeable membrane to separate the dissolved ions under the influence of an electrical potential gradient. The ion exchange membranes have the ability to selectively transport positively or negatively charged ions while restricting the passage of the opposite ones. Thus in an elecrodialysis stack consisting the arrays of alternating negatively and positively charged membranes, the density of charged ions in one compartment increases while dilution occurs in the consecutive one. In electrodialysis reversal, the polarity of the membranes can be changed to control the membrane fouling and scaling [9]. The critical factors affecting the efficiency of electrodialysis or electrodialysis reversal process for the

treatment of brackish water or desalination include the current density of the membrane, the ionic concentration of the solution, membrane fouling, counter effects due to the transport of co-ions, diffusion and osmosis. The laboratory scale testing of electrodialysis systems for the treatment of produced water indicates that treatment cost is highly dependent upon the solution concentration and difference can be as high as 23 times. The main drawbacks of the process include high treatment cost, fouling and the limitation to treat relatively high salinity water [10]. The membrane must be cleaned by using dilute acidic and alkali solutions to restore its performance.

2.3 Non-pressure driven membrane based processes

2.3.1 Forward osmosis

Forward osmosis or natural osmosis utilizes a semi-permeable membrane to separate two solutions with different concentrations. The water from low concentrated solution migrates to the high concentrated solution due to the osmotic pressure gradient across the membrane. The solvent moves due to its natural tendency to migrate from the solution of high osmotic pressure to the lower one, eliminating the need to apply hydraulic pressure. The elimination of applied hydraulic pressure attributes far less fouling in FO than its counterpart RO. Moreover, the developed fouling can be removed by hydraulic washing or chemical cleaning. FO possesses the ability to remove all the particulates matters and almost all the dissolved matters. The theoretical recovery factor obtainable is quite high and, at the same time, the associated energy consumption and chemical demand is very low. The processes based on the osmotic energy have not been practiced yet for the treatment of produced water. However, the lab scale and pilot plant studies of this process for numerous applications have shown a good potential to treat the water with different levels of salinity gradient [11] [12] [13] [14].

2.3.2 Membrane distillation

Membrane distillation is an emerging thermal based membrane process with the potential to be operated on waste or low grade energy. The process owns several advantages over the state-of-the-art thermal and pressure gradient based processes. For membrane distillation process, the possibility to go beyond the concentrations achievable through conventional techniques and the waste grade heat available with the produced water can be very attractive opportunities to treat the produced water [15][16]. Moreover, the produced water coming from the steam assisted gravity drainage may have the temperature even higher than 100^{o}C. The treatment of water with such a high temperature by using RO requires cooling as prerequisite step that adds the additional cost to the process and at the same time causes the waste of the energy associated with this water. Several studies have revealed the potential of membrane distillation to achieve high recovery factor from various types of brine and other concentrated solutions. Similarly, it has been demonstrated through several investigations that membrane distillation has the potential to compete with RO process if the source of waste grade heat or energy is available. In the case of produced water, membrane distillation can be used to achieve the water of very high purity, due to the capability of MD to reject all the salts, metals and other nonvolatile components. MD as an interesting candidate for produced water treatment has been analyzed by Shaffer et al [17].

A few current studies have investigated the potential of membrane distillation to treat the produced water. Singh and Kamlesh [18] have used porous PTFE flat sheet membranes to treat the simulated produced water with temperature raging from 80^{o}C to 130^{o}C corresponding to the feed pressure of 2-3 atm. The salinity level of the water is 10,000 ppm and phenol, cresol and naphthenic acid have also been added to simulate the produced water composition closely. It was found that the water vapor flux remains unchanged with respect to the presence of phenol, cresol and naphthenic acid, however, the

quantity of these compounds in the permeate increases as the feed temperature is increased. It was concluded that the membrane implied maintained its hydrophobic character throughout the experimentation as no sodium traces of sodium chloride were found in the permeate. The quantity of phenol and cresol in distillate was assumed due to the volatile nature of these compounds. The highest flux achieved was as high as 195 kg/m^{2}.h. Alkhudhiri et al [19] have also proved the feasibility of air gap MD for the treatment of produced water. Recently developed thermally rearranged polybenzoxazole membranes, initially developed for gas separation application with extraordinary gas permeability of small gas molecules due to biomodal cavities, exhibited very hydrophobic characteristics showing the flux of about 65 l/m^{2}.hr and virtually no sodium chloride in the permeate of direct contact MD, expected to be feasible for direct contact MD or air gap MD application for produced water treatment. This membrane maintained the hydrophobicity for a prolonged period of time.

A comparison of some desalination techniques on the basis of energy consumption, the handable and achievable salinity level has been shown in Figure 6.3.

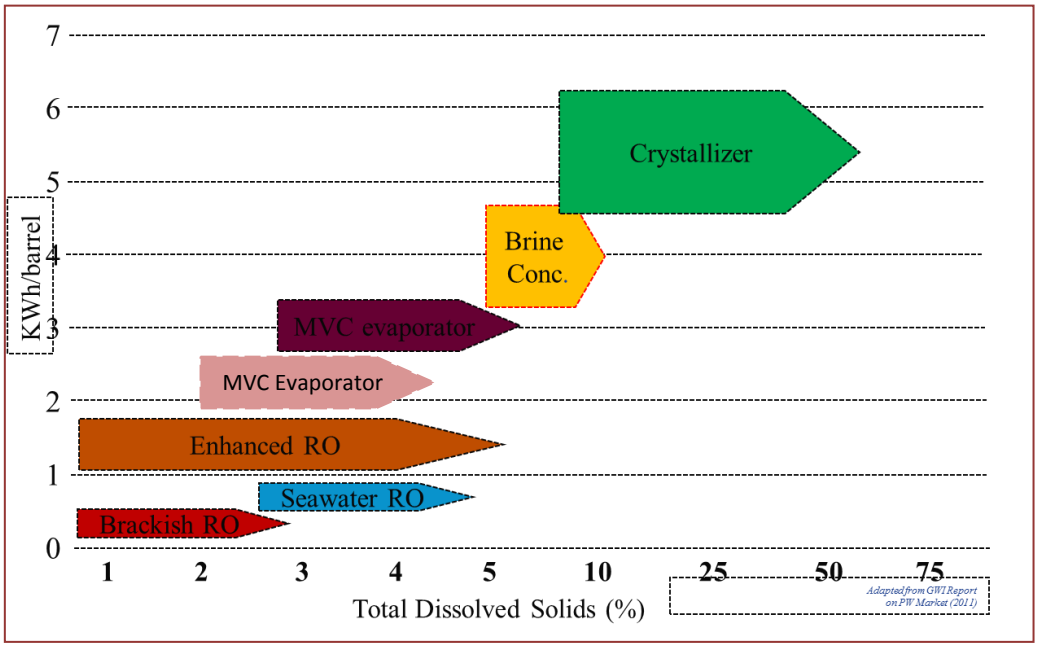

Figure 6.3: A comparison of desalination technologies on the basis of energy consumption, feed concentration and maximum achievable salinity level

The ability of MD to treat the solution beyond their saturation level has been well explored in membrane crystallization (MCr) which is an innovative crystallization concept to carry out finely controlled nucleation and crystal growth. The principles of membrane crystallization can be considered as an extension of the membrane distillation concept, thus providing all the advantages found in MD. The transformation from MD to MCr occurs when the treated solution reaches super-saturation level, thus allowing precipitating and separating the crystals. The advantages of membrane crystallization can be clarified by comparing this technique with a conventional crystallization unit, such as the forced circulation crystallizer. In this type of crystallizer the solvent evaporation and solute crystallization take place in the same location. The temperature gradient and hence the supersaturation is different at different locations in the crystallizer, causing a lower uniformity of the solid products [20]. In MCr a well-controlled nucleation and crystal growth is achieved through uniform evaporation rate through the pores of the membrane. Therefore, MCr produces crystals of much higher quality in

terms of purity, narrow size distribution, etc. with respect to conventional industrial crystallizers. Moreover, MCr is capable to target the polymorphic structure as seen from the crystallization of Na_2SO_4 as Thenardite (anhydrous) from wastewater [21], [22], $MgSO_4$ as Epsomite (heptahydrate) from seawater NF retentate [23], [24] and crystallization of various biomolecules [25]–[27] .

The thermodynamic driving force for the crystallization process is the difference in chemical potential of the crystallizing substance and the solution from where the crystals are formed also referred to as super-saturation. In a crystallization process first nucleation and then crystal growth takes place and agglomeration might occur. The nucleation process is divided into primary and secondary nucleation (Figure 6.4).

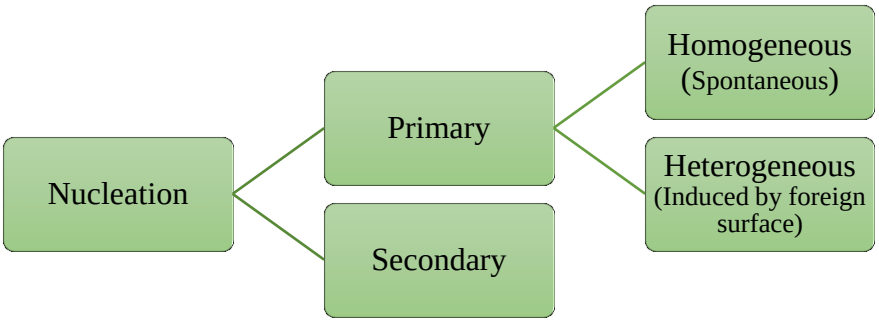

Figure 6.4: Principles of nucleation theory Adapted from [28]

Primary nucleation is new phase formation from a clear liquid or solution. It can be divided into homogeneous and heterogeneous nucleation. The homogeneous nucleation is caused by local fluctuations in concentration which induce formation of clusters. In under-saturated solutions the clusters falls apart, whereas in supersaturated solutions the clusters above a critical size are growing out [28]. The clusters are formed by attachment of single solute entities. Heterogeneous nucleation occurs when the nuclei is formed on already existing surfaces e.g. dust particles. The heterogeneous nucleation requires less energy than a homogeneous nucleation, because the nucleation energy barrier is reduced as no new surfaces have to be created. Hence homogeneous nucleation is rare in practical applications [28]. Secondary nucleation results from the presence of crystals of the crystallizing material that are already present in the solution [28]. Secondary nucleation is dominant in a membrane crystallizer [20]. When the nucleus is formed it can grow and form larger crystals. When the crystal is grown from solution the crystal growth process can be divided in to two main steps: (1) diffusion of growth units towards the crystal-solution interface and (2) subsequent the integration of the growth units into the crystal surface. Impurities in the solution can have a negative effect on the growth rate, due to adsorption on the crystal surface and inhibit the possibility to grow [28].

The current investigation has been carried out with the objective to determine the potentialities of membrane distillation for the purification and reuse of produced water. DCMD configuration has been applied as the first trial. Different membranes with various characteristics and materials of production have been realized for the treatment. The effect of feed temperature and hydrodynamic conditions on the separation achieved has been investigated. Initial studies to check the potential of MCr for recovery of salts from produced water have also been reported.

3. Experimental

3.1 Basic characterization

Produced water for the investigation was kindly provided by Kuwait Institute of Scientific Research (KISR). The water was initially characterized for some basic characteristics including solids present, carbon contents, conductivity and pH. Total carbon (TC), total organic carbon (TOC) and total inorganic carbon (TIC) measurements were carried out using a TOC-V CSN analyzer (Shimadzu). The dissolved solids are those that are not retained by filtration to 0.45 micron. A water sample was filtered through a filter of 0.45 micron, and then 1 g of the filtrate was dried by a thermo-balance (OHAUS MB 45) at a temperature of 105°C to obtain a constant weight. To find out the organic compound present into the water, the gas chromatography-mass spectrometry (GC-MS QP2010S, from Shimadzu) using an Equity 5 column was used. The analysis was carried out using the solid phase micro extraction (SPME) technique, in which the analytes establish equilibrium among the sample matrix and the polymer-coated fused fiber. Then the analytes are desorbed from the fiber to a chromatography column of the GC-MS.

3.2 Membrane used

Two different types of each poly vinyledene fluoride (PVDF) and polypropylene (PP) based hollow fiber membranes were used in the experimentation. The performance of ceramic membranes was also investigated. PVDF membranes were prepared in the laboratory and were assembled into glass module to use them for the experimentation. The polypropylene membranes used were commercial and one was purchased from Microdyn-Nadir (MD020CP2N) in the form of already assembled module while the fibers for other were provided by Membrana (PP Accurel® S6/2) and were assembled in the lab scale glass module. The detailed characteristics of the membranes used in the experimentation are provided in Table 6.1.

Table 6.1: Some basic characteristics of the membrane applied in the study

Fiber type	*Thickness (mm)*	*Emod N/mm²*	*Rm N/mm²*	*break %*	*W Nm*	*PMI bubble point (bar)*	*PMI Pore size (µm)*	*Porosity (%)*
PP1	0.45	103.75	4.16	174.40	1.11	0.76	0.2	73
PP2	0.45	103.75	4.16	174.40	1.11	0.76	0.2	70
PVDF1	0.19	150.53	4.49	223.30	0.34	0.93	0.29	65.44
PVDF2	0.40	65.76	3.86	259.95	0.71	0.87	0.23	80.77
Ceramic							0.2	

3.3 MD experimentation

For the MD tests, for the lab scale module, the initial experimentation was performed with double distilled water as feed and permeate at feed flow rate of 7.4 L/h in lumen side and feed inlet temperature of 50^{o}C. For produced water, the feed was introduced at the inner side of the fiber while the double distilled water was introduced on the shell side of the module. The experimentation has been performed with feed temperature ranging from 50-70 ^{o}C with an interval of 10^{o}C each. Feed flow

rates were varied from 7.4 L/h to 11.4 L/h with an interval of 1.8 L/h. The distillate flow rate and temperature were kept constant at 6 L/h and 25^{o}C, respectively throughout the above experimentation. For the commercial PP hollow fiber module from Microdyn-Nadir, hydrodynamic conditions were varied from feed flow rates of 50L/h to 150L/h with an interval of 50L/h keeping the feed and permeate temperatures at 50^{o}C and 25^{o}C, respectively. For detailed investigation of thermal effects on trans-membrane flux, feed flow rate of 50 L/h was selected and experimentation was accomplished at different feed inlet temperatures of 30^{o}C, 50^{o}C and 60^{o}C, keeping the permeate temperature constant at 25^{o}C.

The experimentation was carried out over an extended period of time for each type of module. The distillate weight was monitored during the experimentation. The possibility of using ceramic membranes for the saline water treatment was also analyzed. For ceramic membranes, the feed temperature was kept at 70^{o}C due to very low flux observed at the lower temperature ranges. For each membrane tested, the flux has been shown over experimental period of time to see the operational stability of the membrane.

3.3.1 MD set-up description

A schematic diagram of the set-up used for the DCMD experimental tests is shown in Figure 6.5. The feed solution is transported to the membrane module (H) from feed tank (F) by using a centrifugal pump (A). The feed is heated by heater (G) before entering into the membrane module. The feed flow rate is monitored by using the flow meter (B). Feed inlet temperature and pressure can be followed by using sensor (T) and monometer (P). Another temperature sensor is devoted to monitor and control the feed-temperature within the tank. Distillate is introduced into the module from distillate tank (D). Transport mechanism, temperature, pressure and flow on the permeate side is essentially similar to that described for the feed side. The distillate weight is scrutinized through a balance (C). Distillate and feed are in counter-flow configuration to ensure a better heat transfer between two streams.

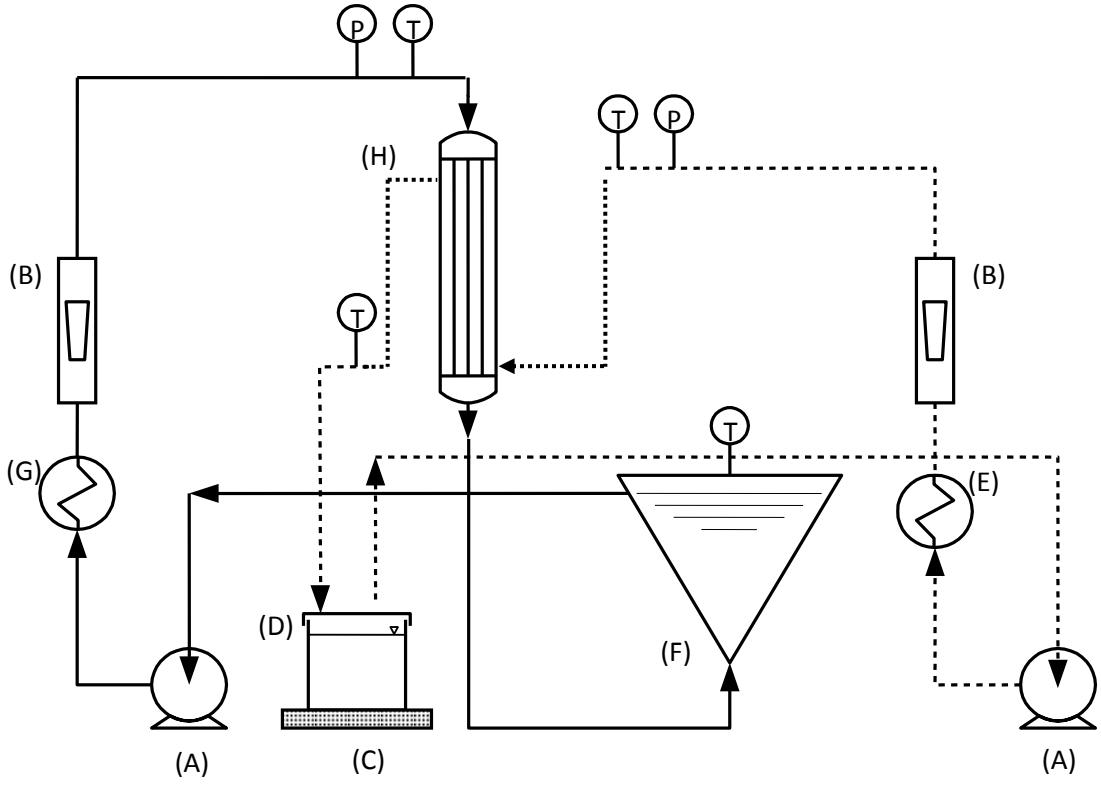

Figure 6.5: Schematic diagram of the set-up used for membrane distillation.

4. Results and discussion

4.1 Basic characterization

The initial experimentation was performed with the intention to characterize the saline water in terms of some basic characteristics. The results of the basic characterization including total carbon, total organic carbon, total solids, total dissolved solids, conductivity and pH obtained according to the procedure described in section 3.1 are given in Table 6.2. The comparison of table with the standard values given in the literature [2,23] indicates that the total organic content of the sample are quite low as compared to the maximum limit (~1700 mg/L) while the level of total solids and total dissolved solids are in medium range. The pH value is approaching to the upper limit mentioned in the literature, indicating very slight acidic nature of the solution. The value of conductivity also lies in intermediate ranges.

Table 6.2: Some basic characteristics of the sample

Total carbon (mg/L)	*Total organic carbon (mg/L)*	*Total solids (g/L)*	*Total dissolved solids (g/L)*	*Conductivity (ms)*	*pH*
50.62	41.072	248.2	247.9	228.2	6.15

Gas chromatography-mass spectrometry analyses of the samples are given in Figure 6.6 a and b which are indicating the presence of 1,2-diethoxy ethane in the sample.

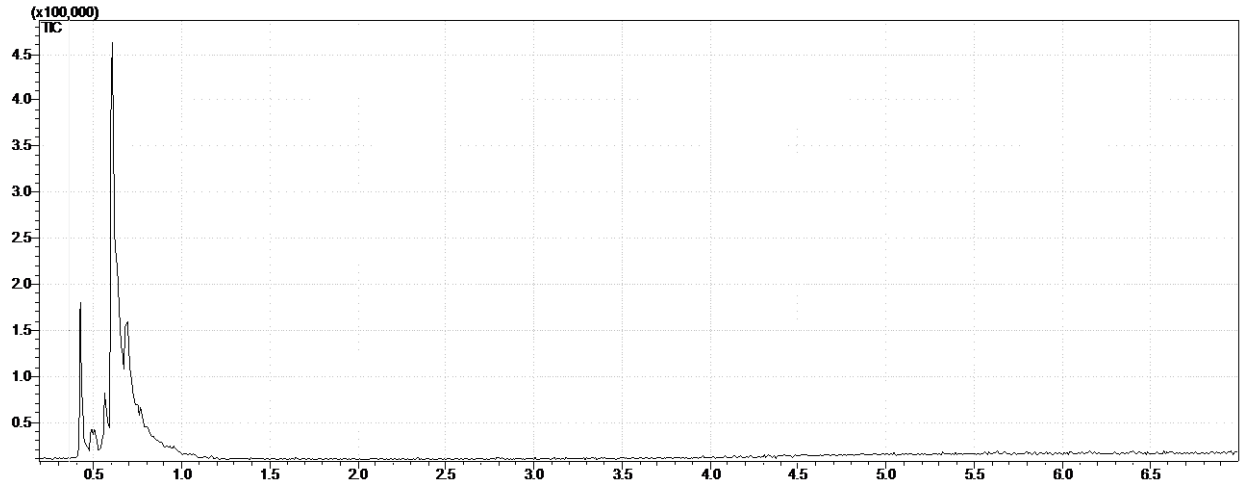

(a)

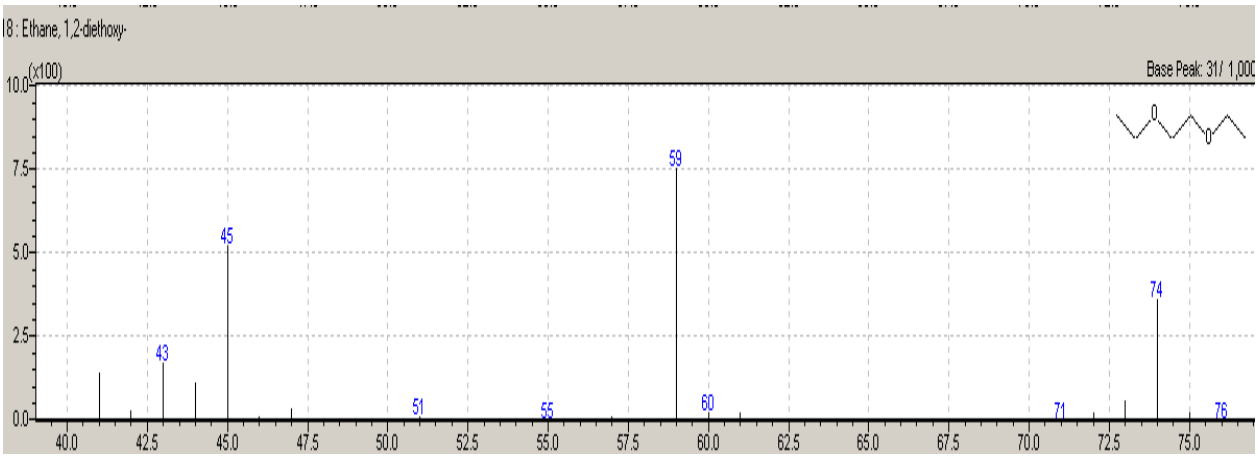

(b)

Figure 6.6: (a) Chromatograph and (b) Mass spectrum confirming the existence of 1,2-diethoxy ethane in the water.

4.2 MD tests

MD tests performed during the first phase aim to provide an indication of the stability of the operation and the comparison of the flux with that for the double distilled water. This objective has been realized by obtaining the flux under constant conditions of temperature and flow rate and monitoring the flux as a function of time. The MD flux for PP1 membrane is shown in Figure 6.7. The results performed by using the double distilled water are also presented for the comparison. Conductivity, ph and total dissolved solids in permeate were measured at the completion of each test and are provided in Table 6.3. The flux for distilled and saline water stays constant during the experimentation. The stable flux combined with the permeate characteristics reported in Table 6.3 indicates that the membrane shows stable behavior during the operation.

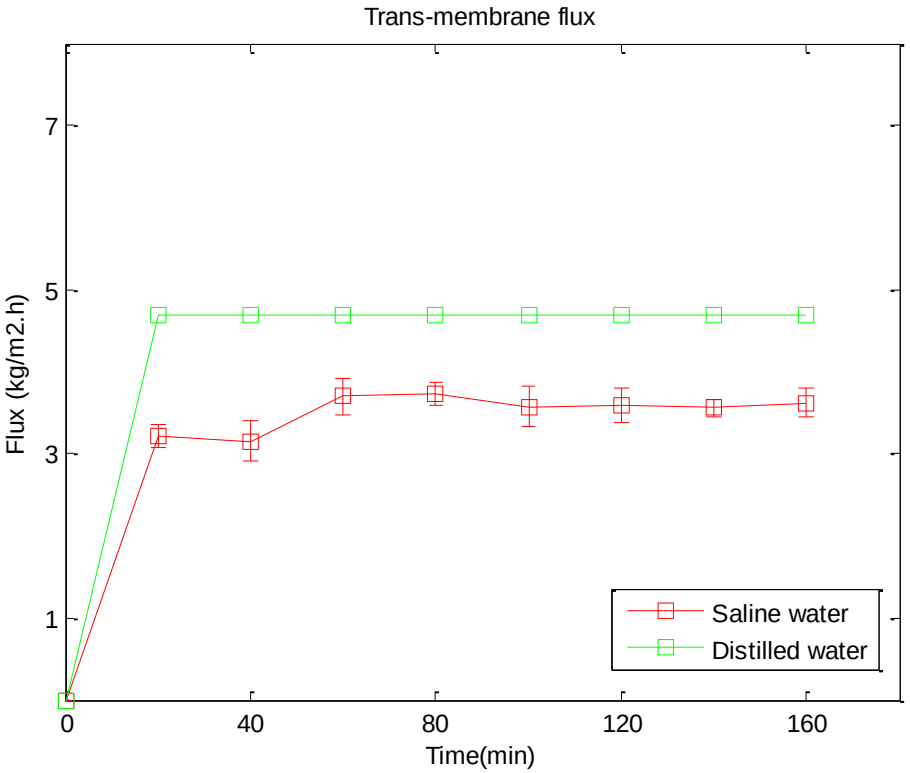

Figure 6.7: Flux obtained by using PP1 based hollow fiber membrane.

Table 6.3: Properties of the permeate obtained

Membrane type	*Conductivity (µs)*	*Total dissolved solids (ppm)*	*Total carbon (mg/L)*	*Total inorganic carbon (mg/L)*	*Total organic carbon (mg/L)*	*pH*	*Rejection Factor*
PP1	817	543	67.55	34.13	33.42	7.15	0.995
PVDF1	650	415	43.17	3.01	40.16	7.21	0.995
PVDF2	614	308	91.36	48.46	42.9	7.15	0.996

The results for the same experimentation carried out by using PVDF based hollow fiber membrane module are expressed in Figure 6.8 and Figure 6.9 (for PVDF1 and PVDF2). The flux for both types of PVDF fibers remains steady during the experimentation. The flux trend combined with the permeate characteristics listed in Table 6.3 implies the suitability of the fibers to treat the saline water.

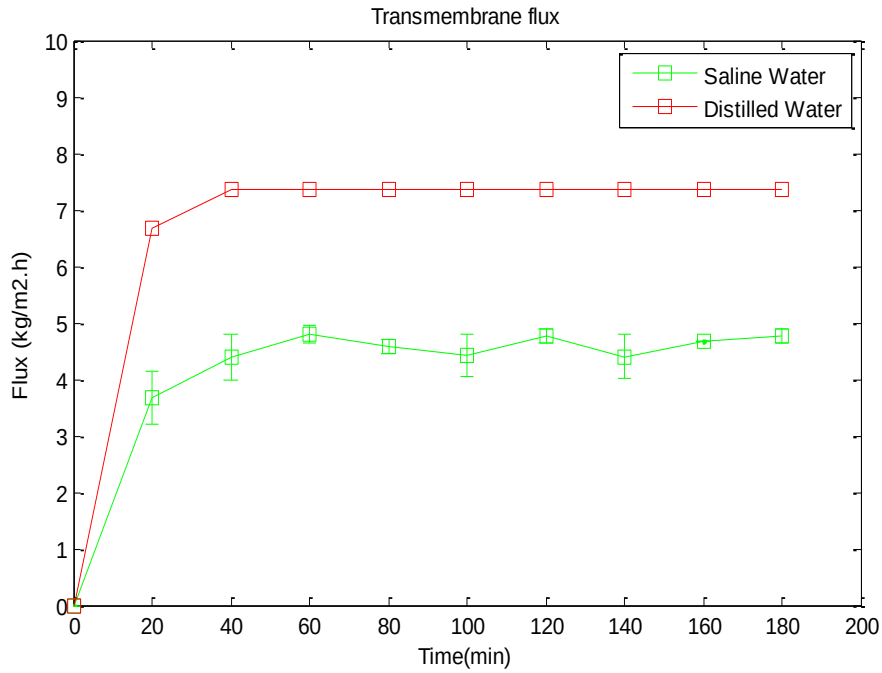

Figure 6.8: Trans-membrane flux obtained by using lab-made PVDF1 based hollow fiber membrane.

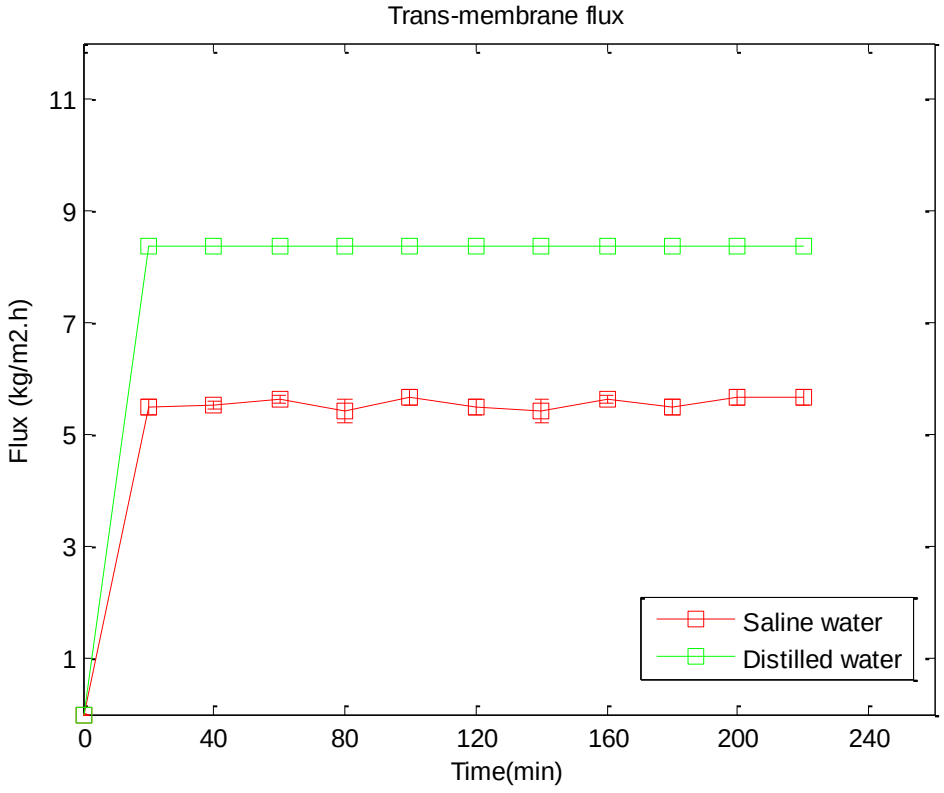

Figure 6.9: Flux obtained by using fiber type PVDF2

Another observation that can be readily made by looking at the Figure 6.7-Figure 6.9 is the lowest value of the flux for both distilled and saline water achieved for PP1 membranes. For PVDF1 membranes, trans-membrane flux is higher than PP and it further increases for PVDF2 membranes. The different flux observed for these membranes can be explained by using the membrane

characteristics provided in Table 6.1. The dependence of flux on membrane characteristics in MD can be expressed by the following relationship.

$$J \propto \frac{\varepsilon r^a}{\delta \tau}$$

Where J is trans-membrane flux, ε is the overall porosity of the membrane, r is the mean pore size, τ is the tortuosity factor and δ is the membrane thickness. For cylindrical pores, the value of 'a' is unity.

As evident from Table 6.1, the porosity of PP1 membranes is less than that for PVDF2 and greater than PVDF1. On the other side, PVDF based membranes have less wall thickness than PP1 while their mean pore size is larger than that of PP. The net result is the lower flux observed in the case of PP1 membranes. While comparing the values of flux for PVDF1 and PVDF2 membranes, it can be noticed that the higher porosity observed for PVDF2 membranes play the decisive role in its higher flux than that for PVDF1 though the wall thickness of PVDF1 membrane is lower than that of PVDF2, however, it might have more thermal polarization that suppresses the flux.

The second observation that can be readily made from Figure 6.7-Figure 6.9 is the difference in trans-membrane flux between distilled water and the saline water. As well acknowledged, the flux in MD is dependent upon the partial pressure gradient created across a microporous, hydrophobic membrane. The dissolved salts present into the produced water reduce the partial pressure of the water as predicted by Raoult's law given below. The consequence is that the flux of saline water is lower than that for the distilled water.

$$P = \gamma(1-x)P^o$$

Where P is the actual vapor pressure, γ is the activity coefficient and, x is the mole fraction of the solute in the solution and P^o is the vapor pressure of pure solvent (water).

The permeate properties summarized in Table 6.3 indicate that all three types of membranes are highly efficient in rejecting the total solids present into the feed and overall rejection factor is greater than 99% in all cases. The comparison of feed and permeate quality listed in Table 6.2 and Table 6.3, respectively designates that MD is not helpful in reducing the organic carbon present into the feed. Most probably, some volatile organic components present into the feed go through the membranes.

The experimentation was also carried out by changing the feed inlet temperature and feed flow rates for both PVDF and PP membranes. The effect of various feed inlet temperatures on trans-membrane flux has been shown in Figure 6.10. The flux increases exponentially by increasing the feed temperature.

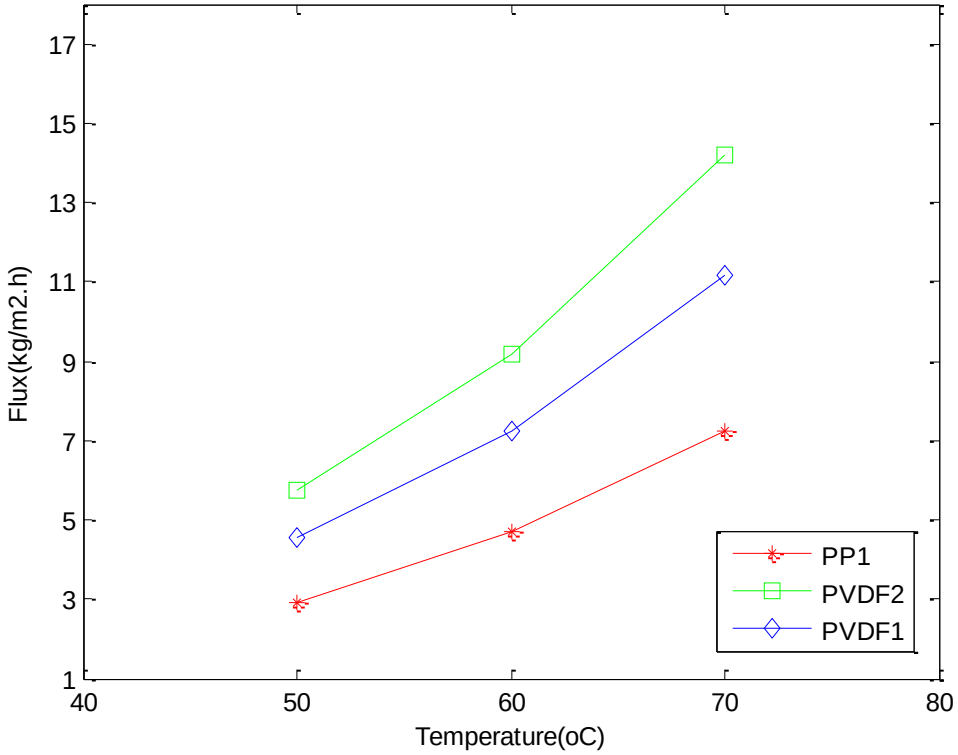

Figure 6.10: Effect of feed temperature on flux for different membranes

In membrane distillation, the flux is proportional to the vapor pressure gradient created across the microporous hydrophobic membrane.

$$J = c\Delta P$$

Where J is the flux, c is a constant depending upon the membrane characteristics and ΔP is the vapor pressure gradient across the membrane.

The vapor pressure is related with temperature by the Antoine's equation given by the following expression.

$$P = \exp\left(A - \frac{B}{T - C}\right)$$

Where A, B and C are constants which depend upon the type of solvent.

By increasing the feed inlet temperature, the vapor pressure gradient across the membrane increases exponentially and consequently we observe a proportional increase in trans-membrane flux.

The effect of feed flow rate for different types of membranes applied in the study is shown in Figure 6.11. It is evident from the figure that by increasing feed flow rate, the flux increase slightly for all the membranes, however, the effect is very low as compared to temperature. Increased feed flow rate favors the mixing of the feed present into the bulk and at the membrane interface. Consequently, the temperature difference between the bulk and the membrane surface decreases and the temperature polarization coefficient goes up. The overall impact is an increase in observed flux, as shown in the Figure 6.11.

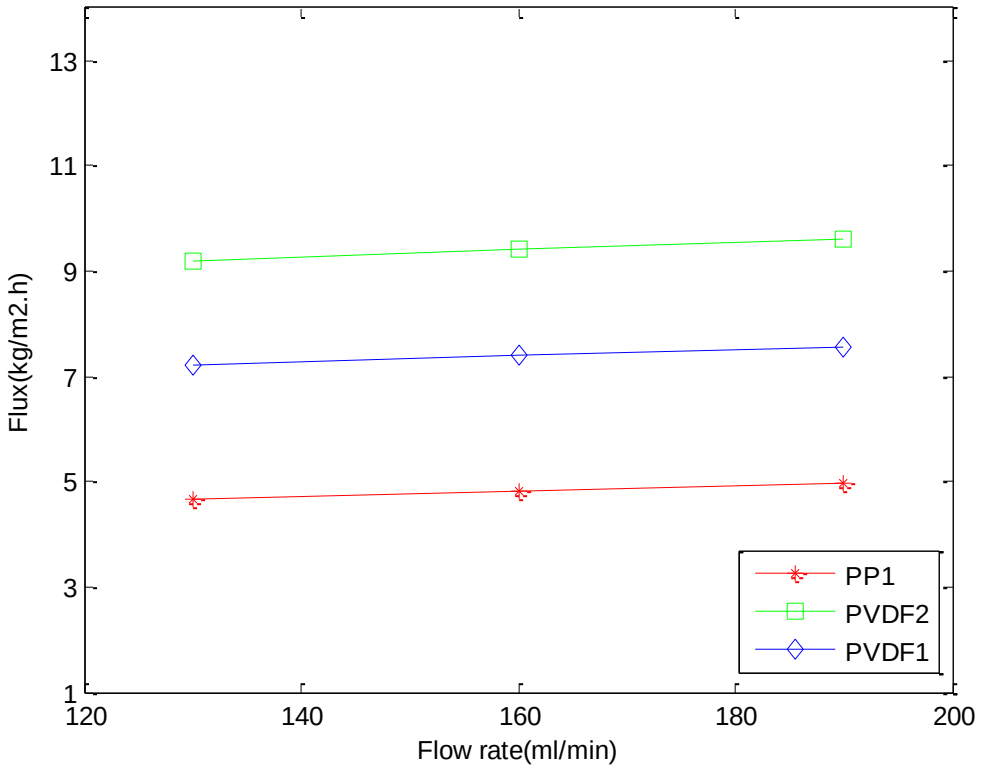

Figure 6.11: Effect of feed flow rates on flux

For detailed investigation of thermal effects on trans-membrane flux by using the commercial module from Microdyn-Nadir (MD020CP2N), feed flow rate of 50 L/h was selected and experimentation was accomplished at different feed inlet temperatures. The trans-membrane flux obtained at various temperatures is shown in Figure 6.12. The observed flux follows the same trend as observed for the other types of the membranes applied in the current study. However, the amount of flux obtained is quite low as compared to the previous results obtained at the same temperature by using other membranes. The comparison of the properties of two types of the PP membrane given Table 6.1 shows that these have essentially similar properties, however, the flux for both types under the same conditions of temperature is quite different. This discrepancy in the flux can be associated with different hydrodynamic conditions to which the membranes are subjected. For the commercial PP modules, two membrane modules were connected in parallel during the operation. Each module contains 40 fibers with length much higher than that for the lab-made PP1 module. Thus the Reynolds number for solution in each fiber would be much lower than that observed for PP1. Secondly, the higher length of the fiber would decrease the effective temperature gradient along the fiber greatly as the feed moves towards the exit point. Another reason that explains the less flux observed in case of PP2 is the fact that this module had been utilized in the past for some desalination related test which possibly has created some irreversible fouling on the membrane surface. All these factors contribute in decreasing the value of the flux. The amount of carbon present in the permeate was considerable at high temperatures and flow rates, the experimentation was also carried out at lower feed flow rates with the expectation of getting less carbon in permeate at lower feed inlet temperatures.

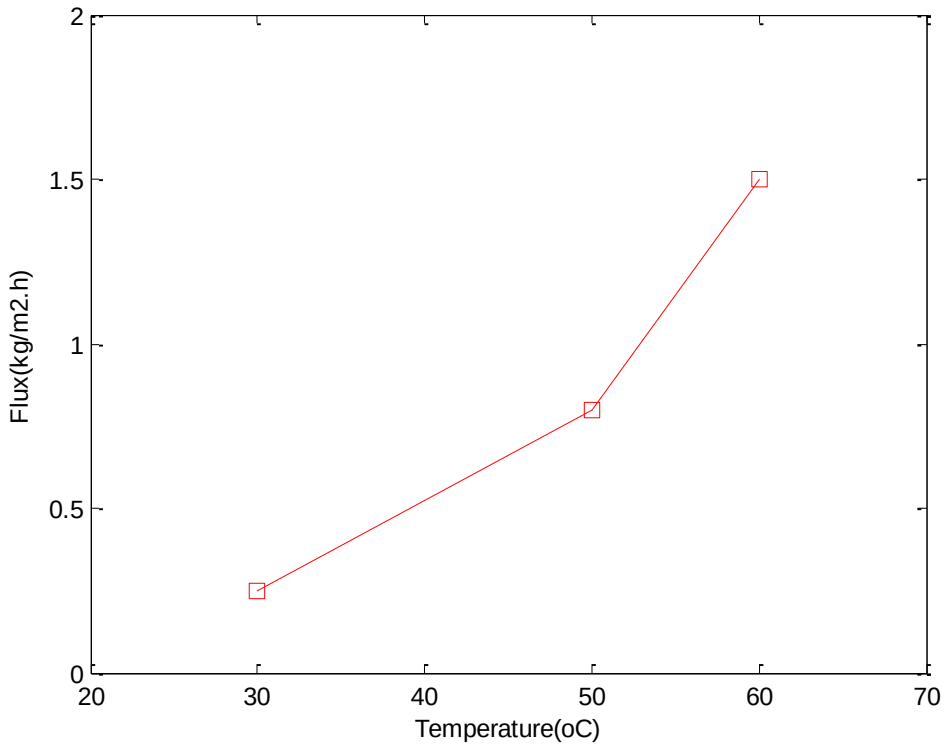

Figure 6.12: Flux obtained at different feed inlet temperatures for feed flow rate of 50L/h

The trans-membrane flux observed at different feed flow rates for feed inlet temperature of 50^{o}C is shown in Figure 6.13. The figure indicates that the trans-membrane flux increase significantly by increasing the feed flow rate which favors the argument raised in the above paragraph to explain the lower flux observed in PP2 than that for PP1. i.e. the hydrodynamic conditions in the commercial module are very poor and retard the flux of the process at the temperatures similar to those used for PP1. It is also clear from the figure that the trans-membrane flux decreases with the passage of time. This reduction can be related with increase in feed concentration as the process goes on. For PP1, PVDF1 and PVDF2, the reduction in flux has not been observed as the permeate collected within the experimental period of time was much less than that for PP2, due to the less surface area of the membranes.

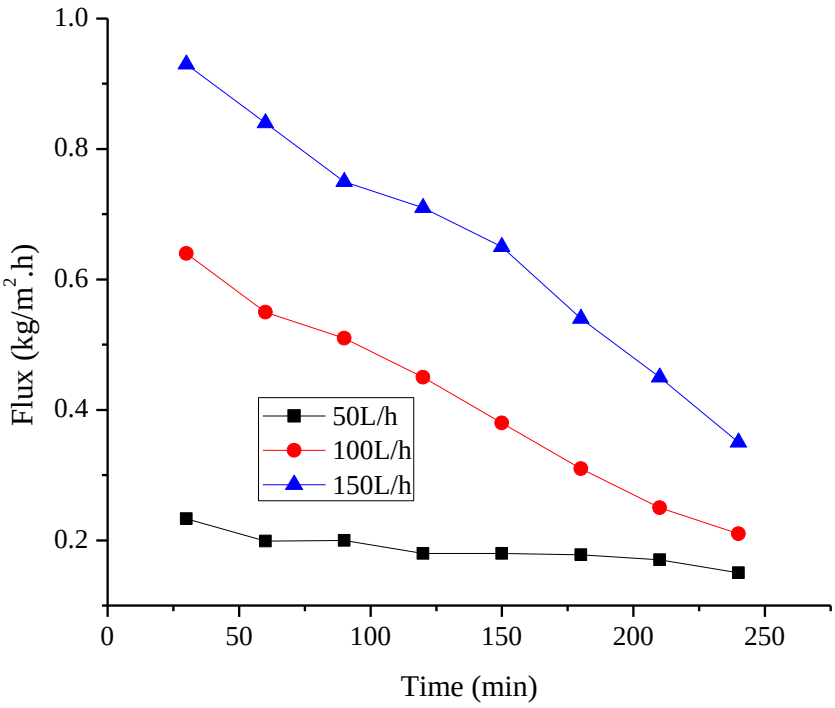

Figure 6.13: Trans-membrane flux obtained at different feed flow rates for feed inlet temperature of 50^{o}C

The properties of the permeate obtained for PP2 are shown in Table 6.4. The table shows that the value of the total dissolved solids decreases slightly by increasing the feed temperature at a particular flow rate while the overall value of total solids increases marginally by increasing the feed flow rate. Total inorganic carbon present into the permeate for all the conditions also shows the same trend. On the other hand, total organic carbon shows the opposite trend i.e. its value decreases by increasing the feed inlet temperature. As explained before, the organic carbon detected in the distillate is most probably due to the presence of volatile that go through the membrane. At high feed temperatures, it is possible that some volatiles are removed when the feed is still in the feed tank. An excellent rejection factor of greater than 99% for solids was observed under all the conditions.

Table 6.4: Properties of permeate obtained by using Mycrodyn-Nadir PP based module

Flow rates (L/h)	*Temperature (^oC)*	*Conductivity (µs)*	*Total dissolved solids(ppm)*	*NaCl (%)*	*Total carbon (mg/L)*	*Total inorganic carbon (mg/L)*	*Total organic carbon (mg/L)*	*pH*	*Rejection Factor*
50	30	72.5	36.1	0.1	55.299	20.955	34.325	7.13	0.994
	50	85	63	0.6	(*)	(*)	(*)	7.14	0.993
	70	142	70.6	0.1	56.713	42.886	13.926	7.13	0.995
100	40	51.2	88	0.1	42.509	21.342	21.167	7.12	0.997
	50	57.2	112.8	0.2	47.006	37.191	9.815	7.1	0.996
150	40	44.5	44	0.1	59.302	42.1	17.202	7.1	0.998
	50	96.7	189	0.2	61.572	49.691	11.881	7.14	0.995

(*) Data not available

The experimentation was also performed with ceramic membranes. The flux observed at feed temperatures of 50^{o}C and 60^{o}C was very low, hence, feed temperature of 70^{o}C was selected for the further experimentation. Preliminary experimentation was performed by using distilled water for the calibration purposes. For both liquids (distilled water and produced water), the feed flow rate was adjusted at 50L/h while the permeate flow rate was kept at 30L/h.

The flux obtained is shown in Figure 6.14. It was observed that the flux decreases as the experimentation goes on. The permeate quality was followed by constantly monitoring the conductivity of the distillate after regular intervals of time. It was seen that with decrease in flux, the conductivity of the distillate goes on increasing. For the new membrane, the flux drops to negligible value after almost 3 hours of operation. The membranes were washed with distilled water and dried and were put into the operation again. The flux was even lower this time and the reduction in flux was observed even earlier which leads to the negligible value of the flux. The properties of the distillate obtained by using ceramic membranes are shown in Table 6.5 which indicates a higher value of conductivity and total solids present into the distillate which is strong evidence of wetting of the membrane.

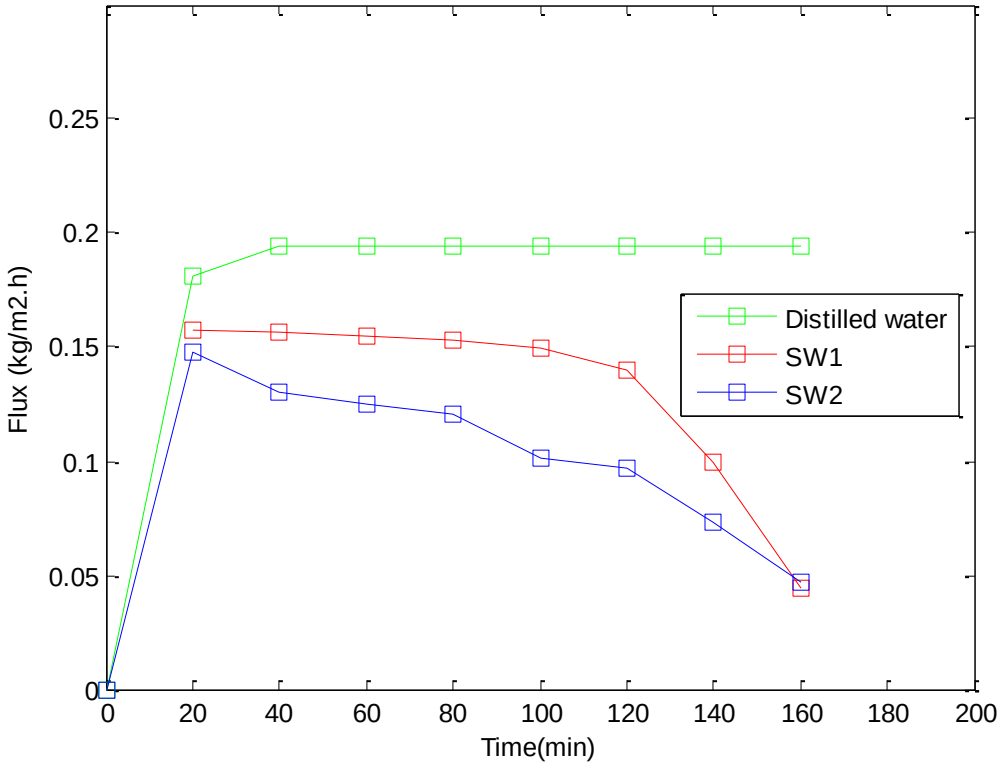

Figure 6.14: Flux obtained by using ceramic membranes. SW1 and SW2 indicate the flux obtained with new membranes and washed membranes after wetting, respectively

Table 6.5: Properties of distillate collected by using ceramic membranes

Membrane type	*Conductivity (ms)*	*Total dissolved solids(g/L)*	*NaCl (%)*	*Total carbon (mg/L)*	*Total inorganic carbon (mg/L)*	*Total organic carbon (mg/L)*	*pH*	*Rejection Factor*
Ceramic	7.45	3.70	-	(*)	(*)	(*)	7.12	-

(*) Data not available

After completion of the first cycle of experimentation with different membranes, the membranes were washed with double distilled water and stored over a period of two months and their reproducibility was tested by putting the membranes in operation under the same initial operating conditions of feed inlet temperature 50^{o}C and feed flow rate of 7.4L/h. The results are illustrated in Figure 6.15 for various membranes used in the study. It was observed that membranes show really reproducible performance even after storage. Flux obtained and the permeate quality remains essentially the same. The comparison of the trans-membrane flux obtained during the first and second cycles is shown in Figure 6.16 while the corresponding properties of the permeate are provided in Table 6.6.

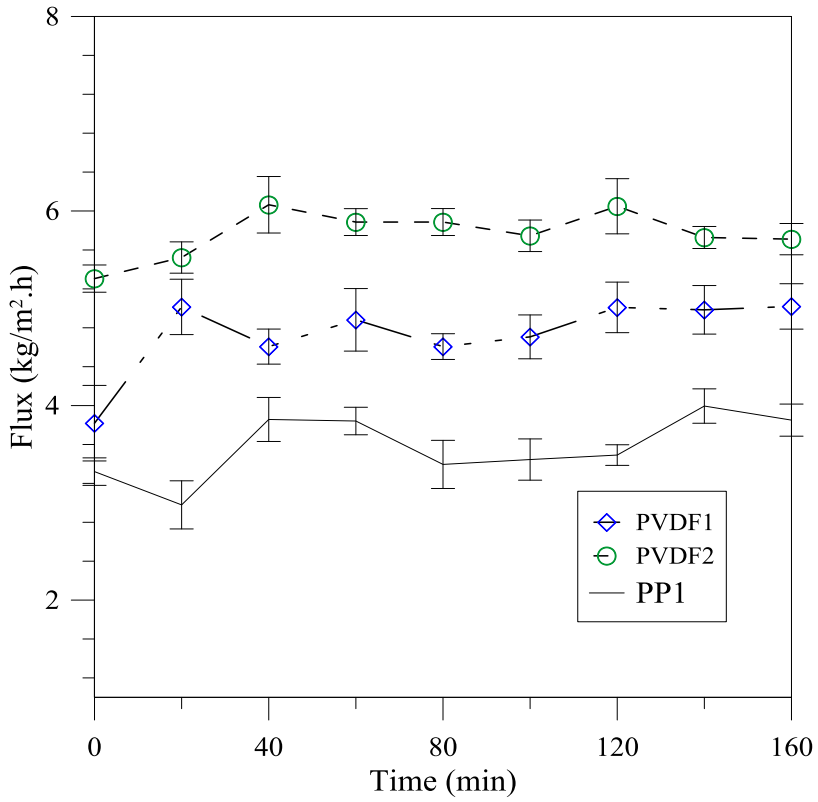

Figure 6.15: Flux obtained for PP1, PVDF1 and PVDF2 membranes after 8 weeks of storage

On the basis of the best performance, PVDF2 membranes were set to operation to see the performance for long term runs. The operation was carried out continuously for 7 hours. The flux obtained is shown in Figure 6.17 while the properties of the corresponding permeate are given in Table 6.7 which clearly points out a stable performance of the membrane throughout the operation. It can also be noted from Figure 6.17 that the flux remains stable during the operational time. The slight decrease in flux is due to the increasing concentration of feed in the feed tank.

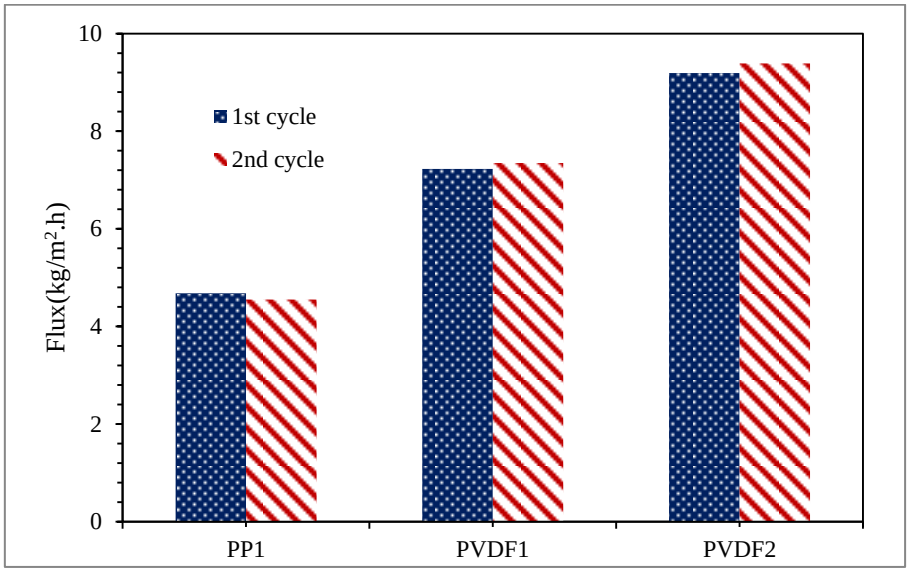

Figure 6.16: Comparison of flux for two cycles of data for different membranes tested

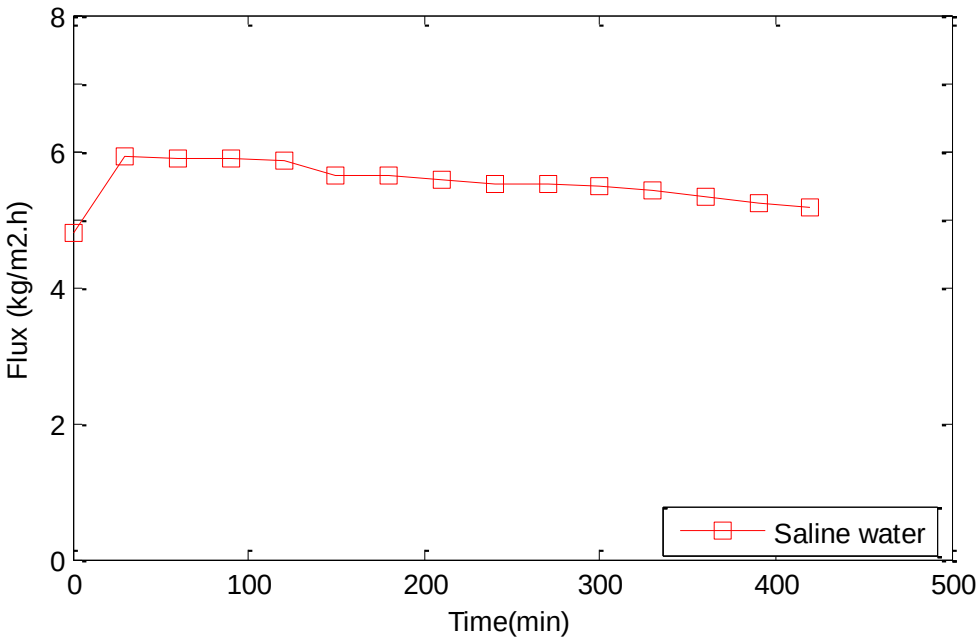

Figure 6.17: Flux obtained by using PVDF2 membranes for 7hours of operation

Table 6.6: Properties of the permeate obtained during reproducibility assessment tests

Membrane type	*Conductivity (µs)*	*Total dissolved solids(ppm)*	*NaCl (%)*	*Total carbon (mg/L)*	*Total inorganic carbon (mg/L)*	*Total organic carbon (mg/L)*	*pH*	*Rejection Factor*
PP1	750	512	1.3	(*)	(*)	(*)	7.12	0.996
PVDF1	735	532	1.6	(*)	(*)	(*)	7.14	0.992
PVDF2	685	367	1.3	(*)	(*)	(*)	7.13	0.994

All the values are averaged
(*) Data not available

Table 6.7: Properties of the permeate obtained after 7 hours of continuous operation

Membrane type	*Conductivity (µs)*	*Total dissolved solids(ppm)*	*NaCl (%)*	*Total carbon (mg/L)*	*Total inorganic carbon (mg/L)*	*Total organic carbon (mg/L)*	*pH*	*Rejection Factor*
PVDF 2	450	212	1	42.26	3.15	41.11	7.10	0.998

The results obtained in the currents study have been compared with some other state-of-the-art techniques mentioned in the literature and the results have been described in Table 6.8. The table indicates that the TDS removal achieved in this study is much higher than the conventional methods applied for treatment of produced water, except that for RSE which is applicable to only the solution with low salinity level. BTP and EDR are much more effective in removing the organics on the other hand. On contrary, MD is able to purify the produced water to the level of drinking quality in terms of TDS (for drinking water, the allowable TDS is 500 ppm while for the agricultural uses, it is 1000 ppm). The only point of concern for MD is to bring the TOC down to the required level.

Table 6.8: Comparison of some of the techniques used to treat produced water

Technique	*TDS removed %*	*TOC removed %*	*Limitation/drawback*	*Ref.*
BTP	9	90	Limited recovery of TDS	[24]
EDR	88.9	93.04	Requires regeneration, Concentration dependent performance	[25]
CDT	>61.9	-	High cost of electrodes, susceptible to fouling	[26]
RSE	99.6	-	Maximum feed concentration<16%, High heating cost	[27]
MD	99.5	93	Removal of volatile organics demands further attention	Current study

(-) Data not provided

BTP Bio treatment process
EDR Electrodialysis reversal
CDT Capacitive deionization technology
RSE Rapid spray evaporation

5. Membrane crystallization of produced water

MCr has been employed for treatment of produced water to recover the contained salts and simultaneously to increase the fresh water production. Analysis of the cations present in the produced water has been carried out by ionic chromatography (Table 6.9). The high amount of sodium might predict in precipitation of sodium chloride crystals. However, the low solubility of calcium in the form of calcium sulphate (gypsum etc.) and calcium carbonate risks to create scaling on the membrane surface. In membrane crystallization, calcium is often removed by chemical treatment to avoid the dangerous phenomena of scaling [29], [30]. Nevertheless, in this study the produced water has not been treated chemically prior to MD and MCr in order to evaluate the behaviour of direct treatment with respect to trans-membrane flux, crystal quality and eventual scaling phenomena.

Table 6.9: Cationic composition of produced water

Component	*Concentration [ppm]*
Sodium Na	76,646
Calcium Ca	6,065
Magnesium Mg	8,361
Potassium K	1,396

The utilized membranes applied in MCr are PP1 and PVDF2 with the operative conditions reported in Table 6.10.

Table 6.10: Operative conditions for MCr of produced water

Membrane	*Temperature [°C]*		*Flow rate [ml/min]*	
	Feed inlet	*Permeate*	*Feed*	*Permeate*
PP1	49	20	70	50
PP1	59	20	70	50
PVDF2	49	20	70	50

The produced water has been treated until super-saturation and the time when crystals have been detected in the feed tank, suspension samples have been withdrawn from the tank and again after 60 minutes. The crystals in the mother liquid have been examined visually by optical microscope. The crystal images obtained from the microscope has been processed by the software ImageJ to determine crystal shape, dimension, crystal size distribution (CSD), coefficient of variation (CV), growth rate (G) and nucleation rate (B^0).

Coefficient of variation (CV) has been estimated through equation 1, whereas growth and nucleation rate has been estimated on the basis of the Randolp-Larson model (equation 2 and 3, respectively):

$$CV = \frac{F_{84\%} - F_{16\%}}{2 \cdot F_{50\%}} \qquad (1)$$

$$\ln(n) = \frac{-L}{Gt} + \ln(n^0) \qquad (2)$$

$$B^0 = n^0 G \qquad (3)$$

where F is the cumulative percent function given by the crystal length at the indicated percentage, n is the crystal population density, L is crystal size, G is growth rate, t is retention time and n^0 is population density at L equal to zero.

Narrow CSD (Figure 6.18) and the low CV (Table 6.11), characterizing the membrane crystallizer, are also obtained in the treatment of produced water. CSD and CV-values suggests a small increase in the size difference of the produced crystals. Nevertheless, CV for all the sample are below 50 % which is the value, in general, obtainable from industrial crystallizers [31]. The lowest CV (26.40 %) and the highest CV (49.07 %) is obtained under the same operative conditions, i.e. PP1 at feed temperature of 59 °C. These results indicate that the small crystals initially produced are getting dissolved due to the higher temperature of the mother liquid, thus the mean diameter and growth rate are also higher for this sample. Nevertheless, the subsequent sample (taken after 60 minutes), the growth rate is depressed and nucleation seems to be the defining parameter, causing a decrease in mean diameter and higher CV because of the many small and fine crystals produced. Noticed by the sample taking time (Table 6.11) for PP1 (T_{feed}: 59 °C), the crystals are detected before due to the fact that the membrane module containing PP1 fibers consist of 4 fibers, making the volume reduction factor higher together with the higher feed temperature causing a higher flux. These factors influence the super-saturation rate and level, therefore the results indicate that these operative conditions might be more uncontrollable in particular with respect to a lower feed temperature.

Crystallization is detected last for the PVDF2 membrane where the module only consists of three fibers. The lowest mean diameter and the lowest growth rate are also obtained for the PVDF2 (Table 6.11). However, the slow crystallization process has a positive effect on CV and in achieving a relative steady nucleation and growth rate with only slight decrease in nucleation and increase in growth rate. Therefore, the crystal size has increased in the sample taken after 60 min, whereas for the PP1 membrane for both the utilized feed temperatures mean diameter, growth rate are decreasing and the nucleation rate is increasing. The results indicate that the PVDF2 membrane is producing crystals of higher quality by a better controllable crystallization process.

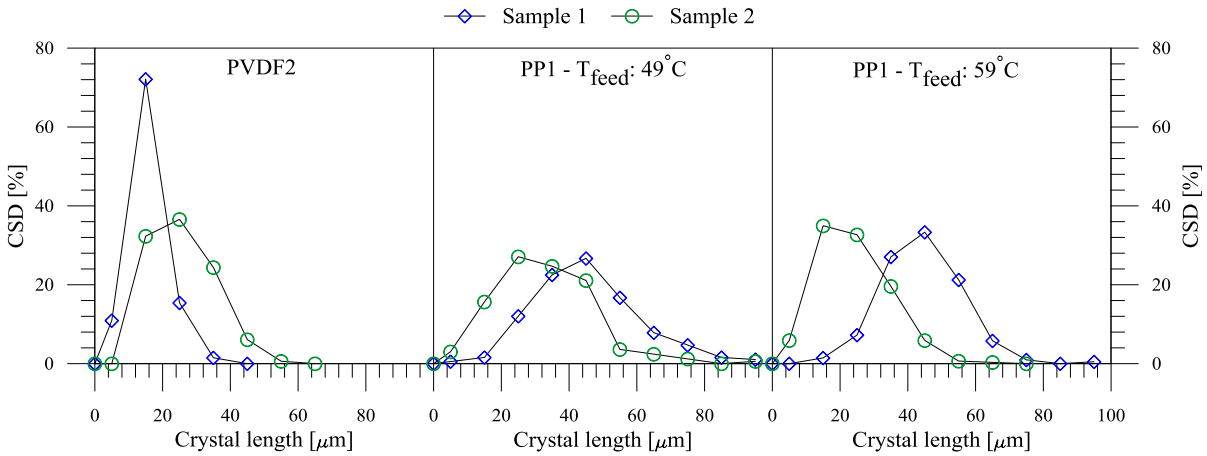

Figure 6.18: Crystal size distribution (CSD) achieved during crystallization of produced water (a) PVDF2, (b) PP1-Tfeed: 49°C, (c) PP1-Tfeed: 59°C.

Table 6.11: Crystal characteristics achieved in the crystallization of produced water

	PVDF2		*PP1 (T_{feed}: 49°C)*		*PP1 (T_{feed}: 59°C)*	
Sample	*1*	*3*	*1*	*3*	*1*	*3*
Sampling time [min]	553	616	304	383	230	310
Number of crystal analyzed	201	164	191	166	207	306
Mean diameter (d_m) [µm]	15.70	25.38	51.00	33.47	46.40	23.71
CV [%]	32.07	40.34	36.89	43.34	26.40	49.07
Growth rate (G) [µm/min]	0,0114	0,0184	0,180	0,0795	0,156	0,0415
Nucleation rate (B^0) [no./(L·min)]	2,31E+05	1,90E+05	9,30E+04	1,13E+05	1,43E+05	2,00E+05

Analysis of the characteristics of the produced water by means of ionic chromatography suggested that the high amount of sodium could precipitate as NaCl crystals. The images obtained from the analysis by optical microscope supports the precipitation of NaCl, where the crystals exhibit the conventional cubic habit characterized by NaCl (Figure 6.19). The cubic habit of the produced crystals has been determined by evaluating the length to width (LW) ratio as shown in Figure 6.20. The majority of the crystals are within the cubic structure (LW < 1.3) also supporting that few or no impurities are incorporated into the crystal lattice, as impurities suppress the cubic structure of NaCl.

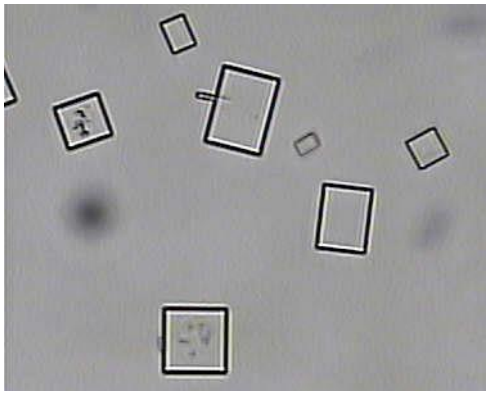

Figure 6.19: Sodium chloride precipitated from produced water.

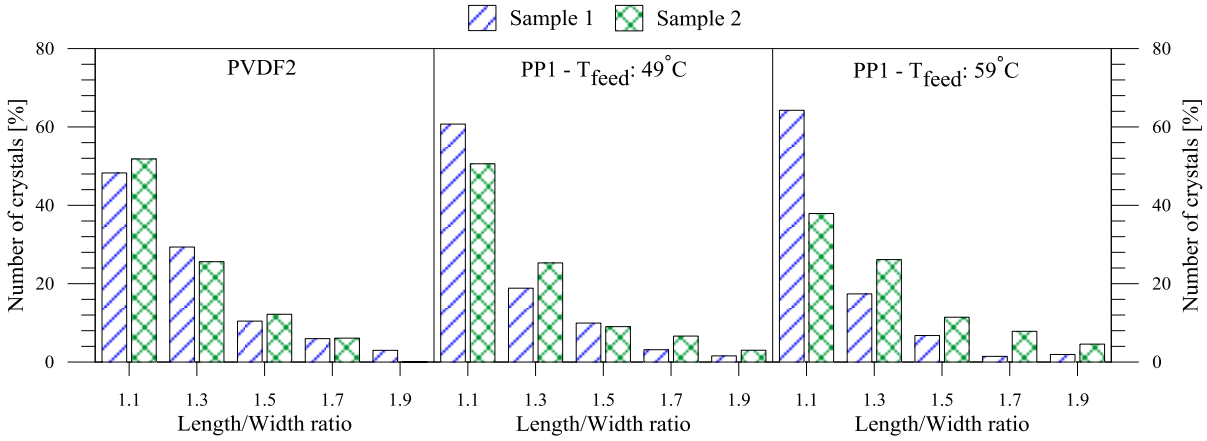

Figure 6.20: Length to width ratio of the obtained crystals.

The recovered crystals from produced water have been analyzed with SEM and energy dispersive x-ray (EDX). SEM images shown in Figure 6.21 at different magnifications are confirming the microscope images of the cubic structure. To analyze the composition of the crystals and to check if any impurities are present, EDX analysis has been performed. The EDX analysis given in Figure 6.22 clearly shows that only sodium chloride without impurities is crystallized from the produced water.

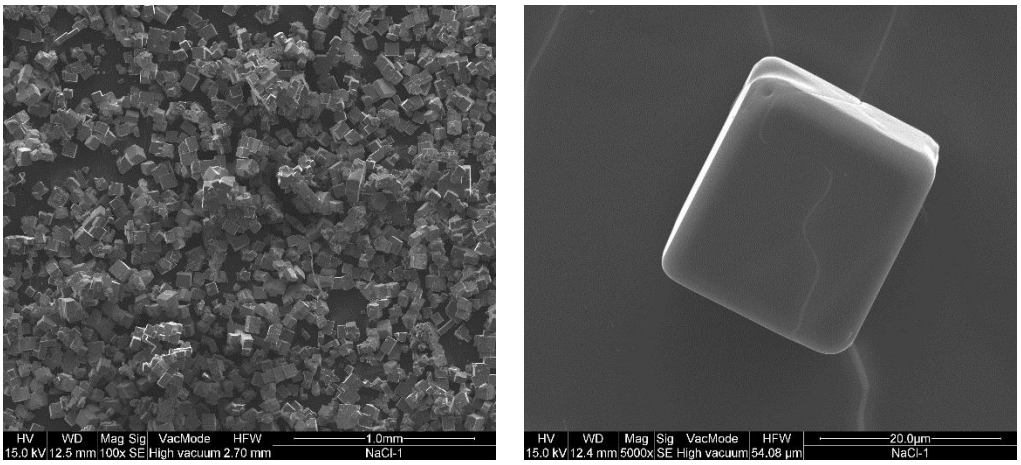

(a) *(b)*

Figure 6.21: SEM images of the crystals precipitated from produced water (a) Area of crystal sample – magnification: 100x, (b) Single crystal – magnification: 5000x

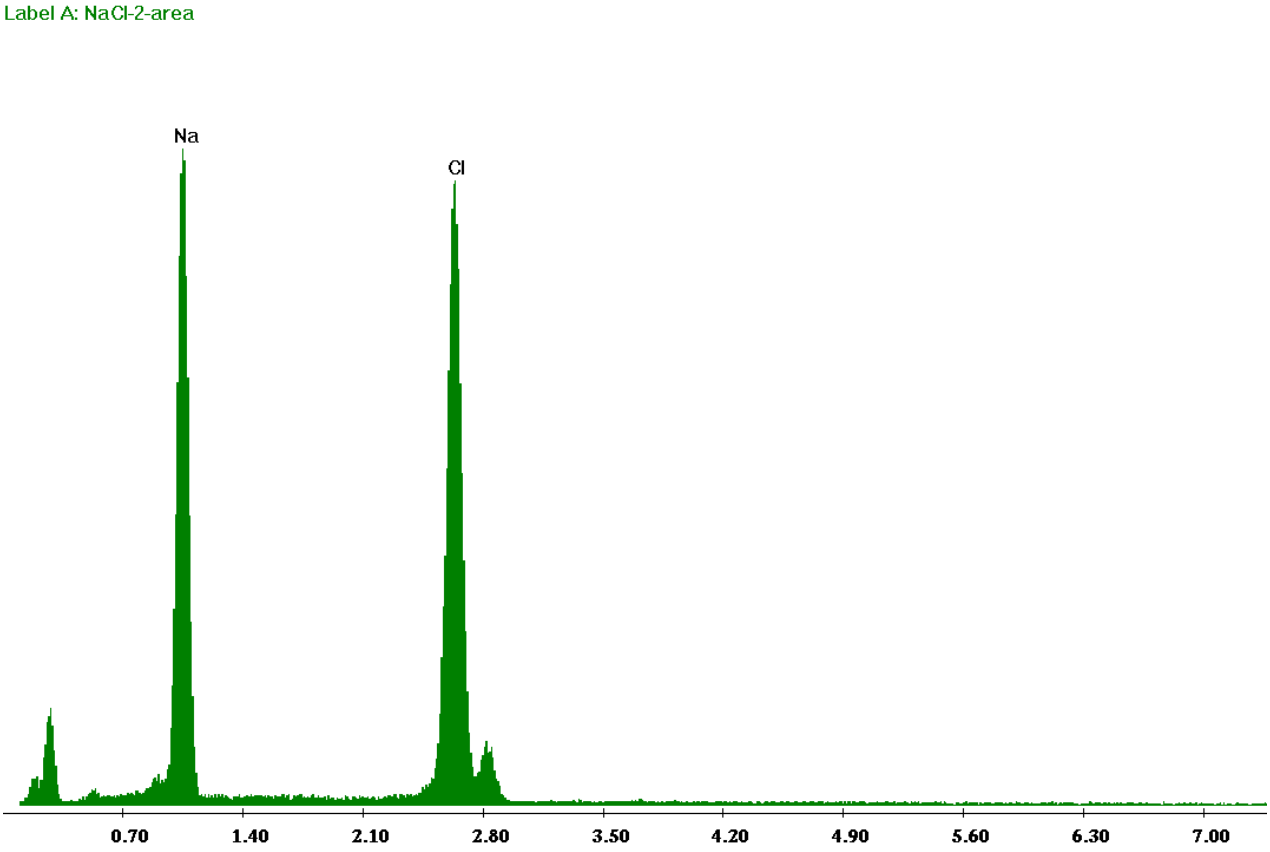

Figure 6.22: Example of EDX spectra obtained for the crystals precipitated from produced water.

6. Conclusions

The stability of PVDF and PP membranes for membrane distillation of the produced water has been confirmed. Membrane distillation tests carried out show an excellent rejection of the total solids present into the feed. The rejection of carbon, however, still needs further investigation. The overall rejection of total solids is greater than 99% in all the cases, however, the chemical analysis of permeate indicates that some volatiles (1,2-diethoxy ethane) go through the membranes. The reproducibility of the membranes has been confirmed by storing the membranes for 8 weeks and then putting into operation again. The best membranes in terms of performance were selected to check their performance stability over longer period of time and it was observed that membranes show quite stable performance even after 7 hours of continuous operation. Ceramic membranes used in the study lose hydrophobic character easily and get wetted.

The produced water contains valuable components including many metals such as lithium, barium, magnesium, aluminum, copper etc. with quite high concentration. The initial results of MCr experimentation show that feasibility of the process. The recovered crystals show very high purity and good quality of the crystals obtained.

References

[1] E. T. Igunnu and G. Z. Chen, "Produced water treatment technologies," *Int. J. Low-Carbon Technol.*, pp. 1–21, Jul. 2012.

[2] *Annual Energy Outlook 2011*, vol. 0383, no. April. 2011.

[3] C. Boyer, R. Lewis, and C. K. Miller, "Shale Gas : A Global Resource,"Oilfield Review pp. 28–39, 23 2011.

[4] US energy adminsitration, "Annual Energy Outlook 2010 With Projections to 2035." U.S Enegy Information Administration, 2010.

[5] D. A. Dzombak, R. D. Vidic, and K. B. Gregory, "Water Management Challenges Associated with the Production of Shale Gas by Hydraulic Fracturing," *Elements*, vol. 7, no. 3. pp. 181–186, 2011.

[6] A. Fakhru'l-Razi, A. Pendashteh, L. C. Abdullah, D. R. A. Biak, S. S. Madaeni, and Z. Z. Abidin, "Review of technologies for oil and gas produced water treatment.," *J. Hazard. Mater.*, vol. 170, no. 2–3, pp. 530–51, Oct. 2009.

[7] K. K. E.J. Sullivan, R.S. Bowman, L. Katz, "Water treatment technology for oil and gas produced water," in *Identifying Technologies to Improve Regional Water Stewardship:*, 2004, no. April, pp. 216–225.

[8] International Energy Agency, "World Energy Investment Outlook 2003,"Internation Energy Agency, 2003.

[9] 07122-12 RPSEA Project, "An Integrated Framework for Treatment and Management of Produced Water,"1st edition, Colorado School of Mines 2009.

[10] T. Sirivedhin, J. McCue, and L. Dallbauman, "Reclaiming produced water for beneficial use: salt removal by electrodialysis," *J. Memb. Sci.*, vol. 243, no. 1–2, pp. 335–343, Nov. 2004.

[11] J. R. Mccutcheon, R. L. Mcginnis, and M. Elimelech, "A novel ammonia--carbon dioxide forward (direct) osmosis desalination process," Desalination vol. 174, pp. 1–11, 2005.

[12] D. K. Anderson, "Concentration of dilute industrial wastes by Direct osmosis," University of Rhode Island, [Kingston], 1977.

[13] R. W. Holloway, A. E. Childress, K. E. Dennett, and T. Y. Cath, "Forward osmosis for concentration of anaerobic digester centrate," Water Res., vol. 41, pp. 4005–4014, 2007.

[14] E. G. York, R. J.; Thiel, R. S.; Beaudry, "Full-Scale Experience of Direct Osmosis Concentration Applied to Leachate Management," in *6th, International waste management and landfill symposium; Sardinia 99*, 1999.

[15] P. Xu, T. Cath, and J. E. Drewes, "Novel and Emerging Technologies for Produced Water Treatment," in *US EPA Technical Workshops for Hydraulic Fracturing*.

[16] L. Camacho, L. Dumée, J. Zhang, J. Li, M. Duke, J. Gomez, and S. Gray, "Advances in Membrane Distillation for Water Desalination and Purification Applications," *Water*, vol. 5, no. 1, pp. 94–196, Jan. 2013.

[17] D. L. Shaffer, L. H. Arias Chavez, M. Ben-Sasson, S. Romero-Vargas Castrillón, N. Y. Yip, and M. Elimelech, “Desalination and reuse of high-salinity shale gas produced water: drivers, technologies, and future directions.,” *Environ. Sci. Technol.*, vol. 47, no. 17, pp. 9569–83, Sep. 2013.

[18] D. Singh and K. K. Sirkar, “Desalination of brine and produced water by direct contact membrane distillation at high temperatures and pressures,” *J. Memb. Sci.*, vol. 389, pp. 380–388, Feb. 2012.

[19] A. Alkhudhiri, N. Darwish, and N. Hilal, “Produced water treatment: Application of Air Gap Membrane Distillation,” *Desalination*, vol. 309, pp. 46–51, Jan. 2013.

[20] E. Curcio, A. Criscuoli, and E. Drioli, “Membrane Crystallizers,” *Ind. Eng. Chem. Res.*, vol. 40, pp. 2679–2684, 2001.

[21] E. Curcio, X. Ji, A. M. Quazi, S. Barghi, G. Di Profio, E. Fontananova, T. Macleod, and E. Drioli, “Hybrid nanofiltration–membrane crystallization system for the treatment of sulfate wastes,” *J. Memb. Sci.*, vol. 360, no. 1–2, pp. 493–498, Sep. 2010.

[22] W. Li, B. Van der Bruggen, and P. Luis, “Integration of reverse osmosis and membrane crystallization for sodium sulphate recovery,” *Chem. Eng. Process. Process Intensif.*, vol. 85, pp. 57–68, Nov. 2014.

[23] E. Drioli, E. Curcio, A. Criscuoli, and G. Di Profio, “Integrated system for recovery of CaCO3, NaCl and MgSO4·7H2O from nanofiltration retentate,” *J. Memb. Sci.*, vol. 239, no. 1, pp. 27–38, Aug. 2004.

[24] F. Macedonio, E. Curcio, and E. Drioli, “Integrated membrane systems for seawater desalination : energetic and exergetic analysis, economic evaluation, experimental study,” *Desalination*, vol. 203, no. May 2006, pp. 260–276, 2007.

[25] G. Di Profio, E. Curcio, A. Cassetta, D. Lamba, and E. Drioli, “Membrane crystallization of lysozyme: kinetic aspects,” *J. Cryst. Growth*, vol. 257, pp. 359–369, Oct. 2003.

[26] G. Di Profio, S. Tucci, E. Curcio, and E. Drioli, “Controlling Polymorphism with Membrane-Based Crystallizers : Application to Form I and II of Paracetamol,” *Chem. Mater.*, vol. 19, pp. 2386–2388, 2007.

[27] G. Di Profio, E. Curcio, S. Ferraro, C. Stabile, and E. Drioli, “Effect of Supersaturation Control and Heterogeneous Nucleation on Porous Membrane Surfaces in the Crystallization of L -Glutamic Acid Polymorphs,” *Cryst. Growth Des.*, vol. 9, pp. 2179–2186, 2009.

[28] J. W. Mullin, *Crystallization*, 4th Editio. Butterworth-Heinemann, 2001.

[29] F. Macedonio, C. A. Quist-jensen, O. Al-harbi, H. Alromaih, S. A. Al-jlil, F. Al Shabouna, and E. Drioli, “Thermodynamic modeling of brine and its use in membrane crystallizer,” *Desalination*, vol. 323, pp. 83–92, 2013.

[30] F. Macedonio and E. Drioli, “Hydrophobic membranes for salts recovery from desalination plants,” *Desalin. Water Treat.*, vol. 18, pp. 224–234, 2010.

[31] S.J. Jancic and P. A. M. Grootscholten, *Industrial crystallization*. Delft, Holland: Delft University Press, 1984.

CHAPTER 7

Fouling in membrane distillation

1. Introduction

In a broader sense fouling is defined as the process of deposition of particles or solute at the membrane surface or inside the pores such that the membrane performance is deteriorated [1]. It has been considered as a major obstacle in wide spread use of membrane technology for a number of applications. Intensive fouling may require rigorous chemical cleaning or membrane replacement, thus contributing to the overall operational cost of a treatment plant. There are several types of foulants encountered in conventional pressure driven processes such as colloidal, biological, organic and scaling. The fouling reduces the permeation of the membrane due to increase in resistance to mass transfer. Figure 7.1 describes the typical resistances that occur during the mass transport in low pressure membrane processes.

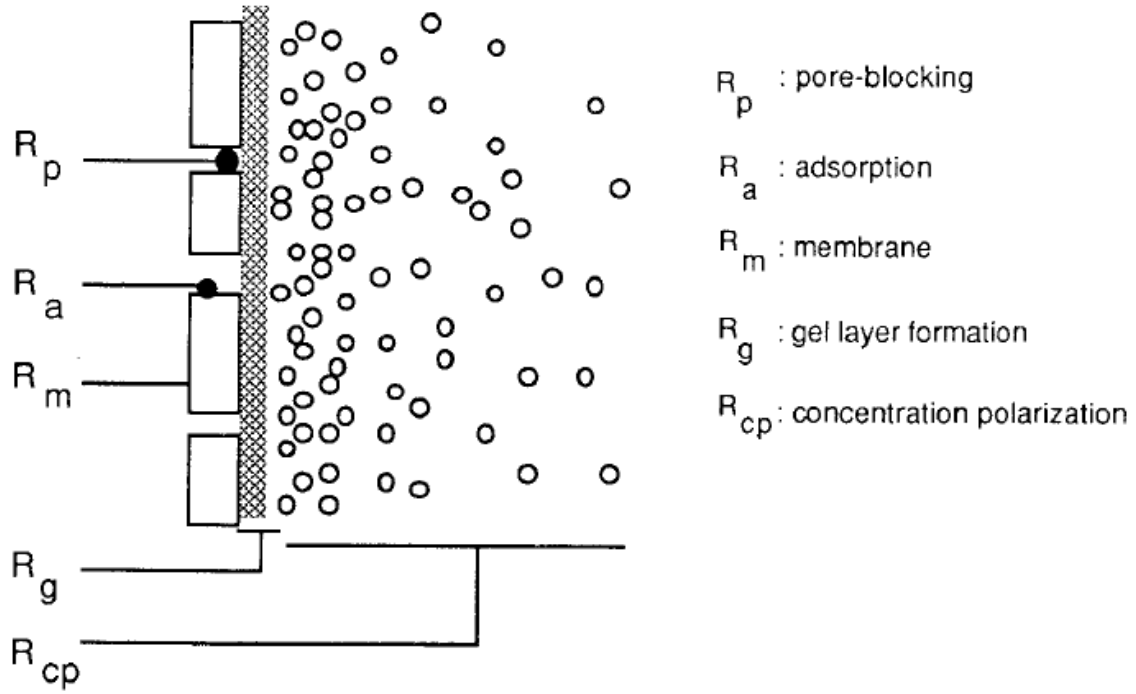

Figure 7.1: Possible resistances to solvent transport encountered in low pressure membrane processes

Due to relatively less convective flux encountered in MD, the effect of concentration polarization is supposed to be very marginal. On the other hand, due to rigorous nature of the salt solutions generally used for MD, the surface scaling can be an additional problem. Moreover as explained in Chapter 2, there are certain other phenomena in MD that have the similar effect as that of the fouling on process performance. Thermal polarization is one of those which can be regarded as the counterpart of concentration polarization in low pressure driven processes. In case of partial wetting, the temperature at the pore mouth can be significantly less than that at the surface and can decrease the temperature polarization coefficient [2]. The possible flux decline parameters for MD have been shown in Figure

7.2. The hydrophobic nature of the membranes used for MD makes the membranes especially vulnerable for attack from organics such as macromolecules present into dairy streams [3].

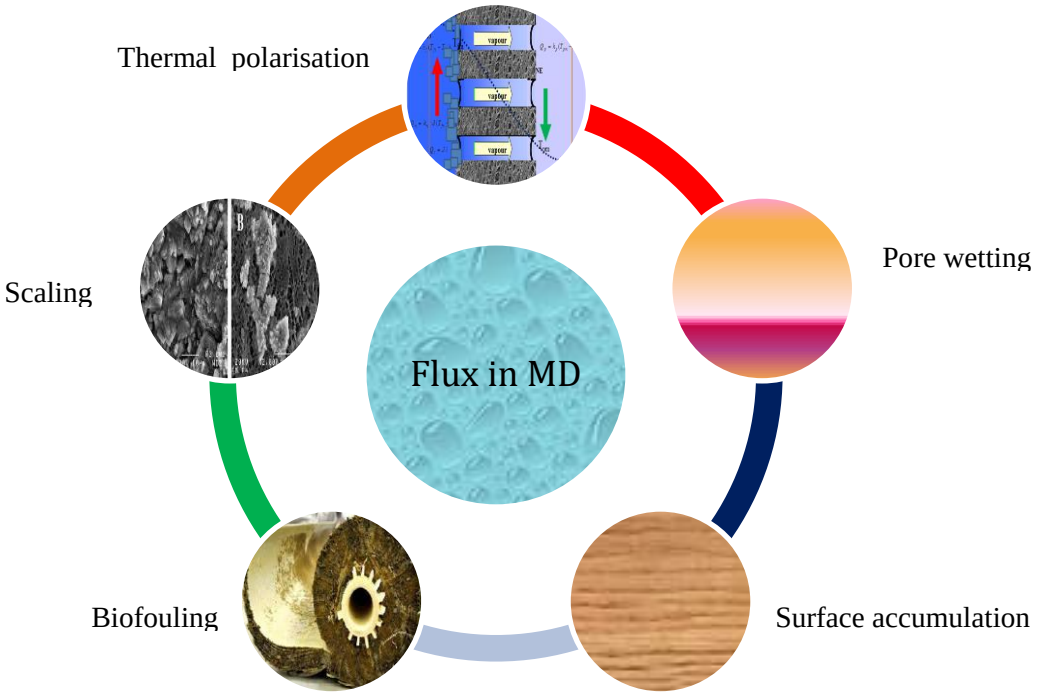

Figure 7.2: Parameters limiting the flux in MD under given process conditions

Similar to the conventional low pressure driven processes, fouling in MD depends upon the feed characteristics, membrane features and the operating conditions used. In current chapter, the fouling tendency of various feeds for membranes with different features has been tested under short experimental time period. The solutions tested include gas field produced water, RO brine; permeate from an MBR plant and whey solution. For first three solutions, lab made PVDF and commercially available PP based hollow fiber membranes have been used while for the whey solution, hydrophilically modified and unmodified PP membrane has been used. Introductory discussion on critical flux has also been included.

2. Theoretical background

2.1. Effect of liquid intrusion (wetting)

The effect of liquid intrusion has been analyzed by using the wetting model proposed by Gilron et al [2]. The details of the analysis can be found in the same reference. The basic heat transfer equation for MD can be written as

$$Q = U_o(T_f - T_p) \qquad (1)$$

Where U_o is the overall heat transfer coefficient and can be represented as following.

$$\frac{1}{U_o} = \frac{2}{h} + \frac{1}{H} \qquad (2)$$

Where

$$H = C\frac{dP}{dT}\Delta H_v + h_m \qquad (3)$$

C represents the effective membrane permeability and can be found by using the flux and vapor pressures at the interfaces for clean membrane and pure water, h_m is the membrane heat transfer coefficient.

Depending upon the characteristics of feed solution and the membrane used, the membranes for MD can prone to wetting. In case of wetting, the effective pore length of the membrane decreases and therefore effective heat transfer coefficient must be corrected based on the length of the wetted pore.

$$\frac{1}{U_o} = \frac{2}{h} + \frac{\delta_m}{\delta_m - \delta_{pl}}\left(C\frac{dP}{dT}\Delta H_v + h_m\right) + \frac{\delta_{pl}}{\varepsilon K_{wt}} \qquad (4)$$

Where, δ_m, δ_{pl}, K_{wt} represent the membrane thickness, the wetted pore length and thermal conductivity of the water, respectively.

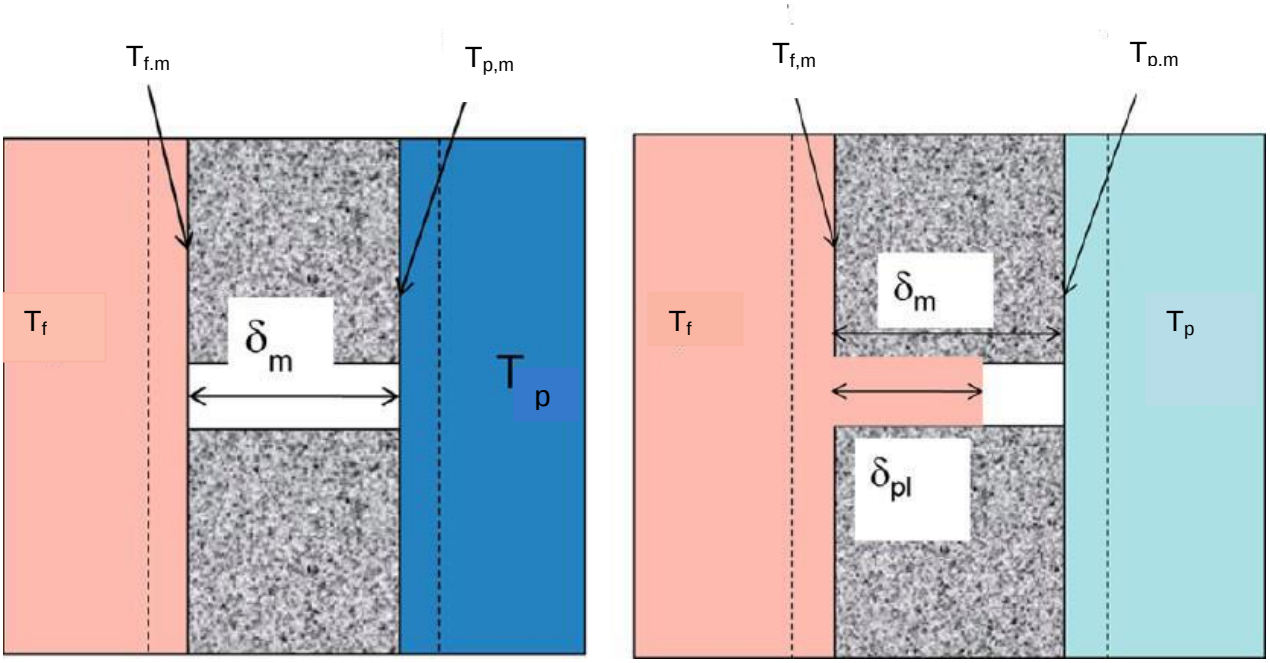

Figure 7.3: Schematic of dry and wet pore in MD (left and right respectively)

The pore wetting (Figure 7.3) plays important role in dictating the heat and mass transfer across the membrane. Due to the wetted portion of the pores, the effective membrane thickness for the mass transfer decreases, however, temperature at pore mouth drops even lower than that at the membrane surface. The cooling caused by evaporation combined with poor hydrodynamic inside the pore can increase the degree of saturation at pore mouth and can cause the scaling within the pores, thus blocking the membrane pores.

The total heat transferred can be found out by applying heat balance on entering and exiting enthalpies of the streams. The heat transfer coefficient for feed and distillate sides can be calculated by using some appropriate relationship. For the current study, the following relationship has been used for determination of *h*.

$$Nu = 1.86\left(\frac{\mathrm{Re}\,\mathrm{Pr}}{L/D}\right)^{1/3} \qquad (5)$$

Once the total heat transferred, *Q*, and heat transfer coefficients, *h*, are known, the temperature at the membrane interface can be calculated by the following expression.

$$Q = h_f (T_f - T_{fm}) \qquad (6)$$

2.2. Effect of physical properties of solution

During the concentration of feed solution in MD/MCr, the physical properties of the solution including viscosity, density and thermal conductivity change. These properties in turn change the hydrodynamic conditions within the membrane fiber that influence the temperature at the membrane surface. Moreover, the increased solution viscosity reduces the diffusion of water molecules from the bulk to the pore mouth where the evaporation takes place, thus contributing negatively to the pure water flux. In order to simplify the calculations, in current analysis, viscosity, density and thermal conductivity of produced water have been assumed equal to that of pure NaCl solution with the same concentration and under the same temperature conditions.

The viscosity of NaCl solution can be related with its mass fraction in the solution at any time by using the following Vogel-Tammann-Fulcher relationship [4].

$$\mu(Pa.s) = 10^{-9} A\sqrt{T}\exp\left(\frac{B}{T - T_0}\right) \qquad (7)$$

Where μ is the solution viscosity, *A, B* and T_o are parameters which depend upon the solution concentration according to the following relationships.

$$A = 4219.6x^2 + 2995.2x + 991.72 \qquad (8)$$

$$B = 300834x^6 - 525458x^5 + 348368x^4 - 106051x^3 + 14531x^2 - 967.34x + 644.92 \qquad (9)$$

$$T_o = 29.088x^2 + 15.881x + 134.68 \qquad (10)$$

The density of the solution as function of concentration can be determined by using the least square fitted parameters provided in [4].

$$\rho = a_1 - b_1(T - 273.15) \qquad (11)$$

Where

$$a_1 = 421.37x^2 + 629.7x + 1012.6 \qquad (12)$$

And

$$b_1 = -168.16x^5 + 206.79x^4 - 89.845x^3 + 17.308x^2 - 0.6854x + 0.4789 \qquad (13)$$

Thermal conductivity of the solution as a function of concentration can be determined by using the Yusufova relationship [5].

$$\frac{\lambda}{\lambda_w} = 1 - (2.3434 \cdot 10^{-3} - 7.924 \cdot 10^{-6} T + 3.924 \cdot 10^{-8} T^2) S + (1.06 \cdot 10^{-5} - 2 \cdot 10^{-8} T + 1.210^{-10} T^2) S^2 \quad (14)$$

Where λ is the thermal conductivity of NaCl solution and λ_w is the thermal conductivity of pure water. T is the temperature and *S* is related with the molality of the solution by following relationship.

$$S = \frac{5844.3 \cdot m}{1000 + 58.443 \cdot m} \quad (15)$$

The values of density, viscosity *Re* and *Pr* calculated on the basis of above equations have been shown in Figure 7.4 and Figure 7.5. *Re* drops from ~400 to ~200 as the solution concentration increases from ~250 g/L to ~500 g/L. Similarly, for the same change in concentration, the solution density changes from ~1160 kg/m^3 to 1380 kg/m^3 while viscosity increases from 0.0008 kg/ms to 0.0018 kg/ms. All these parameters can affect heat and mass transfer during MD process.

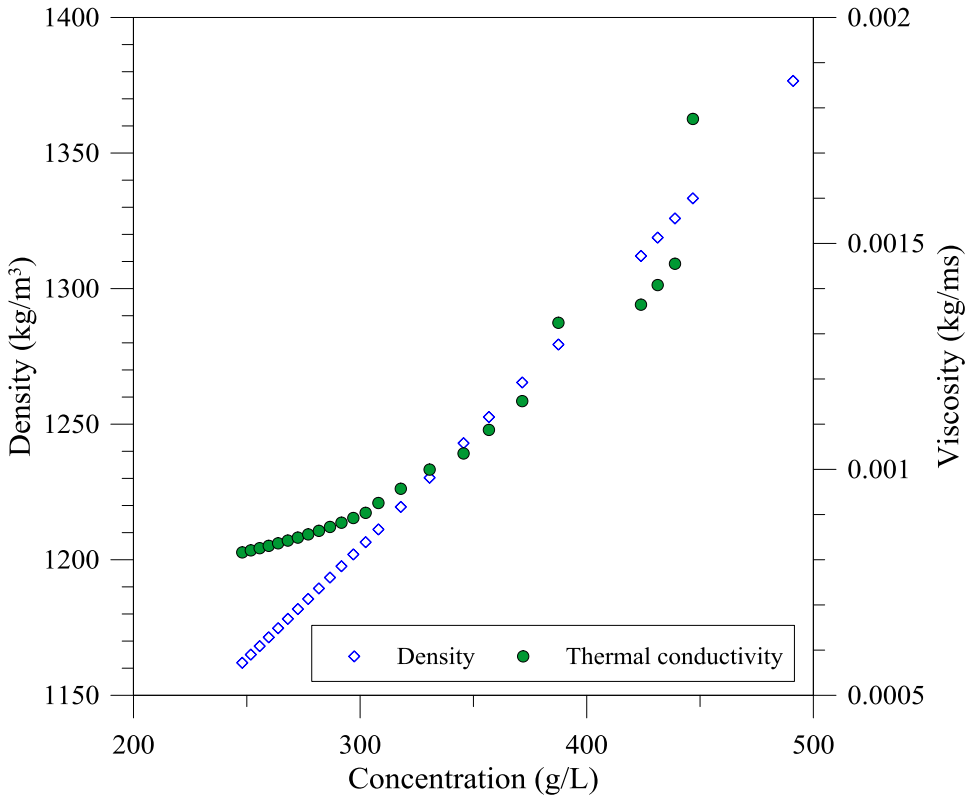

Figure 7.4: Effect of concentration on density and viscosity of solution

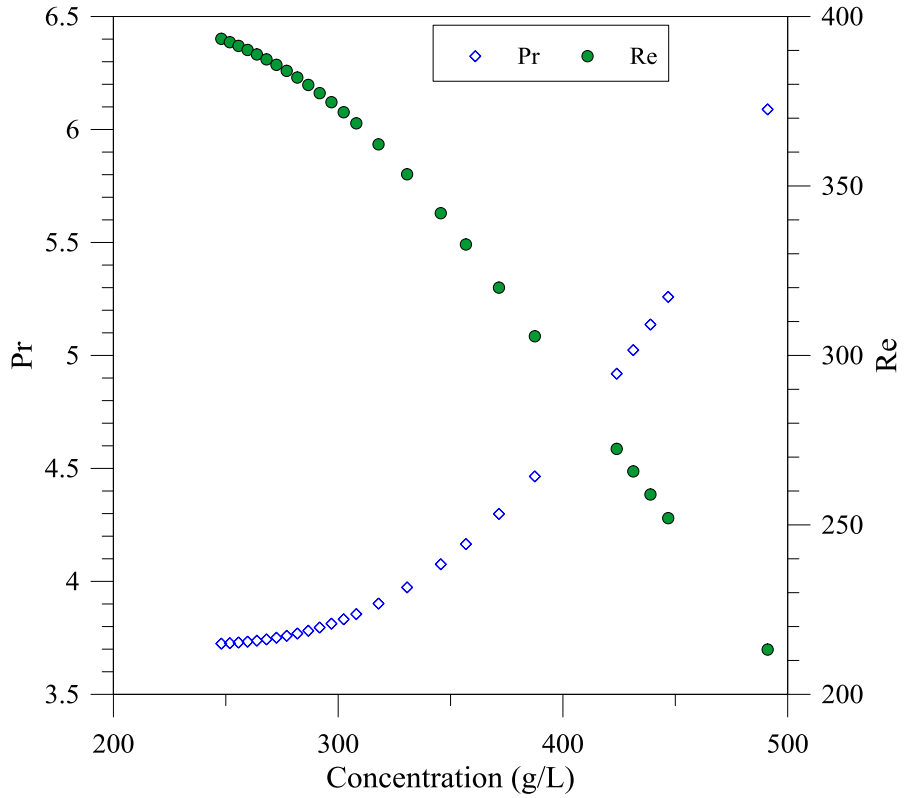

Figure 7.5: Effect of solution concentration on Pr and Re

3. Membrane distillation experimentation

Membrane distillation has been performed at feed and distillate inlet temperatures of 50^{o}C and 10^{o}C, respectively unless otherwise specified. The feed and permeate flow rates were kept constant at 50 ml/min and 30 ml/min, respectively. The detailed set-up description for MD has been shown in Figure 7.6. Three different types of feeds including synthetic brine, produced water and MBR effluent were used in the experimentation. The results achieved by using membranes entitled M3 and PP in Chapter3 have been reported here.

In order to mimic the behavior of most of the solar operated MD plants, the experimentation with produced water and MBR effluent was also performed in intermittent mode: 6-8 hours of operation and then the set-up was left as such overnight before starting up the experimentation for the next day.

3.1 Reverse osmosis brine as feed

The performance of both the membrane was tested against synthetic reverse osmosis brine solution. The composition of the brine used has been provided in Table 7.1. In order to see the effect of humic substances on the operation, 200 ppm of humic acid was also added into the brine solution.

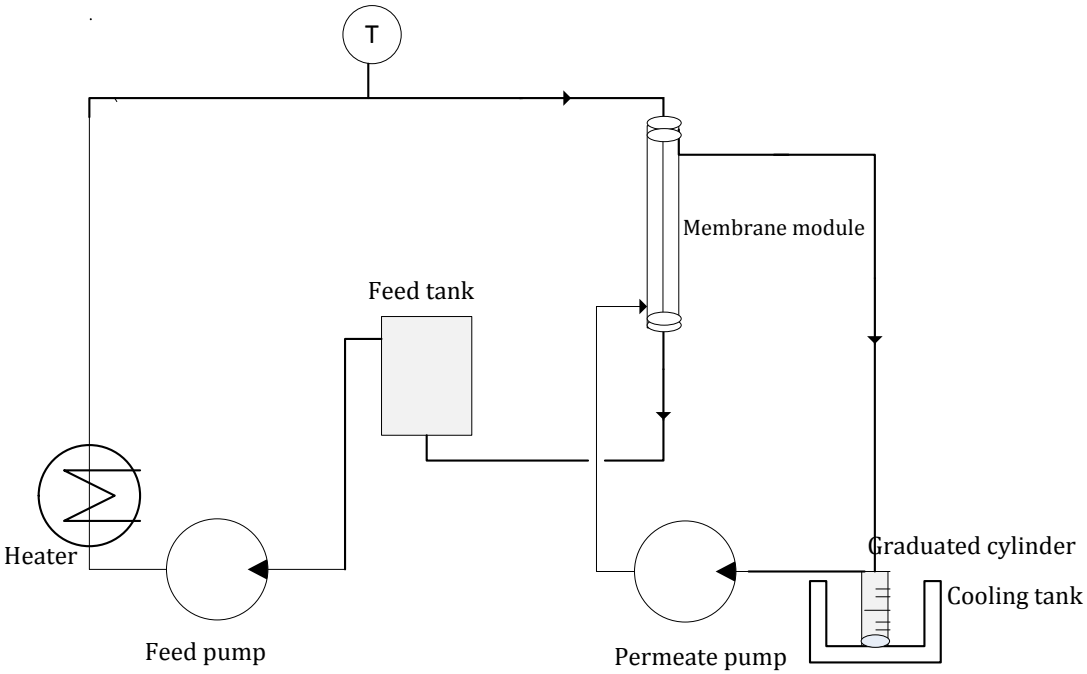

Figure 7.6: Schematic diagram of membrane distillation set-up used

Table 7.1: Composition of synthetic brine

Salt	*Composition (g/L)*
$MgCL_2{\cdot}6H_2O$	25.94
$CaCL_2{\cdot}2H_2O$	3.67
$NaHCO_3$	0.42
NaCl	57.18
Na_2SO_4	9.62
Humic acid	0.2

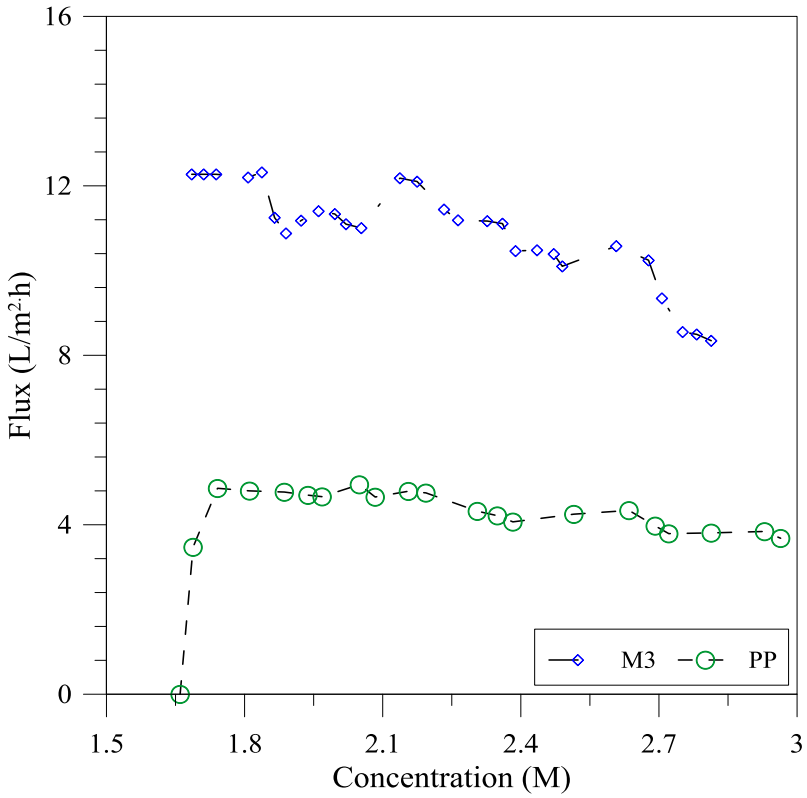

Figure 7.7: Flux as function of concentration for M3 and PP membranes

The flux for both membranes calculated for various brine compositions has been shown in Figure 7.7. The flux decreases with concentration. The most probable causes for flux reduction include reduction in vapor pressure due to increase in concentration, scaling and crystallization at the membrane surface and change in physical properties of solution with increase in concentration that affects the solution hydrodynamic as shown in Figure 7.4 and Figure 7.5. Humic substances present into the solution have tendency to interact with the membrane, and thus can create the fouling at the membrane surface. Relatively more reduction in flux for M3 can be attributed to the presence of macrovoids and relatively less hydrophobicity of PVDF than PP. There is slight increase in the conductivity of the permeate as shown in Table 7.2 which indicates that the wetting mechanism explained in section 2.2 is also partly responsible for observed decrease in flux.

Table 7.2: Properties of permeate from reverse osmosis brine

Membrane type	*Conductivity (µS)*	*TDS (ppm)*
PP	324	668
PVDF	638	1238

3.2 MBR effluent as feed

The experimentation has also been carried out by using MBR effluent obtained from a local industry treating effluent from a local hospital as the feed. The experiment was run for three days with operation carried out only during day time and plant was shut down during night and all the components were left in as-it-is state. The flux obtained for PP membrane has been shown in Figure

7.8. The figure indicates that contrary to RO brine, the flux remains quite stable throughout the operation for the entire period of experimental run. The trend confirms the operational stability of the process. The electrical conductivity and total dissolved solids (TDS) of the distillate were monitored at the end of each run. The properties of feed and average properties of distillate have been given in Table 7.3 which further confirms the operational stability of the process.

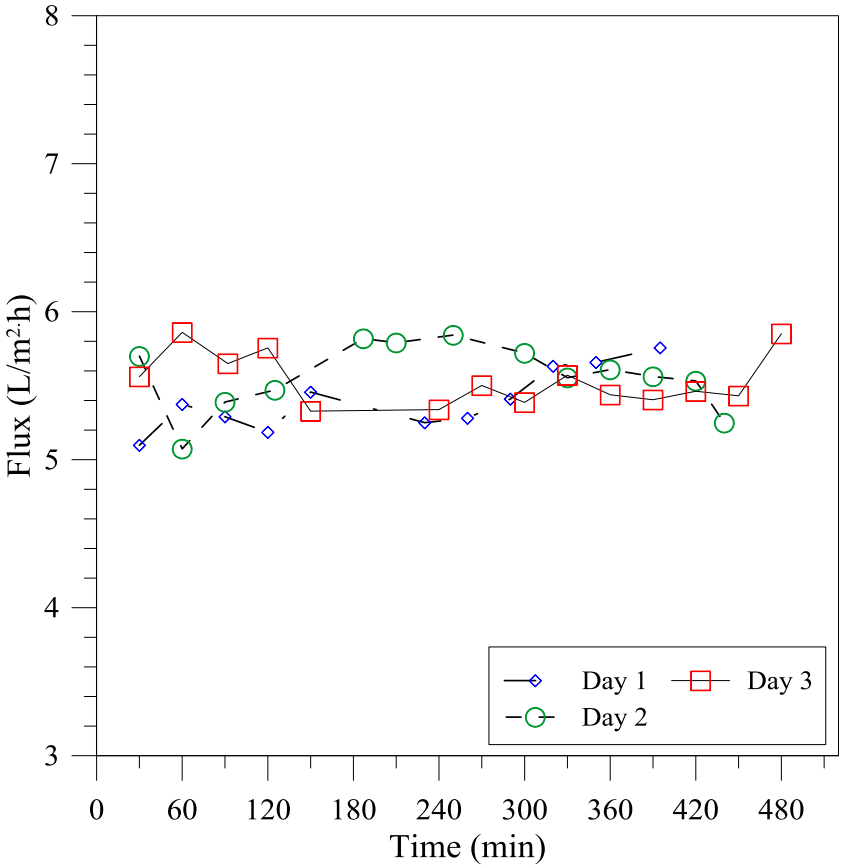

Figure 7.8: Flux obtained for MBR effluent as function of time by using PP membrane

Table 7.3: Properties of MBR effluent feed and distillate

Stream	*TDS (ppm)*	*Condutivity (µS)*	*TC (ppm)*	*TIC (ppm)*	*TOC (ppm)*
Feed	380	761	12.98	12.55	0.43
Permeate	4.86	9.78	5.82	5.1	0.72

As shown in Figure 7.9, the trend observed for M3 membrane is the same as that for PP, however, the value of flux obtained in this case is much higher than that for PP. This effect can be attributed to the lower thickness, high overall porosity and larger mean pore size of M3 membrane as explained in Chapter 3.

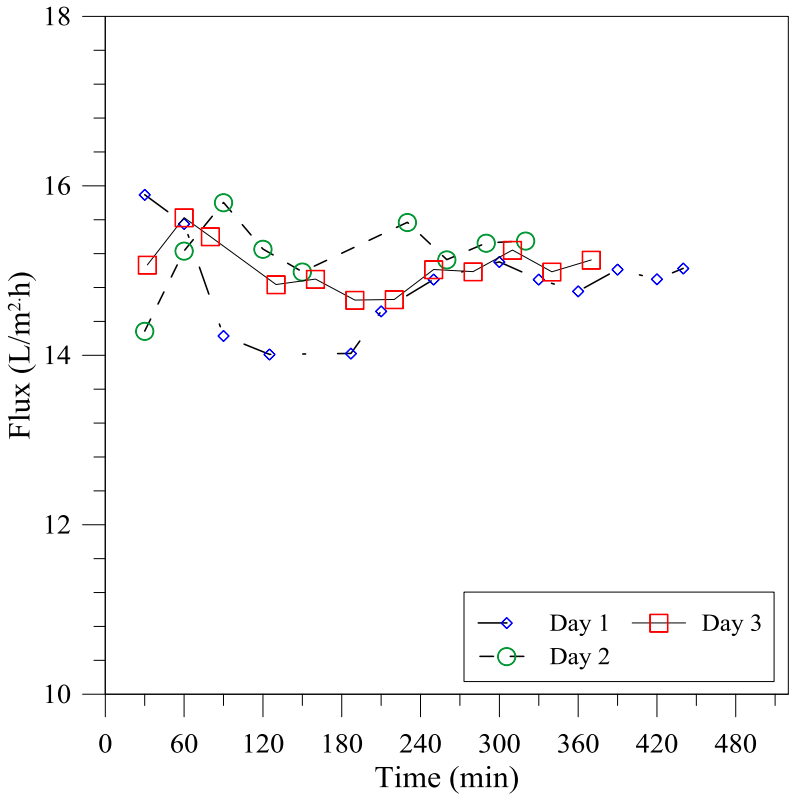

Figure 7.9: Flux obtained for MBR effluent as function of time by using M3 membrane

3.3 Produced water as feed

The experimentation has also been performed by using produced water as feed. Produced water used represents a complex mixture of various fractions. The main characteristics of the water have been provided in Chapter 6 Table 6.2.

3.3.1 Intermittent operation

Membrane distillation has been performed at feed and distillate inlet temperatures of 50^{o}C and 10^{o}C, respectively. The feed flow rate was varied between 50 ml/min to 100 ml/min while the permeate flow rate was kept constant at 30 ml/min. After two days run, the membranes were washed with double distilled water for one hour and at flow rate of 50 ml/min before putting into the next experimental run.

The flux behavior of membrane type M3 before and after washing has been illustrated in Figure 7.10. The flux decreases steeply from ~9 L/m^2.h to ~5 L/m^2.h before achieving a steady value in before washing test. There was no significant increase in solution concentration over the experimental period of time (<5%), thus the effect of solution physical properties discussed in section 2.3 can be neglected. The main reduction in flux can be attributed to the possible wetting of membrane pores that decrease the effective driving force across the membrane. The effect of wetting on different resistances to heat transfer calculated according to the model proposed by Gilron et al [2] has been shown in Figure 7.11. The figure discloses that the resistance offered by the membrane decreases linearly as the wetted length increases. It is due to reduction in effective thickness of the membrane as wetting proceeds. The resistance offered by the wetted pore length rises while the resistance offered by the feed side boundary layer stays constant with rise in wetted pore length. The most interesting observation from the heat transfer point of view is the reduction in temperature at the pore mouth with increase in

wetted pore length. This effect will decrease the effective value of temperature polarization coefficient based on bulk and temperature at the pore mouth and will affect the flux negatively.

The membrane module was left as such overnight without any cleaning or the removal of the feed from the membrane. This is the common practice for most of the solar energy driven membrane distillation pilot plants. It was found out that the flux observed at the start of the next day was significantly lower than the previous one. This behavior can be related with the salt scaling/crystallization occurring at the membrane surface or inside the pores under quiescent conditions maintained overnight. After washing, the flux obtained follows the similar trend as for the first cycle.

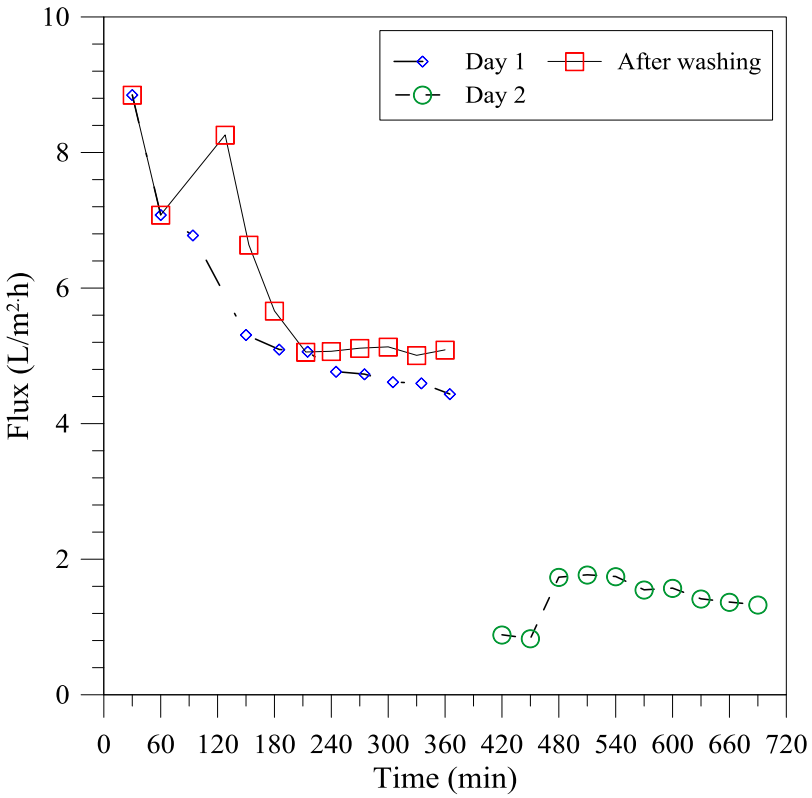

Figure 7.10: Flux as function of time for M3 membrane for produced water as feed

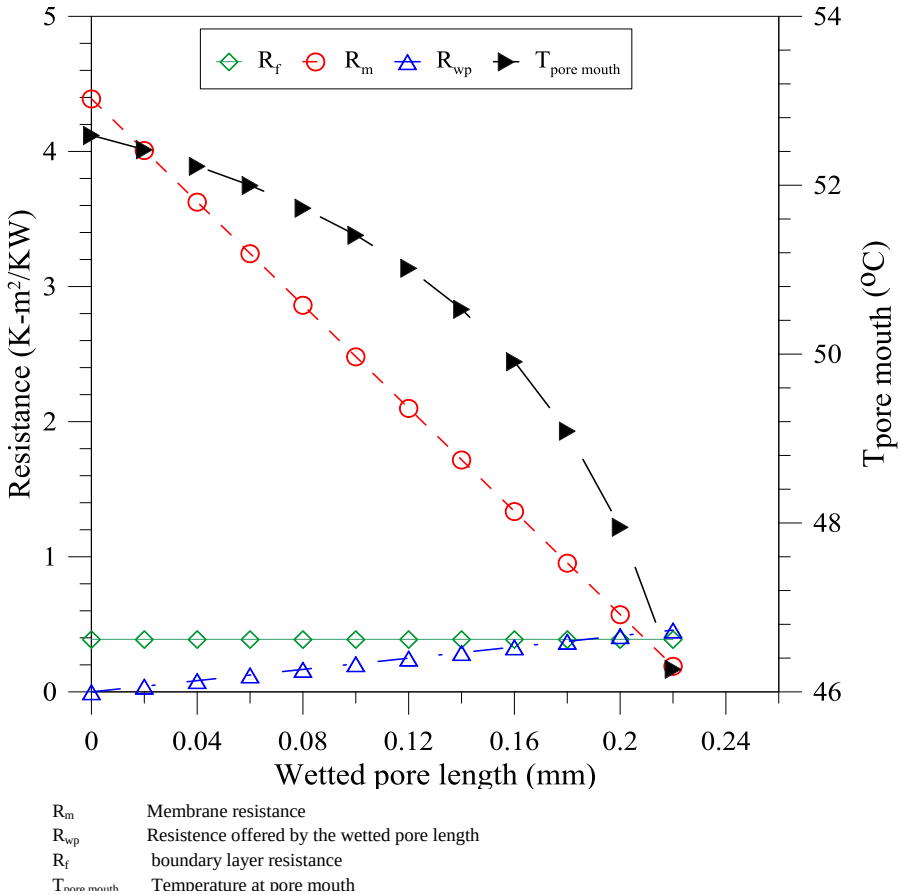

Figure 7.11: Effect of wetted pore length on various resistances to mass transfer

The scaling occurred at the membrane surface of M3 under quiescent conditions maintained over a period of three hours has been shown in Figure 7.12 which confirms the hypothesis of association of flux decline with surface scaling.

Figure 7.12: SEM images of scaling present at surface of M3 at different magnifications

Flux achieved for commercial PP membrane has been shown in Figure 7.13. It is clear from the figure that flux shows almost constant trend over the entire experimental time period for the first day. However, at the start of day 2, similar to M3, the initial flux is much lower than its value for the first day. However, the flux approaches to its steady state value for the first day as the experiment proceeds. The flux is fully recovered after washing the membranes with double distilled water according to the set procedure. This behavior can be attributed to macro-void free structure of PP. Due

to sponge like structure of PP membrane; the scaling is not penetrated deep into the structure and can be washed away relatively easily.

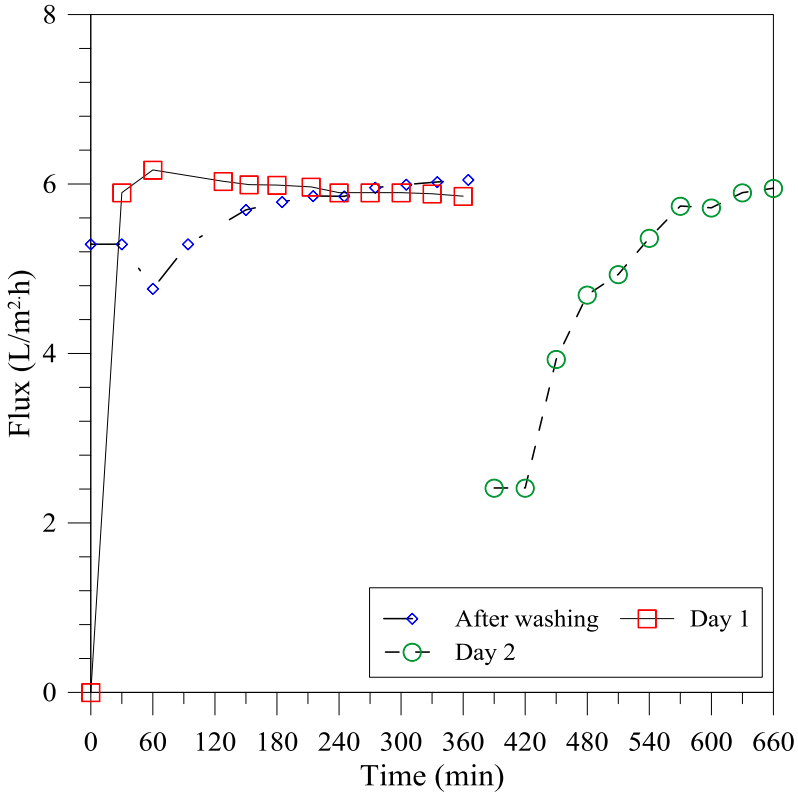

Figure 7.13: Flux as function of time for PP commercial membranes for produced water as feed

The fouling behavior of the membranes investigated can be related with their morphology developed under the operating conditions and dope composition used during the synthesis process. PVDF based membrane (M3) has been prepared by using non-solvent induced phase inversions technique. As explained in Chapter 3, for formation of M3 membrane, relatively low amount of polymer has been used in dope solution. Additionally, maleic anhydride has been applied as a co-pore forming additive into the dope. These factors give rise to the structure containing macro-voids, as evident from Figure 7.14. Such structures may be required from high flux point of view as the resistance to mass transfer offered by such structures would be low. However, for practical application of desalination, the structures with macrovoids are more susceptible to wetting. Moreover, the probability of scaling and crystal formation within the macrovoids is comparatively high. The difference between steady state and unsteady flux for such membrane is quite high and washing does not seem to be very effective for such membranes.

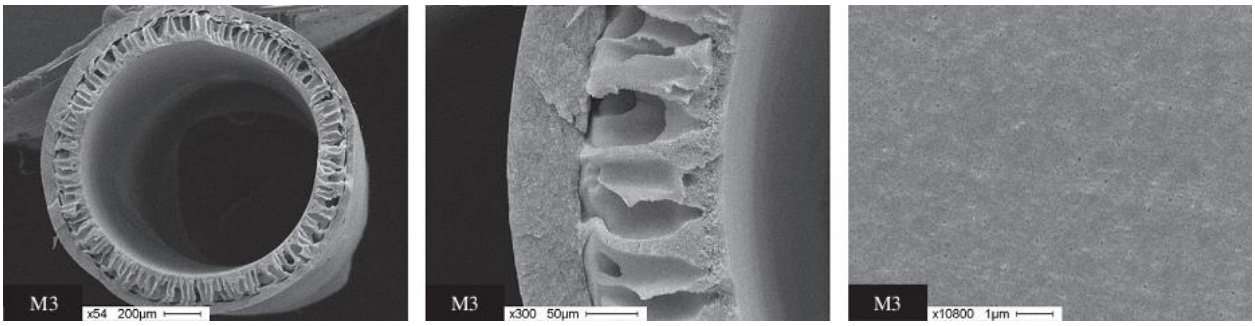

Figure 7.14: SEM picture of fiber type M3

3.3.2 Effect of membrane washing

In order to test the performance of the membrane during crystallization test, the experimentation was carried out by using PP membrane at feed inlet temperature of 50°C. The flux observed has been shown in Figure 7.15.

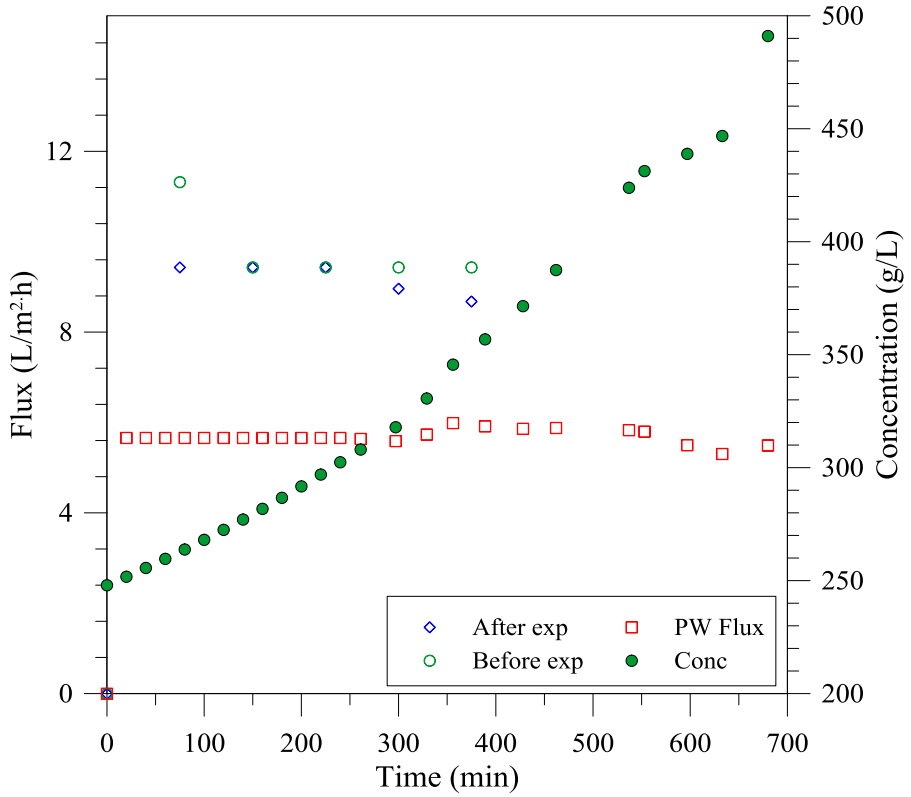

Figure 7.15: Flux for produced water during crystallization and the corresponding concentration along with pure water flux before and after crystallization.

After completing the 1st day experimentation, the membrane was washed with double distilled water. It can be observed from the figure that the starting 2nd day flux (at~350 min) is not affected by the 1st day operation that confirms the efficiency of immediate membrane washing. The pure water fluxes before and after experimentation with produced water has also been provided in the same figure. The figure shows that the flux stays steady throughout the experimental period of time. The similar values of pure water flux before and after the crystallization experiments confirm no residual fouling left on the membrane surface. It is interesting to note that concentration rises almost to double during the experimental time period. The insensitiveness of flux towards increased concentration can be

explained by the high conductivity value at the end of the test (9 mS). Very high conductivity shows that some fraction of the total pore became wet. The passage of pure solution through the wetted pores apparently suppresses the reduction in overall volume on permeate side.

3.4 Whey solution as feed

Comparative study of modules with different characteristics

In order to study the effect of module characteristics on heat and mass transport through the membrane, three different types of modules were used. The first type was fabricated by using simple PP fibers in straight configuration. PP membranes applied in Chapter 5 were used here too. The outer surface of the fibers for the second modules was modified with styrene based monomers prepared by another group according to the procedure described elsewhere [6]. The modification was incorporated in order to render the hydrophilic character to the outer surface of the fiber. The idea was to reduce the protein interactions with the fiber surface and thus to decrease the fouling tendency of the fibers when used for the solutions containing proteins. In third type, the helical configuration was used. The characteristics of the modules used have been shown in Table 7.4.

Table 7.4: Main characteristics of the modules used in the study

Module configuration	*Fibers length (cm)*	*No of fibers*	*Operating configuration*
Straight fibers	20.2	5	Outside-in, Inside-out
Modified straight fibers	21	5	Outside-in
Helically coiled	25.5	6	Inside-out

The pitch of helical module was 4 cm.

Due to the fact that the outer surface of the fibers was modified for hydrophilic character while the benefits of the helical module can be achieved when feed is introduced inside the fibers, both inside-out and outside-in configurations were used for straight fibers for the comparative analysis. Feed temperature was adjusted at 55^{o}C for all the tests. For inside-out configuration, experimentation was carried out at feed Reynolds number of ~880. Due to its rapid fouling nature, whey solution was used as the feed solution.

The flux obtained and the corresponding concentrations for inside-out configuration have been shown in Figure 7.16. As illustrated in the figure, the flux exhibited by the coiled modules is higher than its straight counterpart throughout the experimental run. The improvement can be attributed to reduction in both temperature and concentration polarization achieved in helical modules. The secondary flow induced by the helical structure improves the mixing between the fluid in bulk and boundary layer by forcing the later in lateral direction. The recorded flux for helical modules is up to 25% higher than its straight counterpart.

Another interesting results obtained through the helically coiled module is the high flux even at high feed concentration. The concentrations achieved in helical and straight modules are 18.6% and 13.7%, respectively. The higher concentration does not only cause the concentration polarization and subsequent fouling but also reduces the partial pressure of the solution. All these factors argue in favor of reduced flux. The higher flux for the helical module is due to its superior protagonist to reduce concentration and temperature polarization.

As shown in Figure 7.17, the flux obtained with modified module is significantly less than the both above mentioned modules. The reduction can be ascribed to poor hydrodynamics applied and different configuration (outside-in) used. The feed is introduced on shell side of the module and corresponds to

a Reynolds number of ~810. The figure indicates a sudden decrease in flux for unmodified module which can be probably due to the protein attacked to the hydrophobic surface of the membrane. The flux decreases slightly with time after that. The reduction can be attributed to both the increase in concentration and building up of the fouling layer. On the other hand, the flux for the modified fiber stays almost constant and only a minor drop with time can be observed for the experimentation carried out during the first day. Even after leaving the membrane in contact with the feed overnight, the there is no decrease in starting flux on the next day which indicates no buildup of fouling even under quiescent conditions. The steep decrease in flux can be attributed to increase in overall solution concentration. The modified membranes were tested with pure water immediately after using against whey solution. The results indicated in the same figure reveal quite high flux as compared to that obtained for the solution. It clearly indicates that increased solution concentration over time plays an important role in reduction in flux over time. Furthermore, the recovery of flux with pure water can be attributed to the removal of loosely attached fouling layer on the membrane surface.

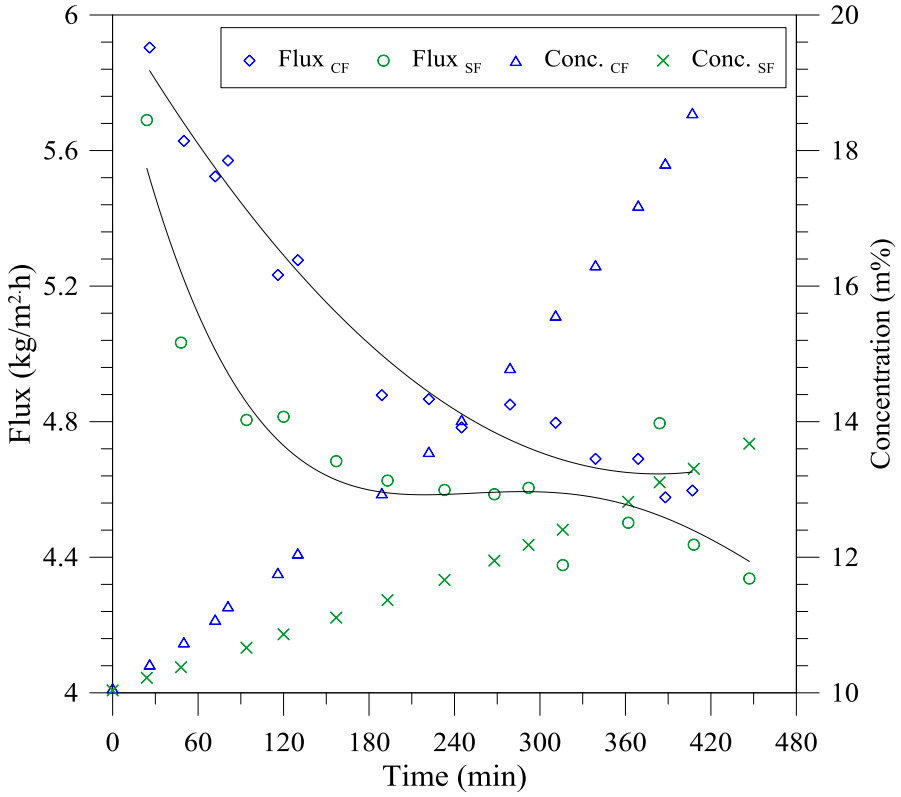

Figure 7.16: Flux and concentration achieved for straight and helical modules with inside-out configuration

When comparing the flux obtained through straight and coiled fiber modules, it should also be noted that residence time of the solution inside the coiled module is high as compared to straight modules due to more resistance offered to the fluid flowing inside the module. Furthermore, the total length of the fiber for helical module used is almost 21% longer than that of the straight one. Higher residence time combined with the relatively longer dimension tend to reduce the overall driving force along the module. The comparative results can be further attractive if the length of fibers in both modules is kept the equal.

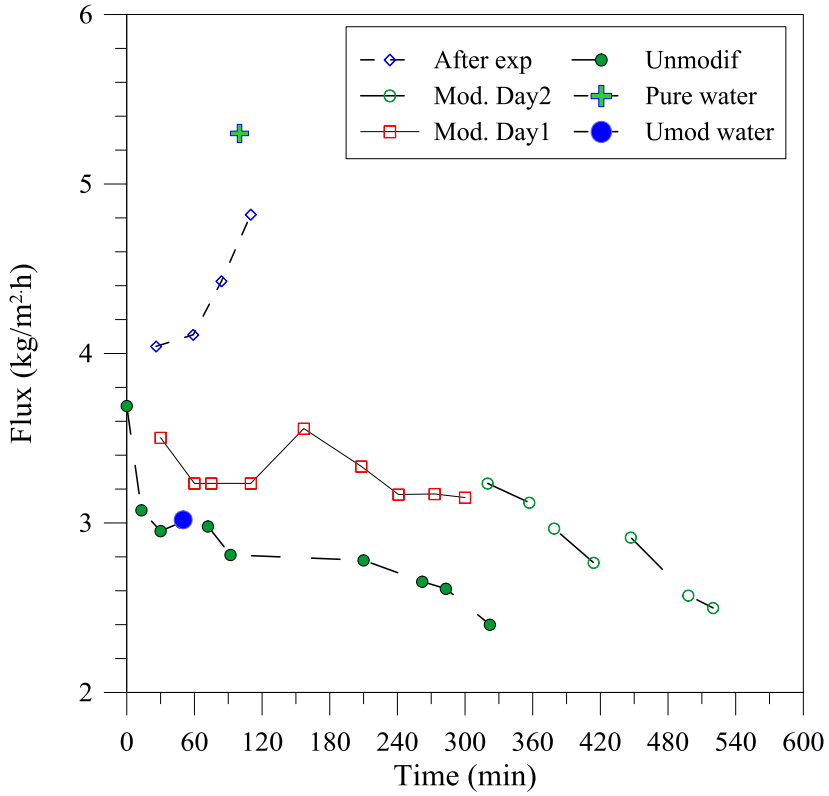

Figure 7.17: Flux achieved for straight fiber modified and unmodified modules with outside-in configuration

4. Critical flux in MD

In case of membrane distillation (MD), the definition of critical flux is much more complex, as the traditional fouling caused by the transfer of liquid through the membrane, encountered in the UF/MF process, is not present. The adsorption phenomenon occurring in subcritical region of the traditional low pressure processes, the crystallization occurring at the membrane surface under saturation conditions, temperature polarization and membrane wetting are the main flux-limiting parameters in case of MD.

If the feed contains organics, the adsorption of organics on hydrophobic membrane surface would be inevitable and it will affect the MD flux considerably. The effect of rate of adsorption on flux depends upon the characteristics of feed and membranes and can be drastic in case of organics-containing feed. Adsorption effect can be divided into two stages for MD: short term or rapid adsorption and a long term adsorption that induces the fouling/scaling which affects the flux. In case of feed containing organics or large molecules, even the short term adsorption can affect the flux significantly, however for salt solutions; the adsorption below saturation level can be negligible. One possibility way of defining critical flux in MD can be based on second stage of adsorption. The effects of true fouling will be prominent only for long term adsorption. This is particularly true for the feed treating the inorganic salts with low adsorption tendency. It is assumed that the salt precipitation at the membrane surface is a result of adsorption of nascent nuclei that grow at the membrane surface or the salt crystals grown in the solution and then adsorbed at the membrane surface.

When the hydraulic pressure exceeds the liquid entry pressure, the membranes are prone to wetting. The effect of wetting is not only possible reduction in flux and degradation of permeate quality but also a severe fouling inside the pores caused by the precipitated/adsorbed materials. For a given feed

and membrane combination, the wetting can be controlled by selecting the appropriate conditions of temperature and flow rate (hydraulic pressure). More comprehensively, feed temperature, feed composition, pore size and hydrophobic character of the membrane combined with the hydraulic pressure applied at the membrane surface will dictate the wetting phenomenon in MD.

$$\Delta P_{ent} = \frac{-2\gamma \cos\theta}{r} \qquad (16)$$

To avoid the wetting, MD operation should always be carried out under sub-wetting-conditions defined by all the features mentioned above. For critical flux, both adsorption and wetting should be avoided (Figure 7.18).

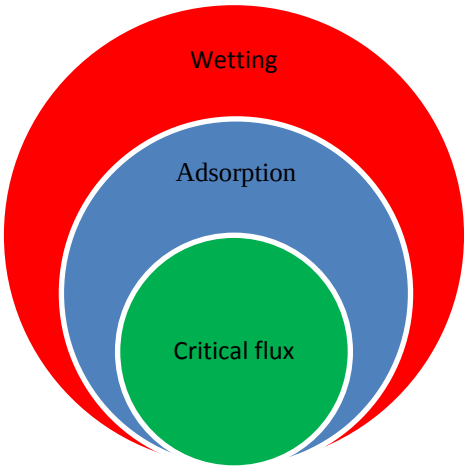

Figure 7.18: Parameters defining the windows for critical flux at a fixed level of thermal polarization

For MD, besides the fouling, temperature polarization also limits the efficiency of the process. Thus in case of MD, the critical flux should be defined for a specific flow rate condition, as the velocity affects the thermal polarization boundary layer. Therefore

$$J_{csMD} = \frac{\Delta p - \Delta \pi}{R_m + R_{TP}} \qquad (17)$$

Where Δp is the vapor pressure of the fluid calculated at the bulk temperature after including the concentration effect and $\Delta \pi$ is the osmotic pressure of the solution that tends to reduce the flux and R_{TP} is the net resistances caused by the boundary layers at both feed and permeate sides.

The weak form of the critical flux can be written in the following way.

$$J_{csMD} = \frac{\Delta p - \Delta \pi}{R_m + R_{TP} + R_{ads,s}} \qquad (18)$$

Here $R_{ads,s}$ represents the short term adsorption. It is valuable to note that in MD, adsorption can lead to continuous buildup of reversible and/or irreversible fouling. On contrary, in low pressure driven processes the filtered volume through the membrane is mainly responsible for the buildup of reversible or irreversible fouling.

4.1 Proposed protocol

The critical flux experimentation for MD may follow the similar steps as described for low pressure membrane processes and RO. For a given combination of feed, membrane and feed inlet temperature, the following step can be carried out.

1. Calculation/determination of the liquid entry pressure measurement/calculation to ensure that the process is always run below the LEP.
2. Circulation of the solution in the set-up to achieve the equilibrium salt adsorption.
3. The flux measurement at constant temperature and flow rate condition under the complete recirculation of the permeate over an extended period of time.
4. Periodic monitoring of solution concentration in the feed tank to see the kinetics of the deposition, if any.
5. Stepwise increase of temperature with a new membrane module and repetition of step 3 and 4.
6. The temperature at which flux start to show decrease with time will be noted, the corresponding flux will be the critical flux under those conditions.
7. The effect of feed flow rate, concentration and membrane characteristics on critical flux can be further explored.

4.2 Kinetics

The ions near the membrane surface will inclined to be spread uniformly into the solution by the diffusion mechanism, whereas, the lateral convection caused by the flux will tend to bring the ions at the membrane surface. The convective axial flow of the solution will direct the ions in axial direction. The interactions among the ions with the membrane surface will also play the role in ionic distribution and therefore, in inducing the concentration polarization and consequently fouling. The condition of critical flux will be achieved under the circumstances where the forces directing the ions towards the membrane (convective flux, interactions between the ions and membranes, interactions between the ions and any absorbed species at the membrane surface) will be balanced by the forces directing the ions away from the membrane (diffusion, repulsion between the particles). Low convective flux combined with the high diffusion coefficient of ions is another element responsible for low fouling in MD during desalination.

The movement of particles or ions towards or away from the membrane will be the results of mainly following factors.

1. The convective flux of vapors will tend to create concentration polarization and thus consequently fouling.
2. The diffusion forces will tend to reduce the effect of concentration polarization. A Peclet number can be defined to see the net effect of each of these parameters.
3. The hydrodynamic conditions applied will drag the particles in axial direction and can interact with the diffusion of the ions.

Convective flux of solute is related with the permeate flux of the solvent and transports the solute to the membrane surface.

The diffusive flux relies on the concentration polarization and tends to transport the solute on the basis of concentration difference.

$$J_{dif} = k(C_b - C_m) \qquad (19)$$

Where k is the solutes mass transfer coefficient and C_b and C_m represent the solute concentration in bulk and at membrane surface, respectively.

k can be calculated by mass transfer analogy of Graetz–Lévêque equation[7].

$$Sh = 1.86 \left(\mathrm{Re}\, Sc \frac{dh}{L} \right)^{0.33} \quad (20)$$

Where Sh and Sc are Sherwood and Schmidt numbers, respectively.

$$Sh = \frac{kdh}{D} \quad (21)$$

$$Sc = \frac{\mu}{\rho D} \quad (22)$$

D is the diffusion coefficient of the solvent.

The concentration at the membrane surface can be calculated by [8]

$$C_m = C_b \exp\left(\frac{J}{\rho k} \right) \quad (23)$$

The convective flux of the solute can be calculated by the following equation.

$$J_{conv} = JC_b \quad (24)$$

The degree of concentration polarization and thickness of concentration boundary layer is expected to be smaller in MD than the conventional pressure driven processes. The scale formation at the membrane surface in NF and RO can be due to bulk crystallization and/or surface crystallization. In first mechanism, the crystals are formed in bulk under superasaturation level followed by the attachment at the membrane surface while according to second mechanism; crystals initiate and grow at the membrane surface. In MD, at low concentration, the crystallization at membrane surface is more probable while at high salt concentration, both mechanisms can be significant.

4.3 Factors affecting CF in MD

4.3.1 Feed temperature

A basic parameter of interest for critical flux in MD would be the feed temperature. While a high temperature may be desired to achieve high flux, thermal efficiency and performance ratio, it may boost membrane fouling at the same time. Feed temperature will affect the flux and therefore the convective force towards the membrane surface and the cooling effect caused at the membrane surface will be stimulated. On the other hand, crystallization at membrane surface can be lowered by increasing overall feed temperature so that the temperature at the membrane surface moves corresponds to sub-saturation conditions. The situation can be relatively simple for the salts exhibiting a negative solubility with temperature. For multicomponent solutions, the saturation level of the first precipitating salt will dictate the conditions achieved for critical flux. To ensure a smooth operation over a longer period of time, the negative impact of temperature must be overcome.

4.3.2 Thermal polarization

Another important factor to be considered is the local increase in superasaturation caused by the temperature polarization induced by the evaporation at the membrane surface and the conductive transfer of heat through the membrane. The salts which have positive solubility with temperature will tend to crystallize if the degree of saturation is achieved under the conditions acquired at the membrane surface. For a given degree of saturation, the effect can be reduced by taking the measures that intend to reduce temperature polarization including feed velocity.

4.3.3 Feed flow rate

The feed flow rate can influence the scale formation in two ways. The concentration boundary layer will be negatively affected due to high feed flow rate and any formed nuclei will be taken away from the membrane. On the other hand, it will decrease thermal boundary layer and thus will lead towards high flux, bringing more ions to the membrane surface. However, it is expected that the first effect will dominate the process and critical flux will increase with feed flow rate. If the salt is prone to suffer shear induced crystallization, then the situation will become more complex.

4.3.4 MD configuration

Under the same operating conditions and membrane features, flux in various configurations of MD can be different. It will change the proportion of diffusional and convective forces. However, the crystallization will occur at the same saturation level for all configurations. Thermal polarization coefficient and therefore, membrane surface temperature might be different for different configurations which imply that saturation level will reach at different values of flux. Thus, critical flux will be different in different configurations, depending upon thermal polarization.

4.3.5 Feed characteristics

The composition of the feed dictates the type of fouling (simple adsorption or crystal adsorption) and the rate of fouling. The feed enriched with proteins and other organics compound is susceptible to induce both short term and long term adsorption on the membrane surface. As evident from many studies, the rate of fouling in MD increases dramatically with feeds congaing organic foulnats in significant quantities. Some studies performed on pressure drive processes indicate the acceleration of organic fouling in presence of salts in the solution. The feeds comprising of easily precipitating salts will lower down the value of critical flux. Moreover, the concentration of solution will dictate the saturation level of the feed and will affect the critical flux.

4.3.6 Feed tank

The structure and conditions imposed inside feed tank can be considerably helpful in controlling the fouling in MD system. The temperature of the feed tank, its structure and area in contact with the feed should be adjusted in such a way that the conditions for crystallization in the feed tank are friendlier than those at the membrane surface. The structure of the feed tank will play an important role in inducing the crystallization process within the feed tank because the interfacial energy between nucleus and a substrate is lower than that of the nucleus and solution. Complex or rougher surfaces can enhance the heterogeneous crystallization. In addition to the appropriate structure, the geometrical design of the tank should emphasis on higher contact area between the solution and the tank surface.

5. Conclusions

The fouling tendency of polymeric membranes towards various types of feeds depends both upon the feed and membrane characteristics. The membrane with macrovoids structure may be attractive to achieve high flux in membrane distillation process; however, the presence of macro-voids deteriorates the performance when the solution to be treated creates some scale forming components. Most of the scaling seems to appear under the quiescent conditions. Temperature polarization becomes worse in case of pore wetting. The helical modules improve the temperature distribution inside the fiber but are not affective in alleviating the protein attack. The hydrophilic modification with the monomers used provides an effective way to reduce the protein fouling at the membrane surface. Some basic discussion on critical flux in MD has also been provided, however, the topic still needs further experimental and theoretical investigations.

References

[1] R. Field, "Fundamentals of Fouling," in in *Membranes for Water Treatment*, vol. 4, K.-V. P. Nunes and S. Pereira, Eds. WILEY-VCH Verlag GmbH & Co. KGaA, Weinheim.

[2] J. Gilron, Y. Ladizansky, and E. Korin, "Silica Fouling in Direct Contact Membrane Distillation," *Ind. Eng. Chem. Res.*, vol. 52, pp. 10521–10529, 2013.

[3] A. Hausmann, P. Sanciolo, T. Vasiljevic, M. Weeks, K. Schroën, S. Gray, and M. Duke, "Fouling mechanisms of dairy streams during membrane distillation," *J. Memb. Sci.*, vol. 441, pp. 102–111, 2013.

[4] G. Colin, L. F. Castillo, and P. Goldstein, "Theoretical basis for the Vogel-Fulcher-Tammann equation," *Phys. Rev. B*, vol. 40, no. 10, pp. 7040–7044, 1989.

[5] H. Ozbek and S. L. P. h i l l i p S, "THERMAL CONDUCTIVITY OF AQUEOUS NaCl SOLUTIONS," Lawrence Barkeley Laboratory, University of California,

[6] Y. Chiag, Y. Chang, W. Chen, and R. Ruaan, "Biofouling Resistance of Ultrafiltration Membranes Controlled by Surface Self-Assembled Coating with PEGylated Copolymers," Langmuir, 28 (2012) pp. 1399-1407.

[7] M. MartõÂnez-DõÂez, L, VaÂzquez-GonzaÂlez, "Temperature and concentration polarization in membrane distillation of aqueous salt solutions," *J. Memb. Sci.*, vol. 156, pp. 265–273, 1999.

[8] R. W. Schofield, a. G. Fane, C. J. D. Fell, and R. Macoun, "Factors affecting flux in membrane distillation," *Desalination*, vol. 77, pp. 279–294, Mar. 1990.

CHAPTER 8

Conclusions and perspectives

The growth and progress in MD have greatly accelerated recently. The increasing interest in this technology has been observed at lab as well as commercial scale. Theoretical and experimental considerations presented in this study clarifies that the availability of appropriate membranes for MD is still an issue. The membranes used in the current study reveal that the membranes prepared through NIPS with structure engineered to increase trans-membrane flux (high porosity and large average pore size) are not appropriate for practical applications of MD. These membranes are prone to wetting and scaling. On the other hand, the membranes with sponge like morphology and relatively narrow pore size exhibit relatively lower flux but stable performance. Thus there exists an optimum between the membrane features suitable for high flux and stable membrane performance. Optimum membrane features can be different for various configurations. There is a requisite to make comparative analysis of membranes performance in various configurations.

New emerging technologies or materials can provide the solution to this problem. The use of nanotechnology to synthesize the membranes comprising of nanofibers is an interesting opportunity to address the challenge of unavailability of appropriate membranes for MD. Incorporation of carbon nanotubes in the membrane structure to enhance the water transport through the membrane is another interesting possibility being investigated. In addition to improving the long term performance, new materials with improved hydrophobicity and mechanical strength can extend the limit of maximum pore size and overall porosity. The use of new high strength/weight ratio material such as graphene can be useful to tune the thickness of the membrane. Similarly, there is possibility to reduce the membrane cost by using the techniques developed in the field of textile to increase the stable hydrophobicity of the fabrics. Similarly, biomimic membranes may become interesting in future for desalination in general. Multilayer (dual or triple layer) membranes with thickness specifically engineered for MD applications are also an interesting emerging candidate. In order to achieve the objective of sustainability, the materials and solvents used for membrane synthesis must also be ‘’green’’.

A significant amount of heat is lost due to thermal polarization, especially in DCMD. It has been shown in present study that the effect of thermal polarization prevails the concentration effects in all practical situations. There is not a single correlation that can be generalized to describe temperature polarization effect in MD. At low *Re*, the experimental heat transfer coefficient falls in the range of theoretical predictions, though no single correlation can predict the results precisely. High deviation of experimental data from theoretical predictions at high *Re* observed in this study can possibly be reduced by further improving the designing of the cell used. There is a strong requisite to extend the thermal polarization analysis further to the membranes with different features and physical configurations. Moreover, appropriate correlations need to be investigated for other configurations of MD too. The effect of membranes characteristics such as surface roughness, overall porosity, pore size distribution etc. on thermal polarization needs to be addressed.

MD has a lot to adopt from active and passive techniques practiced to decrease concentration polarization and fouling in conventional low pressure membrane based processes, and to augment heat transfer in heat transfer applications. The use of these techniques can be helpful in controlling thermal polarization in MD and to decrease the surface fouling/scaling problem. The studies carried out in this

work show that the use of helical and wavy shaped fibers increases the process efficiency and performance ratio. The use of undulating geometries is helpful in decreasing thermal polarization at both up and down stream. However, this technique still needs to be further investigated for membranes with different features and by changing the parameters of helical or wavy fibers. The use of various flow patterns has also been interesting to control thermal polarization in MD. The initial and simple studies carried out in this work show that intermittent and pulsatile flows have significant potential to decrease thermal polarization and to increase the process efficiency without decreasing the overall packing density of the module.

The increased interest of MD for various applications has been seen recently. Besides the conventional attentiveness for seawater desalination, a lot of new interesting applications have been tested. Produced water is an interesting example in this context. This water is characterized generally with presence of very high salt content and small fraction of various hydrocarbons. The treatment of such streams is very challenging for the conventional treatment techniques. The performance of MD to treat gasfield produced water has also been tested during the current PhD. Various operating conditions and membranes have been applied. It has been seen that the membranes in general show excellent performance in terms of quality of the distillate obtained. However, it has been observed that some organic volatiles pass through the membrane pores. However, there is still need to explore the long term performance of various membranes for treatment of this water. It would be interesting to see the performance of other MD configurations for this particular application.

Produced water is enriched with various minerals with concentration much higher than seawater. The use of MD as membrane crystallizer cannot only solve its disposal problem but it can provide an interesting opportunity to further increase the recovery of fresh water and minerals from this waste stream. Initial attempts show that some salts can be recovered from this solution with moderately concentrating it. The recovered salts show very good quality in terms of crystal size, shape and crystal size distribution. Further studies are needed on these lines to characterize the complete spectrum of recoverable salts from this solution.

Pore wetting and scaling are two prominent forms of nontraditional fouling observed in MD. The former depends mainly upon the hydrophobicity of the membrane material, membrane pore size and nature of feed. It has been shown that potential of pore wetting is more for the membranes with pores designed to increase the flux. In current study, produced water characterized with the presence of very high salt and small fractions of petroleum causes the most wetting problem. PP membranes are least susceptible to wetting from brine due to their sponge-like morphology and small pore size. The intrusion of the liquid inside the pores does not only deteriorate the permeate quality but also reduces the process performance. It has been shown that in case of wetting, the temperature of the liquid at pore mouth can be significantly low than its value in the bulk or even at membrane surface. Furthermore, if a wetted membrane is not properly clean, the salts and other contaminants present into the feed can cause surface or internal scaling of the membrane. The membrane scaling and fouling can be decreased by rational operation of the plant. In event of shut down, the membranes must be washed with clean water in order to avoid the surface scaling.

Publications

Journal articles

A. Ali, F. Macedonio, E. Drioli, S. Aljlil, O.A. Alharbi, Experimental and theoretical evaluation of temperature polarization phenomenon in direct contact membrane distillation, *Chemical Engineering Research and Design,* 91 (2013) 1966–1977, http://dx.doi.org/10.1016/j.cherd.2013.06.030

A. Ali, P. Aimar, E. Drioli, Effect of module design and flow patterns on performance of direct contact membrane distillation, *submitted*

A. Ali, C.A. Quist Jensen, F. Macedonio, E. Drioli, Recovery of minerals from produced water, *in preparation*

E. Drioli, **A. Ali**, S. Simone, F. Macedonio, S.A. AL-Jlil, F.S. Al Shabonah, H.S. Al-Romaih, O. Al-Harbi, A. Figoli, A. Criscuoli, Novel PVDF hollow fiber membranes for vacuum and direct contact membrane distillation applications, *Separation and Purification Technology* 115 (2013) 27–38, http://dx.doi.org/10.1016/j.seppur.2013.04.040

F. Macedonio, **A. Ali**, T. Poerio, E. El-Sayed, M. Abdel-Jawad, E. Drioli, Direct contact membrane distillation for treatment of produced water, *Separation and Purification Technology*, 126 (2014) 69-81.

E. Drioli, **A.Ali**, F. Macedonio, Membrane Distillation: Recent progress and perspectives, *Desalination*, *In press*

Editors: E. Drioli, F. Macedonio, **A. Ali**, Membrane Distillation: Basic aspects and applications - A Journal of Membrane Science Virtual Special Issue Journal of MembraneScience. *Elsevier*. Link to Virtual Special Issue: http://www.journals.elsevier.com/journal-ofmembranescience/virtual-special issues/membrane-distillation-basic-aspects-and-applications/

E. Drioli, **A. Ali**, F. Macedonio, Y.M. Lee, S. Al-Sharif, M. Al-Beirutty, Membrane based treatment for produced water, *Submiited*

Conference presentations

A.Ali, F. Macedonio, E. Drioli, Investigation of temperature polarization in membrane distillation and membrane crystallization, *Green Process Engineering* Conference, Seville, Spain, 2014

A. Ali. P. Aimar, E. Drioli, New module designed to reduce thermal polarization in membrane distillation, *10th International congress on membranes and membrane operations (ICOM)*, Suzhou, China 23-26th July, 2014

E. Drioli, F. Macedonio, **A. Ali**, Membrane Engineering for Zero Liquid Discharge in Seawater Desalination, *Annual meeting of AIChE*, Pittsburg, October 28 - November 2, 2012.

A Study of Hydrophobic Micro-Porous Membrane for Membrane Distillation, Annual meeting of AIChE, Pittsburg, October 28 - November 2, 2012 5.

E. Drioli, F. Macedonio, S. Simone, A. Figoli, **A.Ali**, Hydophobic PVDF membrane for use in membrane distillation, Annual meeting of AIChE, Pittsburg, October 28 - November 2, 2012

Poster Presentations

A.Ali, F. Macedonio, E. Drioli, Treatment of produced water by using direct contact membrane distillation, *III International Scientific Conference on Pervaporation, Vapor Permeation and Membrane Distillation*, Toruñ May 2013

A.Ali, F. Macedonio, E. Drioli, Temperature polarization in direct contact membrane distillation, *EMS Summer School*, Essen, Germany, 2013